DISSERTATION / DOCTORAL THESIS

Titel der Dissertation /Title of the Doctoral Thesis

„Jet Shapes with Massive Quarks for e⁺e⁻-Annihilation"

verfasst von / submitted by

Moritz Preißer, BSc MSc

angestrebter akademischer Grad / in partial fulfilment of the requirements for the degree of

Doktor der Naturwissenschaften (Dr. rer. nat.)

Wien, 2018 / Vienna 2018

Abstract

In this thesis mass effects of primary heavy quarks, i.e. heavy quarks that originate directly from the hard process, in global 2-jet event shape observables for e^+e^- annihilation are investigated. Since the original definition of such event-shapes like angularities, thrust, jet masses or C-parameter is not uniform with respect to the treatment of massive particles, definitions which correspond to different schemes regarding the treatment of heavy quark masses (P, E and M-scheme) are considered and their differences analyzed. For the singular dijet-like configuration it is possible to use effective field theory methods, in particular boosted Heavy Quark Effective Theory (bHQET) and Soft-Collinear Effective Theory (SCET), in order to show that the leading cross section contribution for the observables of interest can be factorized in more general building blocks and thereby systematically resum large logarithms present in this limit by utilizing renromalization group methods. At next-to-next-to-leading logarithmic accuracy (NNLL) the effects of heavy quark masses only enter via the so called jet function and it is shown that for the investigated observables different event shapes form classes for which the jet function is universal. Using this, the previously unknown primary massive jet function for the investigated P- and E-scheme event shapes is calculated. Together with the other cross section factors known from the massless case this allows to calculate the singular differential cross section for the discussed event shapes in the context of stable primary heavy quarks at NNLL. For the case of unstable heavy quarks, relevant for top quarks, most of the investigated event shapes are very sensitive to the exact kinematics of the heavy quark decay products which leads to a formally power suppressed but not negligibly small change in the differential cross section. Investigating the underlying mechanisms then leads to an additional factorization of the leading contribution to the differential cross section for unstable heavy quarks into the singular stable cross section and a so called decay function which parametrizes the exact decay kinematics in terms of the event shape of interest. In a next step this factorization is checked numerically using simulations which shows that the theoretical predictions coming from the decay function approach work very well for the investigated observables. Finally the full result for unstable M-scheme C-parameter, which is of interest in the context of MC top quark mass calibrations, is qualitatively compared to pseudo-data from PYTHIA 8.2 which shows that the developed setup leads to a consistent result for such calibrations.

Zusammenfassung

In dieser Arbeit werden Masseneffekte von primären massiven Quarks, das sind massive Quarks die in der harten Wechselwirkung erzeugt wurden, im Rahmen von sogenannten Event-Shape-Verteilungen in Elektron-Positron Kollisionen untersucht. Nachdem die ursprünglichen Definitionen von den meisten dieser Observablen, beispielsweise Angularities, Thrust, Jet Massen oder C-Parameter, in Bezug auf massive Teilchen nicht einheitlich sind, werden Definitionen die in verschiedene Schemen bezüglich der Behandlung von Quarkmassen (P, E und M-Schema) fallen, untersucht. Für singuläre Konfigurationen die einer reinen 2-Jet Situation sehr ähnlich sind, können Werkzeuge aus der effektiven Feldtheorie (EFT), im speziellen boosted Heavy Quark Effective Theory (bHQET) und Soft-Collinear Effective Theory (SCET), benutzt werden um ein Faktorisierungstheorem für die führenden Beiträge des Wirkungsquerschnitts herzuleiten. Die EFT Methode erlaubt es, den Wirkungsquerschnitt als Produkt von allgemeineren Bausteinen zu schreiben und durch das Benutzen von Renormierungsgruppenmethoden sogenannte große Logarithmen zu resummieren, welche in solchen kinematischen Situationen auftreten. Bei der sogenannten "next-to-next-to-leading logarithm"-Genauigkeit (NNLL) gehen die erwähnten Masseneffekte nur über die Jetfunktion in das Faktorisierungstheorem ein, und es stellt sich heraus, dass verschiedene Event-Shape-Observablen Klassen bilden, für welche die Jetfunktion universell ist. Dies wird dann in weiterer Folge benutzt um die bisher nicht bekannte Jetfunktion mit primären massiven Quarks für alle untersuchten Event-Shape-Observablen im P- und E-Schema herzuleiten. Zusammen mit den anderen Bausteinen, die vom masselosen Fall übernommen werden können, lassen sich diese Ergebnisse zur Berechnung des singulären differentiellen Wirkungsquerschnitts mit stabilen primären massiven Quarks verwenden. Im Falle von instabilen schweren Quarks, d.h. für Top-Quarks, zeigen die meisten der untersuchten Event-Shape-Verteilungen eine sehr hohe Sensibilität bezüglich der exakten Kinematik der Zerfallsprodukte was zu einer, formell zwar unterdrückten aber nicht vernachlässigbar kleinen, Modifikationen des differenziellen Wirkungsquerschnitts führt. Im Zuge der Untersuchung der genauen Mechanismen hinter dieser Veränderung kann dann in weiterer Folge gezeigt werden, dass sich für die führenden Beiträge im instabilen Fall eine weitere Faktorisierung in die singulären Beiträge für den stabilen Fall und eine sogenannte Zerfalls-Funktion ("decay function") ergibt. Diese Zerfalls-Funktion parametrisiert die Kinematik der Zerfallsprodukte für die jeweilige Event-Shape-Verteilung. Nachfolgend wird diese Faktorisierung dann anhand von Simulationen überprüft und auch gezeigt dass die resultierende Beschreibung für die untersuchten Fälle gut funktioniert. Abschließend wird dann das Resultat für den sogenannten M-scheme C-Parameter, welcher im Kontext von MC Top Quark Massenkalibrationen von Interesse ist, qualitativ mit pseudo-Daten von PYTHIA 8.2 verglichen. Dieser Vergleich zeigt dass die entwickelte Beschreibung zu einem mit vorherigen Untersuchungen konsistenten Resultat führt.

Acknowledgements

First, I would like to thank my thesis supervisor Prof. André Hoang for his guidance, advice and support during the last few years and also for giving me the opportunity to work as a member of the particle physics group at the University of Vienna.

I would like to thank Prof. Iain Stewart for being a great host during my stay at MIT. I will never forget this very memorable experience and would also like to thank Aditya, Eric, Kristi, Laura, Lina and Patrick for the great time and all the nice memories I brought back with me.

During my time at the University of Vienna I was fortunate to meet many new friends and colleagues. It is impossible to express how profoundly the shared experiences, learned lessons, endured disasters and celebrated successes influenced my whole being and I hope that I was able to give something back to them. This can never be a complete list but I would still like to thank Bahman, Christopher, Daniel, Elke, Judith, Lukas, Manuel, Maximilian, Stefan, Stephan and Vicent for their friendship and support.

Finally I want to thank my other friends and my family for their love and encouragement which I was fortunate enough to receive during my whole life. I am certain that writing this thesis would have been impossible without their support.

Contents

Chapter 1

Introduction

In the modern era of high energy physics the focus of the particle physics community lies on three main objectives which are known as the precision, the energy and the luminosity frontier. While the energy and luminosity frontier usually are understood as being mainly of experimental nature, understanding the origin and decreasing uncertainties is a fundamental aspect of quantitative science. One main interest in the particle physics context is a precise measurement of fundamental theoretical parameters such as coupling strengths of interactions, mixing angles or particle masses. In the context of QCD and confinement fundamental parameters are not directly observable. Instead, fundamental parameters are determined through observable quantities which are highly sensitive to them. The actual determination is then carried out by comparing theoretical predictions and the experimentally measured data. It is well known and in this context intuitive that for such determinations uncertainties are introduced on the experimental side as statistical and systematic uncertainties. Additional theory uncertainties enter because of approximations used in the theoretical descriptions and via uncertainty propagation from parameters which are used as input for the theoretical predictions. One particular example for precision determinations of a theoretical parameter are *determinations of the top quark mass* which in the following will constitute the main application of the work carried out in this thesis.

Since the discovery of the top quark in 1995 at Tevatron [1, 2] its mass has been determined with continuously increasing precision. The most precise determinations reach uncertainties of around 0.5% and a subset of those measurements is given by

$$
\begin{aligned}
m_t &= 174.34 \pm 0.64 \, \text{GeV} & \text{Tevatron Final [3]}, \\
m_t &= 172.44 \pm 0.49 \, \text{GeV} & \text{CMS Run 1 [4]}, \\
m_t &= 172.84 \pm 0.70 \, \text{GeV} & \text{ATLAS Run 1 [5]}.
\end{aligned}
\tag{1.1}
$$

In comparison to other less precise methods (e.g. measurements of the total cross section at hadron colliders) these measurements are obtained in studies using so-called *kinematic reconstruction*. These measurements are based on the idea of a propagating top quark particle, for which highly mass sensitive kinematic distributions, such as the invariant mass distribution can be reconstructed from the momenta of final state objects. This refers to e.g. jets and leptons, which are experimentally identified as decay products of the top quark. On the theory side Monte Carlo (MC) event generators are used since such an identification is theoretically not fully unique due to confinement and also since the used cuts on the final state demand final state information on a highly exclusive level. The measured mass value is then given by the numerical value of the top quark mass parameter which enters the MC simulation for the best fitting reconstructed invariant mass distribution, which is therefore often also referred to as the *Monte Carlo top quark mass parameter*. From the field theoretic side this mass parameter is not yet understood in terms of perturbation theory and it is not yet clear how this quantity can be used for precision calculations without adding an additional uncertainty.

Since direct theoretical calculations for the experimentally measured observables are not yet available one ansatz which was chosen by our collaboration in Ref. [6] is to *extrapolate the prediction of the MC event generator to a process and mass sensitive observable for which precise theoretical calculations at hadron level are possible and extract a numerical relation between the MC top quark mass parameter and a well defined theory mass on the observable level. This approach has been called Monte Carlo top quark mass calibration.* There are not many mass sensitive observables for which precise hadron level predictions are feasible but it turns out that some of the so called event shapes for e^+e^- annihilation can accommodate such investigations which is why the peak region of the 2-jettiness distribution for boosted top quark production was used in the study of Ref. [6]. Apart from a general discussion, the analysis of Ref. [6] will not be discussed in this thesis in detail since most of the conceptual contributions are already described extensively in Refs. [7–9]. My personal contribution to this work was mainly focused on the provision of precise MC data sets and validation checks for the involved extensive numerical implementation. As a next step it would be interesting to investigate the universality of the result obtained in Ref. [6]. One possible approach to this is to investigate alternative observables (in this thesis we will focus on C-parameter). *The main objective of this thesis is to investigate such alternative event shape definitions, identify observables useful for MC top quark mass calibrations and to provide the needed ingredients and if necessary new tools to carry out a calibrations in analogy to the 2-jettiness case of Ref. [6].*

It is well known that for event shapes like 2-jettiness τ the peak region (where $\overline{\tau} \equiv \tau - \tau_{\min} \ll 1$) is populated by events with dijet-like kinematics, for which multiple well separated scales are characteristic. These scales which appear in perturbative fixed order calculations as ratios in potentially large logarithms are given by the hard interaction scale $\mu_h^2 \sim Q^2$ (with Q the center of mass energy), the jet scale which is the typical off-shellness of the collinear particles making up the jet $\mu_c^2 \sim Q^2 \overline{\tau}$ and the soft scale $\mu_s^2 \sim Q^2 \overline{\tau}^2$ which is characteristic for global soft radiation. Using effective field theory tools it is possible to derive a factorization theorem which together with renormalization group evolution techniques can be used to systematically resum the mentioned large logarithms to all orders in perturbation theory. For boosted top quark production where $\Gamma_t > \Lambda_{\rm QCD}$ and where in the peak region $\overline{\tau} \sim \frac{m_t \Gamma_t}{Q^2} \ll \frac{m_t}{Q}$ the suitable framework for carrying out those theoretical calculations is given by boosted Heavy Quark Effective Theory (bHQET) [7, 10, 11] matched onto Soft-Collinear Effective Theory (SCET) [12–15] with massive quarks (compared to only SCET in the collinear sector for $\overline{\tau} \sim \frac{m_t}{Q}$). For this setup the top quark is integrated out and the remaining degrees of freedom are so-called ultracollinear gluons with momentum k^μ interacting with each other and with color sources representing the top quarks which carry the momentum $m_t v^\mu + k^\mu$ (with $v^2 = 1$). The ultracollinear gluons are soft in the rest frame of the top quark with a typical off-shellness $\mu_{uc}^2 \sim \frac{m_t \Gamma_t}{Q^2}$. These ultracollinear gluons are typically much softer than the collinear gluons in SCET $\mu_c^2 \sim \frac{m^2}{Q^2}$.

The origin of the mass sensitivity of the 2-jettiness peak region is already contained in the tree level threshold position which is given by

$$\tau_{\min} = 1 - \sqrt{1 - 4 \frac{m^2}{Q^2}} \;=\; 2 \frac{m^2}{Q^2} + \mathcal{O}\left(\frac{m^4}{Q^4}\right). \tag{1.2}$$

In this context the leading power description from SCET or bHQET for stable top quarks only recovers the leading stable tree level threshold position of $2\frac{m^2}{Q^2}$. The corrections of order $\mathcal{O}(\frac{m^4}{Q^4})$ are formally power suppressed but numerically not at all small. In order to achieve precise predictions for the peak region one nevertheless needs to include these terms in the theoretical description. Since no full description at subleading power is available, usually these subleading contributions are put in "by hand" by shifting the partonic threshold from $2\frac{m^2}{Q^2}$ to $\tau_{\min}$ in order to maintain the full threshold information. Numerical checks with simulation show that for stable heavy quarks this procedure works quite well and thus accounts for the most important effects of these formally power suppressed contributions.

Next, turning to the unstable case and working at leading power, leads to effective field theory predictions which for some event shapes significantly deviate from the distributions obtained from simulations. Looking into this, one can identify the following three effects which possibly lead to major changes for the unstable distribution when compared to the stable case beyond shifting to the full stable threshold position. For illustrative purposes consider the comparison between the case of stable top quark pair production at tree level and the unstable case where these on-shell top quarks decay into massless particles via the weak interaction.

1. *Non-Clustering Event Shapes*
   Some event shapes, e.g. 2-jettiness or jet masses, have a so called clustering property which means that only the total jet momentum enters the calculation of the event shape value. Since energy and momentum are conserved the event shape values for the stable and unstable situation are the same for event shapes with the clustering property. When a massive on-shell particle decays into two massless particles the angle between the two trajectories will be nonzero. Non-clustering event shapes are sensitive to the exact kinematic configuration within the jet, for example to the mentioned nonzero angle between the momentum of the decay products. For such an event shape the measurement will give different results for the stable and the unstable situation.

2. *Non-Collinear Decays*
   For boosted top quark production the decay products are usually collinear with respect to the original top quark which is why we call those *collinear decay events*. Non-collinear decay events are characterized by a final state configuration where one of the decay products is not collinear with respect to the original top quark. Such a situation is power suppressed but still is possible at finite boost. For those events the jet definition (e.g. thrust axis) and the obtained event shape value will be different with respect to the stable top quark case.

3. *Subleading Breit-Wigner effects*

Since the prescription of simply shifting the threshold position, which was used for the stable situation, is not sufficient for the unstable situation, the mentioned numerically important contributions need to be treated more systematically. Working strictly at leading power, terms which are suppressed by $\frac{m^2}{Q^2}$ with respect to the leading terms will be omitted. In order to develop a framework where the above effects can be included, we will adopt the following strategy: *Purely kinematic information about the produced on-shell top quarks (which will also determine the full stable threshold position) will not be expanded in powers of $\frac{m^2}{Q^2}$ but kept to all orders. At the same time dynamical contributions, which are connected to ultracollinear gluon radiation off the top quark, are still treated at leading power in the effective field theory framework.* Using this and a partial narrow width approximation for the top quark it is possible to derive a factorized formula for the unstable singular cross section which is then given by (for some generic event shape e)

$$\frac{\mathrm{d}\sigma^{\mathrm{unstable}}}{\mathrm{d}e} = \int \mathrm{d}\hat{e} \, \frac{\mathrm{d}\sigma^{\mathrm{stable}}}{\mathrm{d}e}(e - \hat{e}) \, F_{\mathrm{decay}}(\hat{e}) \,, \tag{1.3}$$

This formula expresses the unstable singular cross section as a convolution of the stable singular cross section with a so called *decay function*. The decay function parametrizes the kinematics of the decay in terms of the measured event shape and is determined purely by the tree level decay kinematics[1]. As it is shown later, the decay function framework can be used to include contributions related to the three mentioned effects and the subsequent comparison with simulation shows that this framework indeed works very well.

---

[1]Note that a similar setup was used in Ref. [16].

Following the structure of this thesis the studies and strategies which were outlined in this chapter will be developed and discussed in detail. In conclusion a first qualitative comparison between the theoretical prediction and pseudo data from PYTHIA 8.2 for the unstable C-parameter distribution is presented. It will be shown that the results of this comparison are fully compatible with the results from the MC top quark mass calibration which was using 2-jettiness. Since the distinct peak of the stable C-parameter distribution gets smeared out significantly when looking at the unstable case, the estimated calibration precision for this observable turns out the be significantly less than in the case of 2-jettiness and is estimated to be around $1 - 2$ GeV (compared to 200 MeV for 2-jettiness).

The outline of this thesis is as follows: In Chapter 2 the concept of heavy quark masses in perturbative quantum field theory is discussed in general. Apart from reviewing different mass schemes (i.e. pole, $\overline{\text{MS}}$ and MSR mass), also the pole mass renormalon problem and the concept of a MC top quark mass parameter is discussed. The connected publications of Refs [17, 18], which I co-authored, are also summarized in this chapter. Since these works are self-contained and do not widely overlap with the overall objective of this thesis, they will not be discussed in more detail. In the first part of Chapter 3 different event shapes and variants which differ in the way they treat massive quarks are discussed and analyzed with respect to the expected mass sensitivity. In the second part of the same chapter we will then focus on the dijet situation with stable massive quarks, where EFT tools can be used to resum large logarithms. The respective unstable case will be discussed in Chapter 4 and furthermore the mentioned decay function formalism will be developed. In conclusion all of the gathered insights and tools are then combined in different numerical investigations including the mentioned comparison between theory prediction and MC pseudo-data for C-parameter, which is presented in Chapter 5.

Chapter 2

Quark Masses

2.1 Historical Context

When talking about the mass of a particle one usually assumes this to be an unambiguous concept which is distinctly defined throughout physics. Starting with *classical newtonian dynamics* where the mass of some object (or for this purpose a particle) is simply a proportionality factor of how much the object gets accelerated when a force is acting on it. This can also be interpreted as a measure for the inertia of the object, hence we call it the *inertial mass*, which appears in the famous Newton's second law:

$$\vec{F} = m\,\vec{a}\ , \tag{2.1}$$

where $\vec{F}$ is the net force acting on the object, m its inertial mass and $\vec{a}$ the resulting acceleration. Another facet is added to the concept of mass when studying *classical newtonian gravity* where masses attract each other via the gravitational force. There the mass enters in such a way that the resulting gravitational force on mass m_1 (at position $\vec{x}_1$) is proportional to the two involved masses m_1 and m_2 (at position $\vec{x}_2$):

$$\vec{F}_G = G_N\,\frac{m_1 m_2}{r^3}\,(\vec{x}_2 - \vec{x}_1)\ , \tag{2.2}$$

where G_N is Newtons constant and $r = |\vec{x}_2 - \vec{x}_1|$. Since it is the general experience that heavier objects feel a stronger gravitational pull this mass concept is also referred to as the *heavy mass* of an object. In principal these two concepts of mass are a priori two separate ones but from experimental investigations it is known that these two mass concepts coincide which is also referred to as the *weak equivalence principle*.

One important feature of these historical mass definitions is that it was referring to a conserved quantity. This means that if several objects are combined into a bigger one the resulting object has a mass which equals the sum of the mass of the constituents. Starting with the development of *special relativity* this concept was discarded and instead it was realized that in order to consistently unify space and time into a 4-dimensional space-time and also incorporate the concept of relativity and a universal highest speed (the speed of light), mass and energy cannot be treated as independent concepts anymore. The total energy E of an object, which really is a conserved quantity, is now not only related to the momentum $\vec{p}$ but also to the mass of the object via the relation:

$$E^2 = |\vec{p}|^2 c^2 + m^2 c^4\ , \tag{2.3}$$

which means that the energy of a particle in its rest-frame is given by the invariant *rest mass* (or *invariant mass*) which results in the famous equation $E = m\,c^2$. This has far reaching consequences

when considering bound states where the budget of total energy also includes negative binding energy which reduces the mass of the bound state below the sum of the masses of the constituents also known as *mass defect*.

When considering quantum field theory in the context of high energy physics the mass of a particle, for now let us take the electron as an example, is naturally defined as the position of the pole in the propagator of an asymptotically free electron. This definition is therefore also known as *pole mass* and is simply encoding the relation of Eq. (2.3). When interacting theories are considered e.g. Quantumelectrodynamics (QED) we usually have to use perturbation theory and therefore also need to consider radiative corrections to the propagator pole position, hence the mass.
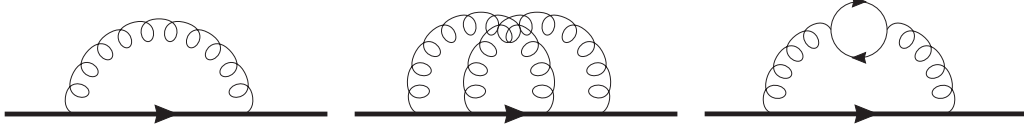

Figure 2.1: Examples for one particle irreducible (1PI) diagrams contributing to radiative corrections of the particle propagator pole position (self energy diagrams).

At tree level the classical (or non-interacting) case is valid. Starting at one loop the corrections which are also known as self energy corrections (shown in Fig. 2.1) lead to divergent contributions which one can deal with via renormalization. The idea is to replace the (infinite) mass parameter in the Lagrangian known as *bare mass* with a finite mass parameter, which needs to be measured, and some infinite part known as counter term, which then cancels the divergence (with the necessary regularization[1]) from the self energy diagram. This procedure has a certain freedom to choose how much of the finite contributions will be canceled in the process which usually leads to what is called mass scheme dependence and we therefore call the finite mass parameter in a certain renormalization scheme m^{scheme}. The self energy contributions which cannot be separated by cutting only one line in the corresponding Feynman diagram are known as one particle irreducible (1PI) contributions which we will denote as

$$i\Sigma(p,m) = i\not{p}\,\Sigma_V(p^2,m^2) + im\,\Sigma_S(p^2,m^2)\,. \tag{2.4}$$

Through reorganizing in a sum of propagators with a different number of 1PI insertions it is possible to formally sum up all corrections to the all order fermion propagator $\Delta_F^{\text{a.o.}}$ via a geometric sum. Without wave function renormalization and only focusing on the part which carries the pole position information we get

$$\Delta_F^{\text{a.o.}}(p,m) = \Delta_F(p,m) \sum_{i=0}^{\infty} \left[\Sigma(p,m)\,\Delta_F(p,m)\right]^i \sim \frac{1}{p^2 - m_0^2 - \Sigma(p,m) + i0}\,, \tag{2.5}$$

where $\Delta_F(p,m)$ is the usual fermion propagator. Next the counterterm δz_m which enters through the replacement of $m_0 = (1 + \delta z_m^{\text{scheme}})\,m^{\text{scheme}}$ cancels the divergence in $\Sigma(p,m)$ order by order. As defined before in the pole mass (also called on-shell) scheme the counterterm is chosen in such a way that it cancels the full 1PI contribution in the denominator of the all order propagator recovering the tree level form of the propagator and with this the kinematical interpretation as the physical mass of an asymptotically free particle as in Eq. 2.3. The on-shell counterterm is then given by

$$\delta z_m^{\text{pole}} = \Sigma_V(m^2,m^2) + \Sigma_S(m^2,m^2)\,. \tag{2.6}$$

Another very popular mass scheme called the $\overline{\text{MS}}$ scheme is defined in such a way that it absorbs only the divergent parts of some amplitude into the counter term and for convenience also the finite

---

[1]From now on we will use dimensional regularization in $d = 4 - 2\varepsilon$ dimensions to regularize divergent expressions of this type.

terms involving γ_E and $\ln 4\pi$ which occur in all loop calculations (realized in dim-reg by using $\tilde{\mu}^2 = \mu^2 \exp(\gamma_E - \ln 4\pi)$ as the renormalization scale). The pole and $\overline{\text{MS}}$ counter terms are given to 4-loop order in Ref. [19].

For the $\overline{\text{MS}}$ mass the interpretation as the physical mass is not possible anymore and one should think about this mass more like a coupling constant which has no kinematic meaning and its numerical value needs to be fixed from comparing an experimental measurement with the corresponding theoretical calculation. The fact that there is no close relation with the physical mass can also be seen from the fact that there are significant (finite) differences between the pole mass and the $\overline{\text{MS}}$ mass. For example in the case of the top quark (with $\overline{\text{MS}}$ mass of $\overline{m}_t \equiv \overline{m}_t(\overline{m}_t) = 163$ GeV) the perturbative conversion formula in QCD looks as follows:

$$m_t^{\text{pole}} = 163 + 7.5040 + 1.6005 + 0.4941 + (0.1944 \pm 0.0004)\,\text{GeV}\,, \tag{2.7}$$

where the terms show the series in powers of the strong coupling[2] $\alpha_s^{(6)}(\overline{m}_t)$ and in the fourth order coefficient the numerical uncertainties from Ref. [19] are quoted.

2.2 The Pole Mass Renormalon

Since all mass schemes must contain the exact same divergences it is also possible to define a mass scheme not by its renormalization procedure but through its finite differences with some other mass scheme, e.g. the pole mass scheme. In the case of the $\overline{\text{MS}}$ mass $\overline{m}_Q \equiv \overline{m}_Q(\overline{m}_Q)$ of some heavy quark Q this defines the coefficients $a_n^{\overline{\text{MS}}}$ as follows:

$$m_Q^{\text{pole}} - \overline{m}_Q = \overline{m}_Q \sum_{n=1}^{\infty} a_n^{\overline{\text{MS}}}(n_Q, n_h = 1) \left(\frac{\alpha_s^{(n_Q+1)}(\overline{m}_Q)}{4\pi} \right)^n , \tag{2.8}$$

where all flavors lighter than the heavy quark ($n_h = 1$) are considered massless and the number of such massless flavors is referred to as n_Q. These coefficients have been calculated up to order $\mathcal{O}(\alpha_s^4)$ in Refs. [19, 23–29] and are given by

$$a_1^{\overline{\text{MS}}}(n_Q, n_h) = \tfrac{16}{3}\,, \tag{2.9}$$

$$a_2^{\overline{\text{MS}}}(n_Q, n_h) = 213.437 + 1.65707\,n_h - 16.6619\,n_Q\,,$$

$$a_3^{\overline{\text{MS}}}(n_Q, n_h) = 12075. + 118.986\,n_h + 4.10115\,n_h^2 - 1707.35\,n_Q + 1.42358\,n_h\,n_Q + 41.7722\,n_Q^2\,,$$

$$a_4^{\overline{\text{MS}}}(n_Q, n_h) = (911588. \pm 417.) + (1781.61 \pm 30.72)\,n_h - (60.1637 \pm 0.6912)\,n_h^2$$
$$- (231.201 \pm 0.102)\,n_h\,n_Q - (190683. \pm 10.)\,n_Q + 9.25995\,n_h^2\,n_Q$$
$$+ 6.35819\,n_h^3 + 4.40363\,n_h\,n_Q^2 + 11105.\,n_Q^2 - 173.604\,n_Q^3\,.$$

Although the pole mass renormalization scheme is gauge-invariant and infrared-safe [23, 30] it receives large corrections in the QCD perturbation series. These large corrections arise because the pole mass scheme leads to subtractions which do not only involve the UV divergent part of the self energy (as for the $\overline{\text{MS}}$ scheme) but also unphysical on-shell self energy corrections from very small momentum fluctuations leading to a factorial growth for high orders. This behavior is also known as the pole mass renormalon (consult Ref. [31] for a review on renormalons).

To see how this factorial growth arises it is instructive to look at so called bubble chain diagrams as depicted in Fig. 2.2 which essentially are one loop quark self energy diagrams with n massless quark

---

[2] The superscript (6) indicates the scheme of the strong coupling constant which includes the top quark as a dynamical flavor in the renormalization group evolution. Following Ref. [20] we use $\alpha_s^{(5)}(m_Z) = 0.11800$ for $m_Z = 91.187$ GeV which by accounting for 5-loop evolution [21] and flavor matching at $\overline{m}_t$ [22] gives $\alpha_s^{(6)}(\overline{m}_t) = 0.10847$.
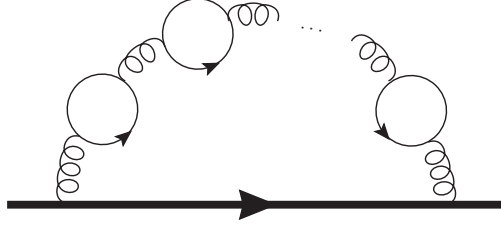
Figure 2.2: Self energy diagram with bubble chain insertion. Here bubble chain refers to a gluon propagator with n insertions of a massless fermion bubble.

bubble insertions and which are the leading contribution in the large β_0/Leading Logarithmic (LL) approximation. Starting with the bubble chain gluon propagator given in Eq. (B.2) (see App. B for more details) one first looks at the $\varepsilon \to 0$ expression for the bubble chain part of the pole mass counter term $Z_m^{\text{pole}} = 1 + \delta_m^{\text{pole}}$ (with the euclidean momentum $k_E = (-ik^0, \vec{k})$):

$$\delta_{m,\text{bubble}}^{\text{pole}} = \tag{2.10}$$

$$- \frac{\alpha_s C_F}{4\pi} \sum_{n=0}^{\infty} \left[\frac{\alpha_s \left(\frac{4}{3} T_F n_f \right)}{4\pi} \right]^n \int_0^\infty \frac{\mathrm{d}k_E^2}{m_Q^2} \left\{ \frac{k_E^2}{2m_Q^2} + \left(1 - \frac{k_E^2}{2m_Q^2} \right) \sqrt{1 + 4\frac{m_Q^2}{k_E^2}} \right\} \ln^n \left(\frac{k_E^2 \mathrm{e}^{-\frac{5}{3}}}{m_Q^2} \frac{m_Q^2}{\mu^2} \right) .$$

Looking at the integrand we can identify two main integral regions which contribute: first the region where $z \equiv (k_E/m_Q)^2$ is large which is where the UV divergences are situated and second the region where z is small and which should give a finite contribution. In the following we are going to focus on the latter and therefore split[3] the integral at $z = \mathrm{e}^{\frac{5}{3}}$ and expand the integrand for small z. Using the replacement $\frac{4}{3}T_F n_f \to -\beta_0$ by which also gluon bubble effects are included, hence often also referred to as *naive nonabelianization* [32], we get (for $\mu = m_Q$)

$$\delta_{m,\text{bubble,IR}}^{\text{pole}} = - \frac{\alpha_s C_F}{4\pi} \sum_{n=0}^{\infty} \left[\frac{\alpha_s(-\beta_0)}{4\pi} \right]^n \int_0^{\mathrm{e}^{5/3}} \mathrm{d}z \left\{ \frac{2}{\sqrt{z}} \right\} \ln^n \left(z\, \mathrm{e}^{-\frac{5}{3}} \right)$$

$$= -4\, \mathrm{e}^{\frac{5}{6}}\, \frac{\alpha_s C_F}{4\pi} \sum_{n=0}^{\infty} \left[\frac{\alpha_s 2\beta_0}{4\pi} \right]^n n! \,, \tag{2.11}$$

which is finite as expected but explicitly shows the factorial growth in n. This factorial growth is also present in the full δ_m^{pole} expression and does not get canceled by the finite terms in the UV part of the integral. This is clear since for $z > \mathrm{e}^{\frac{5}{3}}$ the argument of the logarithm becomes smaller than one leading to an additional alternating sign for the UV part which therefore cannot cancel the non-alternating $n!$ behavior from Eq. (2.11).

Looking at the difference between the pole and the $\overline{\text{MS}}$ mass, the UV divergences which originate from high momenta get canceled and one should be left with a finite difference. Employing the large β_0/LL approximation for which the bubble chain diagrams including naive nonabelianization are the only contribution, the difference is asymptotically given by [20]

$$\left[m^{\text{pole}} - \overline{m}(\mu) \right]_{\beta_0/\text{LL}} \sim \mu \sum_{n=0}^{\infty} \frac{16}{3} \left(2\beta_0^{(n_\ell)} \right)^n n! \left[\frac{\alpha_s^{(n_\ell)}(\mu)}{4\pi} \right]^n , \tag{2.12}$$

which involves (n_ℓ) active flavors for the coefficients of the β function (see App. A) and the strong coupling constant α_s and shows that the pole mass renormalon is both independent of the heavy quark mass and the number of heavy quarks (i.e. only depends on the number of massless quarks n_ℓ).

---

[3]The used choice is arbitrary but is a good separation value, especially for large n, because the argument of the involved logarithm is then one.

In a next step let us look at the Borel transform of Eq. (2.10). For a given function $f(\alpha_s)$ with the associated power series $R_f(\alpha_s) = \sum_{n=0}^{\infty} b_n \alpha_s^n$ the Borel transform is defined as $B[R_f](t) = \sum_{n=0}^{\infty} b_n t^n / n!$ with t being the Borel variable. If the Borel integral (or inverse Borel transform), which is given by $\tilde{f}(\alpha_s) = \int_0^{\infty} \mathrm{d}t \, \mathrm{e}^{-t/\alpha_s} B[R_f](t)$ exists, the series $R_f(\alpha_s)$ is called *Borel summable*. Furthermore if $R_f(\alpha_s)$ is summable then $\tilde{f}(\alpha_s) = R_f(\alpha_s)$ holds. For the case that there are singularities along the integration path (postive real axis) in the Borel variable plane the function $\tilde{f}(\alpha_s)$ is defined ambiguously. In this case the Borel integral must be defined by deforming the integration contour around these singularities and its result in general depends on the deformation.

It is also interesting to look at the Borel transform of the sum of counter term diagrams with insertions of all orders of bubble chain gluon propagators (also see Eq. (B.3)). The pole mass counter term originating from bubble chain diagrams (in analogy to Eq. (2.10)) is then given by

$$
B\big[\delta_{m,\text{bubble}}^{\text{pole}}\big](u) = -\frac{C_F}{\beta_0} \int_0^{\infty} \mathrm{d}z \left\{ \frac{z}{2} + \left(1 - \frac{z}{2}\right)\sqrt{1 + \frac{4}{z}} \right\} \left(z \, \mathrm{e}^{-\frac{5}{3}} \frac{m_Q^2}{\mu^2} \right)^{-u}
$$

$$
= \frac{C_F}{\beta_0} \frac{6}{\sqrt{\pi}(u-2)} \left(4 \frac{m_Q^2}{\mu^2} \mathrm{e}^{-\frac{5}{3}} \right)^{-u} \Gamma\big(\tfrac{1}{2} - u\big) \Gamma\big(u\big), \tag{2.13}
$$

where we used the modified Borel variable $u = \frac{t\beta_0}{4\pi}$. When examining the above expression in more detail one finds poles at $u = \frac{2m+1}{2}$ with $m \in \mathbb{N}_0$ which originate from the IR region of the integral (this can be seen by splitting the integral in the same way as before), poles at $u = -m$ with $m \in \mathbb{N}$ which originate from the UV region of the original integral as well as a single IR pole at $u = 2$. The additional pole at $u = 0$ corresponds to the usual UV divergences which would also be regularized in dimensional regularization and vanish after renormalization. Since the bare mass should be free of any ambiguity (which is associated with a pole in the Borel plane) the above expression contains the same singularities as the pole mass itself in the large β_0/LL approximation (also see Ref. [33]).

Due to the exponential suppression in the Borel integral the pole associated with $u = \frac{1}{2}$ does contribute the biggest part to the pathological behavior of the perturbative series and it is therefore called the leading IR renormalon. The fact that this pole contains the leading IR sensitivity can also be seen when investigating the IR region of the integral (e.g. using a hard cutoff as before) with the bubble chain and expanding the u independent part of the integrand. The leading contribution then gives rise to the pole at $u = \frac{1}{2}$ represented by a linear dependence on $|k_E|/m_Q$ while the higher orders give rise to the subleading poles e.g. the pole at $u = \frac{3}{2}$ is connected to a cubic momentum dependence and so on.

Furthermore at least the scaling of the ambiguity coming from the leading IR renormalon can be estimated by the difference of the integral when deforming the path above or below the pole which therefore is given by the residuum of the pole at $u = \frac{1}{2}$:

$$
\text{Res}_{u=\frac{1}{2}}\Big[B\big[m_Q \, \delta_m^{\text{pole}}\big](u) \Big] \sim \lim_{u \to \frac{1}{2}} \mu \, \mathrm{e}^{-\frac{4\pi u}{\alpha_s(\mu)\beta_0}} = \mu \, \mathrm{e}^{-\frac{2\pi}{\alpha_s(\mu)\beta_0}} = \Lambda_{\text{QCD}}^{\text{LL}}. \tag{2.14}
$$

Taking this scaling argument[4] into account several estimates for the actual numerical size of the ambiguity have been proposed. In Ref. [34] the ambiguity is estimated via the normalization factor of the $u = \frac{1}{2}$ renormalon pole when doing the full calculation (for further information also see Ref. [17]) which is usually referred to as $N_{1/2}$. The normalization factor is formally given by $N_{1/2} = \lim_{n \to \infty} a_n^{\overline{\text{MS}}}(n_Q, 0)/d_n^{\text{asy}}(n_Q)$ with the coefficients of a pure Λ_{QCD} renormalon series $d_n^{\text{asy}}(n_Q)$, i.e. $a_n^{\overline{\text{MS}},\text{asy}}(n_Q, n_h) = a_n^{\overline{\text{MS}},\text{asy}}(n_Q, 0) = N_{1/2} \, d_n^{\text{asy}}(n_Q)$. The asymptotic coefficients are given in terms

---

[4]Using the same procedure it is easy to see that the pole at $u = \frac{3}{2}$ gives rise to an ambiguity scaling like $(\Lambda_{\text{QCD}}^{\text{LL}})^3$ and analogously for the other subleading poles.

of beta function coefficients and defined by [17,35]

$$d_n^{\text{asy}}(n_Q) = 4\pi (2\beta_0)^{n-1} \sum_{k=0}^{\infty} g_k \frac{\Gamma(n + \hat{b}_1 - k)}{\Gamma(1 + \hat{b}_1)} \ , \tag{2.15}$$

with (n_Q) active massless flavors and $(\hat{b}_0 = g_0 = 1)$

$$\hat{b}_{n+1} = 2 \sum_{i=0}^{n} \frac{\hat{b}_{n-i}\, \beta_{i+1}}{(-2\beta_0)^{i+2}} \ , \qquad\qquad g_{n+1} = \frac{1}{1+n} \sum_{i=0}^{n} (-1)^i\, \hat{b}_{i+2}\, g_{n-i} \ . \tag{2.16}$$

Using all the available information for the coefficients of the $\overline{\text{MS}}$ mass and beta function coefficients, the normalization factor is determined to be $N_{1/2}(n_Q = 5) = 0.4616^{+0.027}_{-0.070} \pm 0.002$. This result is compatible with the determination from the so called renormalon sum rule which is defined in Ref. [17] giving $N_{1/2}(n_Q = 5) = 0.446 \pm 0.026$. Using the result for the normalization factor and estimating the ambiguity introduced by the ill-definedness of the top quark pole mass by taking the imaginary part of the Borel integral divided by π the ambiguity estimate of Ref. [34] is 110 MeV. In the context of other analysis, like the one of Ref. [20] which estimates the ambiguity to be 250 MeV, the obtained value from [34] is very optimistic.

The effects of lighter massive quark flavors cause the reduction of active flavors in Eq. (2.12). This is the case since the mass of a virtual quark in on-shell self energy diagrams acts as an effective infrared cutoff which causes the light quark to decouple at higher orders which means that those terms will not grow factorially anymore and the asymptotic high order region is governed by contributions from scales $\lesssim \Lambda_{\text{QCD}}$. The fact that the renormalon pattern of the pole mass is changed by the mass effects of light quarks means that the light quark mass corrections show renormalon behavior themselves. In Ref. [20] a systematic study on how to include massive lighter quark flavors q (still $m_q > \Lambda_{\text{QCD}}$) into the pole-$\overline{\text{MS}}$ relation from Eq. (2.8) was developed. This was realized by introducing a renormalization group framework based on the MSR mass (see Sec. 2.3) which allows to systematically implement the subsequent decoupling of the light massive quark mass effects and resum large logarithms of quark mass ratios which arise for this multi-scale problem. With this the top quark pole-$\overline{\text{MS}}$ relation can be evaluated at arbitrary scales. For example at very low scales $R < \overline{m}_c$ it is given by the expression of Eq. (2.8) with reduced number of active flavors at R and a couple of renormalization group evolution contributions and matching coefficients as follows:

$$\begin{aligned}
m_t^{\text{pole}} = \ &\overline{m}_t + \Delta m_t^{(6\to5)}(\overline{m}_t) + \Delta m^{(5)}(\overline{m}_t, \overline{m}_b) + \delta_{b,c}^{(t\to b)}(\overline{m}_b, \overline{m}_c) \\
&+ \Delta m_b^{(5\to4)}(\overline{m}_b) + \Delta m^{(4)}(\overline{m}_b, \overline{m}_c) + \delta_c^{(b\to c)}(\overline{m}_c) \\
&+ \Delta m_c^{(4\to3)}(\overline{m}_c) + \Delta m^{(3)}(\overline{m}_c, R) + R \sum_{n=1}^{\infty} a_n^{\overline{\text{MS}}}(n_\ell = 3, 0) \left(\frac{\alpha_s^{(3)}(R)}{4\pi} \right)^n \ ,
\end{aligned} \tag{2.17}$$

where $\Delta m^{(n)}(R, R') = m_Q^{\text{MSR}}(R') - m_Q^{\text{MSR}}(R)$ are the resummed contributions from R-evolution with (n) active flavors, $\Delta m_Q^{(n_Q+1\to n_Q)}(\overline{m}_Q)$ denotes contributions from the heavy quark Q MSR-$\overline{\text{MS}}$ matching coefficient and $\delta_Q^{(Q'\to Q)}(\overline{m}_Q)$ encodes Q'-Q matching contributions encoding heavy quark symmetry breaking effects. For more details see Ref. [20].

At finite order the best estimate for the full expression which is represented by an asymptotic series is obtained when the sum is truncated after the minimal correction term. In Ref. [20] the uncertainty associated with the determination of this minimal term was taken as an estimate for the pole mass renormalon ambiguity. In general there is not only one distinct minimal term but rather a region of terms of similar size which is usually referred to as the "flat region". Using the previously discussed framework to determine the $\overline{\text{MS}}$-pole mass difference to very high accuracy (including light massive

quarks) and the overall scale variations of the terms contributing to the flat region as an uncertainty estimate of the minimal term, the ambiguity associated with the pole mass renormalon was estimated to be around 250 MeV in Ref. [20]. Since this method uses heavy quark symmetry as a guiding principle and extensions of methods well established for convergent series we expect this method to give a conservative and reliable ambiguity estimate.

2.3   The MSR mass

Although the $\overline{\text{MS}}$ mass does not suffer from the same renormalon ambiguities as the pole mass it still is not always convenient to use since for observables sensitive to low scales it usually leads to rather large perturbative corrections which can impair the convergence of the perturbative series (see for example [7]). To overcome this disadvantage different *short distance mass schemes* (no linear low momentum sensitivity i.e. only sensitive to short distances) such as the kinetic mass [36], the potential-subtracted (PS) mass [37], the 1S mass [38–40], the renormalon-subtracted (RS) mass [41], the jet mass [7, 42] or the MSR mass [17, 43] have been developed.

The MSR mass which depends on some scale R is obtained by taking Eq. (2.8) and literally replacing $a_n^{\overline{\text{MS}}}(n_Q, 1) \to a_n^{\overline{\text{MS}}}(n_Q, 0)$, $\overline{m}_Q \to R$ and $\alpha_s^{(n_Q+1)} \to \alpha_s^{(n_Q)}$. The pole-MSR mass difference is then given by[5]

$$m_Q^{\text{pole}} - m_Q^{\text{MSR}}(R) = R \sum_{n=1}^{\infty} a_n^{\overline{\text{MS}}}(n_Q, 0)\left(\frac{\alpha_s^{(n_Q)}(R)}{4\pi}\right)^n , \tag{2.18}$$

with the coefficients $a_n^{\overline{\text{MS}}}$ which were already encountered for the pole-$\overline{\text{MS}}$ mass relation and are given in Eq. (2.9). The MSR mass is the proper extension of the $\overline{\text{MS}}$ mass concept to scales below the heavy quark mass which is achieved by two main points. First, virtual heavy quark loops are explicitly removed. Second, the above definition of the MSR mass is designed in a way so that the MSR mass is free of the linear scale dependence of the pole mass at any loop order. It can therefore be interpreted (concerning the leading IR behavior) as the pole mass minus all self-energy corrections related to *scales below R*. Also, the above expression explicitly implements the asymptotic behavior of the analog expression for the case of the $\overline{\text{MS}}$ mass in the large β_0/LL approximation which was given in Eq. (2.12).

Furthermore the MSR mass has a non-trivial renormalization group flow in R which can be expressed by the following R-RGE equation:

$$R\frac{\text{d}}{\text{d}R}m_Q^{\text{MSR}}(R) = -R\gamma^R\big[\alpha_s(R)\big] = -R\sum_{n=0}^{\infty}\gamma_n^R\left(\frac{\alpha_s(R)}{4\pi}\right)^{n+1} , \tag{2.19}$$

with the R anomalous dimension $\gamma^R\big[\alpha_s(R)\big]$. The coefficients of the perturbative series, here called γ_n^R, are given by [17]

$$\gamma_0^R = a_1^{\overline{\text{MS}}} ,$$
$$\gamma_1^R = a_2^{\overline{\text{MS}}} - 2\,\beta_0\,a_1^{\overline{\text{MS}}} ,$$
$$\gamma_2^R = a_3^{\overline{\text{MS}}} - 4\,\beta_0\,a_2^{\overline{\text{MS}}} - 2\,\beta_1\,a_1 , \tag{2.20}$$
$$\gamma_n^R = a_{n+1}^{\overline{\text{MS}}} - 2\sum_{j=0}^{n-1}(n-j)\,\beta_j\,a_{n-j}^{\overline{\text{MS}}} .$$

---

[5]In Ref. [17] the so called natural and practical versions of the MSR mass are defined. Here only the natural definition is employed. It turns out that for most numerical analysis the difference is negligible in comparison to other involved uncertainties (e.g. higher order corrections).

Solving the R-evolution equation (which can be done numerically or was done analytically in Ref. [43, 44]) it is possible to sum potentially large logarithms in $m_Q^{\mathrm{MSR}}(R_0) - m_Q^{\mathrm{MSR}}(R_1)$ in a renormalon free way as long as $R_0, R_1 > \Lambda_{\mathrm{QCD}}$ [17, 43]. This can explicitly and easily be seen in the large β_0/LL approximation by comparing the pole-MSR mass difference and the difference of the MSR mass at two different scales R_0 and R_1. The first difference is given to all orders by [43]

$$\left[m_Q^{\mathrm{pole}} - m_Q^{\mathrm{MSR}}(R)\right]_{\beta_0/\mathrm{LL}} = \frac{a_1^{\overline{\mathrm{MS}}}}{2\beta_0} \sum_{n=0}^{\infty} \left(\frac{\beta_0\,\alpha_s(R)}{2\pi}\right)^{n+1} n!\, R \,. \tag{2.21}$$

By definition this expression shows the leading renormalon behavior (at least asymptotically we have seen this in Eq. (2.12) which is the analog expression involving the $\overline{\mathrm{MS}}$ mass) and which certainly does not converge. Looking at the second difference one finds:

$$\left[m_Q^{\mathrm{MSR}}(R_0) - m_Q^{\mathrm{MSR}}(R_1)\right]_{\beta_0/\mathrm{LL}} = \frac{a_1^{\overline{\mathrm{MS}}}}{2\beta_0} \sum_{n=0}^{\infty} \left(\frac{\beta_0\,\alpha_s(R_1)}{2\pi}\right)^{n+1} n!\left[R_1 - R_0 \sum_{k=0}^{n} \frac{1}{k!} \ln^k \frac{R_1}{R_0}\right], \tag{2.22}$$

which can be seen to be convergent illustrating the original statement.

2.4   The Monte Carlo Top Quark Mass and its Calibration

It is well known that top quark mass determinations which employ reconstruction of the top kinematics from lepton and jet momenta currently allow for the most precise top mass extractions from hadron collider data. Although the underlying procedure is well defined on parton level it is not well defined on the level of jets due to confinement which makes it impossible to uniquely identify a subset of final state particles/momenta which originate only from the initially produced top quark and its decay products. Nevertheless the idea of reconstructing the top quark kinematics is used as a guiding principle to construct highly mass sensitive observables. A drawback of such observables is that traditional analytical calculations are not feasible for these observables and the mass is then extracted by employing so called parton shower Monte Carlo (MC) event generators. In such determinations the extracted top quark mass is simply the numerical input value which leads to the best fit of the experimental distribution. Clearly this procedure gives rise to different systematical uncertainties as expected from traditional theoretical calculations which need to be addressed separately. One particular example which is less straightforward to estimate is an inherent uncertainty with respect to the exact definition of the extracted mass value as a meaningful parameter in QFT which is usually avoided to address by the notion of the *Monte Carlo top quark mass*. In the following we aim to give a consistent presentation of the involved complications and how this relates to what is known as *Monte Carlo Top Quark Mass Calibrations* [6].

Traditional theoretical calculations for observables used in top quark mass determinations from kinematic reconstruction are currently not feasible[6]. This is the case since the experimental selection cuts used in the observable definition require highly exclusive event information on particle level, which is theoretically not accessible due to the lack of understanding of non-perturbative QCD effects. The theoretical description for these observables is therefore based on simulations from parton shower MC event generators (subsequently referred to as MCs - see Ref. [45]) which circumvent this problem by modelling the relevant non-perturbative physics. What is then determined as the top quark mass is the numerical value of the input top quark mass parameter in the MC program which leads to the best fit of the experimental and simulated distribution. The state of the art MC programs for top

---

[6]A promising approach to circumvent some of the problem which are discussed here is to use light soft drop jet grooming - see Ref. [16].

production at a *pp* collider first produce parton level predictions[7] for top quark production and subsequent decay. Afterwards, collinear and soft gluon radiation off the top quark and its color charged decay products is taken into account via a parton shower and finally nonperturbative QCD effects are modelled by a hadronization model leading to exclusive particle level predictions for the observables of interest. For more details on the used mass determination strategies see Ref. [47] and references therein.

In recent years this method (and similar procedures) of determining the top quark mass led to increasingly high precision for the obtained top mass value with uncertainties of well below $1\,\mathrm{GeV}$ [3–5, 48]. At such high precision a detailed discussion of the involved sources of uncertainties needs to be carried out and it is important to make sure that all relevant uncertainties are considered. The uncertainty budget can be roughly categorized as follows:

1. Statistical and systematical experimental uncertainties e.g. jet energy scale (JES), b-tagging efficiency, etc.

2. Scale uncertainties: Uncertainties from not included subleading higher order contributions (NNLO) to the hard scattering cross section are usually estimated by scale variations[8]. The subsequent parton shower (PS) is then matched to the NLO matrix elements (ME). The introduced uncertainties can also be estimated by varying the scale at which the matching happens.

3. Parton shower: To estimate the uncertainty in the perturbative description of parton showers automated estimation procedures similar to scale variations have been introduced recently in the most common parton shower MC programs (see e.g. [49, 50]).

4. Nonperturbative effects: Uncertainties from mismodeling underlying event/multi parton interactions (UE/MPI), color reconnection and hadronization can not be estimated just from the model itself. As it will be explained below, an estimate which is tied together with estimates for other sources of uncertainties can still be reached by using different MC setups/tunes.

5. "Mass scheme uncertainty": For achieving high precision it is crucial to investigate if the measured quantity is theoretically well defined (at least at a level subleading to other systematics). A priori it is unclear how the interplay between the ME-PS matching, the PS, the shower cutoff and the employed models for non-perturbative QCD effects affect the extracted numerical value of the top quark mass parameter since all of these steps are tied together in a non-trivial way. For estimating the uncertainties introduced in previous points it is assumed that none of those steps has any influence on the numerical value of the extracted mass parameter which at this point is not justified. It was argued that if one interprets the extracted quantity in terms of some perturbatively defined mass parameter (e.g. the pole mass) without further investigation one should assign an uncertainty which is regularly considered to be around $1\,\mathrm{GeV}$ [51].

Usually Points 1-4 are addressed by the experimental collaborations carrying out the top quark mass determination. It was already mentioned and it is clear to see that it is not possible to estimate the theoretical uncertainties from Point 4 without a deeper understanding of the involved nonperturbative physics. Nevertheless if one uses several MC programs which are sufficiently different for the choice of PS and nonperturbative QCD implementation (equivalent for everything which is not tied to tuning, e.g. the description of the hard scattering process) together with appropriate tunes, the difference is considered to be a good estimate of the uncertainty associated with Points 3 and 4 together. Investigating and understanding Point 5 is still work in progress and it is clear that such investigations are necessary for each of the used MC setups separately.

---

[7]Numerical fixed order calculations are available at NLO [46] which are used in NLO matched MC programs.

[8]In principle also uncertainties on the finite statistics for the MC phase space integration need to be considered although these will usually be small compared to the ones from higher orders and can be easily decreased by investing more computing power.

Recently a different approach to reduce uncertainties from Points 2-4 employing jet grooming techniques was explored in [52], where the estimate for the sum of these uncertainties was called "inherent ambiguity of the MC top quark mass" reflecting that these uncertainties are inherent to the mass extraction using a MC event generator. Since it is in principle possible to systematically improve on these uncertainties by improving the perturbative description and the employed models, this terminology might be misleading and it is important not to confuse this with what was described in Point 5 and connected remarks which ultimately tries to quantify the missing theoretical understanding in terms of an uncertainty of the measured quantity which here is the top quark mass parameter of the used MC.

In the context of top quark mass determinations it is interesting to note that usually Point 5 is not addressed properly, in the sense that it is circumvented by the caveat that the theoretical meaning of the determined quantity is unclear and an additional uncertainty should be considered. Although this is a valid approach, in practice this additional uncertainty is often not estimated and the determined quantity is then interpreted as the pole mass of the top quark, which is claimed to be natural since the pole mass was implemented in the ME stage of the event simulation. Apart from the fact that this direct identification with the pole mass is unjustified, using the pole mass also introduces an additional significant source of uncertainty due to the $\mathcal{O}(\Lambda_{\mathrm{QCD}})$ pole mass renormalon ambiguity (see Sec. 2.2) which could be avoided by relating the measured quantity to a short distance mass scheme instead of the pole mass. Furthermore in Ref. [53] it was shown that for angular ordered parton showers the employed mass scheme effectively corresponds to a short distance mass scheme (free of the leading renormalon) dependent on the shower cutoff. This is quite remarkable since for the first time it was shown that the mass scheme which effectively is used within the MC program at parton level is not equal to the pole mass and thereby the previously mentioned identification is indeed not only unjustified but incorrect. The effect of the hadronization model in this context still remains to be understood.

Extending the usual strategy of avoiding the complication of the used mass scheme is to call the numerical quantity which is obtained from such mass determinations *the MC top quark mass* although at this point it is not clear in which sense this notion is well defined. To illustrate this in more detail, let us now consider a mass determination where only one process (p), one observable (o) and one MC event generator setup (MCs) is used. Next we would like to write down a numerical relation between a well defined field theory mass and the obtained MC top quark mass $(m_t^{\mathrm{MC}})_{\mathrm{MCs}}^{\mathrm{p,o}}$ which is a priori process, observable and MC setup dependent. Due to the unclear separation between perturbative and non-perturbative effects on the extracted top mass value it cannot be assumed that such a relation can be established on the level of perturbation theory. Nevertheless one can establish such a relation on the particle level i.e. relate the numerical values of the input parameter of the MC with the numerical value for a well defined perturbative mass scheme which enters a proper theoretical calculation. This can be achieved by comparing the predicted values or distributions for mass dependent observables and identify the input mass values for which the distributions fit best. If one understands the following relation like that it is possible to write

$$m_t^{\mathrm{pole}} = \left(m_t^{\mathrm{MC}}\right)_{\mathrm{MCs}}^{\mathrm{p,o}} + \left(\Delta_t^{\mathrm{pole}}\right)_{\mathrm{MCs}}^{\mathrm{p,o}} , \qquad (2.23)$$

for the case of the pole mass and where the shift in the fitted mass with respect to the pole mass is denoted as $(\Delta_t^{\mathrm{pole}})_{\mathrm{MC}}^{\mathrm{p,o}}$. Of course an analogous expression for other mass schemes e.g. for the MSR mass (see Sec. 2.3) can also be written down:

$$m_t^{\mathrm{MSR}} = \left(m_t^{\mathrm{MC}}\right)_{\mathrm{MCs}}^{\mathrm{p,o}} + \left(\Delta_t^{\mathrm{MSR}}\right)_{\mathrm{MCs}}^{\mathrm{p,o}} . \qquad (2.24)$$

It should be emphasized that it is not clear if $(\Delta_t^{\mathrm{scheme}})_{\mathrm{MCs}}^{\mathrm{p,o}}$ is, in any way, universal[9] and how

---

[9]Heuristic arguments given in Ref. [51] and the already discussed result from Ref. [53] would suggest process universality as well as a partial observable universality at parton level but in general and at hadron level claiming universality is at this point not justified.

relevant possible universality breaking contributions are compared to other involved uncertainties, hence it would only be sensible to speak of a MC top quark mass m_t^{MC} (which is still specific for one MC setup) if process and observable universality can be established.

In general the described approach of course is not feasible because of the missing theoretical calculation for arbitrary observables which otherwise would render the usage of MC event generators for top mass determinations unnecessary in the first place. Following the presented strategy but using an extrapolation of the MC predictions to observables where theoretical calculations are possible is called *MC top quark mass calibration* in the literature. In Ref. [6] such a calibration was carried out for the case of the peak region of the 2-jettiness[10] distribution in e^+e^- annihilation with PYTHIA 8.2 [54]. For many event shapes and for this observable in particular it is possible to obtain precise hadron level predictions by using a factorized approach together with the corresponding renormalization group evolution to resum large logarithms to all orders in perturbation theory, as well as an appropriate nonperturbative model function (for details concerning this setup see Chap. 3).

The precise predictions obtained with the described setup as well as pseudo-data generated by the mentioned MC setup can then be used to fit for the value of some well defined theory mass (here pole or MSR mass) in a relation which is analogous to Eq. (2.23). Using high statistics (10^7 events) and several different values for the energy it is then possible to achieve a precise calibration. The described overall calibration uncertainty is split in two parts: (1) The perturbative uncertainty which is estimated by scanning over the different possible choices for the involved free renormalization scales (implemented by a scan over the profile function parameters, see Sec. 3.8). (2) The so called MC incompatibility uncertainty which originates from actual differences in what is implemented in the theory code and the MC simulation. This source of uncertainty is estimated by the changes induced for using different combinations of definitions of the peak region and different sets of energies considered simultaneously in the fit.

The result of the calibration is then a relation of the MC top quark mass $\left(m_t^{\mathrm{MC}}\right)_{\mathtt{PYTHIA8.2}}^{e^+e^-,\tau_2}$ (subsequently only called m_t^{MC}) and the considered mass scheme as well as the corresponding overall calibration uncertainty [55] and reads

$$m_t^{\mathrm{MC}} = m_t^{\mathrm{MSR}}(R = 1\,\mathrm{GeV}) + (0.18 \pm 0.22)\ \mathrm{GeV}\ , \tag{2.25}$$

$$m_t^{\mathrm{MC}} = m_t^{\mathrm{pole}} \qquad\qquad\quad + (0.29 \pm 0.40)\ \mathrm{GeV}\ , \tag{2.26}$$

which was checked to be valid for MC top quark mass values between 172 and 174 GeV. From this results it is easy to see that for both investigated mass schemes an identification of the MC top quark mass and the respective mass scheme is possible, however for the MSR mass within a significantly smaller uncertainty.

In the future it is important to investigate observable universality of such relations and to do that it is necessary to consider (sufficiently) different observables. One aim of this work is to identify such observables and deliver all needed ingredients to carry out a similar calibration. Due to its relatively high mass sensitivity, the different behavior concerning soft particles (with respect to 2-jettiness) and the additional sensitivity to the exact decay kinematics of the top quark (see Chap. 4), a mass sensitive version of C-parameter (more precisely M-scheme C-parameter, see Chap. 3) is a promising observable and will therefore be of special interest throughout this thesis. Furthermore a qualitative comparison for the respective theory result with MC data is shown as a preliminary result in Sec. 5.3.

---

[10]Later discussed as M-scheme thrust, see Sec. 3.2 for more details.

Chapter 3

Event Shapes for Massive Quarks in e^+e^--Annihilation

3.1 General Remarks and Definitions

Since the late 1970s a class of observables called *event shapes* was used to test and determine fundamental properties of QCD (for a review see [56,57]), most notably α_s-measurements. As the name suggests these observables contain information about the geometric momentum distribution of the final state particle momenta. The (historic) main field of application is e^+e^--annihilation and deep inelastic scattering (DIS) but today there also exist adaptations developed specifically for hadronic collision experiments (e.g. pp) [58,59].

In the historical context of e^+e^--annihilation a variety of such observables was studied both theoretically and also experimentally in great detail. An incomplete list involves thrust[1] τ [60,61], C-parameter C [62], invariant hemisphere jet masses ρ [63–65] and angularities τ_a [66,67] (with $0 \le a \le 1$). Using the center-of-mass energy Q and the sum of the modulus of final state particle 3-momenta Q_p, explicitely given by

$$Q = \sum_j p_j^0 \,, \qquad\qquad Q_p = \sum_j |\vec{p}_j| \,, \qquad\qquad (3.1)$$

the mentioned observables were defined in the literature in terms of final state particle momenta as follows:

$$\tau = 1 - T = 1 - \max_{\hat{t}} \frac{\sum_i |\vec{p}_i \cdot \hat{t}|}{Q_p} = \frac{1}{Q_p} \min_{\hat{t}} \sum_i \left(|\vec{p}_i| - |\hat{t} \cdot \vec{p}_i| \right) \,, \qquad (3.2)$$

$$\tau_a = \frac{1}{Q} \sum_i \frac{p_i^0}{|\vec{p}_i|} p_i^\perp e^{-|\eta_i|(1-a)} = \frac{1}{Q} \sum_i \frac{p_i^0}{|\vec{p}_i|} \left(|\vec{p}_i| - |\hat{t} \cdot \vec{p}_i| \right)^{\frac{2-a}{2}} \left(|\vec{p}_i| + |\hat{t} \cdot \vec{p}_i| \right)^{\frac{a}{2}} \,, \qquad (3.3)$$

$$\rho_\pm = \frac{\left(\sum_i p_i \, \theta(\pm\hat{t} \cdot \vec{p}_i) \right)^2}{Q^2} \,, \qquad \rho_h = \max(\rho_+, \rho_-) \,, \qquad \rho_l = \min(\rho_+, \rho_-) \,, \qquad (3.4)$$

$$C = \frac{3}{2} \frac{\sum_{i,j} |\vec{p}_i||\vec{p}_j| \sin^2(\theta_{ij})}{Q_p^2} = \frac{3}{2} \left[1 - \frac{1}{Q_p^2} \sum_{i,j} \frac{(\vec{p}_i \cdot \vec{p}_j)^2}{|\vec{p}_i||\vec{p}_j|} \right] \,. \qquad (3.5)$$

---

[1]Originally the variable T was defined as thrust but for consistency with the general properties of (2-jet) event shape distributions it is convenient to change that definition to $\tau = 1 - T$.

The so-called thrust axis $\hat{t}$ is determined as the axis which maximizes the projection of final state particle 3-momenta on that axis. Angularities are originally expressed in terms of the transverse momentum $p^{\perp}$ and pseudorapidity η of the final state particles with respect to the thrust axis but for ease of comparison we rewrote the above expression in analogy with the other event shapes. Note that for massless particles thrust is recovered from angularities for $a \to 0$. Furthermore, the orthogonal plane to the thrust axis defines two hemispheres (a particle with momentum p belongs to hemisphere $+$ if $\hat{t} \cdot \vec{p} > 0$ and otherwise to $-$) which defines the two hemisphere jet masses $\rho_{\pm}$. Light jet mass ρ_{l} (LHM) and heavy jet mass ρ_{h} (HJM) are then given by the lighter and heavier one, respectively. C-parameter is originally derived from the linearized momentum tensor [68, 69] $\theta^{kl} = (1/Q_p) \sum_i (p_i^k p_i^l)/|\vec{p}_i|$ which is a symmetric 3×3 matrix made up of products of final state particle 3-momentum components. Together with energy-momentum conservation this leaves two degrees of freedom which are known as the C- and D-parameter [62] (for a more detailed review see also [70]).

Due to its relevance in the literature we also want to mention total jet broadening [71] which can be recovered for massless particles from angularities for a $\to 1$ and is given by

$$B_T = \frac{1}{2Q_p} \sum_i |\hat{t} \times \vec{p}_i| = \frac{1}{2Q_p} \sum_i p_i^{\perp} = \frac{1}{2Q_p} \sum_i (|\vec{p}_i| - |\hat{t} \cdot \vec{p}_i|)^{\frac{1}{2}} (|\vec{p}_i| + |\hat{t} \cdot \vec{p}_i|)^{\frac{1}{2}} = \frac{\tau_{\mathrm{a} \to 1}^P}{2} . \qquad (3.6)$$

In general the discussed event shapes (also called 2-jet event shapes[2]) measure how closely the geometric 3-momentum distribution resembles an event with two very narrow back-to-back jets in the center of mass frame. Usually small event shape values (for the massless case, for the massive case event shape values close to the minimal value) correspond to a very dijet-like event while larger values correspond to events which are more isotropic in their momentum distribution. The asymmetrically peaked differential cross section distribution is then roughly split into three parts, i.e. the peak region which contains events which are very dijet like, the tail region with events with three well separated jets and the far tail region which corresponds to a multijet event.

3.2 Schemes for Treating Quark Masses

In high energy experiments most of the time it is sufficient to use the approximation that all final state particles are massless. If one is interested in high precision calculations or more obvious in non-zero mass effects this approximation is (a priori) no longer valid. Most of the earlier investigations where massive particles were considered in event shape distributions were concerned with the effects of finite hadron masses on nonperturbative power corrections [72, 73]. Since the generalization of the used event shape variables to the massive case is not unique we use different definitions of an event shape with the same massless limit and categorize similarly constructed observables into *schemes for treating quark masses*. In this context the following schemes are defined (in analogy with [72]):

1. *P-scheme:* All particle energies which occur are replaced by the modulus of the corresponding 3-momentum i.e. $(p_i^0, \vec{p}_i) \to |\vec{p}_i| (1, \vec{p}_i/|\vec{p}_i|)$. From the above examples thrust, C-parameter and jet broadening are originally defined in this scheme which means that only 3-momenta and their absolute values appear.

2. *E-scheme:* All particle momenta which occur are replaced by momenta which point in the same direction but with modulus of the energy of the corresponding particle i.e. $(p_i^0, \vec{p}_i) \to p_i^0 (1, \vec{p}_i/|\vec{p}_i|)$. From the list of observables which we have considered so far angularities in their original definition belong to this scheme.

---

[2]In analogy one can also define N-jet event shapes which measure how closely an event resembles a N-jet event, e.g. D-parameter is an example for a 3-jet event shape.

3. *M*-scheme: The jet masses do not fall in either of these classes and similarly constructed observables should therefore be categorized as defined in the *massive scheme* (for simplicity we call this the *M*-scheme), which will usually retain full momentum information.

In the following we will try to extend this line of thought and work out how different scheme choices change the situation in the context of massive partonic final state particles. For different schemes different simplifications are possible, e.g. in the center-of-mass (c.o.m.) frame $\sum_i p_i^0 \, \vec{p}_i/|\vec{p}_i| \neq \sum_i \vec{p}_i = 0$, which is why changing scheme might be ambiguous. It turns out that in order to correctly recover the expressions used in the literature one should start by defining event shapes in the *M*-scheme, then rewrite everything in particle energies and 3-momenta and lastly carry out all simplifications possible involving $\sum_i \vec{p}_i = 0$. After that, the usual replacement rules are used to derive the *P*- and *E*-scheme expressions. A consistent setup can be found by defining the following expressions as the *M*-scheme version of the discussed event shapes (using transverse mass $m^\perp = \sqrt{|\vec{p}^\perp|^2 + m^2}$ and rapidity y measured with respect to the thrust axis $\hat{t}$):

$$\tau^M = \frac{1}{Q} \min_{\hat{t}} \sum_i \left(p_i^0 - |\hat{t} \cdot \vec{p}_i| \right) , \tag{3.7}$$

$$\tau_a^M = \frac{1}{Q} \sum_i m_i^\perp \mathrm{e}^{-|y_i|(1-a)} = \frac{1}{Q} \sum_i \left(p_i^0 - |\hat{t} \cdot \vec{p}_i| \right)^{\frac{2-a}{2}} \left(p_i^0 + |\hat{t} \cdot \vec{p}_i| \right)^{\frac{a}{2}} , \tag{3.8}$$

$$\rho_\pm^M = \rho_\pm , \tag{3.9}$$

$$C^M = \frac{3}{2} \left[2 - \sum_{i \neq j} \frac{(p_i \cdot p_j)^2}{(p_i \cdot q)(p_j \cdot q)} \right] \overset{\text{(c.o.m.)}}{=} \frac{3}{2} \left[2 - \frac{1}{Q^2} \sum_{i \neq j} \frac{(p_i \cdot p_j)^2}{p_i^0 p_j^0} \right]$$

$$= \frac{3}{2} \left[1 - \frac{1}{Q^2} \sum_{i,j} \frac{(\vec{p}_i \cdot \vec{p}_j)^2}{p_i^0 p_j^0} \right] + \frac{3}{2Q^2} \left[Q^2 + \sum_i |\vec{p}_i|^2 \frac{|\vec{p}_i|^2 - 2(p_i^0)^2}{(p_i^0)^2} - \sum_{i \neq j} p_i^0 p_j^0 \right] . \tag{3.10}$$

Note that τ^M is also known as 2-jettiness τ_2 [74]. For the *M*-scheme angularities the relation $\tau^M = \tau_{a \to 0}^M$ still holds. For *C*-parameter we used an expression given in terms of Lorentz invariants [62] with $q = \sum_i p_i$ the sum of all particle momenta. This form was shown to be convenient in the context of massive final state particles [70, 75] and as expected reduces to the original definition for massless particles in the center-of-mass frame. Thrust and *C*-parameter are originally given in the *P*-scheme which we recover via the replacement $(p_i^0, \vec{p}_i) \to |\vec{p}_i| \, (1, \vec{p}_i/|\vec{p}_i|)$ (note that this also changes $Q \to Q_p$):

$$\tau^P = \tau , \tag{3.11}$$

$$\tau_a^P = \frac{1}{Q_p} \sum_i p_i^\perp \mathrm{e}^{-|\eta_i|(1-a)} = \frac{1}{Q_p} \sum_i \left(|\vec{p}_i| - |\hat{t} \cdot \vec{p}_i| \right)^{\frac{2-a}{2}} \left(|\vec{p}_i| + |\hat{t} \cdot \vec{p}_i| \right)^{\frac{a}{2}} , \tag{3.12}$$

$$\rho_\pm^P = \frac{1}{Q_p^2} \sum_{i,j \in \pm} \left(|\vec{p}_i||\vec{p}_j| - \vec{p}_i \cdot \vec{p}_j \right) , \tag{3.13}$$

$$C^P = C . \tag{3.14}$$

Using the analogous replacement of $(p_i^0, \vec{p}_i) \to p_i^0 \, (1, \vec{p}_i/|\vec{p}_i|)$ we get the *E*-scheme expressions, which

allows us to recover the original definition for angularities. The E-scheme expressions read

$$\tau^E = \frac{1}{Q} \min_{\hat{t}} \sum_i \frac{p_i^0}{|\vec{p}_i|} \left(|\vec{p}_i| - |\hat{t} \cdot \vec{p}_i| \right) , \tag{3.15}$$

$$\tau_a^E = \tau_a , \tag{3.16}$$

$$\rho_{\pm}^E = \frac{1}{Q^2} \sum_{i,j \in \pm} \frac{p_i^0 p_j^0}{|\vec{p}_i||\vec{p}_j|} \left(|\vec{p}_i||\vec{p}_j| - \vec{p}_i \cdot \vec{p}_j \right) , \tag{3.17}$$

$$C^E = \frac{3}{2} \left[1 - \frac{1}{Q^2} \sum_{i,j} \frac{p_i^0 \, p_j^0 \, (\vec{p}_i \cdot \vec{p}_j)^2}{|\vec{p}_i|^2 |\vec{p}_j|^2} \right] . \tag{3.18}$$

Note that the form of the M-scheme C-parameter in Eq. (3.10) is convenient for this presentation since for both, the P- and E-scheme C-parameter the second part of this expression vanishes and only the first part contributes to the familiar form.

Mass sensitivity

When studying the mass sensitivity of the discussed observables at parton level[3] already the leading order contribution for $e^+ e^-$ annihilation where a heavy quark-antiquark pair is produced without additional radiation, i.e. $e^+ e^- \rightarrow \gamma^*, Z^0 \rightarrow Q\overline{Q}$, can contribute. For this case it is straightforward to see that the thrust axis will be (anti-)parallel with the momentum of the (anti-)quark which makes it quite easy to calculate the two-particle threshold for 2-final state particles with the mass m.

	τ	τ_a	C	$\rho_{\pm}$
M-scheme	$1 - \beta$	$(1-\beta)^{\frac{2-a}{2}}(1+\beta)^{\frac{a}{2}}$	$12\hat{m}^2(1-\hat{m}^2)$	$\hat{m}^2$
P- & E-scheme	0	0	0	0

Table 3.1: Threshold position $e_{\min}$ for primary production of a stable quark-antiquark pair for different event shape definitions, using $\beta = \sqrt{1 - 4\hat{m}^2}$ and $\hat{m} = m/Q$.

The results in Tab. 3.1 show that for events in which a massive stable quark-antiquark pair is produced (*primary production*) only the M-scheme observables are sensitive to the quark mass at leading order while P- and E-scheme observable definitions are not. The expressions for the threshold position represent minimal values which get modified when considering radiation off the primary heavy quarks. This will also add subleading mass sensitivity (suppressed by a factor of α_s) even in the P- and E-scheme but does not change the leading sensitivity of the M-scheme definitions realized by the mass dependence of the tree-level peak position.

From this we can already conclude that for the production of primary stable heavy quarks the M-scheme definitions are generally favorable if the aim is a mass-sensitive observable (e.g. for quark mass determinations) which is also why such event shapes were already used in several investigations with that aim [6, 16]. In case that a mass insensitive observable is favored the P- and E-scheme observable definitions should be the better choice.

If the massive partons enter the final state not at leading order but rather via gluon splitting in a massive quark-antiquark pair (*secondary production*) the sensitivity to the quark mass will be further suppressed (at least by a total factor of α_s^2). Apart from this observation it is not possible to make any general statement without a thorough investigation which is beyond the scope of this work.

---

[3]In the following we will consider pure QCD final states, except top quark decay products in Chap. 4.

3.3 Dijet Kinematics and Large Logarithms

In the following section we want to pay closer attention to the singular limit which for the considered (global 2-jet) event shapes is reached for events with dijet kinematics (two very narrow/light pencil-like back-to-back jets), i.e. $e \to e_{\min}$. For non-global versions of the considered event shapes the singular limit is reached for the analog kinematics which is a very narrow/light jet.

When looking at this kinematic situation and the observables of interest it is clear that several well separated scales will appear $\mu_h \gg \mu_j \gg \mu_s \gg \Lambda_{\text{QCD}}$: (1) The hard scale μ_h which is the scale at which the initial parton was produced $\mu_h \sim Q$. (2) The jet scale μ_j which is the scale of the typical transverse momentum of collinear particles. It can be written as $\mu_j \sim Q\Lambda$ by using some power counting parameter Λ (e.g. for jet masses we have $\Lambda^2 = [(\sum_{i \in \text{jet}} p_i)^2 - m^2]/Q^2$). (3) The soft[4] scale μ_s denoting the scale at which additional softer radiation happens. For this it is sensible to write $\mu_s \sim Q\Lambda^2$ which encodes the fact that this radiation will not disturb the structure of the collinear radiation making up the jet. (4) $\Lambda_{\text{QCD}} \sim 1$ GeV which is the scale of non-perturbative QCD contributions at which for example hadronization happens.

It is well known that in fixed-order (FO) perturbation theory ratios of the involved characteristic scales[5] will enter in logarithms which in the case of event shapes in the singular limit gives rise to so-called *large logarithmic corrections*. For a generic 2-jet event shape e one typically finds $\Lambda^2 \sim e$ and a generic form for the cumulative fixed order cross section (integrated differential cross section) for the massless case is then given by

$$\frac{1}{\sigma_0} \Sigma(e) = \int_0^e \mathrm{d}e' \frac{1}{\sigma_0} \frac{\mathrm{d}\sigma}{\mathrm{d}e'} = 1 + \frac{\alpha_s C_F}{4\pi} \left[a_2^e \ln^2 e + a_1^e \ln e + a_0^e \right] + \mathcal{O}(\alpha_s^2) , \tag{3.19}$$

where a_i^e are some event shape specific $\mathcal{O}(1)$ coefficients which are independent of the value of e. It can now be seen that if the logarithms from Eq. (3.19) scale like $\log \sim \alpha_s^{-1}$, the associated contributions will spoil the convergence of the perturbative series. This effect renders traditional FO perturbative results less useful for jet-like kinematics in the context of event shape observables, even without considering contributions from non-perturbative physics (i.e. $\alpha_s \ll 1$).

The exact structue of large logarithms appearing in cross sections which are not fully inclusive over final state hadrons and how they can be organized was investigated in Refs. [78, 79]. These studies were carried out in the context of event-shapes for $e^+ e^- \to$ hadrons with massless quarks[6] and it turns out that the perturbative part[7] of the cumulative cross section for a generic event shape e including all orders of perturbation theory (also called the *radiator*) can be organized as follows:

$$\frac{1}{\sigma_0} \Sigma(e) = \int_0^e \mathrm{d}e' \frac{1}{\sigma_0} \frac{\mathrm{d}\sigma}{\mathrm{d}e'} = C[\alpha_s] R[e, \alpha_s] + D[e, \alpha_s] ,$$

$$\ln R[e, \alpha_s] = \left[L \sum_{i=1}^\infty g_{0i} (a_s L)^i \right]_{\text{LL}} + \left[\sum_{i=1}^\infty g_{1i} (a_s L)^i \right]_{\text{NLL}} + \left[a_s \sum_{i=1}^\infty g_{2i} (a_s L)^i \right]_{\text{NNLL}} + \dots ,$$

$$C[\alpha_s] = \sum_{i=0}^\infty c_i a_s \tag{3.20}$$

---

[4]Note that this scale is also called the ultrasoft scale which distinguishes this from the situation of a recoil sensitive event shape e.g. jet broadening where "soft" interjet radiation scales like $\mu_s \sim \mu_j \sim Q\Lambda$.

[5]This discussion is valid for the situation of the event shapes which were discussed before. Which of the mentioned scales appear in the ratios is in general observable dependent since different observables involve modes with different typical off-shellness. As mentioned before an example which behaves differently than what we have seen so far is given by total jet broadening which was investigated in Refs. [76, 77].

[6]Nevertheless this still applies qualitatively to the massive case.

[7]A discussion on nonperturbative effects and how they can be treated is given in Sec. 3.7.

with $a_s = \frac{\alpha_s}{4\pi}$. The appearing function R contains all the potentially large logarithms $L \equiv \ln e$ and can be written as an exponential, C is a function containing non-log terms and D is a remainder function vanishing for $e \to 0$. The fact that the final expression and therefore the function R is finite (which we know from experiment and the fact that the nonperturbative contribution should be small) is known as *Sudakov suppression*. Employing the log counting $\log \sim \alpha_s^{-1}$ one can reorganize $\ln R$ which appears in the all order radiator function into towers (already suggested in Eq. (3.20)) of the most leading logarithms (LL), next-to-leading logarithms (NLL) and so on which are separated by one power of α_s. During the last decades different techniques have been developed to deal with large logarithmic corrections in event shape distributions [7, 78, 80, 81] which make it possible to systematically resum these towers of logarithms into the final result which is then called a *resummed cross section* (at a certain order in the employed log counting).

Resummation of Large Logarithms

In the following large logarithms will be treated within the framework of Effective Field Theories [82] (EFTs), which are constructed for the specific kinematical situation at hand. Soft-Collinear Effective Theory [12–15] (short version SCET, for a review / pedagogical introduction also see [9, 70, 83, 84]) is used to describe general dijet like configurations where one finds well separated scales, i.e. a hard interaction scale ($\mu_h \sim Q$), a jet scale or typical jet off-shellness, $\mu_j \sim Q\lambda$ with the SCET power counting parameter (e.g. for jet masses) $\lambda^2 \sim s/Q^2 \equiv [(\sum_{i \in \text{jet}} p_i)^2 - m^2]/Q^2 \ll 1$ and a soft scale (soft global radiation, $\mu_s \sim Q\lambda^2$). SCET is used for massless jets ($m = 0$) and also for jets originating from heavy quarks if the mass of the initially produced quark fulfills $m \lesssim Q\lambda$ [85]. For the observables of interest the involved soft, n-collinear and $\bar{n}$-collinear modes then scale like[8] $p_s^\mu = (p^+, p^-, p^\perp) \sim Q(\lambda^2, \lambda^2, \lambda^2)$, $p_n^\mu \sim Q(\lambda^2, 1, \lambda)$ and $p_{\bar{n}}^\mu \sim Q(1, \lambda^2, \lambda)$, respectively.

In case the heavy quark mass is large enough or if the jet is narrow enough one enters the regime of boosted Heavy Quark Effective Theory [7] (a boosted version of HQET [10, 11], for a pedagogical introduction also see [9]) where $s/(mQ) \ll m/Q$. Here the heavy quark which carries the momentum $mv + k^\mu$ (with $v^2 = 1$) gets integrated out as a dynamical degree of freedom and the remaining degrees of freedom are so-called ultracollinear gluons which carry the residual momentum k^μ. The ultracollinear gluons, which are soft in the top quark rest frame $k^\mu \sim \Delta(1, 1, 1)$ (with some low scale $\Delta < m$), interact with each other and with color sources representing the integrated out heavy quarks. The typical off-shellness of such ultracollinear gluons is softer than for collinear gluons which are part of SCET jets. For boosted top quark pair production two versions which are boosted into back-to-back directions are then used and subsequently matched onto SCET in order to account for global soft radiation. For the observables of interest the involved soft, n-ultracollinear and $\bar{n}$-ultracollinear modes then scale like $p_s^\mu = (p^+, p^-, p^\perp) \sim Q(\lambda^2, \lambda^2, \lambda^2)$, $p_n^\mu \sim \frac{\Delta}{m}(\frac{m^2}{Q^2}, 1, \frac{m}{Q})$ and $p_{\bar{n}}^\mu \sim \frac{\Delta}{m}(1, \frac{m^2}{Q^2}, \frac{m}{Q})$, respectively and where $\lambda^2 = \frac{m\Delta}{Q^2}$.

Using this framework it is possible to derive factorization theorems [7, 81] which effectively separate physics at the different involved scales which works because the involved cross section factors account for physics from the different kinematical regions. This means generically they will consist of a hard, jet and a soft function accounting for physics coming from the corresponding scales discussed before. Utilizing the renormalization group evolution (RGE) behavior of each of these factors it is then possible to resum the encountered large logarithms in a systematic way.

---

[8]Using light-cone momentum components $p^\mu = (p^+, p^-, p^\perp)$.

Amending Boosted Heavy Quark Effective Theory (bHQET)

As already mentioned in bHQET the heavy quark gets integrated out and the remaining collinear degrees of freedom are given by gluons which are soft in the rest frame of the top quark, also called ultracollinear gluons. The momentum of the heavy quark p_Q can therefore be written in terms of a non-dynamical part and the residual momentum coming from interactions with ultracollinear gluons:

$$p_Q = (p_Q^+, p_Q^-, \vec{p}_Q^{\perp}) = m\, v_Q + k_Q \,, \tag{3.21}$$

where k_Q is the residual heavy quark momentum in the center-of-mass frame. The scaling of the residual momenta in the top rest frame is $\hat{k} = (\hat{k}^+, \hat{k}^-, \hat{\vec{k}}^{\perp}) \sim \Delta(1,1,1)$ with some power counting parameter $\Delta^2/m^2 \ll 1$. When boosting from the heavy quark rest frame to the c.o.m. frame (let us assume the heavy quark moving along the z-axis) one gets[9] the following in terms of light cone momentum components:

$$\hat{p}_Q = m(1,1,\vec{0}) + \left(\hat{k}_Q^+, \hat{k}_Q^-, \hat{\vec{k}}_Q^{\perp}\right) \qquad \longrightarrow \qquad p_Q = \left(\gamma(1-\beta)\hat{p}_Q^+, \gamma(1+\beta)\hat{p}_Q^-, \hat{\vec{p}}_Q^{\perp}\right) \,, \tag{3.22}$$

where the boost factors are given by

$$\gamma(1-\beta) = v^+ = \frac{Q}{2\,m}\left(1 - \sqrt{1 - 4\frac{m^2}{Q^2}}\right) = \frac{Q}{m}\left(\frac{m^2}{Q^2} + \frac{m^4}{Q^4} + \dots\right) \,, \tag{3.23}$$

$$\gamma(1+\beta) = v^- = \frac{Q}{2\,m}\left(1 + \sqrt{1 - 4\frac{m^2}{Q^2}}\right) = \frac{Q}{m}\left(1 - \frac{m^2}{Q^2} + \dots\right) \,. \tag{3.24}$$

Next we use this to write down the heavy quark momentum in analogy to Eq. (3.21) and adopt the following prescription: *Terms which only contain kinematical information about the initially produced on-shell heavy quark are not expanded in powers of $\frac{m^2}{Q^2}$ but kept to all orders. Dynamical contribtuions, which are connected to interactions with ultracollinear gluons, are treated at leading power.* With this the heavy quark momentum in the c.o.m. frame is then given by

$$p_Q = m\, v_Q + k_Q \tag{3.25}$$

$$= Q\left(\frac{1}{2}\left[1 - \sqrt{1 - 4\frac{m^2}{Q^2}}\right], \frac{1}{2}\left[1 + \sqrt{1 - 4\frac{m^2}{Q^2}}\right], \vec{0}\right) + Q\left(\frac{m\hat{k}_Q^+}{Q^2}, \frac{\hat{k}_Q^-}{m} - \frac{m\hat{k}_Q^-}{Q^2}, \frac{\hat{\vec{k}}_Q^{\perp}}{Q}\right) + \mathcal{O}\left(\frac{m^3\Delta}{Q^4}\right) \,.$$

In the literature (see Refs. [7,8]) also terms which are non-dynamical but suppressed by a factor of $\frac{m^2}{Q^2}$ over the leading term are neglected due to them being formally suppressed. In this situation Eq. (3.25) gets reduced to:

$$p_Q = Q\left(\frac{m}{Q}, 1, 0\right) + Q\left(\frac{m\hat{k}_Q^+}{Q^2}, \frac{\hat{k}_Q^-}{m} - \frac{m\hat{k}_Q^-}{Q^2}, \frac{\hat{\vec{k}}_Q^{\perp}}{Q}\right) + \mathcal{O}\left(\frac{m^4}{Q^4}, \frac{m^3\Delta}{Q^4}\right) \,. \tag{3.26}$$

Considering top quark pair production at a c.o.m. energy of $Q = 700$ GeV as a realistic numerical example one can see that the terms of order $\mathcal{O}\left(\frac{m^4}{Q^4}\right)$ which are omitted when going from Eq. (3.25) to Eq. (3.26), although they are formally suppressed, are not small and should be kept if possible. Using a top quark mass of $m = 173\,\text{GeV}$ and its width as a typical off-shellness of $\Gamma = \Delta = 1.4\,\text{GeV}$ the size of the different involved terms is given by

$$\frac{m^2}{Q^2} = 0.06108 \,, \qquad\qquad \frac{m^4}{Q^4} = 0.00373 \,, \qquad\qquad \frac{m^6}{Q^6} = 0.00023 \,, \tag{3.27}$$

$$\frac{m\Gamma}{Q^2} = 0.00049 \,, \qquad\qquad \frac{m^3\Gamma}{Q^4} = 0.00003 \,, \qquad\qquad \frac{\Gamma^2}{Q^2} \sim 4 \cdot 10^{-6} \,. \tag{3.28}$$

---

[9]In the following momenta with hat e.g. $\hat{p}$ denote the corresponding momentum in the rest frame of the particle.

Interpreting these numbers as shifts in the 2-jettiness threshold which is given by $\tau_2^{\min} = 1 - \sqrt{1 - 4\frac{m^2}{Q^2}}$ leads to the following shifts in the corresponding extracted mass:

$$\frac{m^2}{Q^2} : 33.108\,\text{GeV}\,, \qquad \frac{m^4}{Q^4} : 2.277\,\text{GeV}\,, \qquad \frac{m^6}{Q^6} : 140\,\text{MeV}\,, \qquad (3.29)$$

$$\frac{m\Gamma}{Q^2} : 304\,\text{MeV}\,, \qquad \frac{m^3\Gamma}{Q^4} : 19\,\text{MeV}\,, \qquad \frac{\Gamma^2}{Q^2} : 2\,\text{MeV}\,. \qquad (3.30)$$

This makes it clear that the subleading purely non-dynamical terms are numerically not small and should therefore not be neglected. In the following we will keep the full pure $\frac{m}{Q}$ dependence in a consistent manner, hence use $m(v^+, v^-, 0)$ and not $Q(\frac{m^2}{Q^2}, 1, 0)$ as usually done in the literature. This makes it also possible to naturally recover the full threshold position as given in Tab. 3.1 which up to now was set to the full expression by hand.

3.4 Factorization and Resummation

Factorization formula for dijet kinematics such as the one used in the context of SCET (see Sec. 3.4.2) rely on the fact that at leading order in the appropriate powercounting it is possible to write the event shape formula in the dijet limit as a sum of contributions of $n(\overline{n})$-collinear, soft perturbative and soft nonperturbative particles [73, 81] ($\overline{e}$ denotes the event shape e in the dijet limit at leading order):

$$\overline{e} = e_n + e_{\overline{n}} + e_s + e_\Lambda\,. \qquad (3.31)$$

If the event shape is given by a single sum of final state particle momenta (as it is the case for thrust or angularities) this statement is trivial. In the case that the definition of the event shape correlates momenta of a pair of final state particles (i.e. the definition will involve a double sum) the situation is more complicated. In this case one has to show explicitly that in this kinematic limit the leading contribution to the event shape can be written in the form of Eq. (3.31), which for example was done in Ref. [86] for C^P and in Ref. [70] for C^M.

3.4.1 Measurement Factorization in the Dijet Limit

Measurement Factorization in SCET

In the following we want to study different mass scheme definitions of the considered event shapes in the dijet limit while considering the power counting of SCET (for details see Sec. 3.3 and references therein). In this situation it is possible to characterize each event shape by a function[10] $f_e(r_i, y_i)$ in the following way:

$$\overline{e} = \frac{1}{Q}\sum_i m_i^\perp\, f_e(r_i, y_i)\,, \qquad (3.32)$$

where $m_i^\perp = \sqrt{(p_i^\perp)^2 + m_i^2}$ is the transverse mass using $p_i^\perp = |\vec{p}_i^\perp|$, $r_i = p_i^\perp / m_i^\perp$ is the transverse velocity and y_i is the rapidity of the i-th final state particle again with respect to the thrust axis. Obviously if one can show that an event shape observable takes this form in the dijet limit, Eq. (3.31) trivially follows. As an example for how this calculation works let us now consider the M-scheme jet mass ρ_+^M for the SCET case with a primarily produced stable massive quark-antiquark pair.

---

[10]This form was also employed in [73] where the used J-scheme coincides with the M-scheme in the dijet limit for the case that soft particles are massless.

When considering the fact that particles can be either soft, n-collinear or $\bar{n}$-collinear which scale like $p_s^\mu = (p^+, p^-, p^\perp) \sim Q(\lambda^2, \lambda^2, \lambda^2)$, $p_n^\mu \sim Q(\lambda^2, 1, \lambda)$ and $p_{\bar{n}}^\mu \sim Q(1, \lambda^2, \lambda)$ respectively, we can write:

$$\rho_+^M = \sum_{\substack{a \in \{s,n,\bar{n}\} \\ b \in \{s,n,\bar{n}\}}} \rho_{+,ab}^M = \frac{1}{Q^2} \sum_{\substack{a \in \{s,n,\bar{n}\} \\ b \in \{s,n,\bar{n}\}}} \sum_{\substack{i \in a \\ j \in b}} (p_i \cdot p_j)\, \theta(\hat{t} \cdot \vec{p}_i)\, \theta(\hat{t} \cdot \vec{p}_j)\,, \tag{3.33}$$

where a and b correspond to either the soft, n-collinear or $\bar{n}$-collinear sector. Calculating all the ingredients gives

$$\rho_{+,ss}^M = 0 + \mathcal{O}(\lambda^4)\,, \tag{3.34}$$

$$\rho_{+,sn}^M = \rho_{+,ns}^M = \frac{1}{Q^2} \sum_{\substack{i \in n \\ j \in s}} \left[(p_i^+ p_j^- + p_i^- p_j^+)/2 - \vec{p}_i^\perp \vec{p}_j^\perp \right] \theta(\hat{t} \cdot \vec{p}_j) = \frac{1}{2\,Q^2} \sum_{\substack{i \in n \\ j \in s}} p_i^- p_j^+\, \theta(\hat{t} \cdot \vec{p}_j) + \mathcal{O}(\lambda^4)$$

$$= \frac{1}{2\,Q} \sum_{j \in s} p_j^+\, \theta(\hat{t} \cdot \vec{p}_j) + \mathcal{O}(\lambda^4)\,, \tag{3.35}$$

$$\rho_{+,nn}^M = \frac{1}{Q^2} \sum_{\substack{i \in n \\ j \in n}} \left[(p_i^+ p_j^- + p_i^- p_j^+)/2 - \vec{p}_i^\perp \vec{p}_j^\perp \right] = \frac{1}{Q} \sum_{i \in n} p_i^+\,, \tag{3.36}$$

$$\rho_{+,s\bar{n}}^M = \rho_{+,\bar{n}s}^M = \rho_{+,n\bar{n}}^M = \rho_{+,\bar{n}n}^M = \rho_{+,\bar{n}\bar{n}}^M = 0\,, \tag{3.37}$$

where we used that $\sum_{i \in n/\bar{n}} \vec{p}_i^\perp = 0 + \mathcal{O}(Q\lambda^2)$ and that each collinear sector carries half of the center of mass energy (up to soft corrections) i.e. $\sum_{i \in n} p_i^- = \sum_{i \in \bar{n}} p_i^+ = Q + \mathcal{O}(Q\lambda^2)$. Starting with the definition of rapidity (measured with respect to the thrust axis) we find

$$y_i = \frac{1}{2} \ln\left(\frac{p_i^0 + \hat{t} \cdot \vec{p}_i}{p_i^0 - \hat{t} \cdot \vec{p}_i} \right) \quad \Longrightarrow \quad |y_i| = \frac{1}{2} \ln\left(\frac{p_i^0 + |\hat{t} \cdot \vec{p}_i|}{p_i^0 - |\hat{t} \cdot \vec{p}_i|} \right) \quad \Longrightarrow \quad \mathrm{e}^{-|y_i|} = \sqrt{\frac{p_i^0 - |\hat{t} \cdot \vec{p}_i|}{p_i^0 + |\hat{t} \cdot \vec{p}_i|}}\,. \tag{3.38}$$

With $\theta(y_i) = \theta(\hat{t} \cdot \vec{p}_i)$ and $m_i^\perp = \sqrt{(p_i^\perp)^2 + m^2} = \sqrt{(p_i^0)^2 - |\hat{t} \cdot \vec{p}_i|^2}$ it is now straightforward to conclude that Eq. (3.32) is fulfilled for the case of ρ_+^M:

$$\rho_+^M = \frac{1}{Q} \sum_i m_i^\perp\, \theta(y_i) \mathrm{e}^{-y_i} = \frac{1}{Q} \sum_i (p_i^0 - |\hat{t} \cdot \vec{p}_i|) = \frac{1}{Q} \sum_i p_i^+ \theta(\hat{t} \cdot \vec{p}_i) \quad \Longrightarrow \quad f_{\rho+}^M(r,y) = \theta(y)\mathrm{e}^{-y}\,. \tag{3.39}$$

To arrive at similar and also simple expressions for P- and E-scheme event shape definitions it is convenient to introduce pseudorapidity η and the velocity v of a particle which are defined in terms of the transverse velocity $r = p^\perp/m^\perp$ and rapidity y by

$$\eta = \eta(r,y) = \ln\left(\frac{\sqrt{r^2 + \sinh^2 y} + \sinh y}{r} \right)\,, \qquad v = v(r,y) = \frac{\sqrt{r^2 + \sinh^2 y}}{\cosh y}\,. \tag{3.40}$$

Using this it is easy to extract the expressions for $f_e^{P/E}(r,y)$. The derivation for the other discussed event shapes is now straightforward and completely analogous to the example case and therefore not discussed in more detail. The obtained results are summarized in Tab. 3.2 from which we can observe the following relation of the M-scheme with the corresponding P- and E-scheme expressions for $f_e^{P/E}(r,y)$:

$$f_e^P(r,y) = r\, f_e^M(r, \eta(r,y))\,, \qquad\qquad f_e^E(r,y) = \frac{r}{v(r,y)}\, f_e^M(r, \eta(r,y))\,. \tag{3.41}$$

$f_e(r, y)$	τ	τ_a	C	$\rho_\pm$
M-scheme	$\mathrm{e}^{-|y|}$	$\mathrm{e}^{-|y|(1-a)}$	$\frac{3}{\cosh y}$	$\theta(\pm y)\mathrm{e}^{\mp y}$
P-scheme	$r\mathrm{e}^{-|\eta|}$	$r\mathrm{e}^{-|\eta|(1-a)}$	$\frac{3r}{\cosh \eta}$	$r\theta(\pm \eta)\mathrm{e}^{\mp \eta}$
E-scheme	$\frac{r}{v}\mathrm{e}^{-|\eta|}$	$\frac{r}{v}\mathrm{e}^{-|\eta|(1-a)}$	$\frac{r}{v}\frac{3}{\cosh \eta}$	$\frac{r}{v}\theta(\pm \eta)\mathrm{e}^{\mp \eta}$

Table 3.2: Coefficient function $f_e(r, y)$ for the used event shape definitions in the singular limit according to Eq. (3.32).

Measurement Factorization in bHQET

When considering the power counting of bHQET (see Sec. 3.3 and references therein), which is characteristic for the peak/resonance region in boosted top quark production, it turns out that in the dijet limit the expression of Eq. (3.32) takes an even simpler form (at least for the event shapes which are considered here):

$$\overline{e} = e_{\min} + \frac{1}{Q} \sum_i k_i^\perp f_{B,e}(y_i) \,, \tag{3.42}$$

where the expressions for the first part are given in Tab. 3.1 and which originates equally from the two ultracollinear sectors. The second part does now not depend on the mass of the heavy quark, hence it is independent of the used event shape scheme, and takes the same functional form than its SCET counterpart i.e. $f_{B,e}(y) = f_e^M(1, y)$ when given in terms of residual particle momenta only.

To see this explicitly let us again consider the example of ρ_+^M, now with the bHQET power counting. Starting with Eq. (3.33) and considering that the heavy (anti-)quark is part of the $(\overline{n})n$-ultracollinear sector, it is easy to see that all the expressions except the one for $\rho_{+,nn}^M$ are the same as in the SCET case. In the top quark rest frame ultracollinear gluons are soft i.e. their momentum scales like $\hat{k}^\mu = (\hat{k}^+, \hat{k}^-, \hat{k}^\perp) \sim \Delta(1, 1, 1)$ with some low scale $\Delta < m$. Using this the involved soft, n-ultracollinear and $\overline{n}$-ultracollinear modes then scale like $k_s^\mu \sim Q(\lambda^2, \lambda^2, \lambda^2)$, $k_n^\mu \sim \frac{\Delta}{m}(\frac{m^2}{Q^2}, 1, \frac{m}{Q})$ and $k_{\overline{n}}^\mu \sim \frac{\Delta}{m}(1, \frac{m^2}{Q^2}, \frac{m}{Q})$, respectively and where $\lambda^2 = \frac{m\Delta}{Q^2}$. The missing contribution is then given by

$$
\begin{aligned}
\rho_{+,nn}^M &= \frac{1}{Q^2}\left\{ p_Q \cdot p_Q + 2 p_Q \cdot \sum_{i\in x} p_i + \sum_{i,j\in x} p_i \cdot p_j \right\} \\
&= \frac{m^2}{Q^2} + \frac{1}{Q}\left[\sum_{i\in n} k_i^+ + \frac{m}{Q}\sum_{i\in n} k_i^- \right] + \mathcal{O}(m^3\Delta/Q^4) \\
&= \frac{m^2}{Q^2} + \frac{1}{Q}\sum_{i\in n} k_i^+ + \mathcal{O}(m^3\Delta/Q^4) \,, \tag{3.43}
\end{aligned}
$$

which confirms the general form of Eq. (3.42) and where x is the set of ultracollinear gluons (set of ultracollinear particles excluding the heavy quark). Furthermore we used the following argument: each ultracollinear region carries energy $Q/2$ up to soft radiation. From that one can then follow that

$$
\begin{aligned}
2\sum_{i\in n} p_i^0 = \sum_{i\in n}\left(p_i^+ + p_i^- \right) &= Q\left(1 + \mathcal{O}(\lambda^2)\right) \\
&= \frac{Q}{m}\left[\frac{k_Q^-}{Q} + \sum_{i\in x}\frac{k_i^-}{Q} \right] + Q\left(1 + \mathcal{O}(m\Delta/Q^2)\right) \,, \tag{3.44}
\end{aligned}
$$

$$\frac{Q}{m}\sum_{i\in n}\frac{k_i^-}{Q} = 0 + \mathcal{O}(m\Delta/Q^2) \qquad \longrightarrow \qquad \frac{m}{Q}\sum_{i\in n}\frac{k_i^-}{Q} = 0 + \mathcal{O}(m^3\Delta/Q^4) \,. \tag{3.45}$$

Verifying the form of Eq. (3.42). The discussion for the other event shapes of interest is again straightforward and completely analogous, hence not discussed here.

3.4.2 Factorization Formula and Mass Scenarios

Using the same argumentation as in Refs. [7, 8, 73, 81] we can write down the factorization formula for the most singular part of the differential cross section with respect to a recoil free massive e^+e^- event shape. It was discussed extensively in Refs. [9, 84, 87–89] how to setup a consistent variable flavor number scheme to account for effects of the mass of primarily and secondarily produced heavy quarks. As explained before we want to work out the expressions for different mass scheme definitions for primary heavy quark production in e^+e^- annihilation (here in the singular limit). For this case three scenarios distinguished by their hierarchy of scales with respect to the heavy quark mass m are relevant, where each of them has a different factorization theorem and renormalization group evolution setup. In the following discussion we adopt the established nomenclature from the relevant literature where the not mentioned Scenario I refers to a scale hierarchy with $m > \mu_h$ which implies that no primary heavy quark production is possible. In the following we will only discuss factorization theorems valid for global observables[11]. As an example we will use the case of thrust but the factorization theorem will take an analogous form for many other event shapes like angularities (for small a) or C-parameter (often it is more convenient to use the rescaled C-parameter which is given by $\tilde{C} = C/6$).

Scenario IV: $\mu_h > \mu_j > \mu_s > m$

For this scenario the mass is below any of the kinematical scales. Because of that the effects of the mass enter all of the ingredients of the factorization theorem and the renormalization group evolution of all involved factors will involve $(n_\ell + 1)$ active flavors. As our default we will set the global renormalization scale to $\mu = \mu_j$ which leads to the factorization theorem given by:

$$
\frac{\mathrm{d}\sigma_{\mathrm{IV}}^{\mathrm{sing}}}{\mathrm{d}\tau} = \sum_{i=v,a} Q\,\sigma_0^i\, H^{(n_\ell+1)}(Q,\mu_h)\, U_H^{(n_\ell+1)}(Q,\mu_h,\mu) \int \mathrm{d}s\,\mathrm{d}\ell\, J_\tau^{(n_\ell+1)}(s,m,\mu)
$$
$$
\times\, U_{S,\tau}^{(n_\ell+1)}(\ell,\mu,\mu_s)\, S_\tau^{(n_\ell+1)}\!\left(Q\,\tau - \frac{s}{Q} - \ell, m, \mu_s\right) . \tag{3.46}
$$

The appearing factors contain SCET matrix elements and can be calculated individually. This allows us to separate the involved kinematical scales and subsequently use renormalization group running (via the also appearing evolution kernels denoted by U, see Sec. 3.4.3) from a natural scale (which minimizes the involved logarithms) to a common global scale, here $\mu = \mu_j$, which leads to a resummation of the mentioned large logarithms. The cross-section factors are[12]:

- The *hard function* $H(Q,\mu) = |C(Q,\mu)|^2$ which is given by the squared renormalized matching coefficient $C(Q,\mu)$ of the SCET current onto the QCD current, thus universal for all e^+e^- annihilation observables. The unrenormalized matching coefficient is given by

$$
\langle Q\bar{Q}|\, \mathcal{J}_{\mathrm{QCD},i}^\mu\, |0\rangle_{m^2 \ll Q^2} = C^0(Q,\mu)\, \langle Q\bar{Q}|\, J_{\mathrm{SCET},i}^\mu\, |0\rangle \ , \tag{3.47}
$$

---

[11] For non-global observables which only consider part of the event (e.g. hemisphere jet masses) the factorization theorem needs to be modified (partly discussed in [90]) and will in general also involve so-called *non-global logarithms* [91].

[12] From now on we will keep the explicit flavor number dependence on the cross section factors only when stating the factorization theorem and take them otherwise as implicit. The flavor number states how many active flavors need to be considered during renormalization group evolution and the flavor number scheme of the involved α_s.

where the vector/axial-vector $Q\bar{Q}$ current in QCD $\mathcal{J}^{\mu}_{\text{QCD},i}$ and SCET $J^{\mu}_{\text{SCET},i}$ are given by

$$\mathcal{J}^{\mu}_{\text{QCD},i} = \overline{\psi}\,\Gamma^{\mu}_i\,\psi\,, \qquad \text{with} \qquad \Gamma^{\mu}_v = \gamma^{\mu}\,,\ \ \Gamma^{\mu}_a = \gamma^{\mu}\gamma_5\,, \qquad (3.48)$$

$$J^{\mu}_{\text{SCET},i} = \overline{\chi}_n\,Y^{\dagger}_n S^{\dagger}_n\,\Gamma^{\mu}_i\,S_{\overline{n}}Y_{\overline{n}}\,\chi_{\overline{n}}\,, \qquad (3.49)$$

with the quark field ψ, the jet field χ_n and the ultrasoft and mass mode Wilson lines Y_n and S_n (for further information see Sec. 3.3 and references therein).

- The (global) *jet function* which is a convolution of the n- and the $\overline{n}$-collinear jet functions $J_e = J_{n,e} \otimes J_{\overline{n},e}$. The n- and $\overline{n}$-collinear jet function is then given in terms of a collinear event shape measurement on matrix elements of collinear fields. This can be interpreted as the probablility of forming a jet (up to soft corrections and power corrections) which contributes the n-collinear part e_n to the total event shape value $\overline{e}$ of the event. The jet function accounts for the dynamics of the collinear particles within the jet and for some generic event shape e (such as thrust, angularities or C-parameter) is given by [7,8,81] (with implicit color- and spin-trace)

$$J_{n,e}(s,m,\mu) = \frac{1}{8\pi}\int \mathrm{d}k^+\,\mathrm{d}k^-\,\mathrm{d}^2(\vec{k}_\perp)\,\delta(k^- - Q)\,\delta^{(2)}(\vec{k}_\perp)\,\mathcal{J}_{n,e}(s,k,m,\mu)\,, \qquad (3.50)$$

$$\mathcal{J}_{n,e}(s,k,m,\mu) = \frac{1}{N_c}\int \mathrm{d}^4x\,\mathrm{e}^{i\,k\,x}\,\mathrm{Tr}\left[\langle 0|\,\slashed{\overline{n}}\chi_n(x)\,\delta(s - Q^2\hat{e}_n)\,\overline{\chi}_n(0)\,|0\rangle\right]\,, \qquad (3.51)$$

with the n-collinear event shape operator acting on some final state like

$$\hat{e}_n\,|X\rangle = e_n(X)\,|X\rangle\,. \qquad (3.52)$$

- The *soft function* which accounts for soft radiation and soft cross-talk between the jets. Due to their large separation in momentum the soft gluons only see highly boosted color charges along the n- and $\overline{n}$-direction with which they interact via eikonal interactions (see for example Ref. [83]), hence the soft function has no information on the mass of the primary produced collinear quarks and only involves soft Wilson lines $Y_n, \overline{Y}_{\overline{n}}$. The perturbative part of the soft function for some generic event shape e (such as thrust, angularities or C-parameter) is given by [81] (with implicit color- and spin-trace)

$$S_{\text{pert},e}(\ell,m,\mu) = \frac{1}{N_c}\,\langle 0|\,(\overline{Y}^{\dagger}_{\overline{n}}Y^{\dagger}_n)(0)\,\delta(\ell - Q\hat{e}_s)\,(Y_n\,\overline{Y}_{\overline{n}})(0)\,|0\rangle\,. \qquad (3.53)$$

with the soft event shape operator acting on some final state like

$$\hat{e}_s\,|X\rangle = e_s(X)\,|X\rangle\,. \qquad (3.54)$$

Since the soft function accounts for all soft radiation it also has non-perturbative contributions. Due to a lack of understanding of this non-perturbative part it has to be modelled and the full soft function is then given by a convolution of the perturbative part and a non-perturbative shape-function as shown in Eq. (3.163). More details on the used shape-function (sometimes also called soft model function) and connected issues are given in Sec. 3.7.

From their definition it is clear that the hard function does not depend on the quark mass while the same is true for the soft function up to NLO. In the following we are only interested in NLO for which the mass independent results are well known. The expressions for $H(Q,\mu)$ is known at 3-loop accuracy [92,93] and at NLO the QCD-SCET matching coefficient, the corresponding counter term

and the hard function are given by

$$Z_C(Q,\mu) = 1 - \frac{\alpha_s C_F}{\pi}\left\{\frac{1}{2\,\varepsilon^2} + \frac{3}{4\,\varepsilon} + \frac{1}{2\,\varepsilon}\ln\frac{\mu^2}{-Q^2 - i0}\right\} + \mathcal{O}(\alpha_s^2)\,, \tag{3.55}$$

$$C(Q,\mu) = 1 - \frac{\alpha_s C_F}{\pi}\left\{\frac{3}{4}\ln\frac{\mu^2}{-Q^2 - i0} + \frac{1}{4}\ln^2\frac{\mu^2}{-Q^2 - i0} + 2 - \frac{\pi^2}{24}\right\} + \mathcal{O}(\alpha_s^2)\,, \tag{3.56}$$

$$H(Q,\mu) = |C(Q,\mu)|^2 = 1 + \frac{\alpha_s C_F}{\pi}\left\{-\frac{3}{2}\ln\frac{\mu^2}{Q^2} - \frac{1}{2}\ln^2\frac{\mu^2}{Q^2} - 4 + \frac{7\pi^2}{12}\right\} + \mathcal{O}(\alpha_s^2)\,. \tag{3.57}$$

The corresponding expressions for S_{τ_a} (with $S_\tau = S_{\tau_a \to 0}$) and $S_{\tilde{C}}$ (with $\tilde{C} = C/6$) and the associated counter terms (details on renormalization and renormalization group evolution of the cross section factors are discussed in Sec. 3.4.3) are given in Refs. [8, 86, 94–96] and Ref. [86] respectively, and at NLO read (using $\tilde{\ell} = l/\mu$)

$$\mu\, Z_{S,\tau_a}(l,\mu) = \delta(\tilde{l}) + \frac{\alpha_s C_F}{\pi}\left\{-\delta(\tilde{l})\frac{1}{(1-a)\,\varepsilon^2} + \frac{2}{(1-a)\varepsilon}\left[\frac{\theta(\tilde{l})}{\tilde{l}}\right]_+\right\} + \mathcal{O}(\alpha_s^2)\,, \tag{3.58}$$

$$Z_{S,\tilde{C}}(\ell,\mu) = Z_{S,\tau}(\ell,\mu) = Z_{S,\tau_a \to 0}(\ell,\mu)\,, \tag{3.59}$$

$$\mu\, S_{\text{pert},\tau_a}(\ell,m,\mu) = \delta(\tilde{l}) + \frac{\alpha_s C_F}{\pi}\left\{\delta(\tilde{l})\frac{1}{1-a}\frac{\pi^2}{12} - \frac{4}{1-a}\left[\frac{\theta(\tilde{l})\ln\tilde{l}}{\tilde{l}}\right]_+\right\} + \mathcal{O}(\alpha_s^2)\,, \tag{3.60}$$

$$\mu\, S_{\text{pert},\tilde{C}}(\ell,m,\mu) = \delta(\tilde{l}) + \frac{\alpha_s C_F}{\pi}\left\{\delta(\tilde{l})\frac{\pi^2}{4} - 4\left[\frac{\theta(\tilde{l})\ln\tilde{l}}{\tilde{l}}\right]_+\right\} + \mathcal{O}(\alpha_s^2)\,. \tag{3.61}$$

The massless jet function for $\rho_\pm$ (which is the same as the n-collinear jet function for τ and $\tilde{C} = C/6$) is known to two loop order [87, 97] while the massless one loop τ_a jet function is given in Ref. [95]. For the primary massive situation the n-collinear jet function is known at one loop for M-scheme jet masses, thrust and the modified C-parameter ($\tilde{C} = C/6$) [7, 8]. In Sec. 3.5 we are going to discuss the analog jet function calculation for the corresponding P- and E-scheme event shape definitions.

In contrast to earlier work concerning the primary massive jet function (see Refs. [98] and [7, 8]) the general calculation (and in particular the one of Sec. 3.5) cannot be based on taking the imaginary part of an inclusive jet function which would require the collinear measurement to only depend on the total jet momentum and not on momenta of the individual particles. One possible approach, which we will follow, is to use an explicit collinear final state[13]. This approach was also used in the case of the massless broadening jet function in Ref. [76] and in a modified version for the massless angularities jet function[14] in Ref. [95].

Now let us take a closer look at the n-collinear jet function[15] for an event shape e. We start from Eq. (3.51) and use a n-collinear version of the final state completeness relation. Next an additional translation $\chi_n(x) \to \chi_n(0)$ is performed and after some manipulations we finally get:

$$\mathcal{J}_{n,e}(s,k,m,\mu) = \frac{1}{N_c}\sum_{X_n}\int \mathrm{d}\Pi_{X_n}\,(2\pi)^d\,\delta^{(d)}(k - P_n)\,\delta(s - Q^2 e_n(X))$$

$$\times \operatorname{Tr}\left[\langle 0|\, \slashed{\bar{n}}\chi_n(0)\,|X_n\rangle\,\langle X_n|\,\overline{\chi}_n(0)\,|0\rangle\right]\,, \tag{3.62}$$

---

[13]Using explicitly factorized final states $|X\rangle = |X_n\rangle|X_{\bar{n}}\rangle|X_s\rangle$ and performing the measurement on them is one possibility to calculate the jet function for an aribtrary event shape (i.e. one for which more differential information than just jet momentum information is needed).

[14]An analogous approach to an explicitly factorized final state is to define modified *Cutkosky rules* as it was done in [95] where this approach was called "Cutting rules for weighted matrix elements".

[15]By replacing $n \leftrightarrow \bar{n}$ and $k^+ \leftrightarrow k^-$ one gets the jet function in $\bar{n}$ direction which is defined analogously.

where P_n is the overall final state jet momentum. For the jet function calculation done in Sec. 3.5.1 it seems more instructive to write the matrixelement part of the above jet function definition with explicit dirac indices in the form of 1-jet amplitudes (the color trace is still implicit):

$$\text{Tr}\left[\langle 0 | \not{n} \chi_n(0) \, |X_n\rangle \langle X_n| \, \overline{\chi}_n(0) \, |0\rangle \right] = (\not{n}\gamma_0)_{\alpha\beta} \, \langle 0 | (\overline{\chi}_n^\dagger)^\beta(0) \, |X_n\rangle \langle X_n| (\overline{\chi}_n)^\alpha(0) \, |0\rangle$$

$$= (\not{n}\gamma_0)_{\alpha\beta} \, (\mathcal{M}_{n,1-\text{jet}}^\dagger)^\beta (\mathcal{M}_{n,1-\text{jet}})^\alpha \, . \tag{3.63}$$

Scenario III: $\mu_h > \mu_j > m > \mu_s$

For this scenario the mass is between the jet and soft scale, hence the hard and jet function evolution happens again above the mass threshold $\mu_m \sim m$ and the corresponding sectors involve $(n_\ell + 1)$ active flavors. The soft function evolution on the other hand, which starts with (n_ℓ) active flavors, crosses the mass threshold which means that virtual quark mass effects need to be included in the running of the soft function above μ_m and also threshold corrections enter at the mass scale via a matching coefficient. Putting everything together one then recovers the $(n_\ell + 1)$ flavor soft function running from scenario IV above the mass scale (see also Sec. 3.4.4). The factorization theorem for $\mu = \mu_j$ then reads

$$\frac{d\sigma_{\text{III}}^{\text{sing}}}{d\tau} = \sum_{i=v,a} Q \, \sigma_0^i \, H^{(n_\ell+1)}(Q, \mu_h) \, U_H^{(n_\ell+1)}(Q, \mu_h, \mu) \int ds \, d\ell \, d\ell' \, d\ell'' \, J_\tau^{(n_\ell+1)}(s, m, \mu)$$

$$\times U_{S,\tau}^{(n_\ell+1)}(\ell'', \mu, \mu_m) \, \mathcal{M}_S^{(n_\ell+1)}(\ell' - \ell'', m, \mu_m)$$

$$\times U_{S,\tau}^{(n_\ell)}(\ell - \ell', \mu_m, \mu_s) \, S_\tau^{(n_\ell)}\left(Q\tau - \frac{s}{Q} - \ell, \mu_s\right) , \tag{3.64}$$

where the involved hard and jet functions are identical to the ones in scenario IV. At one loop the soft function does not depend on the heavy flavor which was integrated out and therefore the related matching coefficient $\mathcal{M}_S^{(n_\ell+1)}$ starts to be non-trivial at two-loop level. It involves large rapidity logarithms which can be resummed via simple exponentiation [99]. The soft function matching coefficient was determined in Ref. [88] and reads

$$\mu_s \, \mathcal{M}_S(\ell, m, \mu_m) = \delta(\tilde{\ell}) \tag{3.65}$$

$$+ \left[\delta(\tilde{\ell}) C_F T_F \left(\frac{\alpha_s(\mu_m)}{4\pi} \right)^2 \ln\left(\frac{\mu_s^2}{\mu_m^2} \right) \left\{ \frac{8}{3} L_m^2 + \frac{80}{9} L_m + \frac{224}{27} \right\} \right]_{\mathcal{O}(\alpha_s)} + \mathcal{O}(\alpha_s^2) \, ,$$

with $\tilde{\ell} = \ell/\mu_s$, $L_m = \ln(m^2/\mu_m^2)$ and where the subscript $\mathcal{O}(\alpha_s)$ indicates that the involved rapidity logarithm is counted as $\alpha_s^2 \log \sim \alpha_s$ which means that we need to include it at N^{2}LL for consistency (the same size as $\mathcal{O}(\alpha_s)$ matrix element corrections, see also Sec. 3.4.3). Furthermore μ_s indicates some scale which scales like $\mu_s \sim Qe$ so that all large logarithms are explicit [88]. The remaining α_s^2 terms only involve L_m and constants which are omitted while at higher order only terms contributing at N^{3}LL appear.

bHQET Scenario: $\mu_h > m > \mu_{jB} > \mu_s$

For the case that the mass scale is bigger than the jet scale[16] μ_{jB}, which typically only (if at all) happens in the peak/resonance region of (2-jet) event shape distributions, one needs to employ a different effective field theory setup involving a boosted version of HQET (bHQET, see Sec. 3.3 and references therein) which allows for a typical jet off-shellness of $P_n^2 - m^2 \sim \mu_{jB}^2 \ll m^2$, while for

---

[16]Since μ_j and μ_{jB} have different canonical scaling we differentiate these two "jet scales" - see Sec. 3.8.

SCET $P_n^2 - m^2 \sim m^2$ holds. In this kinematical regime the heavy quark needs to be integrated out as a dynamical degree of freedom and gluons which are soft in the heavy quark rest frame are the remaining degrees of freedom. Using two versions of bHQET (one for each collinear direction) and matching them onto SCET leads to the bHQET factorization theorem [7,8] which in analogy to Eq. (3.46) and Eq. (3.64) then reads (with $\mu = \mu_{jB}$)

$$
\frac{\mathrm{d}\sigma_{\mathrm{bHQET}}^{\mathrm{sing}}}{\mathrm{d}e} = \sum_{i=v,a} Q\, \sigma_0^i\, H^{(n_\ell+1)}(Q, \mu_h)\, U_H^{(n_\ell+1)}(Q, \mu_h, \mu_m)\, H_M^{(n_\ell+1)}(m, \mu_m)\, U_M^{(n_\ell)}(\tfrac{Q}{m}, \mu_m, \mu)
$$
$$
\times \int \mathrm{d}s\, \mathrm{d}\ell\, J_{B,e}^{(n_\ell)}(s, m, \mu)\, U_{S,e}^{(n_\ell)}(\ell, \mu, \mu_s)\, S_e^{(n_\ell)}(Q\, e - \frac{s}{Q} - \ell, \mu_s)\,. \tag{3.66}
$$

Here the hard function gets evolved with $(n_\ell + 1)$ flavors down to the mass scale μ_m at which the heavy quark gets integrated out (matching the bHQET current onto the SCET current, see Ref. [99]). The remaining evolution down to the global scale μ is then continued with the reduced (n_ℓ) flavor running of the hard function together with the (n_ℓ) flavor running of the squared bHQET to SCET current matching coefficient, denoted by $U_M^{(n_\ell)} = U_H^{(n_\ell)} U_{H_M}^{(n_\ell)}$. The involved squared current matching coefficient H_M is given by [8,99]

$$
H_M(m, \mu_m) = 1 + \frac{\alpha_s(\mu_m)\, C_F}{4\pi}\left\{2L_m^2 - 2L_m + 8 + \frac{\pi^2}{3}\right\} \tag{3.67}
$$
$$
+ \left[C_F T_F \left(\frac{\alpha_s(\mu_m)}{4\pi}\right)^2 \ln\left(\frac{Q^2}{\mu_m^2}\right)\left\{-\frac{8}{3}L_m^2 - \frac{80}{9}L_m - \frac{224}{27}\right\}\right]_{\mathcal{O}(\alpha_s)} + \mathcal{O}(\alpha_s^2)\,,
$$

with $L_m = \ln(m^2/\mu_m^2)$ and where the subscript $\mathcal{O}(\alpha_s)$ indicates that the involved rapidity logarithm is again counted as $\alpha_s^2 \log \sim \alpha_s$, hence included at N²LL. The soft function and the corresponding (n_ℓ) flavor evolution in Eq. (3.66) is identical with scenario III. The jet function does now involve matrix elements of bHQET fields (see Sec. 3.3 and references therein) and is given by

$$
J_{B,n,e}(s, m, \mu) = \frac{1}{8\pi} \int \mathrm{d}k^+\, \mathrm{d}k^-\, \mathrm{d}(\vec{k}_\perp^2)\, \delta(k^-)\, \delta^{(2)}(\vec{k}_\perp^2)\, \mathcal{J}_{B,n,e}(s, k, m, \mu)\,, \tag{3.68}
$$

$$
\mathcal{J}_{B,n,e}(s, k, m, \mu) = \frac{1}{N_c} \sum_{X_n} \int \mathrm{d}\Pi_{X_n} (2\pi)^d\, \delta^{(d)}(mv + k - P_n)\, \delta(s - Q^2 e_n(X)) \tag{3.69}
$$
$$
\times \mathrm{Tr}\left[\langle 0| \not{\bar{n}}\, W_n^\dagger\, h_{v^+}(0)\, |X_n\rangle \langle X_n|\, \bar{h}_{v^+}\, W_n(0)\, |0\rangle\right]\,,
$$

with $J_{B,e} = J_{B,n,e} \otimes J_{B,\bar{n},e}$. Later it will be useful to employ a simplification like in Eq. (3.63) to express everything in 1-jet amplitudes:

$$
\mathrm{Tr}\left[\langle 0| \not{\bar{n}}\, W_n^\dagger h_{v^+}(0)\, |X_n\rangle \langle X_n|\, \bar{h}_{v^+}\, W_n(0)\, |0\rangle\right] = (\not{\bar{n}}\gamma_0)_{\alpha\beta}\, \langle 0|\, (\bar{h}_{v^+} W_n)^{\dagger\beta}(0)\, |X_n\rangle \langle X_n|\, (\bar{h}_{v^+} W_n)^\alpha(0)\, |0\rangle
$$
$$
= (\not{\bar{n}}\gamma_0)_{\alpha\beta}\, (\mathcal{M}_{B,n,1-\mathrm{jet}}^\dagger)^\beta (\mathcal{M}_{B,n,1-\mathrm{jet}})^\alpha\,, \tag{3.70}
$$

which is the form that will be used in Sec. 3.5.2 to calculate the bHQET jet function for the mentioned event shape variables. Note that in the literature the bHQET jet function is usually written in terms of the natural jet function variable $\hat{s} = \frac{s}{m}$ which renders the jet function free of explicit logarithms of the form $\ln \frac{m}{\mu}$. To have a more uniform presentation of all the scenarios and a more natural transition between scenarios we choose to use s for the most part of this work.

3.4.3 Anomalous Dimension, Resummation and Evolution Kernels

As already mentioned in Sec. 3.3 the previously discussed factorization theorems allow us to resum large logarithms appearing in fixed order cross section calculations. This can be achieved by utilizing

the renormalization group evolution of the different involved factors [7, 8] which is encoded into their respective anomalous dimensions. In momentum space the renormalization for the jet and soft function works via a convolution due to their distributional nature while the hard function renormalization is multiplicative:

$$H^0(Q, \mu) = Z_H(Q, \mu) H(Q, \mu) , \tag{3.71}$$

$$J^0_{n,e}(s, m, \mu) = \int \mathrm{d}s' \, Z_{J,n,e}(s - s', \mu) \, J_{n,e}(s', m, \mu) , \tag{3.72}$$

$$S^0_e(\ell, m, \mu) = \int \mathrm{d}\ell' \, Z_{S,e}(s - s', \mu) \, S_e(s', m, \mu) . \tag{3.73}$$

By using the Fourier-transform of the jet function $\tilde{J}(y) = \mathcal{F}(J(s)) = \int \mathrm{d}s \exp(-iys) J(s)$ and soft function $\tilde{S}(y) = \mathcal{F}(S(\ell)) = \int \mathrm{d}\ell \exp(-iy\ell) S(\ell)$ we can write[17]

$$F^0(y, \mu) = Z_F(y, \mu) F(y, \mu) , \tag{3.74}$$

with $F = H, \tilde{J}, \tilde{S}$. The renormalization group evolution (RGE) equation then reads

$$\mu \frac{\mathrm{d}}{\mathrm{d}\mu} F(y, \mu) = \gamma_F(y, \mu) F(y, \mu) . \tag{3.75}$$

This equation depends on the anomalous dimension γ_F which in general can be written as

$$\gamma_F(y, \mu) = \frac{2 \Gamma_F[\alpha_s(\mu)]}{j} L_F(y, \mu) + \gamma_F[\alpha_s(\mu)] , \tag{3.76}$$

with $j \in \{1, 2\}$ which keeps track of the powers of μ for the different cross section factors (for hard and jet function $j = 2$, for the soft function $j = 1$) as well as the so-called *cusp* anomalous dimension $\Gamma_F[\alpha_s]$ and *non-cusp* anomalous dimension $\gamma_F[\alpha_s]$. These are defined in terms of a perturbative expansion as follows:

$$\Gamma_F[\alpha_s(\mu)] = \sum_{n=0} \Gamma_{F,n} \left(\frac{\alpha_s(\mu)}{4\pi} \right)^{n+1} , \qquad \gamma_F[\alpha_s(\mu)] = \sum_{n=0} \gamma_{F,n} \left(\frac{\alpha_s(\mu)}{4\pi} \right)^{n+1} . \tag{3.77}$$

Explicit expressions for the anomalous dimension coefficients for the different cross section factors can be found in App. A. Additionally Eq. (3.76) involves the logarithm function $L_F(t, \mu)$ which for the different functions is given by

$$L_H(y, \mu) = \ln \frac{\mu^2}{Q^2} , \qquad L_{\tilde{J}/\tilde{S}}(y, \mu) = \ln \left(iy\mu^j e^{\gamma_E} \right) , \tag{3.78}$$

with $y \equiv y + i0$. Solving the generic RGE equation from Eq. (3.75) one gets

$$F(y, \mu) = U_F(y, \mu, \mu_0) F(y, \mu_0) , \tag{3.79}$$

$$U_F(y, \mu, \mu_0) = \exp \left[\omega_F(\mu, \mu_0, \Gamma_F, j) L_F(y, \mu_0) + K_F(\mu, \mu_0, \Gamma_F, \gamma_F) \right] . \tag{3.80}$$

The introduced functions ω_F and K_F play a central role in the evolution kernels and are defined as follows:

$$\omega_F(\mu, \mu_0, \Gamma_F, j) = \frac{2}{j} \int_{\alpha_s(\mu_0)}^{\alpha_s(\mu)} \mathrm{d}\alpha \frac{\Gamma_F[\alpha]}{\beta[\alpha]} , \tag{3.81}$$

$$K(\mu, \mu_0, \Gamma_F, \gamma_F) = 2 \int_{\alpha_s(\mu_0)}^{\alpha_s(\mu)} \mathrm{d}\alpha \frac{\Gamma_F[\alpha]}{\beta[\alpha]} \int_{\alpha_s(\mu_0)}^{\alpha} \frac{\mathrm{d}\alpha'}{\beta[\alpha']} + \int_{\alpha_s(\mu_0)}^{\alpha_s(\mu)} \mathrm{d}\alpha \frac{\gamma_F[\alpha]}{\beta[\alpha]} , \tag{3.82}$$

---

[17]In the following we will consider dependence on m or Q as implicit and therefore omit them from the list of variables the functions depend on.

which involve the QCD beta function given by

$$\beta[\alpha_s(\mu)] = \frac{d\alpha(\mu)}{d\ln\mu} = -2\varepsilon\alpha_s(\mu) - \frac{\alpha_s(\mu)^2}{2\pi}\sum_{n=0}\beta_n\left(\frac{\alpha_s(\mu)}{4\pi}\right)^n. \tag{3.83}$$

Explicit expressions for ω_F, K_F and the beta function coefficients are also given in App. A. Using the inverse Fourier transform $F(y) = \mathcal{F}^{-1}(\tilde{F}(t)) = \int \frac{dt}{2\pi}\exp(ity)\tilde{F}(t)$ one gets the momentum space jet and soft function evolution kernel [7] which is given by

$$U_{J/S}(t,\mu,\mu_0) = \frac{e^{K_F}\left(e^{\gamma_E}\right)^{\omega_F}}{\mu_0^j\,\Gamma(-\omega_F)}\left[\frac{\theta(\tilde{t})}{\tilde{t}^{1+\omega_F}}\right]_+, \tag{3.84}$$

with ω_F and K_F as in Eq. (3.80), $\tilde{t} = \frac{t}{\mu_0^j}$ and again j the mass dimension of the variable[18] t.

Due to the fact that only a finite number of terms in the perturbative expansion of the anomalous dimension for the different cross section factors is known, only the resummation of large logarithms to a corresponding finite order (in the log counting) is possible. How the resummation of logarithms according to a specified counting can be achieved consistently was clarified and reviewed in Ref. [79]. Adopting the convention of Ref. [100] the perturbative order at which the different ingredients have to be entered to achieve a certain logarithmic accuracy are given in Tab. 3.3.

	Γ_F	γ_F	Matching	Non-Singular
LL	1	0	0	0
NLL	2	1	0	0
NLL$'$	2	1	1	1
N^{2}LL	3	2	1	1
N^{2}LL$'$	3	2	2	2

Table 3.3: Needed perturbative order of different ingredients to achieve a certain order of resummation of large logarithms (in α_s). Apart from the cusp and non-cusp anomalous dimensions which enter into the evolution kernels also the different cross section factors ("Matching") and non-singular contributions have to be included to a certain perturbative order to achieve a consistent resummation of large logarithms (conventions adopted from Ref. [100]).

3.4.4 Choice of General Renormalization Scale μ and Consistency Relations

The global renormalization scale μ has no predefined value and in principle can be freely chosen. In order to allow any value, the discussed factorization theorems of Sec. 3.4.2 need to be generalized to the case $\mu \neq \mu_j$ and $\mu \neq \mu_{jB}$ for the different scenarios.

Starting with the bHQET scenario (see Sec. 3.4.2), the correct factorization theorem for the more general case $\mu_m > \mu \neq \mu_{jB}$ is constructed by using the evolution of the bHQET jet function $J_{B,n,e}(\mu) = U_B(\mu,\mu_j) \otimes J_{B,n,e}(\mu_j)$ while everything else stays the same. For the alternative factorization theorem which is valid for $\mu > \mu_m > \mu_j$ the soft function evolution then crosses the mass threshold and is therefore given by the setup used for scenario III which introduces the matching coefficient $\mathcal{M}_S^{(n_\ell+1)}$ from Eq. (3.65). The jet function will then also cross the mass threshold, thus one starts with the bHQET jet function which first gets evolved with (n_ℓ) flavors up to the mass

---

[18]To make this more clear, the variable t corresponds to s for the jet function with $j = 2$ and to ℓ for the soft function with $j = 1$.

threshold. After matching onto the SCET jet function the evolution continues with $(n_\ell + 1)$ flavors. The mentioned matching is usually implemented in the following way [8]:

$$J_{n,e}(s,m,\mu_m)^{(n_\ell+1)} = \int \mathrm{d}s' \, \mathcal{M}_{J,n}^{(n_\ell+1)}(s-s',m,\mu_m) J_{B,n,e}^{(n_\ell)}(s',m,\mu_m) + \mathcal{O}\left(\frac{P_n^2 - m^2}{m^2}\right) , \qquad (3.85)$$

where the omitted terms correspond to the non-distributional terms in the SCET jet function and the matching coefficient $\mathcal{M}_{J,n}^{(n_\ell+1)}$ is given by [8,88]

$$
\begin{aligned}
\mu_j^2 \, \mathcal{M}_{J,n}^{(n_\ell+1)}(s,m,\mu_m) = {} & \delta(\tilde{s}) \left[1 + \frac{\alpha_s^{(n_\ell+1)}(\mu_m) \, C_F}{4\pi} \left\{ L_m^2 - L_m + 4 + \frac{\pi^2}{6} \right\} \right] \\
& + \delta(\tilde{s}) \left[C_F T_F \left(\frac{\alpha_s^{(n_\ell+1)}(\mu_m)}{4\pi} \right)^2 \ln\left(\frac{\mu_j^2}{\mu_m^2}\right) \left\{ -\frac{8}{3} L_m^2 - \frac{80}{9} L_m - \frac{224}{27} \right\} \right]_{\mathcal{O}(\alpha_s)} + \mathcal{O}(\alpha_s^2) ,
\end{aligned}
$$
$$(3.86)$$

with $\tilde{s} = \frac{s}{\mu_j^2}$, $L_m = \ln \frac{m^2}{\mu_m^2}$ and (as in the case of $\mathcal{M}_S$) with the additional scale μ_j scaling like $\mu_j \sim Q\sqrt{e}$ again to make all large logarithms explicit.

For scenario III the more general factorization theorem for $\mu_j \neq \mu > \mu_m$ is then found in analogy to the bHQET scenario by using the SCET jet function evolution $J_{n,e}(\mu) = U_J(\mu,\mu_j) \otimes J_{n,e}(\mu_j)$ while everything else again stays the same. For the different scale hierarchy of $\mu_j > \mu_m > \mu$ the soft function now evolves completely with (n_ℓ) flavors while the hard and jet function start with $(n_\ell + 1)$ flavor evolution and subsequently have to cross the mass threshold. The hard function evolution is implemented as in the bHQET case for the default hierarchy $\mu_m > \mu$ while the jet function evolution is basically given by the inverse evolution of the jet function in the case of bHQET with hierarchy $\mu > \mu_m > \mu_j$ (ignoring bHQET power corrections - see Sec. 3.6 for a discussion)

In case of scenario IV again the SCET jet function evolution is used to find the appropriate factorization theorem for the hierarchy $\mu_j \neq \mu, \mu_s > \mu_m$. For $\mu_j > \mu_m > \mu$ not only the hard and jet functions but now also the soft function start their respective evolution with $(n_\ell + 1)$ flavors, cross the mass threshold and finally continue their evolution with (n_ℓ) active flavors. For the hard and jet function the detailed implementation for this particular scale hierarchy is the same as for scenario III. The soft function evolution is now given by the inverse evolution of the soft function in scenario III with $\mu > \mu_m > \mu_s$.

Consistency Relations for Matching Coefficient

Next let us consider the factorization theorems for the two different hierarchies between μ_m and the jet scale $\mu_{j(B)}$ which were discussed for each scenario. For the case where $\mu = \mu_{j(B)}$ the two results should give the same. This allows us to extract a consistency relation which holds for the used matching coefficients. It is given by

$$H_M(m,\mu_m)\,\delta(s) = \int \mathrm{d}\ell \, \mathcal{M}_J(s - Q\,\ell, m, \mu_m) \, \mathcal{M}_S(\ell, m, \mu_m) , \qquad (3.87)$$

where we used the definition $\mathcal{M}_J = \mathcal{M}_{J,n} \otimes \mathcal{M}_{J,\bar{n}}$. This relation can be checked to be true at $\mathcal{O}(\alpha_s)$ by considering the corresponding expressions from Eqs. (3.65), (3.67) and (3.86) and that $\ln\left(\frac{\mu_j^4}{\mu_s^2 \mu_m^2}\right) = \ln\left(\frac{Q^2}{\mu_m^2}\right)$ up to higher order corrections.

Consistency Relations for Anomalous Dimensions

Checking the μ independence of the factorization theorem entails other consistency relations which should hold for the anomalous dimensions. Starting with scenario IV and $\mu > \mu_m$ let us next look

at the Fourier transform (as before $\tilde{F}$ denotes the Fourier transform of the function F) of the cross section formula and take the derivative with respect to μ. One then gets the following:

$$\frac{\mathrm{d}}{\mathrm{d}\ln\mu} H\, \tilde{J}_n\, \tilde{J}_{\bar{n}}\, \tilde{S} = \left(\gamma_H + 2\,\gamma_{\tilde{J}} + \gamma_{\tilde{S}}\right) H\, \tilde{J}_n\, \tilde{J}_{\bar{n}}\, \tilde{S} = 0 \qquad \Rightarrow \qquad \left(\gamma_H + 2\,\gamma_{\tilde{J}} + \gamma_{\tilde{S}}\right) = 0\,, \qquad (3.88)$$

where all the anomalous dimensions are evaluated with $(n_\ell + 1)$ flavors and the jet function now refers to the hemisphere jet function. Using Eq. (3.76) the above expression can be split into three (by comparing the coefficients of the different involved logarithms) relations:

$$\left(\Gamma_H[\alpha_s] - \Gamma_S[\alpha_s]\right)\ln(\mu/Q) = 0\,, \qquad (3.89)$$

$$\left(\Gamma_J[\alpha_s] + \Gamma_S[\alpha_s]\right)\ln\left(iy\mu^2\mathrm{e}^{\gamma_E}\right) = 0\,, \qquad (3.90)$$

$$\gamma_H[\alpha_s] + 2\,\gamma_J[\alpha_s] + \gamma_S[\alpha_s] = 0\,, \qquad (3.91)$$

which tells us $\Gamma_H = -\Gamma_J = \Gamma_S$ as well as $\gamma_H + 2\,\gamma_J + \gamma_S = 0$. Analog relations can be derived for the other scale hierarchies as well and all of them can explicitly be checked by using the expressions from App. A.

3.5 Jet Function at NLO

As discussed in Sec. 3.4.1 it is possible to find a function $f_e(r, y)$ which is characteristic for each event shape discussed earlier. Since $f_e \sim \lambda^2$ it is straightforward to show that the collinear measurement which is the relevant one for the jet function calculation is the same for P- and E-scheme at leading order:

$$v = \frac{|\vec{p}_i|}{p_i^0} = \frac{|\vec{p}_i|}{\sqrt{|\vec{p}_i|^2 + m_i^2}} = 1 - \frac{1}{2}\frac{m_i^2}{|\vec{p}_i|^2} + \mathcal{O}(\lambda^4) \quad \text{for } i \in n\text{-collinear}\,,$$

$$f_{e,n}^P(r, \eta(r, y)) = v\, f_{e,n}^E(r, \eta(r, y)) = f_{e,n}^E(r, \eta(r, y)) + \mathcal{O}(\lambda^4)\,, \qquad (3.92)$$

which is why we only distinguish M- and P-scheme jet function from now on. Futhermore it is easy to see that $C_n^{M/P} = 6\,\tau_n^{M/P} = 6\,\rho_{+,n}^{M/P}$, hence all of them can be calculated from the corresponding angularities via the limit $a \to 0$.

3.5.1 SCET Jet Function for P-scheme Angularities

To calculate the jet function for the P-scheme definition of angularities we need to evaluate the expressions given in Eqs. (3.50),(3.62) and (3.63) with the appropriate measurement delta function from Tab. 3.2. The leading contribution to the n-collinear part of the P-scheme definition of angularities can be written as

$$\tau_{a,n}^P = \frac{1}{Q}\sum_{i\in n}(m_i^\perp)r\mathrm{e}^{-|\eta|(1-a)} = \frac{1}{Q}\sum_i \left(p_i^-\right)^{a-1}\left(p_i^+ p_i^- - m_i^2\right)^{\frac{2-a}{2}}\,. \qquad (3.93)$$

At NLO there are two possible final states for 1-jet production: a single massive quark $|Q\rangle$ or a massive quark together with a radiated gluon $|Qg\rangle$. The diagrams involved in the NLO jet function calculation where the pole mass scheme[19] is used are shown in Fig. 3.1. In the following we are going to discuss the corresponding contributions to the SCET jet function calculation.

---

[19]Alternative mass schemes can be implemented by using the finite difference to the pole mass and expanding for small α_s up to the appropriate order.
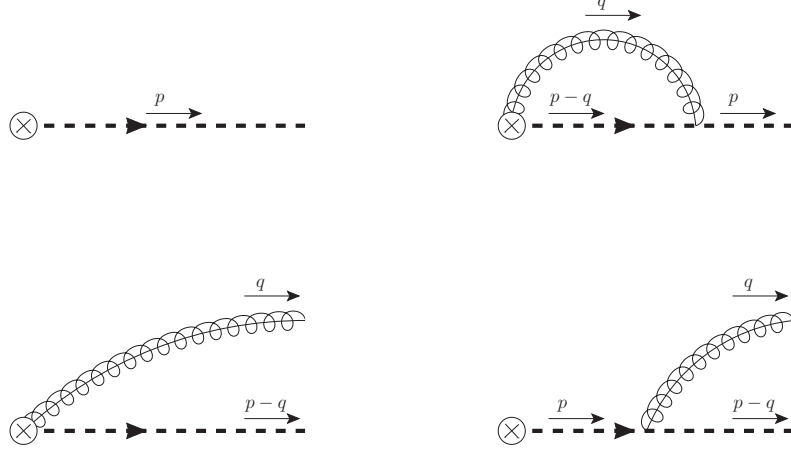
Figure 3.1: Relevant diagrams for calculating 1-jet amplitudes needed for the jet function calculation. The upper two diagrams contribute to the $|Q\rangle$ final state while the lower two diagrams contribute to the $|Qg\rangle$ final state.

Single Quark Contribution

The definition of the jet function, see Eq. (3.62), involves unrenormalized (bare) fields. To be efficient we rewrite everything in terms of renormalized fields and then simply calculate the usual amputated diagrams which do not include self energy corrections of external fields:

$$(\mathcal{M}^{Q}_{n,1-\text{jet}})^{\alpha} = \langle q_n | (\overline{\chi}^0_n)^{\alpha} | 0 \rangle = \left[1 + \frac{1}{2} \delta z^{\text{OS}}_{\psi} + \mathcal{O}(\alpha_s^2) \right] \langle q_n | (\overline{\chi}_n)^{\alpha} | 0 \rangle \ , \tag{3.94}$$

where $\delta z^{\text{OS}}_{\psi} = \frac{\alpha_s C_F}{4\pi} \left[-\frac{3}{\varepsilon} + 3 \ln \frac{m^2}{\mu^2} - 4 \right]$ is the one loop field renormalization counter term in the on-shell scheme in $d = 4 - 2\varepsilon$ dimensions.

For the single quark contributions we have to evaluate the upper two diagrams of Fig. 3.1 which give (involving $u_n(p,s) = \frac{1}{4}(\slashed{n}\slashed{\bar{n}})u(p,s)$ the n-collinear SCET analog of the dirac spinor $u(p,s)$)

$$(\mathcal{M}^{Q}_{n,1-\text{jet}})^{\alpha} = \overline{u}^{\alpha}_n(p,s) \left[1 + \frac{1}{2} \delta z^{\text{OS}}_{\psi} + 8 \, i\pi \, \alpha_s C_F \frac{\slashed{\bar{n}}}{2} \frac{\slashed{n}}{2} \, \mathcal{I}_{\text{virt}}(p,m) + \mathcal{O}(\alpha_s^2) \right] , \tag{3.95}$$

where we used the strong coupling constant $\alpha_s = g_s^2/(4\pi)$ and defined the integral (details on the calculation are given in App. C.1)

$$\mathcal{I}_{\text{virt}}(p,m) = \tilde{\mu}^{4-d} \int \frac{\mathrm{d}^d q}{(2\pi)^d} \frac{p^- - q^-}{[(p-q)^2 - m^2 + i0][q^- + i0][q^2 + i0]} \ . \tag{3.96}$$

Next we evaluate the square of the matrix element, carry out the spin sum and all involved traces (color trace is implicit) and get

$$(\slashed{\bar{n}}\gamma_0)_{\alpha\beta} \sum_{\text{spins}} (\mathcal{M}^{Q \ \dagger}_{n,1-\text{jet}})^{\beta} (\mathcal{M}^{Q}_{n,1-\text{jet}})^{\alpha}$$

$$= 4 \, N_c \, p^- \left[1 + \delta z^{\text{OS}}_{\psi} + 16\pi \, \alpha_s C_F \, \text{Re}\left(i \, \mathcal{I}_{\text{virt}}(p,m) \right) + \mathcal{O}(\alpha_s^2) \right] , \tag{3.97}$$

where we used the appropriate powercounting to obtain the leading contribution to the spin sum[20] $\sum_s u^\alpha_{n,a}(p,s)\overline{u}^\beta_{n,b}(p,s) = \frac{1}{2}p^- \delta_{ab}\slashed{n}^{\alpha\beta}$. With this it is then easy to carry out the trivial phase space integral (only involving one massive on-shell final state particle) and evaluate all involved delta functions:

$$
J^Q_{n,\tau_a}(s,m,\mu) = \frac{1}{8\pi N_c} \int \mathrm{d}k^+ \, \mathrm{d}k^- \, \mathrm{d}^2(\vec{k}_\perp) \, \delta(k^- - Q)\, \delta^{(2)}(\vec{k}_\perp) \int \frac{\mathrm{d}^4 p}{(2\pi)^d} (2\pi)^d \delta^{(d)}(k-p)
$$

$$
\times (2\pi)\theta(p^0)\delta(p^2 - m^2)\, \delta\!\left[s - Q(p^-)^{a-1}(p^+ p^- - m^2)^{\frac{2-a}{2}} \right] \tag{3.98}
$$

$$
\times 4N_c \, p^- \left[1 + \delta z^{\mathrm{OS}}_\psi + 16\pi\,\alpha_s C_F \operatorname{Re}\!\left(i\, \mathcal{I}^1_{\mathrm{virt}}(p,m) \right) + \mathcal{O}(\alpha_s^2) \right],
$$

which directly leads to the final result for the single quark part of the jet function as defined in Eq. (3.50). The result is split in three parts:

$$
J^Q_{n,\tau_a}(s,m,\mu) = J^0_{n,\tau_a} + J^a_{n,\tau_a} + J^b_{n,\tau_a} + \mathcal{O}(\alpha_s^2), \tag{3.99}
$$

$$
\mu^2 J^0_{n,\tau_a} = \delta(\tilde{s}), \tag{3.100}
$$

$$
\mu^2 J^a_{n,\tau_a} = \delta(\tilde{s})\frac{\alpha_s C_F}{\pi}\left[-\frac{3}{4\varepsilon} + \frac{3}{4}\ln\frac{m^2}{\mu^2} - 1 \right], \tag{3.101}
$$

$$
\mu^2 J^b_{n,\tau_a} = \delta(\tilde{s})\frac{\alpha_s C_F}{\pi}\left[\frac{1}{2\varepsilon^2} + \frac{1}{\varepsilon}\left(1 - \frac{1}{2}\ln\frac{m^2}{\mu^2} \right) + 2 + \frac{\pi^2}{24} - \ln\frac{m^2}{\mu^2} + \frac{1}{4}\ln^2\frac{m^2}{\mu^2} \right], \tag{3.102}
$$

with $\tilde{s} = s/\mu^2$ and where the first term corresponds to the tree level contribution, the second term originates from the field renormalization counter term and the third term represents the virtual contributions to the NLO jet function.

Real Radiation Contribution

At one loop order one also needs to take care of real radiation contributions which correspond to a $|Qg\rangle$ final state. The diagrams we need to address are shown in the lower line of Fig. 3.1 and give rise to the amplitude[21]

$$
(\mathcal{M}^{Qg}_{n,1-\mathrm{jet}})^\alpha = \overline{u}^\alpha_n(p-q,s)\varepsilon^\nu_A(q,\lambda)g_s T^A \tilde{\mu}^\varepsilon \left[R_{1,\nu}(p,q) + R_{2,\nu}(p,q)\frac{\slashed{\overline{n}}\slashed{n}}{4} \right] + \mathcal{O}(g_s^2), \tag{3.103}
$$

$$
R_{1,\nu}(p,q) = \frac{\overline{n}_\nu}{q^- + i0}, \tag{3.104}
$$

$$
R_{2,\nu}(p,q) = -\frac{p^-}{p^2 - m^2 + i0}\left(n_\nu + \frac{\gamma^\perp_\nu(\slashed{p}^\perp + m)}{p^-} + \frac{(\slashed{p}^\perp - \slashed{q}^\perp - m)\gamma^\perp_\nu}{p^- - q^-} \right.
$$

$$
\left. - \frac{(\slashed{p}^\perp + m)(\slashed{p}^\perp - \slashed{q}^\perp - m)}{p^-(p^- - q^-)}\,\overline{n}_\nu \right), \tag{3.105}
$$

where $R_{1,\nu}(p,q)$ is related to the contribution from the diagram involving a collinear Wilson line and $R_{2,\nu}(p,q)$ to the contribution from the diagram with a collinear gluon vertex.

Following the strategy used for the single quark contributions we next square the amplitude, carry

---

[20]In the following a,b indicate color indices (fundamental representation) while α,β correspond to Dirac indices.

[21]From now on we also use μ,ν for Lorentz indices and A as a color index (adjoint representation).

out spin and polarization sums and also take the color trace (implicit):

$$(\not{\!n}\gamma_0)_{\alpha\beta} \sum_{\substack{\text{spins}\\ \text{pol}}} (\mathcal{M}^{\text{Qg}\,\dagger}_{n,1-\text{jet}})^\beta (\mathcal{M}^{\text{Qg}}_{n,1-\text{jet}})^\alpha$$

$$= -g_s^2 \, N_c \, C_F \, (p^- - q^-) \, \tilde{\mu}^{2\varepsilon} \, \text{Tr}\left\{ \not{\!n}\gamma_0 \left[(R_1^\mu)^\dagger + \frac{\not{\!n}\not{\!n}}{4}(R_2^\mu)^\dagger \right] \gamma_0 \frac{\not{\!n}}{2} \left[R_{1,\mu} + R_{2,\mu}\frac{\not{\!n}\not{\!n}}{4} \right] \right\} \tag{3.106}$$

$$= -4\pi \, \alpha_s \, N_c \, C_F \, (p^- - q^-) \, \frac{\tilde{\mu}^{2\varepsilon}}{2} \, \text{Tr}\left\{ \not{\!n}\not{\!n} \left[(R_1^\mu)^\dagger + (R_2^\mu)^\dagger \right] \left[R_{1,\mu} + R_{2,\mu} \right] \right\}, \tag{3.107}$$

where we used $\sum_\sigma (\varepsilon_A^\mu(q,\sigma))^* \varepsilon_B^\nu(q,\sigma) = -g^{\mu\nu}\delta_{AB}$ and also the following easy to check identities $[\gamma_\mu^\perp, \not{\!n}\not{\!n}] = 0$, $[\gamma_\perp^\mu, \gamma_0] = 0$, $\gamma_0\not{\!n} = \not{\!n}\gamma_0$ and $(\not{\!n}\not{\!n})\not{\!n} = 4\not{\!n}$. Next we can already use that the total jet momentum will be set to $p^\mu = (p^+, p^-, \vec{p}^{\,\perp}) = (k^+, Q, 0)$ which happens due to a delta function integration and can be seen in Eq. (3.50). With this and simplifying the involved expressions we then find

$$(R_1^\mu)^\dagger R_{1,\mu} \sim \bar{n} \cdot \bar{n} = 0, \tag{3.108}$$

$$(R_1^\mu)^\dagger R_{2,\mu} + (R_2^\mu)^\dagger R_{1,\mu} = -2\,\text{Re}\left[\frac{Q\,\bar{n}\cdot n}{(q^- + i0)(Qk^+ - m^2 - i0)} \right] = -\frac{4\,Q}{q^-(Qk^+ - m^2)}, \tag{3.109}$$

$$(R_2^\mu)^\dagger R_{2,\mu} = \frac{Q^2}{(Qk^+ - m^2)^2}\left[\left(n^\mu - \frac{\gamma^{\perp,\mu}(\not{\!q}^\perp - m)}{Q - q^-} - \frac{m\gamma^{\perp,\mu}}{Q} - \frac{m(\not{\!q}^\perp - m)}{Q(Q - q^-)}\bar{n}^\mu \right) \right.$$

$$\left. \times \left(n_\mu + \frac{\gamma_\mu^\perp m}{Q} - \frac{(\not{\!q}^\perp + m)\gamma_\mu^\perp}{Q - q^-} + \frac{m(\not{\!q}^\perp + m)}{Q(Q - q^-)}\bar{n}_\mu \right) \right]$$

$$= \frac{Q^2(d - 2)}{(Qk^+ - m^2)^2\,(Q - q^-)}\left[m^2\left(\frac{2\,d}{(d - 2)Q} - \frac{Q - q^-}{Q^2} - \frac{1}{Q - q^-} \right) - \frac{(\vec{q}^{\,\perp})^2}{Q - q^-} \right] \tag{3.110}$$

$$+ \text{ terms with odd } \# \text{ of } \gamma\text{'s}.$$

In the next step we put everything together, simplify the involved expressions and arrive at the phase space integrals which we have to calculate in order to get the final result (if not stated dependence on m, Q and μ is implicit):

$$J^{Qg}_{n,\tau_a}(s, m, \mu) = J^c_{n,\tau_a} + J^d_{n,\tau_a} + \mathcal{O}(\alpha_s^2), \tag{3.111}$$

$$J^c_{n,\tau_a} = \frac{\alpha_s C_F}{\pi} \int dt \, \frac{8\pi\,\tilde{\mu}^{4-d}}{t - m^2} \int \frac{d^d q}{(2\pi)^d} \, (2\pi)^2 \theta(p^0 - q^0)\theta(q^0)\delta((p - q)^2 - m^2)\delta(q^2) \, \frac{Q - q^-}{q^-}$$

$$\times \delta\left\{ Q(Q - q^-)^{a-1}\left[(Q - q^-)(\frac{t}{Q} - q^+) - m^2 \right]^{\frac{2-a}{2}} + Q(q^-)^{a-1}\left[q^+ q^- \right]^{\frac{2-a}{2}} - s \right\}, \tag{3.112}$$

$$J^d_{n,\tau_a} = -\frac{\alpha_s C_F}{\pi} \int dt \, \frac{2\pi\,Q^2\,\tilde{\mu}^{4-d}}{(t - m^2)^2} \int \frac{d^d q}{(2\pi)^d} \, (2\pi)^2 \theta(p^0 - q^0)\theta(q^0)\delta((p - q)^2 - m^2)\delta(q^2)$$

$$\times (d - 2)\left[\frac{m^2}{Q^2}\left(\frac{2d}{d - 2} - \frac{Q - q^-}{Q} - \frac{Q}{Q - q^-} \right) - \frac{Q}{Q - q^-}\frac{q_\perp^2}{Q^2} \right] \tag{3.113}$$

$$\times \delta\left\{ Q(Q - q^-)^{a-1}\left[(Q - q^-)(\frac{t}{Q} - q^+) - m^2 \right]^{\frac{2-a}{2}} + Q(q^-)^{a-1}\left[q^+ q^- \right]^{\frac{2-a}{2}} - s \right\},$$

with $t = Qk^+$. Evaluating these integrals is a rather long process which is why we present details on

the calculation in App. C.2. The result of this calculation is as follows:

$$\mu^2 J_{n,\tau_a}^c = \frac{\alpha_s C_F}{\pi} \Bigg\{ \delta(\tilde{s}) \bigg[\frac{1}{2(1-a)\varepsilon^2} + \frac{1}{2(1-a)\varepsilon} \bigg((1-a)\ln\frac{m^2}{Q^2} + a\ln\frac{Q^2}{\mu^2} \bigg) $$

$$+ \frac{1-4a+2a^2}{24(1-a)}\pi^2 + \frac{1}{4(1-a)} \bigg((1-a)\ln\frac{m^2}{\mu^2} + a\ln\frac{Q^2}{\mu^2} \bigg)^2 \bigg]$$

$$- \frac{1}{(1-a)} \bigg[\frac{\theta(\tilde{s})}{\tilde{s}} \bigg]_+ \bigg[\frac{1}{\varepsilon} + (1-a)\ln\frac{m^2}{\mu^2} + a\ln\frac{Q^2}{\mu^2} \bigg] + \frac{2}{(1-a)} \bigg[\frac{\theta(\tilde{s})\ln\tilde{s}}{\tilde{s}} \bigg]_+ \tag{3.114}$$

$$- \frac{\theta(\tilde{s})}{\tilde{s}} \bigg[\ln\bigg(1 + \frac{(\tilde{s}\,\mu^2/Q^2)^{\frac{2}{2-a}}}{m^2/Q^2} \bigg) $$

$$+ \frac{2}{2-a} \,_2F_1\bigg(1, 1-\frac{a}{2}; 2-\frac{a}{2}; -\frac{m^2}{\mu^2}\bigg(\frac{Q^2}{\mu^2}\bigg)^{\frac{a}{2-a}} \tilde{s}^{\frac{2}{a-2}} \bigg) + \frac{2}{2-a} \mathcal{I}_1(s;a) \bigg] \Bigg\},$$

$$\mu^2 J_{n,\tau_a}^d = \frac{\alpha_s C_F}{\pi} \Bigg\{ \delta(\tilde{s}) \bigg[\frac{1}{2\varepsilon} + \frac{1}{2}\bigg((1-a)\ln\frac{m^2}{\mu^2} + a\ln\frac{Q^2}{\mu^2} \bigg) \bigg] - \bigg[\frac{\theta(\tilde{s})}{\tilde{s}} \bigg]_+ $$

$$+ \theta(\tilde{s}) \bigg[\frac{2-a}{2}\frac{\mu^2}{m^2}\bigg(\frac{m^2}{Q^2}\bigg)^{\frac{a}{2}} \Gamma\bigg(1-\frac{a}{2}\bigg)\Gamma\bigg(\frac{a}{2}\bigg)$$

$$- \frac{2-a}{a}\frac{\mu^2}{m^2}\bigg(\frac{Q^2}{\mu^2}\bigg)^{\frac{-a}{2-a}} \tilde{s}^{\frac{a}{2-a}} \,_2F_1\bigg(1, \frac{a}{2}; \frac{2+a}{2}; -\frac{\mu^2}{m^2}\bigg(\frac{Q^2}{\mu^2}\bigg)^{\frac{-a}{a-2}} \tilde{s}^{\frac{2}{2-a}} \bigg) \tag{3.115}$$

$$- \frac{2}{2-a}\frac{1}{\tilde{s}}\mathcal{I}_1(s;a) + \frac{1}{2-a}\frac{1}{\tilde{s}}\mathcal{I}_2(s;a) + \frac{2}{2-a}\frac{1}{\tilde{s}}\mathcal{I}_3(s;a) \bigg] \Bigg\},$$

with $\tilde{s} = s/\mu^2$. In order to extract analytic expressions it was necessary to employ subtractions which are contained in the integral expressions denoted as $\mathcal{I}_i(s;a)$. All terms of the form $\frac{\theta(s)}{s}f(s)$ which appear in Eqs. (3.115) and (3.114) are finite and integrable in s. The appearing integral expressions read:

$$\mathcal{I}_1(s;a) = \frac{m^2}{Q^2}\int_0^1 dx\, x\,(1-x) \Bigg\{ \bigg[\bigg(\frac{s}{Q^2}\bigg)^{\frac{2}{2-a}} \bigg(\frac{x^{1-a}(1-x)^{1-a}}{x^{1-a}+(1-x)^{1-a}} \bigg)^{\frac{2}{2-a}} + m^2\,x^2 \bigg]^{-1} \tag{3.116}$$

$$- \bigg[\bigg(\frac{s}{Q^2}\bigg)^{\frac{2}{2-a}} x^{\frac{2(1-a)}{2-a}} + m^2\,x^2 \bigg]^{-1} \Bigg\},$$

$$\mathcal{I}_2(s;a) = \bigg(\frac{s}{Q^2}\bigg)^{\frac{2}{2-a}}\int_0^1 dx\, x\, \bigg[\bigg(\frac{s}{Q^2}\bigg)^{\frac{2}{2-a}} + \frac{m^2}{Q^2}x^{\frac{2}{2-a}}\bigg(1 + \frac{x^{1-a}}{(1-x)^{1-a}} \bigg)^{\frac{2}{2-a}} \bigg]^{-1}, \tag{3.117}$$

$$\mathcal{I}_3(s;a) = \frac{m^4}{Q^4}\int_0^1 dx\, x^3\,(1-x) \Bigg\{ \bigg[\bigg(\frac{s}{Q^2}\bigg)^{\frac{2}{2-a}} \bigg(\frac{x^{1-a}(1-x)^{1-a}}{x^{1-a}+(1-x)^{1-a}} \bigg)^{\frac{2}{2-a}} + \frac{m^2}{Q^2}\,x^2 \bigg]^{-2} \tag{3.118}$$

$$- \bigg[\bigg(\frac{s}{Q^2}\bigg)^{\frac{2}{2-a}} x^{\frac{2(1-a)}{2-a}} + \frac{m^2}{Q^2}\,x^2 \bigg]^{-2} \Bigg\}.$$

NLO Result

When putting the expressions from the two final state contributions together there are some simplifications and we arrive at the result for the renormalized NLO primary massive P-scheme angularities

jet function and the corresponding counter term:

$$\mu^2 Z_{J,n,\tau_a}(s,\mu) = \delta(\tilde{s}) + \frac{\alpha_s C_F}{\pi} \left\{ \delta(\tilde{s}) \left[\frac{1 - a/2}{(1-a)\varepsilon^2} + \frac{3}{4\varepsilon} + \frac{a}{2(1-a)\varepsilon} L_Q \right] \right.$$

$$\left. + \left[\frac{\theta(\tilde{s})}{\tilde{s}} \right]_+ \frac{1}{(1-a)\varepsilon} \right\} + \mathcal{O}(\alpha_s^2) , \tag{3.119}$$

$$\mu^2 J_{n,\tau_a}(s,m,\mu) = \delta(\tilde{s})$$

$$+ \frac{\alpha_s C_F}{\pi} \left\{ \delta(\tilde{s}) \left[\frac{\pi^2}{24} \frac{(2 - 5a + 2a^2)}{1-a} + 1 + \frac{2-a}{4} L_m^2 + \left[\frac{1-2a}{4} + \frac{a}{2} L_Q \right] L_m \right. \right.$$

$$\left. + \frac{a}{2} \left[\frac{a/2}{1-a} L_Q + 1 \right] L_Q \right]$$

$$- \left[\frac{\theta(\tilde{s})}{\tilde{s}} \right]_+ \left[L_m + \frac{a}{1-a} L_Q + 1 \right] + \frac{2}{1-a} \left[\frac{\theta(\tilde{s}) \ln(\tilde{s})}{\tilde{s}} \right]_+ \tag{3.120}$$

$$+ \theta(\tilde{s}) \left[-\frac{1}{\tilde{s}} \ln \left(1 + \frac{Q^2}{m^2} \left(\frac{\mu^2}{Q^2} \tilde{s} \right)^{\frac{2}{2-a}} \right) - \frac{2}{2-a} \frac{1}{\tilde{s}} \, _2F_1 \left(1, 1 - \frac{a}{2}; 2 - \frac{a}{2}; -\frac{m^2}{Q^2} \left(\frac{\mu^2}{Q^2} \tilde{s} \right)^{\frac{-2}{2-a}} \right) \right.$$

$$+ \frac{2-a}{2} \frac{\mu^2}{m^2} \left(\frac{m^2}{Q^2} \right)^{\frac{a}{2}} \Gamma \left(1 - \frac{a}{2} \right) \Gamma \left(\frac{a}{2} \right) - \frac{2-a}{a} \frac{\mu^2}{m^2} \left(\frac{\mu^2}{Q^2} \tilde{s} \right)^{\frac{a}{2-a}} \, _2F_1 \left(1, \frac{a}{2}; 1 + \frac{a}{2}; -\frac{Q^2}{m^2} \left(\frac{\mu^2}{Q^2} \tilde{s} \right)^{\frac{2}{2-a}} \right)$$

$$\left. \left. - \frac{4}{2-a} \frac{1}{\tilde{s}} \mathcal{I}_1(s;a) + \frac{1}{2-a} \frac{1}{\tilde{s}} \mathcal{I}_2(s;a) + \frac{2}{2-a} \frac{1}{\tilde{s}} \mathcal{I}_3(s;a) \right] \right\} + \mathcal{O}(\alpha_s^2) ,$$

with $\tilde{s} = \frac{s}{\mu^2}$, $L_m = \ln \frac{m^2}{\mu^2}$ and $L_Q = \ln \frac{Q^2}{\mu^2}$. Again all terms of the form $\frac{\theta(s)}{s} f(s)$ are finite and integrable in s.

3.5.2   bHQET Jet Function for P-scheme Angularities

Calculating the P-scheme angularities jet function in bHQET is very similar to the SCET case. It is straightforward to calculate that the one loop single quark contributions (virtual contributions) to the bHQET jet function are scaleless[22] and we therefore get:

$$\mu^2 J_{B,n,\tau_a}^0 = \delta(\tilde{s}) , \tag{3.121}$$

$$J_{B,n,\tau_a}^a = J_{n,\tau_a}^b = 0 . \tag{3.122}$$

Real Radiation Contribution

In the case of the real radiation contributions one first needs to look into the measurement delta function. With a residual heavy quark momentum k^μ the delta functions from Eqs. (3.68) and (3.69) set the total heavy quark momentum to $p^\mu = (p^+, p^-, \vec{p}^\perp) = (mv^+, mv^-, 0) + (k^+, 0, 0)$. With this we then get for the (leading) measurement of the P-scheme angularities in bHQET[23]:

$$\tau_{a,n}^P = \frac{1}{Q} (mv^- - q^-)^{a-1} \left((mv^+ + k^+ - q^+)(mv^- - q^-) - m^2 \right)^{\frac{2-a}{2}} + \frac{1}{Q} (q^-)^{a-1} \left(q^+ q^- \right)^{\frac{2-a}{2}}$$

$$= \left(\frac{mv^-}{Q} \right)^{a-1} \left[\frac{mv^-}{Q} \frac{k^+}{Q} - \left(\frac{mv^-}{Q} \frac{q^+}{Q} + \frac{mv^+}{Q} \frac{q^-}{Q} \right) \right]^{\frac{2-a}{2}} + \left(\frac{q^-}{Q} \right)^{\frac{a}{2}} \left(\frac{q^+}{Q} \right)^{\frac{2-a}{2}} + \mathcal{O}(\Delta^2/Q^2) . \tag{3.123}$$

---

[22]As a consequence of the heavy quark being on-shell the residual heavy quark momentum is set to zero i.e. $k = 0$ which leads to scaleless integrals.

[23]Same momentum assignment than in SCET, see Fig. 3.1.

Following the procedure lined out for the SCET jet function we find the following for the bHQET case (again with an implicit color trace on the left hand side):

$$(\not{\bar{n}}\gamma_0)_{\alpha\beta} \sum_{\substack{\text{spins} \\ \text{pol}}} (\mathcal{M}_{n,1-\text{jet}}^{\text{Qg}\,\dagger})^\beta (\mathcal{M}_{n,1-\text{jet}}^{\text{Qg}})^\alpha = \frac{\alpha_s C_F}{\pi} 16\pi^2 N_c \tilde{\mu}^{2\varepsilon} \left\{ \frac{2m(v^-)^2}{q^-(v\cdot k)} - \frac{mv^-}{(v\cdot k)^2} \right\}. \tag{3.124}$$

Putting everything together we arrive at the final phase space integrals (dependence on m, Q and μ is implicit) which by using Eq. (3.123) and $t = mv^- k^+$ are given by

$$J_{B,n,\tau_a}^{Qg}(s,m,\mu) = J_{B,n,\tau_a}^c + J_{B,n,\tau_a}^d + \mathcal{O}(\alpha_s^2), \tag{3.125}$$

$$J_{B,n,\tau_a}^c = \frac{\alpha_s C_F}{\pi} \int dt \frac{8\pi\tilde{\mu}^{2\varepsilon}}{t} \int \frac{d^d q}{(2\pi)^d}$$
$$\times (2\pi)^2 \theta(p^0 - q^0)\theta(q^0)\delta((p-q)^2 - m^2)\delta(q^2) \frac{mv^-}{\bar{n}\cdot q} \delta\left\{ s - Q^2 \tau_{a,n}^P \right\}, \tag{3.126}$$

$$J_{B,n,\tau_a}^d = -\frac{\alpha_s C_F}{\pi} m^2 \int dt \frac{8\pi\tilde{\mu}^{2\varepsilon}}{t^2} \int \frac{d^d q}{(2\pi)^d}$$
$$\times (2\pi)^2 \theta(p^0 - q^0)\theta(q^0)\delta((p-q)^2 - m^2)\delta(q^2) \delta\left\{ s - Q^2 \tau_{a,n}^P \right\}. \tag{3.127}$$

NLO Result

The result for the bHQET P-scheme angularities jet function and the corresponding counter term at NLO can then be obtained by evaluating the real radiation integrals (details in App. C.4) and adding them to the tree level contributions from Eq. (3.121). The final result is then given by

$$\mu^2 Z_{B,n,\tau_a}(s,\mu) = \delta(\tilde{s}) + \frac{\alpha_s C_F}{\pi} \left\{ \delta(\tilde{s}) \left[\frac{1}{2(1-a)\varepsilon^2} + \frac{1}{2(1-a)\varepsilon}((1-a)L_m + aL_Q) + \frac{1}{2\varepsilon} \right] \right.$$
$$\left. - \frac{1}{(1-a)\varepsilon} \left[\frac{\theta(\tilde{s})}{\tilde{s}} \right]_+ \right\} + \mathcal{O}(\alpha_s^2), \tag{3.128}$$

$$\mu^2 J_{B,n,\tau_a}(s,m,\mu) = \delta(\tilde{s}) + \frac{\alpha_s C_F}{\pi} \left\{ \delta(\tilde{s}) \left[\frac{1}{4(1-a)}((1-a)L_m + aL_Q)^2 \right. \right.$$
$$\left. + \frac{1}{2}((1-a)L_m + aL_Q) + \frac{1-4a+2a^2}{24(1-a)} \pi^2 \right]$$
$$\left. - \left[\frac{\theta(\tilde{s})}{\tilde{s}} \right]_+ \left[L_m + \frac{a}{1-a} L_Q + 1 \right] + \frac{2}{1-a} \left[\frac{\theta(\tilde{s})\ln\tilde{s}}{\tilde{s}} \right]_+ \right\} + \mathcal{O}(\alpha_s^2), \tag{3.129}$$

with $\tilde{s} = \frac{s}{\mu^2}$, $L_m = \ln\frac{Q^2}{\mu^2}\frac{v^+}{v^-}$ and $L_Q = \ln\frac{Q^2}{\mu^2}$.

Using the natural bHQET jet function variable $\hat{s} = s/(Q\sqrt{v^+/v^-}) = \frac{s}{m}[1 + \mathcal{O}(m^2/Q^2)]$ the above result can be written without explicit logarithms of the form $\ln\frac{m}{\mu}$. It is changed with respect to Ref. [8] where it was defined as $\hat{s} = \frac{s}{m}$. This is the case because here the full kinematical information about the initial heavy quark is included to all orders while in the case of Ref. [8] only the leading order in $\frac{m^2}{Q^2}$ is used.

Since this will only have a very small effect on the overall event shape distribution and in order to be consistent with other contributions for which those subleading corrections are not known (e.g. SCET non-singular - see Sec. 3.6.2) only the leading terms will be used for numerical implementations, hence $\ln\frac{Q^2}{\mu^2}\frac{v^+}{v^-} \to \ln\frac{m^2}{\mu^2}$.

3.5.3 Jet Function for other Event-Shapes

It turns out that using the same procedure as before it is not feasible to calculate the massive M-scheme angularities jet function (for the SCET and the bHQET case). When following the same steps as in Sec. 3.5.1 one first needs to consider the leading contribution to the n-collinear part of the M-scheme angularities which can be written as

$$\tau_{a,n}^M = \frac{1}{Q} \sum_{i \in n} (m_i^\perp) \exp^{-|y_i|(1-a)} = \frac{1}{Q} \sum_i \left(p_i^-\right)^{\frac{a}{2}} \left(p_i^+\right)^{\frac{2-a}{2}} . \tag{3.130}$$

Using this and proceeding as before one will encounter the following delta function in analogy to Eq. (C.7) for the first real radiation diagram:

$$\delta\left\{\left(z + \frac{m^2}{Q^2}\right)^{\frac{2-a}{2}} (1-x)^{a-1} + z^{\frac{2-a}{2}} x^{a-1} - \frac{s}{Q^2}\right\} . \tag{3.131}$$

For the P-scheme case this delta function can be used to carry out the z integration. For the M-scheme case this is not a fruitful approach because it is not possible to find a root of the delta function argument which can be written in terms of simple functions. Furthermore changing the order of integration using it to carry out some other integration does also not lead to a successful calculation of the massive jet function for M-scheme angularities which is therefore considered beyond the scope of this work.

Still it is possible to check that the $a \to 0$ limit, which usually is referred to as the hemisphere mass jet function, can be calculated with the procedure outlined for the P-scheme angularities calculation which works well. The result which first was calculated in Ref. [8] is given in Sec. 3.5.4 and as explained before (up to different threshold positions $e_{\min}$) is closely related to the single hemisphere parts of the M-scheme thrust and C-parameter jet function by the relation $J_{(B),n,\tau^M}(s) = J_{(B),n,\tilde{C}^M}(s) = J_{(B),n,C^M}(s/6)/6 = J_{(B),n,\rho_+^M}(s)$.

3.5.4 The $a \to 0$ Limit

SCET $a \to 0$ Limit: P-scheme Jet Mass

As already pointed out the calculation of the P-scheme angularities jet function allows us to extract the P-scheme jet (hemisphere) mass (and with this trivially the thrust and C-parameter) jet function via the limit $a \to 0$ which can be achieved in a straightforward calculation. The expressions which have to be integrated numerically given in Eqs. (3.116),(3.117) and (3.118) can be solved analytically for this case and with $z = m^2/s$ give

$$\mathcal{I}_1(s;0) = \frac{1 - z + z^2 \ln z}{(1-z)^2} - \frac{(1+z)\ln(1+z)}{z} , \tag{3.132}$$

$$\mathcal{I}_2(s;0) = \frac{z\left(1 - z^2 + 2 z \ln z\right)}{2(1-z)^3} , \tag{3.133}$$

$$\mathcal{I}_3(s;0) = \frac{2 - 4z}{(1-z)^2} - \frac{z^2(1+z)\ln z}{(1-z)^3} - \frac{(2+z)\ln(1+z)}{z} . \tag{3.134}$$

Furthermore the $a \to 0$ limit of the remaining non-distributional parts is also easy to achieve and by

considering

$$\lim_{a\to 0} {}_2F_1\left(1, 1-\frac{a}{2}; 2-\frac{a}{2}; -\frac{m^2}{Q^2}(\frac{Q^2}{s})^{\frac{2}{2-a}}\right) = \frac{s}{m^2}\ln\left(1+\frac{m^2}{s}\right), \tag{3.135}$$

$$\lim_{a\to 0}\left[\frac{2-a}{2}\left(\frac{m^2}{Q^2}\right)^{\frac{a}{2}}\Gamma\left(1-\frac{a}{2}\right)\Gamma\left(\frac{a}{2}\right) - \frac{2-a}{a}\left(\frac{s}{Q^2}\right)^{\frac{a}{2-a}}{}_2F_1\left(1, \frac{a}{2}; 1+\frac{a}{2}; \frac{Q^2}{m^2}\left(\frac{s}{Q^2}\right)^{\frac{2}{2-a}}\right)\right]$$
$$= \ln\left(1+\frac{m^2}{s}\right), \tag{3.136}$$

together with the trivial limit of the distributional contributions we get the primary massive P-scheme jet mass jet function which reads:

$$\mu^2 Z_{J,n,\rho_+^P}(s,\mu) = \delta(\tilde{s}) + \frac{\alpha_s C_F}{\pi}\left\{\delta(\tilde{s})\left[\frac{1}{\varepsilon^2}+\frac{3}{4\,\varepsilon}\right] - \left[\frac{\theta(\tilde{s})}{\tilde{s}}\right]_+\frac{1}{\varepsilon}\right\} + \mathcal{O}(\alpha_s^2), \tag{3.137}$$

$$\mu^2 J_{n,\rho_+^P}(s,m,\mu) = \delta(\tilde{s}) + \frac{\alpha_s C_F}{\pi}\left\{\delta(\tilde{s})\left[\frac{\pi^2}{12}+1+\frac{1}{4}L_m+\frac{1}{2}L_m^2\right] - \left[\frac{\theta(\tilde{s})}{\tilde{s}}\right]_+\left[L_m+1\right]\right. \tag{3.138}$$
$$\left. + 2\left[\frac{\theta(\tilde{s})\ln\tilde{s}}{\tilde{s}}\right]_+ + \theta(\tilde{s})\frac{\mu^2}{4(s-m^2)^3}\left[s\,(s-8m^2)+7m^4-2s\,(2s-5m^2)\ln\frac{s}{m^2}\right]\right\} + \mathcal{O}(\alpha_s^2),$$

with $\tilde{s} = \frac{s}{\mu^2}$ and $L_m = \ln\frac{m^2}{\mu^2}$.

SCET $a \to 0$ Limit: M-scheme Jet Mass

The $a \to 0$ limit for the M-scheme angularities SCET jet function leads to the so-called hemisphere mass SCET jet function which was first calculated in Ref. [8] and is given by

$$\mu^2 Z_{J,n,\rho_+^M}(s,\mu) = \delta(\tilde{s}) + \frac{\alpha_s C_F}{\pi}\left\{\delta(\tilde{s})\left[\frac{1}{\varepsilon^2}+\frac{3}{4\,\varepsilon}\right] - \left[\frac{\theta(\tilde{s})}{\tilde{s}}\right]_+\frac{1}{\varepsilon}\right\} + \mathcal{O}(\alpha_s^2), \tag{3.139}$$

$$\mu^2 J_{n,\rho_+^M}(s,m,\mu) = \delta(\tilde{s}) + \frac{\alpha_s C_F}{\pi}\left\{\delta(\tilde{s})\left[-\frac{\pi^2}{12}+2+\frac{1}{4}L_m+\frac{1}{2}L_m^2\right] - \left[\frac{\theta(\tilde{s})}{\tilde{s}}\right]_+\left[L_m+1\right]\right. \tag{3.140}$$
$$\left. + 2\left[\frac{\theta(\tilde{s})\ln\tilde{s}}{\tilde{s}}\right]_+ + \theta(\tilde{s})\frac{\mu^2}{4}\left[\frac{s-m^2}{s^2} - 4\frac{\ln\frac{s}{m^2}}{s-m^2}\right]\right\} + \mathcal{O}(\alpha_s^2),$$

with $\tilde{s} = \frac{s-m^2}{\mu^2}$ and $L_m = \ln\frac{m^2}{\mu^2}$. When used in the context of the appropriate factorization theorem the full threshold of the considered observable might not coincide with the squared jet mass threshold of m^2/Q^2. To account for that s usually is modified to $s \to s + m^2 - Q^2 e_{\min}^n$ where $e_{\min}^n$ is the n collinear contribution to the full threshold (for jet masses $\rho_{\min}^n = \rho_{\min}$ and for thrust, angularities and C-parameter $e_{\min}^n = e_{\min}/2$).

bHQET $a \to 0$ Limit: P-scheme Jet Mass

The $a \to 0$ limit for the P-scheme angularities bHQET jet function is trivially obtained from Eqs. (3.128) and (3.129) and we get

$$\mu^2 Z_{B,n,\rho_+^P}(s,\mu) = \delta(\tilde{s}) + \frac{\alpha_s C_F}{\pi}\left\{\delta(\tilde{s})\left[\frac{1}{2\,\varepsilon^2}+\frac{1}{2\,\varepsilon}(1+L_m)\right] - \frac{1}{\varepsilon}\left[\frac{\theta(\tilde{s})}{\tilde{s}}\right]_+\right\} + \mathcal{O}(\alpha_s^2), \tag{3.141}$$

$$\mu^2 J_{B,n,\rho_+^P}(s,m,\mu) = \delta(\tilde{s}) + \frac{\alpha_s C_F}{\pi} \Bigg\{ \delta(\tilde{s}) \left[\frac{\pi^2}{24} + \frac{1}{2} L_m + \frac{1}{4} L_m^2 \right]$$

$$- \left[\frac{\theta(\tilde{s})}{\tilde{s}} \right]_+ \left[L_m + 1 \right] + 2 \left[\frac{\theta(\tilde{s}) \ln \tilde{s}}{\tilde{s}} \right]_+ \Bigg\} + \mathcal{O}(\alpha_s^2) , \qquad (3.142)$$

with $\tilde{s} = \frac{s}{\mu^2}$ and $L_m = \ln \frac{Q^2}{\mu^2} \frac{v^+}{v^-}$.

bHQET $a \to 0$ Limit: M-scheme Jet Mass

The $a \to 0$ limit for the M-scheme angularities bHQET jet function leads to the so-called hemisphere mass bHQET jet function which was first calculated in Ref. [8] and is given by

$$\mu^2 Z_{B,n,\rho_+^M}(s,\mu) = \delta(\tilde{s}) + \frac{\alpha_s C_F}{\pi} \Bigg\{ \delta(\tilde{s}) \left[\frac{1}{2\,\varepsilon^2} + \frac{1}{2\,\varepsilon}(1 + L_m) \right] - \frac{1}{\varepsilon} \left[\frac{\theta(\tilde{s})}{\tilde{s}} \right]_+ \Bigg\} + \mathcal{O}(\alpha_s^2) , \qquad (3.143)$$

$$\mu^2 J_{B,n,\rho_+^M}(s,m,\mu) = \delta(\tilde{s}) + \frac{\alpha_s C_F}{\pi} \Bigg\{ \delta(\tilde{s}) \left[-\frac{\pi^2}{8} + 1 + \frac{1}{2} L_m + \frac{1}{4} L_m^2 \right]$$

$$- \left[\frac{\theta(\tilde{s})}{\tilde{s}} \right]_+ \left[L_m + 1 \right] + 2 \left[\frac{\theta(\tilde{s}) \ln \tilde{s}}{\tilde{s}} \right]_+ \Bigg\} + \mathcal{O}(\alpha_s^2) , \qquad (3.144)$$

with $\tilde{s} = \frac{s - Q^2 e_{\min}^n}{\mu^2}$ and $L_m = \ln \frac{Q^2}{\mu^2} \frac{v^+}{v^-}$.

3.5.5 Massless Limit

In this subsection the cross check of taking the massless limit of Eq. (3.120) will be carried out and we expect to arrive at the massless angularities jet function which first was calculated in Ref. [95]. Taking the massless limit directly from Eq. (3.120) is not straightforward since the numerical integrals given in Eq. (3.116), (3.117) and (3.118) are only valid for $m \neq 0$. Since the original integrals were expanded for small ε (dim-reg with $d = 4 - 2\varepsilon$ was used) while assuming a non-zero quarkmass, the mentioned numerical integrals are not regulated properly in the limit $m \to 0$, which is why the calculation has to be done again for the massless case.

It is easy to see that in case of a massless quark the integrals which appear in the calculation of the single quark contribution are scaleless in dim-reg which then leads to

$$\mu^2 J_{n,\tau_a,\mathrm{ml}}^0 = \delta(\tilde{s}) , \qquad (3.145)$$

$$J_{n,\tau_a,\mathrm{ml}}^a = J_{n,\tau_a,\mathrm{ml}}^b = 0 . \qquad (3.146)$$

Including the real radiation contributions $J_{n,\tau_a,\mathrm{ml}}^c$ and $J_{n,\tau_a,\mathrm{ml}}^d$ as calculated in App. C.3 and given in Eq. (C.27) and Eq. (C.28) we find the following result for the massless limit of the NLO primary massive P-scheme angularities jet function and the corresponding counter term:

$$\mu^2 Z_{J,n,\tau_a,\mathrm{ml}}(s,\mu) = \delta(\tilde{s}) \qquad (3.147)$$

$$+ \frac{\alpha_s C_F}{\pi} \Bigg\{ \delta(\tilde{s}) \left[\frac{(1 - a/2)}{(1 - a)} \left(\frac{1}{\varepsilon^2} - \frac{a/2}{(1 - a/2)\,\varepsilon} L_Q \right) + \frac{3}{4\,\varepsilon} \right] - \left[\frac{\theta(\tilde{s})}{\tilde{s}} \right]_+ \frac{1}{(1 - a)\,\varepsilon} \Bigg\} + \mathcal{O}(\alpha_s^2) ,$$

$$\mu^2 J_{n,\tau_a,\mathrm{ml}}(s,\mu) = \delta(\tilde{s}) +$$

$$+ \frac{\alpha_s C_F}{\pi} \Bigg\{ \delta(\tilde{s}) \left[\frac{a^2}{8(1 - a/2)(1 - a)} L_Q^2 + \frac{3a}{8(1 - a/2)} L_Q + f(a) \right] \qquad (3.148)$$

$$- \left[\frac{\theta(\tilde{s})}{\tilde{s}} \right]_+ \left[\frac{1}{2(1 - a/2)} \left(\frac{3}{2} + \frac{a}{1 - a} L_Q \right) \right] + \left[\frac{\theta(\tilde{s}) \ln \tilde{s}}{\tilde{s}} \right]_+ \frac{1}{(1 - a)(1 - a/2)} \Bigg\} + \mathcal{O}(\alpha_s^2) ,$$

44

with $\tilde{s} = s/\mu^2$, $L_Q = \ln \frac{Q^2}{\mu^2}$ and the function $f(a)$ which is given by

$$f(a) = \frac{1}{1 - a/2} \left[\frac{7 - 13a/2}{4} - \frac{\pi^2}{12} \frac{3 - 5a + 9a^2/4}{1 - a} - \int_0^1 \mathrm{d}x \frac{1 - x + x^2/2}{x} \ln \left(x^{1-a} + (1 - x)^{1-a} \right) \right] .$$

This result agrees with the one given in Ref. [95].

3.6 General Setup, Continuity and Non-Singular Contributions

After discussing singular contributions and how factorization theorems can be utilized to resum large logarithms (see Sec. 3.4), as well as the calculation of the NLO jet function needed for most of the discussed event shapes (in Sec. 3.5), let us now focus on how to achieve precise prediction for event shape distributions involving primary massive quarks across the whole range of possible values for the investigated event shapes. For most part the strategy on how to put the different scenarios together and how to include subleading corrections (power corrections in the EFT) was already laid out in Ref. [9] for which $\mu = \mu_j$ was considered. Furthermore in Sec. 3.4.4 different hierarchies of μ and μ_m for different scenarios were discussed. In the following the usual implementation of power corrections via so-called *non-singular* contributions will be reviewed and finally a general factorization formula which covers all event shape values with arbitrary scale hierarchies will be provided.

3.6.1 bHQET Non-Singular

In general the natural choice for the involved scales will be depending on the value of the event shape variable (see Sec. 3.8) itself while the mass scale μ_m will not. For a consistent description of the whole event shape distribution the different scenarios need to be patched together at the point where the hierarchies with respect to μ_m change. For the special case of transitioning from the SCET scenario III to the bHQET scenario, contributions which are power suppressed in the bHQET jet function are commonly omitted, as can be seen from the $\mathcal{O}\left(\frac{P_n^2 - m^2}{m}\right)$ terms in Eq. (3.85). Due to the resulting difference this would then lead to a discontinuous transition at the matching point of the two scenarios. This can be reconciled by defining an adapted bHQET jet function which will automatically account for a smooth matching to the SCET jet function[24] and which is given by

$$J_{B,n,e}^{(n_\ell),\mathrm{sub}}(s, m, \mu) = J_{B,n,e}^{(n_\ell)}(s, m, \mu) + \int \mathrm{d}s' \, J_{n,e,\mathrm{nd}}^{(n_\ell)}(s - s', m, \mu) \left(\mathcal{M}_{J,n}^{(n_\ell+1)} \right)^{-1}(s', m, \mu_m, \mu) , \quad (3.149)$$

where $\mathcal{M}_{J,n}^{(n_\ell+1)}$ is defined in Eq. (3.86) and where $J_{n,e,\mathrm{nd}}^{(n_\ell)}$ is the non-distributional part of the SCET jet function with (n_ℓ) active flavors. The non-distributional part of the SCET jet function is defined by

$$J_{n,e,\mathrm{nd}}^{(n_\ell)} = J_{n,e}^{(n_\ell+1)} - \mathcal{M}_{J,n}^{(n_\ell+1)} \otimes J_{B,n,e}^{(n_\ell)} . \tag{3.150}$$

The second term of Eq. (3.149) now gives the proper power corrections at order α_s including the discussed rapidity logarithms and will remove the mentioned discontinuity. The matching from Eq. (3.85) can now be written as

$$J_{n,e}^{(n_\ell+1)}(s, m, \mu) = \int \mathrm{d}s' \, \mathcal{M}_{J,n}^{(n_\ell+1)}(s - s', m, \mu_m, \mu) J_{B,n,e}^{(n_\ell),\mathrm{sub}}(s', m, \mu) + \mathcal{O}(\alpha_s^2) , \tag{3.151}$$

which is not valid beyond order α_s.

---

[24]Note that this is a slightly different approach than in Ref. [9].

3.6.2 SCET Non-Singular

Very similar to the previous case, terms which are subleading in the SCET power counting will in general be omitted in the EFT although in the tail region they become more and more important as the powercounting parameter $\lambda \sim \mu_j/Q$ becomes larger (and eventually $\lambda \sim \mathcal{O}(1)$). The usual strategy employed in the literature [6, 86, 100] is to calculate the full QCD NLO distribution and subtract the singular contributions evaluated with all scales set to a common scale μ_{ns}:

$$\frac{d\sigma^{\text{nonsing}}}{de} = \frac{d\sigma^{\text{QCD}}}{de} - \frac{d\sigma^{\text{sing}}}{de}\bigg|_{\mu=\mu_s=\mu_j=\mu_h=\mu_{\text{ns}}} . \tag{3.152}$$

In the context of massive heavy quark production in e^+e^- annihilation this was worked out explicitly at one loop for some of the event-shapes of interest, for example 2-jettiness [9, 84, 87] and M-scheme C-parameter [70]. For massless jets also numerical extractions from numerical fixed-order calculations were used at one-loop [101] and also at higher loop order [86, 100].

Especially if one is interested in a general treatment or only an estimate of the non-singular contributions the latter approach is favorable also for the massive case. The analytic calculation for a specific event shape can be quite demanding and in most cases the needed accuracy does not justify the effort. Using a numerical FO calculation, here we use `WHIZARD` [102], it is straightforward to extract the non-singular contributions via Eq. (3.152).
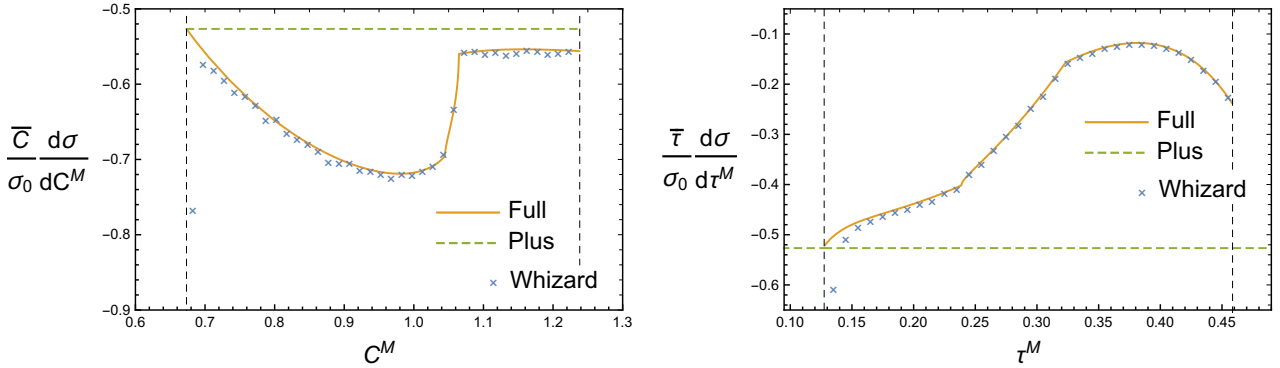

Figure 3.2: The $(\alpha_s C_F/\pi)$ coefficient of the non-singular cross section times $\bar{e} = (e - e_{\text{min}})$ extracted from `WHIZARD` with 10^8 $e^+e^- \to t\bar{t}g$ events (blue crosses) and for comparison the full analytic (orange) and the plus distribution part of the analytic result (green dashed). The kinematical endpoints (for $t\bar{t}g$) e_{min} and e_{max} are also shown (black dashed).

To see that this also works quite well for heavy quark production, let us consider the full result for the non-singular cross section of the M-scheme thrust and C-parameter which is known analytically and compare with the extraction based on a data sample with 10^8 $e^+e^- \to t\bar{t}g$ events from `WHIZARD`. For the singular part of the 2-jettiness differential cross section and for $\tau^M \neq \tau^M_{\text{min}}$ it is straightforward to obtain the following expression:

$$\frac{1}{\sigma_0}\frac{d\sigma^{\text{sing}}}{d\tau^M}(\tau^M, m, \mu = Q) = \frac{\alpha_s C_F}{\pi}\left[-\frac{2}{\bar{\tau}^M}\left(1 + \ln\frac{m^2}{Q^2}\right) - \frac{2}{\bar{\tau}^M}\ln\left(1 + \frac{Q^2}{m^2}\bar{\tau}^M\right) + \frac{\bar{\tau}^M}{2\left(\frac{m^2}{Q^2} + \bar{\tau}^M\right)^2} \right], \tag{3.153}$$

which is the same for the case of M-scheme C-parameter C^M and which uses $\bar{e} = (e - e_{\text{min}})$. The obtained result is illustrated in Fig. 3.2 where we show $\bar{e} \cdot 1/\sigma_0 \cdot d\sigma^{\text{nonsing}}/de$ as extracted from the numerical calculation (blue crosses) and for comparison the analytic result (orange) as well as the part of the analytic result which only involves a plus distribution $(\frac{1}{\bar{e}})_+$ (green dashed).

As expected the numerical FO calculation which is based on a MC integration does not put enough events into the singular phase space region, hence does not sample the distribution in the singular region correctly. Because of that the nonsingular distribution gets more negative than the analytic result. Apart from that (expected) deviation the numerical non-singular cross section is very similar to the full result and the same method could be used for other event-shapes where no analytic result is known or its calculation feasible with reasonable effort.

Note that in the massive case the coefficient of the plus distribution $(\frac{1}{\bar{e}})_+$ in the non-singular cross section is nonzero, i.e. the value of $\bar{e} \cdot d\sigma^{\text{nonsing}}/de$ at $e_{\min}$ is not zero but a constant (see Fig. 3.2). In the massless case one expects no distributions in the non-singular cross section but in the massive case it is possible to have distributions which are formally power suppressed by factors of $\lambda \sim \frac{m}{Q}$. Sometimes it is profitable (with respect to convergence studies) to absorb these distributions into the singular part before resummation which is shown in more detail in Ref. [9].
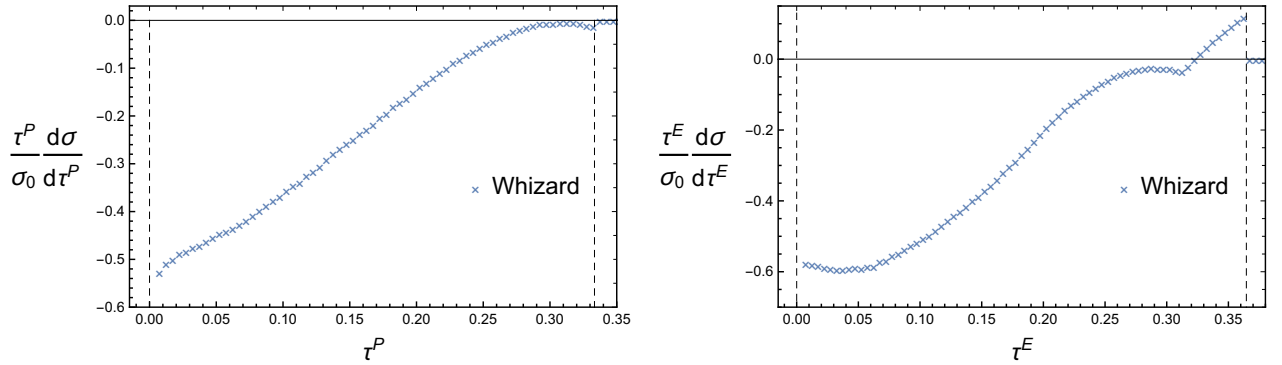

Figure 3.3: The $(\alpha_s C_F/\pi)$ coefficient of the non-singular cross section times $\bar{e} = (e - e_{\min})$ extracted from `WHIZARD` with 10^8 $e^+e^- \to t\bar{t}g$ events (blue crosses). The kinematical endpoints (for $t\bar{t}g$) $e_{\min}$ and $e_{\max}$ (obtained via the last nonzero bin in the numerical FO calculation) are also shown (black dashed)

Using the insights from the case of M-scheme thrust and C-parameter let us next consider the example of P- and E-scheme thrust which will be used in Sec. 5.1. By using the new P/E-scheme thrust jet function of Eq. (3.138) it is easily possible to calculate the singular part of the P-scheme thrust differential cross section to be

$$\frac{1}{\sigma_0}\frac{d\sigma^{\text{sing}}}{d\tau^P}(\tau^P, m, \mu = Q) = \frac{\alpha_s C_F}{\pi}\left[-\frac{2}{\tau^P}\left(1 + \ln\frac{m^2}{Q^2}\right)\right.$$
$$\left. + \frac{1}{2\left(\tau^P - \frac{m^2}{Q^2}\right)^3}\left(\tau^P\left(\tau^P - 8\frac{m^2}{Q^2}\right) + 7\frac{m^4}{Q^4} - 2\tau^P\left(2\tau^P - 5\frac{m^2}{Q^2}\right)\ln\frac{Q^2}{m^2}\tau^P\right)\right], \quad (3.154)$$

which is the same for the case of E-scheme thrust τ^E, simply because the two jet functions are the same.

Using this result it is now straightforward to again extract the non-singular cross section for the mentioned P/E-scheme versions of thrust by comparison with the already mentioned numerical FO calculation. The obtained results are illustrated in Fig. 3.3.

It was already mentioned that for event shapes in the massive case the non singular terms include formally power suppressed distributions, in particular a plus distribution $(\frac{1}{\bar{e}})_+$ and delta function. The plus distribution can be fitted from the numerical FO results by using enough events and the $1/\bar{e}$ behavior for $e \neq e_{\min}$. There are different possibilities to extract the delta function coefficient: (1) Integrating the non-distributional and plus distribution part and subtracting this from the known integrated cross section gives the coefficient of the delta function (although involving only analytic

expressions a similar approach was employed in [70]). (2) It is possible to use the so-called two cutoff phase space slicing method [103] to extract the analytic nonsingular delta function coefficient which was used for 2-jettiness in [9]. Since the focus of this work lies on the peak region and because the P-scheme thrust seems to behave similar to the well studied M-scheme case, for which the singular contributions already give a very good approximation, the SCET non-singular contributions will not be used for any numerical analysis. Because of that, no explicit calculation of the non-singular delta function coefficient is needed at this point.

3.6.3 General Setup

At this point all necessary ingredients to provide a general factorization theorem which covers the whole event shape range and all possible scale hierarchies for the production of primary massive quarks at N²LL+NLO have been collected and discussed. The general factorization theorem which is formulated in analogy to the ones stated in Sec. 3.4.2 reads

$$\frac{1}{\sigma_0}\frac{\mathrm{d}\sigma}{\mathrm{d}e} = Q\,H(Q,\mu_h)\,U_H(Q,m,\mu_h,\mu)$$

$$\times\left[U_J(s,m,\mu,\mu_j)\otimes J_e(s,m,\mu_j)\otimes U_s(\ell,m,\mu,\mu_s)\otimes S_e(\ell,m,\mu_s)\right] + \frac{1}{\sigma_0}\frac{\mathrm{d}\sigma^{\mathrm{nonsing}}}{\mathrm{d}e}\,. \tag{3.155}$$

It is clear that this factorization theorem again involves all the factors which appeared before. The generalized hard, jet and soft function as well as the non-singular cross section is given by:

- Hard function: always above the mass scale, thus defined with $(n_\ell + 1)$ active flavors and reads

$$H(Q,\mu_h)\equiv H^{(n_\ell+1)}(Q,\mu_h) \tag{3.156}$$

- Generalized jet function: again defined via $J_e = J_{n,e}\otimes J_{\bar{n},e}$ and given by

$$J_e(s,m,\mu_j) = \begin{cases} J_e^{(n_\ell+1)}(s,m,\mu_j) & (\mu_j > \mu_m) \\ J_{B,e}^{(n_\ell),\mathrm{sub}}(s,m,\mu_j) & (\mu_m > \mu_j) \end{cases} \tag{3.157}$$

  where $J_{B,e}^{(n_\ell),\mathrm{sub}}(s,m,\mu_j)$ now includes the bHQET non-singular contributions (see Sec. 3.6.1).

- Generalized soft function:

$$S_e(\ell,\mu_s) = \begin{cases} S_e^{(n_\ell+1)}(\ell,\mu_s) & (\mu_s > \mu_m) \\ S_e^{(n_\ell)}(\ell,\mu_s) & (\mu_m > \mu_s) \end{cases} \tag{3.158}$$

- SCET non-singular cross section: incorporates formally power suppressed contributions and was discussed in detail in Sec. 3.6.2.

Additionally the factorization theorem also involves evolution kernels which take care of resumming large logarithms. These might involve an additional matching coefficient when crossing the mass scale and are given by:

- Hard function evolution kernel:

$$U_H(Q,m,\mu_h,\mu) = \begin{cases} U_H^{(n_\ell+1)}(Q,\mu_h,\mu) & (\mu > \mu_m) \\ U_H^{(n_\ell+1)}(Q,\mu_h,\mu_m)\,H_M^{(n_\ell+1)}(m,\mu_m)\,U_M^{(n_\ell)}(\frac{Q}{m},\mu_m,\mu) & (\mu_m > \mu) \end{cases} \tag{3.159}$$

48

- Jet function evolution kernel:

$$
U_J(s, m, \mu, \mu_j) = \begin{cases}
U_J^{(n_\ell+1)}(\mu, \mu_j) & (\mu, \mu_j > \mu_m) \\
U_J^{(n_\ell+1)}(\mu_j, \mu_m) \otimes \left[\mathcal{M}_J^{(n_\ell+1)}(m, \mu_m)\right]^{-1} \otimes U_J^{(n_\ell)}(\mu_m, \mu) & (\mu_j > \mu_m > \mu) \\
U_J^{(n_\ell+1)}(\mu, \mu_m) \otimes \mathcal{M}_J^{(n_\ell+1)}(m, \mu_m) \otimes U_J^{(n_\ell)}(\mu_m, \mu_j) & (\mu > \mu_m > \mu_j) \\
U_J^{(n_\ell)}(\mu, \mu_j) & (\mu_m > \mu, \mu_j)
\end{cases}
\tag{3.160}
$$

- Soft function evolution kernel:

$$
U_S(\ell, m, \mu, \mu_s) = \begin{cases}
U_S^{(n_\ell+1)}(\mu, \mu_s) & (\mu, \mu_s > \mu_m) \\
U_S^{(n_\ell+1)}(\mu_s, \mu_m) \otimes \left[\mathcal{M}_S^{(n_\ell+1)}(m, \mu_m)\right]^{-1} \otimes U_S^{(n_\ell)}(\mu_m, \mu) & (\mu_s > \mu_m > \mu) \\
U_S^{(n_\ell+1)}(\mu, \mu_m) \otimes \mathcal{M}_S^{(n_\ell+1)}(m, \mu_m) \otimes U_S^{(n_\ell)}(\mu_m, \mu_s) & (\mu > \mu_m > \mu_s) \\
U_S^{(n_\ell)}(\mu, \mu_s) & (\mu_m > \mu, \mu_s)
\end{cases}
\tag{3.161}
$$

Note that, to save space, for the jet and soft function evolution kernel we have omitted the arguments s and ℓ, that appear in each factor on the right hand side.

3.7   Non-perturbative Corrections and Gap Formalism

Up to this point only partonic final states were discussed, while in experiments hadronic final states are detected. To describe such realistic final states one has to account for non-perturbative effects of QCD. Since it is not known how to calculate them from first principles, we adopt the approach to employ models to account for such hadronization effects.

In the context of event shape distributions a versatile and widely used approach is based on using a so-called *shape function* [104] $F_e^{\mathrm{mod}}(e)$ (also *model function*) which depends on the observable of interest and at leading order should not depend on any hard scale, e.g. the mass of a heavy quark, due to the wide separation of relevant scales i.e. $m \gg \Lambda_{\mathrm{QCD}}$. For event shapes the shape function typically is implemented in terms of a convolution with the partonic cross section. The hadron level cross section is then given by

$$
\frac{\mathrm{d}\sigma}{\mathrm{d}e} = \int \mathrm{d}e' \, \frac{\mathrm{d}\sigma^{\mathrm{part}}}{\mathrm{d}e}(e - e') \, F_e^{\mathrm{mod}}(e') \,,
\tag{3.162}
$$

but it is more common to use a dimensionful model $S_e^{\mathrm{mod}}(\ell) = F_e^{\mathrm{mod}}(\ell/Q)/Q$. Using this soft model function the shape function is then absorbed into the soft function as follows [8, 105]:

$$
S_e(\ell) = \int \mathrm{d}\ell' \, S_{\mathrm{part},e}(\ell, \mu) \, S_e^{\mathrm{mod}}(\ell) \,.
\tag{3.163}
$$

Furthermore it is possible to perform an operator product expansion (OPE) for the tail region of the soft function which is given by [100]

$$
S_e(\ell, \mu) = S_e^{\mathrm{part}}(\ell, \mu) - \frac{\mathrm{d}S_e^{\mathrm{part}}(\ell, \mu)}{\mathrm{d}\ell} \, \overline{\Omega}_1^e + \dots \,,
\tag{3.164}
$$

with $\overline{\Omega}_1^e$ the first moment of the soft model function given by $\overline{\Omega}_1^e = \int d\ell\, \ell\, S_e^{\mathrm{mod}}(\ell)$. In absence of hadron mass effects this first moment is proportional to a universal non-perturbative matrix element common to all event shapes [106] and related to it by a calculable coefficient. Using this it is possible to relate the first moment of the soft model for different event shape observables to the one of thrust[25] in the following way:

$$\overline{\Omega}_1^{\tilde{C}} = \overline{\Omega}_1^C /6 = \frac{\pi}{4}\,\overline{\Omega}_1^\tau \,, \qquad\qquad \overline{\Omega}_1^{\tau_a} = \frac{1}{1-a}\,\overline{\Omega}_1^\tau \,. \tag{3.165}$$

As a parametrization for the soft model function several different versions were used in the past. Originally a physically reasonable function with a few free parameters was setup and subsequently fitted to data. Alternatively one can for example use the ansatz of Ref. [107] where a linear combination of N (in principle infinitely many) basis functions[26] is used. The general ansatz is given by

$$\hat{S}_e^{\mathrm{mod}}\big(\ell,\xi,p,\{c_i^e\}\big) = \frac{1}{\xi}\left[\sum_{n=0}^{N} c_n^e\, f_n\Big(p,\frac{\ell}{\xi}\Big)\right]^2 \,, \tag{3.166}$$

where the involved basis functions are given in terms of Legendre polynomials P_n by

$$f_n(p,x) = \sqrt{\frac{(2n+1)\,x^p\,(1+p)^{1+p}}{\Gamma(1+p)}}\,\exp\left(-\frac{1+p}{2}\,x\right) P_n\big(y(p,x)\big)\,, \tag{3.167}$$

$$y(p,x) = 1 - 2\,\exp\big(-(1+p)\,x\big)\sum_{i=0}^{p}\left[\frac{(1+p)^i}{\Gamma(i+1)}\,x^i\right]\,. \tag{3.168}$$

With $\sum_i (c_i^e)^2 = 1$ this model function is normalized to 1, positive definite, has support for $(0,\infty)$ and fulfills $\hat{S}_e^{\mathrm{mod}}(0) = 0$. This type of shape function was used in the version where $p = 3$ in a variety of investigations among others also in Refs. [6, 86, 100]. Often also the most simple example which is further specified by $\{c_0 = 1, c_{i\neq 0} = 0\}$ is useful as a test-model and as such it will be used in Sec. 5.3.2. For this case the parameter ξ can be interpreted as the first moment which means

$$\Omega_1^{c_0=1} = \xi\,. \tag{3.169}$$

Historically the shape function has support for $(0,\infty)$ but it turns out that implementing a so-called *gap* Δ which simply is a shift of the model function i.e. $S_e^{\mathrm{mod}}(\ell) \to S_e^{\mathrm{mod}}(\ell-\Delta)$ has several advantages. In terms of the observable this gap can be interpreted as the minimal hadronic energy deposit (e.g. at least two pions for e^+e^- annihilation) and since it needs to be fitted to experimental data anyways it can be used to absorb the leading IR renormalon of the soft function.

3.7.1 Soft Function Renormalon

The already discussed $\mathcal{O}(\Lambda_{\mathrm{QCD}})$ pole mass renormalon (see Sec. 2.2) enters in the result for the massive quark jet function. It is easy to avoid the pathological asymptotic factorial growth, which also at low orders can spoil the perturbative convergence, by using a so-called short distance mass scheme such as the $\overline{\mathrm{MS}}$ or MSR mass[27]. Apart from the pole mass renormalon one also finds an $\mathcal{O}(\Lambda_{\mathrm{QCD}})$ IR

---

[25]For now hadron mass effects (see Ref. [73]) are neglected, thus distinguishing different mass schemes is not necessary.

[26]In the end one of course still only wants to fit for a small number of free parameters. This is why the basis functions are chosen (from experience) so that for the used observables the leading basis function covers already most of the relevant shape. This is then systematically improvable by including more and more of the basis functions.

[27]Which short distance mass scheme is producing the best perturbative convergence depends on the observable. When using effective field theory it is additionally important to make sure that the induced subtractions are compatible with the power counting of the theory.

renormalon in the soft function usually referred to as the soft renormalon. To see this let us use the rescaled M-scheme C-parameter (given by $\tilde{C}^M = C^M/6$) as an example and have a closer look at the perturbative soft function calculation. Considering the two non-zero diagrams (which correspond to the two diagrams given in Fig. 3.4 without the bubble insertions) one finds [70, 86]

$$\mu S_{\tilde{C}^M}(\ell, \mu) = \delta(\tilde{\ell}) + 32\,\pi^2 (\mathrm{e}^{\gamma_E})^\varepsilon \frac{\alpha_s C_F}{\pi} \int \frac{\mathrm{d}^d \tilde{k}}{(2\pi)^d} \operatorname{Im}\left[\frac{1}{-\tilde{k}^2 - i0}\right] \frac{\theta(\tilde{k}^0)}{\tilde{k}^+ \tilde{k}^-} \delta\left(\ell - \frac{\tilde{k}^+ \tilde{k}^-}{\tilde{k}^+ + \tilde{k}^-}\right) + \mathcal{O}(\alpha_s^2) \tag{3.170}$$

with $\tilde{\ell} = \ell/\mu$ as well as $\tilde{k} = k/\mu$ and where the imaginary part of the gluon propagator enforces the on-shellness of the gluon. Calculating the result leads to the expressions already given in Eqs (3.59) and (3.61).
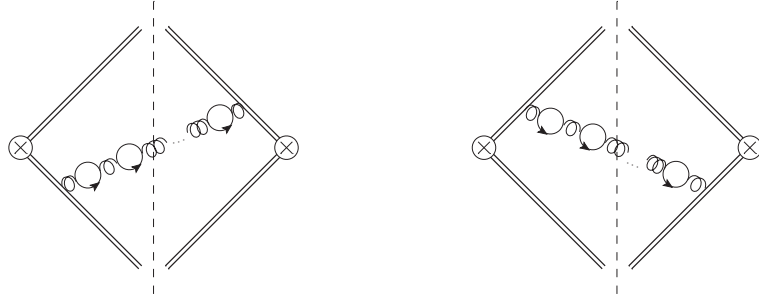

Figure 3.4: Diagrams contributing to the soft function with bubble chain insertion which are non-zero. Furthermore the same diagrams without the inserted fermionic bubbles are the only non-zero one-loop integrals contributing to the soft function (for more details see for example [70]).

Next we look at the Borel transform of the sum of soft function diagrams with insertions of all orders of bubble chain gluon propagators (also see Eq. (B.3)). For this situation the relevant types of diagrams are shown in Fig. 3.4. As we have seen in Sec. 2.2 it is useful to use the Borel transform of the gluon propagator to obtain the Borel transform of the whole quantity of interest. Following Ref. [105] and as long as the measurement is inclusive with respect to the massless quark bubbles it is sufficient to take the calculation from Eq. (3.170) and replace the intermediate gluon propagator with the Borel transformed gluon bubble chain propagator from Eq. (B.3). The Borel transform of the rescaled M-scheme C-parameter soft function with bubble chain insertion (therefore the tree level is not contained - superscript (1)) is then given by

$$B\big[\mu S^{(1)}_{\tilde{C}^M}(\ell, \mu)\big](u) = \frac{4C_F}{\beta_0} \frac{(\mathrm{e}^{\gamma_E})^\varepsilon}{\Gamma(1-\varepsilon)} \tag{3.171}$$

$$\times \int \mathrm{d}\tilde{k}^+ \mathrm{d}\tilde{k}^- \operatorname{Im}\left[\int_0^\infty \mathrm{d}(\tilde{k}_\perp^2) \frac{(\tilde{k}_\perp^2)^{-\varepsilon}}{\left[\tilde{k}_\perp^2 - (\tilde{k}^+ \tilde{k}^- + i0)\right]^{1+u}}\right] \frac{\mathrm{e}^{\frac{5u}{3}}}{\pi} \frac{\theta(\tilde{k}^+ + \tilde{k}^-)}{\tilde{k}^+ \tilde{k}^-} \delta\left(\ell - \frac{\tilde{k}^+ \tilde{k}^-}{\tilde{k}^+ + \tilde{k}^-}\right),$$

where $\mathrm{d}^d k = \frac{1}{4} \mathrm{d}\Omega^{d-2}_{\mathrm{tot}} \mathrm{d}k^- \mathrm{d}k^+ \mathrm{d}(k_\perp^2)(k_\perp^2)^{-\varepsilon} \theta(k_\perp^2)$ with $k_\perp = |\vec{k}_\perp|$ was used and again with $\tilde{\ell} = \ell/\mu$ and $\tilde{k} = k/\mu$. Taking the involved imaginary part which is given by

$$\operatorname{Im}\left[\int_0^\infty \mathrm{d}(\tilde{k}_\perp^2) \frac{(\tilde{k}_\perp^2)^{-\varepsilon}}{\left[\tilde{k}_\perp^2 - (\tilde{k}^+ \tilde{k}^- + i0)\right]^{1+u}}\right] = \frac{(\tilde{k}^+ \tilde{k}^-)^{-\varepsilon-u}\,\Gamma(1-\varepsilon)\,\pi}{\Gamma(1+u)\Gamma(1-\varepsilon-u)}, \tag{3.172}$$

the remaining integrations are trivial and the final result reads

$$B\big[\mu S^{(1)}_{\tilde{C}^M}(\ell, \mu)\big](u) = \frac{4C_F}{\beta_0} \frac{(\mathrm{e}^{\gamma_E})^\varepsilon \mathrm{e}^{\frac{5u}{3}} \mathrm{B}(\varepsilon + u, \varepsilon + u)}{\Gamma(1+u)\Gamma(1-\varepsilon-u)} \tilde{\ell}^{-1-2u-2\varepsilon}, \tag{3.173}$$

51

with the Beta function $B(a, b) = \frac{\Gamma(a)\Gamma(b)}{\Gamma(a+b)}$. As expected this result gives the one loop result for $u = 0$ where $\varepsilon \neq 0$ regularizes the contained UV divergences (also the additional factor $\frac{\alpha_s \beta_0}{4\pi}$ needs to be included to recover the correct gluon propagator). Investigating the result for $u \neq 0$ and $\varepsilon = 0$ one finds that the renormalon poles are now contained in the distributive structure. The leading renormalon pole is again situated at $u = \frac{1}{2}$ and in terms of distributions given by

$$\tilde{\ell}^{-1-2u}\Big|_{u=\frac{1}{2}} = \frac{1}{2(u - \frac{1}{2})}\delta'(\tilde{\ell}) + \mathcal{O}((u - \frac{1}{2})^0) . \tag{3.174}$$

Furthermore the subleading renormalon poles[28] are situated at $u = (2k+1)/2$ with $k \in \mathbb{N}$ and in general are connected to derivatives of the delta function by

$$\tilde{\ell}^{-1-2u}\Big|_{u=\frac{2k+1}{2}} = -\frac{(-1)^{2k+1}}{2(2k+1)!(u - \frac{2k+1}{2})}\delta^{(2k+1)}(\tilde{\ell}) + \mathcal{O}((u - \frac{2k+1}{2})^0) . \tag{3.175}$$

It is even more illustrative to look at the logarithm of the Fourier transform of the partonic soft function with bubble chain insertions (including tree level) $\tilde{S}(y) = \mathcal{F}(S(\ell)) = \int d\ell \exp(-iy\ell) S(\ell)$ and subsequently take the Borel transform of the leading term of $\ln \tilde{S}_{CM}$. From this we get

$$B\left[\ln \tilde{S}_{CM}(y, \mu)\right](u) = \frac{4C_F}{\beta_0} \frac{e^{\frac{5u}{3}} \Gamma(u)^2 \Gamma(-2u)}{\Gamma(1+u)\Gamma(1-u)\Gamma(2u)} (iy\mu)^{2u} . \tag{3.176}$$

In this expression the poles and also the distributive structure is now explicit for different values of u when taking into account that the Fourier transform of the derivatives of the delta function is given by $\mathcal{F}(\delta^{(n)}(\ell))(y) = (iy\mu)^n$.

Note for the interested reader: the result of the analog calculation for the collinear-soft function where the soft drop groomed jet mass is measured, shows that the corresponding leading soft renormalon is situated between $(\frac{1}{2}, 1)$ depending on how strong the grooming is performed. Details as well as the mentioned calculation are given in App. D

3.7.2 Gap Formalism

The already mentioned gap parameter Δ of the soft model function can now be used (following Refs. [100, 105]) to absorb the pathological renormalon behavior and thereby render the soft function free of the leading renormalon. After introducing a gap the full soft function is given by

$$S_e(\ell, \mu_s) = \int d\ell' S_e^{\text{part}}(\ell - \ell', \mu_s) S_e^{\text{mod}}(\ell' - \Delta) = \int d\ell' S_e^{\text{part}}(\ell' - \Delta, \mu_s) S_e^{\text{mod}}(\ell - \ell') \tag{3.177}$$

Next the gap parameter is split in a non-perturbative part $\overline{\Delta}$ (which still has to be determined from data) and a subtraction which can be written as a perturbative series δ_e which is designed to cancel the pathological renormalon behavior. The exact form of δ_e is scheme dependent and not unique. The resulting form of Δ then reads

$$\Delta = \overline{\Delta}(R_\Delta, \mu_s) + \delta_e(R_\Delta, \mu_s) , \tag{3.178}$$

where μ_s is the scale of the partonic soft function and R_Δ is the subtraction scale at which this relation is defined.

---

[28] Naively one would also find poles in the distributive structure at integer values for u but this gets canceled by the $1/\Gamma(1-u)$ in the prefactor giving a finite result.

A convenient definition for δ_e, called *gap subtraction* has been proposed in Refs. [42, 105] and reads:

$$\delta_e(R_\Delta, \mu_s) = R_\Delta \, e^{\gamma_E} \left[\frac{d}{d \ln(iy)} \ln \tilde{S}_e^{\text{part}}(y, \mu_s) \right]_{y = (iR_\Delta \, e^{\gamma_E})^{-1}} , \tag{3.179}$$

which is suggested by the form of the inverse Fourier transform of the partonic soft function given by

$$S_e^{\text{part}}(\ell' - \Delta, \mu_s) = \int dy \, \exp \left[iy(\ell' - \overline{\Delta}(R_\Delta, \mu_s)) + \ln \tilde{S}_e^{\text{part}}(y, \mu_s) - iy \, \delta_e(R_\Delta, \mu_s) \right] . \tag{3.180}$$

Using this together with Eq. (3.176) it is clear that for the example of M-scheme C-parameter the renormalon pole at $u = \frac{1}{2}$ cancels:

$$B \left[\ln \tilde{S}_{CM}^{\text{part}}(y, \mu_s) - iy \, \delta_{CM}(R_\Delta, \mu_s) \right]_{u = \frac{1}{2}}$$

$$= \frac{4C_F}{\beta_0} \frac{e^{\frac{5u}{3}} \Gamma(u)^2 \Gamma(-2u)}{\Gamma(1+u)\Gamma(1-u)\Gamma(2u)} \mu^{2u} \left[(iy)^{2u} - 2u \, iy \left(R_\Delta \, e^{\gamma_E} \right)^{1-2u} \right]_{u = \frac{1}{2}} = 0 . \tag{3.181}$$

Additionally we note that for other event shapes the same type of subtraction will successfully cancel the renormalon associated with the $\delta'(\ell)$ which in this case lies at $u = \frac{1}{2}$ (an example with $u \neq \frac{1}{2}$ can be found in App. D). We note that any occurring (subleading) renormalons associated with higher derivatives of $\delta(\ell)$ will not be sufficiently treated by a simple subtraction implemented in the gap of the soft model function.

The gap subtraction can be written as a perturbative series as follows:

$$\delta_e(R_\Delta, \mu_s) = R_\Delta e^{\gamma_E} \sum_{n=1} \delta_{e,n}(R_\Delta, \mu_s) \left(\frac{\alpha_s C_F}{4\pi} \right)^n , \tag{3.182}$$

where for event shapes like thrust, the rescaled C-parameter $\tilde{C} = C/6$ or angularities the first two orders are given by [70]

$$\delta_{e,1} = 2\Gamma_{s,0} \, L_{\mu R} , \tag{3.183}$$

$$\delta_{e,2} = 2 \, s_1^e \, \beta_0 + \gamma_{s,1} + 2 \, \Gamma_{s,1} L_{\mu R} + 2 \, \beta_0 \, \Gamma_{s,0} \, L_{\mu R}^2 , \tag{3.184}$$

with $L_{\mu R} = \log(\mu_s / R_\Delta)$ and $\Gamma_{s,i}$ denoting the cusp and $\gamma_{s,i}$ the non-cusp anomalous dimension of the soft function which was defined in Eq. (3.77). Furthermore s_1^e corresponds to the one loop constant term of the Fourier transform of the partonic soft function divided by $\alpha_s C_F / (4\pi)$. For the different event shapes of interest this coefficient is given by

$$s_1^{\tau_a} = -\frac{\pi^2}{(1-a)} , \qquad s_1^\tau = -\pi^2 , \qquad s_1^{\tilde{C}} = -\frac{\pi^2}{3} . \tag{3.185}$$

In the literature [86, 100] a reference value for the gap parameter $\overline{\Delta}(R_\Delta, \mu_s)$ is often defined at low perturbative scales e.g. $R_{\Delta,0} = \mu_{s,0} = 2$ GeV. Since this parameter enters the factorization theorem at different scales (see Sec. 3.8), one needs to evolve the gap in μ_s and R_Δ. Similar to the MSR mass (see Sec. 2.3) the gap parameter $\overline{\Delta}(R_\Delta, \mu_s)$ has non trivial renormalization group flow in R_Δ. The evolution in μ_s and R_Δ can be expressed in terms of the following RGE equations:

$$\frac{d\overline{\Delta}(R, \mu)}{d \ln \mu} = -R \, \gamma_{\overline{\Delta}}^\mu \left[\alpha_s(\mu) \right] , \qquad \gamma_{\overline{\Delta}}^\mu \left[\alpha_s(\mu) \right] = \sum_{i=0} \gamma_{\overline{\Delta},n}^\mu \left(\frac{\alpha_s(\mu) C_F}{4\pi} \right)^{n+1} , \tag{3.186}$$

$$\frac{d\overline{\Delta}(R, R)}{d \ln R} = -R \, \gamma_{\overline{\Delta}}^R \left[\alpha_s(R) \right] , \qquad \gamma_{\overline{\Delta}}^R \left[\alpha_s(R) \right] = \sum_{i=0} \gamma_{\overline{\Delta},n}^R \left(\frac{\alpha_s(R) C_F}{4\pi} \right)^{n+1} . \tag{3.187}$$

For the gap parameter the μ evolution is completely governed by the μ evolution of the partonic soft function and for the R_Δ evolution the first two anomalous dimension coefficients are given by

$$\gamma^R_{\Delta,0} = 0 \,, \qquad\qquad\qquad \gamma^R_{\Delta,1} = \mathrm{e}^{\gamma_E}\left(2\,s^e_1\,\beta_0 + \gamma_{s,1}\right) \,. \qquad\qquad (3.188)$$

These evolution equations can be solved numerically or analytically as shown in Refs. [43, 44]. The solution of the μ_s and R_Δ evolution equations of $\overline{\Delta}(R_\Delta,\mu_s)$ at NNLL from $(R_{\Delta,0},\mu_{s,0})$ to (R_Δ,μ_s) is then given by

$$\overline{\Delta}(R_\Delta,\mu_s) = \overline{\Delta}(R_{\Delta,0},\mu_{s,0}) - 2\,R_{\Delta,0}\,\mathrm{e}^{\gamma_E}\,\omega^{\mathrm{NLL}}(R_{\Delta,0},\mu_{s,0},\Gamma_s,2) - 2\,R_\Delta\,\mathrm{e}^{\gamma_E}\,\omega^{\mathrm{NLL}}(\mu_s,R_\Delta,\Gamma_s,2)$$
$$- \Lambda^{\mathrm{NNLL}}_{\mathrm{QCD}}\,S_1\,\mathrm{e}^{i\pi\hat{b}_1}\left[\Gamma\left(-\hat{b}_1 - 1,-\frac{2\pi}{\beta_0\,\alpha_s(R_\Delta)}\right) - \Gamma\left(-\hat{b}_1 - 1,-\frac{2\pi}{\beta_0\,\alpha_s(R_{\Delta,0})}\right)\right] \,,$$
$$(3.189)$$

with $\hat{b}_i$ already given in Eq. (2.16), $S_1 = \gamma^R_{\Delta,1}/(2\beta_0)^2$ and $\Lambda^{\mathrm{NNLL}}_{\mathrm{QCD}}$ which is given by [43]

$$\Lambda^{\mathrm{NNLL}}_{\mathrm{QCD}} = R_\Lambda \exp\left(-\frac{2\pi}{\beta_0\,\alpha_s(R_\Lambda)}\right)\left(\frac{2\pi}{\beta_0\,\alpha_s(R_\Lambda)}\right)^{\hat{b}_1}\exp\left(\frac{\hat{b}_2\,\beta_0\,\alpha_s(R_\Lambda)}{2\pi}\right) \,. \qquad (3.190)$$

where the choice $R_\Lambda = 100$ GeV is typical for numerical implementations. Furthermore note that since the evolution function ω does not appear in the exponential as it does for the μ evolution of cross section factors as given in Eq. (3.80), ω^{NLL} is sufficient at NNLL.

3.8 Profile Functions

In fixed order perturbation theory it is well known that one needs to choose a scale and appropriate variations to obtain a result with reliable theoretical uncertainties. A good scale choice is usually characterized by minimizing the logarithms which appear in perturbative results. This of course only works well for problems involving a single scale but not if several well separated characteristic scales appear which will then lead to large logarithms. Already when discussing the resummation of large logarithms by using factorization theorems and connected renormalization group evolution it became clear that for the individual cross section factors a suitable scale choice is necessary to achieve properly convergent cross section predictions. Furthermore we note that the logarithms which appear in the factors of the factorization theorem depend on the value of corresponding typical kinematical scales which in general will depend on the event kinematics, hence depend on the event shape value itself. This means that for resummed cross section calculations the problem of choosing an appropriate scale now is generalized to finding an appropriate function for all μ_i's appearing in functions of factorization theorems which are usually called *profile function*.

For event shapes involving massless particles appropriate profile functions have been constructed for example in Refs. [86, 100]. From those investigations one can see that the natural scaling for the involved hard, jet and soft scale in the different regions is given by

$$
\begin{array}{llll}
\text{peak:} & \mu_h \sim Q \,, & \mu_j \sim \sqrt{\Lambda_{\mathrm{QCD}}\,Q} \,, & \mu_s \sim \Lambda_{\mathrm{QCD}} \,, \\
\text{tail:} & \mu_h \sim Q \,, & \mu_j \sim Q\sqrt{e} \,, & \mu_s \sim Q\,e \,, \\
\text{far-tail:} & \mu_h = \mu_j = \mu_s \sim Q \,,
\end{array}
\qquad (3.191)
$$

which is determined by the typical scale appearing in the corresponding cross section factors. The scaling in the peak region represents the fact that this region is dominated by nonperturbative physics which is why usually the perturbative scales will be frozen at a perturbative value (i.e. $\gtrsim 1$ GeV) when

entering the peak region. Furthermore in the far tail one needs to make sure to recover the full fixed order result where all scales are joined together at the hard scale.

In between those regions an "interpolation" function is used which ensures that the resulting profile function is continuous and has a continuously differentiable transition between the different regions. For this purpose we will subsequently use a double quadratic function. As the name suggests, it is made of two quadratic functions which are joined in the middle (also continuous and continuously differentiable). This transition function which is denoted by $\zeta(a_1, a_2; b_1, b_2)$ is completely defined by the two linear functions $f_1(x) = a_2 x + a_1$ and $f_2(x) = b_2 x + b_1$, giving the value and first derivative at the start and end point of the transition, respectively (more details on this can be found in Ref. [9]).

The soft scale profile function for the massless case is then given by [86, 100]

$$
\mu_s(e) = \begin{cases}
\mu_0 & (e \leq e_0) \\
\zeta(\mu_0, 0; 0, \mu_h r_s) & (e_0 < e \leq e_1) \\
\mu_0 r_s e & (e_1 < e \leq e_2) \\
\zeta(0, \mu_h r_s; \mu_h, 0) & (e_2 < e \leq e_s) \\
\mu_h & (e_s < e)
\end{cases}
\tag{3.192}
$$

with the hard scale $\mu_h = \varepsilon_h Q$, the transition points $e_0(Q) = n_0/Q$, $e_1(Q) = n_1/Q^\beta$, e_2 as well as e_s and the slope in the canonical region $r_s = r_{\mathrm{ml}} (1 + \varepsilon_s)$. The gap scale R_Δ and jet scale μ_j for the massless case are based on the soft scale via the following relation:

$$
R_\Delta(e) = \begin{cases}
R_0 & (0 < e \leq e_0) \\
\zeta(R_0, 0; 0, \mu_h r_s) & (e_0 < e \leq e_1) \\
\mu_s(e) & (e_1 < e)
\end{cases}
\tag{3.193}
$$

$$
\mu_j(e) = \begin{cases}
\left[1 + \varepsilon_j \left(e_s - e \right)^2 \right] \sqrt{\mu_h \, \mu_s(e)} & (e \leq e_s) \\
\mu_h & (e_s < e)
\end{cases}
\tag{3.194}
$$

From Refs. [86, 100] and Ref. [9] one can see that this parametrization and the corresponding parameter choices[29] shown in Tab. 3.4 lead to a well convergent perturbative result over the whole cross section region for the case of massless thrust and C-parameter. To estimate the uncertainty from higher orders in the nonsingular contributions the uncertainty is estimated by varying the nonsingular scale in the following way:

$$
\mu_{\mathrm{ns}}(e) = \begin{cases}
\left(\mu_h + \mu_j(e) \right)/2 & (n_{\mathrm{ns}} = -1) \\
\mu_h & (n_{\mathrm{ns}} = 0) \\
\left(3\mu_h - \mu_j(e) \right)/2 & (n_{\mathrm{ns}} = 1)
\end{cases}
\tag{3.195}
$$

The case of primary massive stable (and to some extent also unstable) quarks was investigated for the case of 2-jettiness in Ref. [9] and it is straightforward to extend this to other event shapes. For

---

[29]Due to the fact that between Ref. [100] and [9] the parametrization changed from $e_1 = n_1/Q$ to $e_1 = n_1/Q^\beta$ with $\beta = 3/4$ also the default value for n_1 changed which in the case of thrust led to the new default value of 2.25 GeV compared to the old one of 10 GeV. To account for this change in the case of C-parameter we changed the default value so that we get the same ratio between the old and new value as for thrust which gives $25/10 * 2.25\,\mathrm{GeV} = 5.625\,\mathrm{GeV}$.

this case the jet scale needs to be generalized for $\mu_j < \mu_m = \sqrt{\varepsilon_h}\, m$ to account for the characteristic scaling of the bHQET jet scale given by

$$\mu_{jB} = \frac{\mu_h\, \mu_s(e)}{\mu_m} \; .$$

(3.196)

The generalized massive jet scale can then be written as

$$\mu_j^m(e) = \begin{cases} \mu_{jB}(e) & (\mu_j(e) \leq \mu_m) \\ \mu_j(e) & (\mu_m < \mu_j(e)) \end{cases}$$

(3.197)

To account for the additional freedom of the heavy quark mass the parametrization from Eqs. (3.192), (3.193) and (3.194) needs to be changed. Involving $\hat{m} = m/Q$ the resulting expressions read [9]

$$e_0(m, Q) = \frac{n_0}{Q} + \frac{d_0}{Q^{0.5}} + e_{\min}(\hat{m}) \;, \qquad\qquad e_1(m, Q) = \frac{n_1}{Q^\beta} + \frac{d_1}{Q^{0.5}} + e_{\min}(\hat{m}) \;,$$

(3.198)

$$e_2(\hat{m}) = e_2(0) + [e_{\max}(\hat{m}) - e_{\max}(0)] \;, \qquad\qquad e_s(\hat{m}) = e_s(0) + [e_{\max}(\hat{m}) - e_{\max}(0)] \;.$$

(3.199)

$$r_s^e(\hat{m}) = r_{\mathrm{ml}} \left[1 + \varepsilon_s \left(\frac{e_s(0)}{e_s(\hat{m}) - e_{\min}(\hat{m})} \right) \right] \;, \qquad\qquad d(\hat{m}) = -\,e_{\min}(\hat{m}) r_s(\hat{m}) + d_{\mathrm{var}} \;,$$

(3.200)

$$e_j(\hat{m}) = e_{j,\mathrm{ml}} \left[\frac{e_s(0) - e_0(0, Q)}{e_s(\hat{m}) - e_0(m, Q)} \right]^2 \;,$$

(3.201)

with $e_{\min}$ from Tab. 3.1.

e	τ		C	
μ_0	1.1(3.00)	–	1.1	–
R_0	0.7(2.25)	–	0.7	–
n_0	2	–	12	–
n_1	2.25	–	5.625	–
e_2	0.25	[0.225, 0.275]	0.67	[0.64, 0.70]
e_s	0.40	[0.375, 0.425]	0.83	[0.80, 0.86]
r_{ml}	2	–	0.33	–
n_{ns}	0	$\{-1, 0, 1\}$	0	$\{-1, 0, 1\}$
ε_s	0	[−0.115, 0.13]	0	[−0.115, 0.13]
ε_j	−1.5	[−3, 0]	0	[−0.5, 0.5]
ε_h	1	[0.5, 2]	1	[0.5, 2]
d_0	0	[−0.05, 0.05]	0	[−0.05, 0.05]
d_1	0	[−0.05, 0.05]	0	[−0.05, 0.05]
abs	1(0)	–	1	–

Table 3.4: Default profile parameter choices (with $\beta = 3/4$) and their variation for thrust and C-parameter with stable (unstable) primary quarks. Details can be found in Refs. [9, 86, 100]. All parameter choices for C-parameter which do not originate from the massless analysis are extrapolated from the thrust case.

Chapter 4

Event Shapes and Unstable Heavy Quarks in e^+e^--Annihilation

4.1 Introducing Unstable Heavy Quarks

4.1.1 Inclusive Decay

When considering physical processes involving one or several (anti-)top quarks the large width ($\Gamma > \Lambda_{\text{QCD}}$) of the top quark needs to be taken into account even at parton level. Already in the discussion of Refs. [7,8], which was in the context of the double differential hemisphere mass and the differential 2-jettiness cross section, the fact that the top quark is unstable and has nonzero width was discussed. In this work it was shown that the bHQET jet function with nonzero width can be written as a convolution of a Breit-Wigner function with the stable bHQET jet function:

$$J_{B,n,e}^{\Gamma}(s,m,\mu) = \frac{Q}{m}\,\hat{J}_{B,n,e}^{\Gamma}(\hat{s},\delta m,\mu) = \frac{Q}{m}\int \mathrm{d}\hat{s}'\,\hat{J}_{B,n,e}(\hat{s}-\hat{s}',\delta m,\mu)\frac{\Gamma}{\pi\big[(\hat{s}')^2+\Gamma^2\big]}\ . \tag{4.1}$$

This was shown by taking the approach of calculating the imaginary part of the inclusive jet function $\mathfrak{J}_{B,n,e}(s,m,\mu)$, rather than calculating the jet function with exclusive jet final states as in Sec. 3.5. By shifting the pole of the jet function (in the variable s), which corresponds to the pole in the top quark propagator, to an imaginary value it is possible to derive the relation of (4.1). The involved expressions are given by [8]

$$J_{B,n,e}^{\Gamma}(s,m,\mu) = \mathrm{Im}\Big[\mathfrak{J}_{B,n,e}\big(s+i\Gamma+i0,m,\mu\big)\Big]\ , \tag{4.2}$$

$$\mathfrak{J}_{B,n,e}\big(Qp^+,m,\mu\big) = \frac{-i}{4\pi N_c Q}\int \mathrm{d}^4x\,e^{ip\cdot x}\,\langle 0|\,T\Big\{(\overline{h}_{v^+}W_n)(0)\,(W_n^{\dagger}h_{v^+})(x)\Big\}|0\rangle\ . \tag{4.3}$$

Taking the full factorization theorem and inserting Eq. (4.1) for the jet function it is straightforward to see that one can also implement the convolution with the Breit-Wigner function on the cross section level:

$$\frac{1}{\sigma_0}\frac{\mathrm{d}\sigma^{\Gamma}}{\mathrm{d}e} = \int \mathrm{d}\hat{e}\,\frac{1}{\sigma_0}\frac{\mathrm{d}\sigma^{\Gamma=0}}{\mathrm{d}e}(e-\hat{e})\frac{\frac{m\,\alpha\,\Gamma}{Q^2}}{\pi\Big[\hat{e}^2+\big(\frac{m\,\alpha\,\Gamma}{Q^2}\big)^2\Big]}\ , \tag{4.4}$$

with an event shape specific factor α. This factor is $\alpha = 2$ for thrust (and the rescaled C-parameter $\tilde{C} = C/6$) and originates from the exact form of the ultracollinear measurement. For example because of the factor 6 in the ultracollinear measurement of the M-scheme C-parameter with respect to thrust

the final convolution will involve a Breit-Wigner distribution with $\alpha = 12$. On the other hand since one of the hemisphere jet functions will not contribute to the heavy jet mass distribution the factor will be $\alpha = 1$.

We note that this treatment is derived for observables like M-scheme jet masses ρ_+^M for which the convolution variable s coincides with the jet off-shellness. For other event shapes the convolution variable s only coincides with α times the jet off-shellness at leading power. By using the decay-function framework it is also possible to include subleading Breit-Wigner effects (corresponding to subleading width effects of the form $\Gamma \to (1 + \frac{m^2}{Q^2} + \mathcal{O}(\frac{m^4}{Q^4}))\Gamma$) modifying the relation of Eq. (4.4) which is discussed in Sec. 5.2.

4.1.2 Checking with Simulation

From the result of Eq. (4.4) one would expect that a generic event shape distribution for unstable top quark pair production is simply given by the stable distribution convoluted with a Breit-Wigner (BW) function. To check how well this expectation captures all effects of having an unstable heavy quark in the final state we next compare several event shape distributions for stable and unstable top quark pair production which are obtained from a general purpose Monte Carlo event generator. In particular we take the distributions after the parton shower step and convolute them with a simple analytic hadronization model. For the model we use the simple analytic test-model which was already defined in Sec. 3.7, with $\{c_0 = 1, c_{i\neq0} = 0\}$, $\xi = \Omega_1$. The resulting distributions are then analyzed in comparison to the theoretical expectation.

First, let us consider M-scheme thrust (alternatively 2-jettiness) and C-parameter for $e^+e^- \to t\bar{t} \to X$ with $m_t = 173$ GeV and a center of mass energy of $Q = 700$ GeV. Using PYTHIA 8.2 [54] to generate 10^7 simulated events we produce the results shown in Fig. 4.1 where the comparison plots are shown for M-scheme thrust (left) and C-parameter (right). For both observables the resulting distributions are shown for the stable (blue) and the unstable (orange) situation at parton shower level (dashed) and at hadron level (solid). In general we used a comparably large first model moment which is just for illustrative purposes and in case of C-parameter we used the relation of Eq. (3.165) to estimate a reasonable first moment.
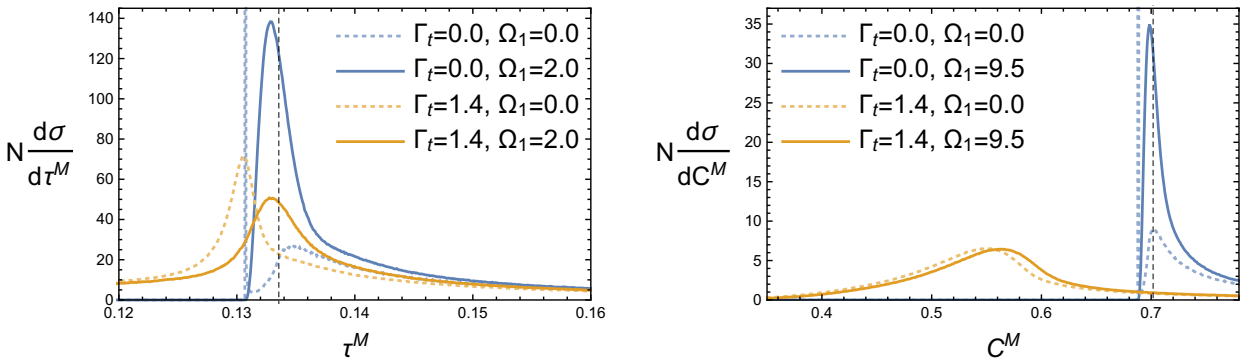

Figure 4.1: Differential distributions (PYTHIA parton level + analytic hadronization) for M-scheme thrust (N chosen so that the distribution is self-normalized within $[0, 0.5]$) and C-parameter (self-normalized within $[0.35, 0.85]$) for stable top (blue) and unstable top (orange), at parton shower level (dashed) or at hadron level (solid). For comparison also the peak position for the stable tree level case (black dashed) $e_0 = e_{\min} + \Omega_1/Q$ is shown.

Analyzing the results shown in Fig. 4.1 we note the following:

- **M-scheme thrust:** Comparing the unstable to the stable situation one can observe that the peak position is stable and that the peak gets wider. This is consistent with the theoretical treatment and can be expected from the *clustering property* of these observables (i.e. they only depend on the total jet momentum, like M-scheme thrust or jet masses). Since energy and momentum are conserved the event shape value is not changed and the inclusive treatment of the BW convolution is sufficient to describe the unstable case. In addition, the unstable distribution develops a small feature (in the following we will call it "decay-shoulder") left of the peak which at this point is not expected.

- **M-scheme C-parameter:** Comparing the unstable to the stable situation the peak position changes significantly. Furthermore the overall shape and width of the distribution changes beyond what one would expect from the convolution with a BW.

Next let us consider the P-scheme versions of the same observables as before. The corresponding results are shown in Fig. 4.2.
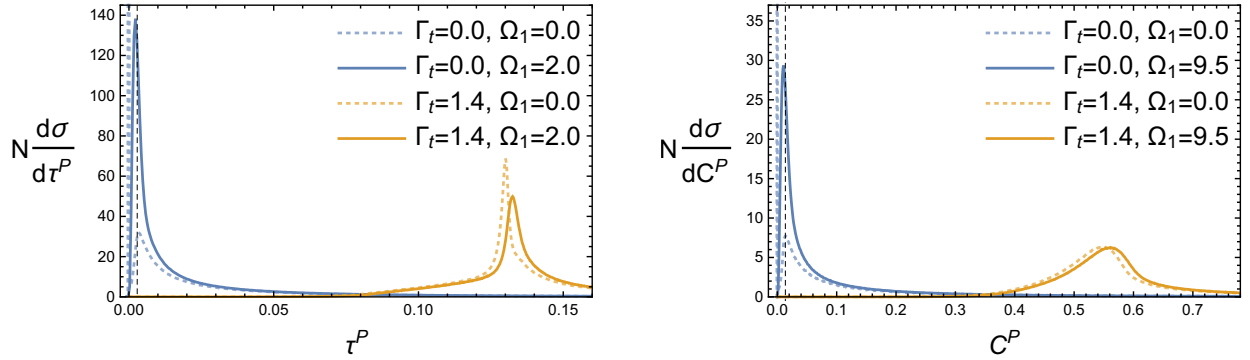

Figure 4.2: Differential distributions (`PYTHIA` parton level + analytic hadronization) for P-scheme thrust (N chosen so that the distribution is self-normalized within $[0, 0.5]$) and C-parameter (self-normalized within $[0, 1]$) for stable top (blue) and unstable top (orange), at parton shower level (dashed) or at hadron level (solid). For comparison also the peak position for the stable tree level case (black dashed) $e_0 = \Omega_1/Q$ is shown ($e_{\min} = 0$).

Again, comparing the unstable to the stable case it is clear that here in both cases the convolution of the stable distribution with a Breit-Wigner function will not be sufficient to recover the full unstable case. An argument why this could already be expected at least for thrust is related to the fact that the fully decayed final state involves (almost) massless particles. For massless final state particles P- and M-scheme definition of an event shape coincide and since for the M-scheme the stable and unstable situation are very similar the difference between the stable and unstable P-scheme distributions should be similar to the difference between the stable P- and M-scheme definitions, which is significant.

On a qualitative level we find that for event shapes with the clustering property (i.e. they only depend on the total jet momentum and one expects those not to be decay sensitive due to energy-momentum conservation) the unstable situation can be recovered by convolution of the stable distribution with a Breit-Wigner function. Furthermore we also note that for other event shapes, which are sensitive to more exclusive final state information, this prescription will in general not work well.

4.1.3 Dependence on the Heavy Quark Decay Kinematics

In order to understand the results from the previous subsection our next aim is to identify the different relevant kinematical situations and also to understand how they contribute to the final distribution

of the full unstable case.

For event shapes with the clustering property any effect from the decay beyond the convolution with a Breit-Wigner is expected to be small. This is the case because for large boost (i.e. $Q \gg m$) basically all the decay products stay in the jet, thus the jet momentum does not change, which because of the clustering property and energy momentum conservation means that the event shape value of the event does not change. We call such events *aligned decay events.* Due to the large boost the situation, where decay products are not contained in the same jet anymore, is power suppressed. For this situation the event shape value will change with respect to the corresponding stable situation and from now on we will refer to them as *misaligned decay events.*
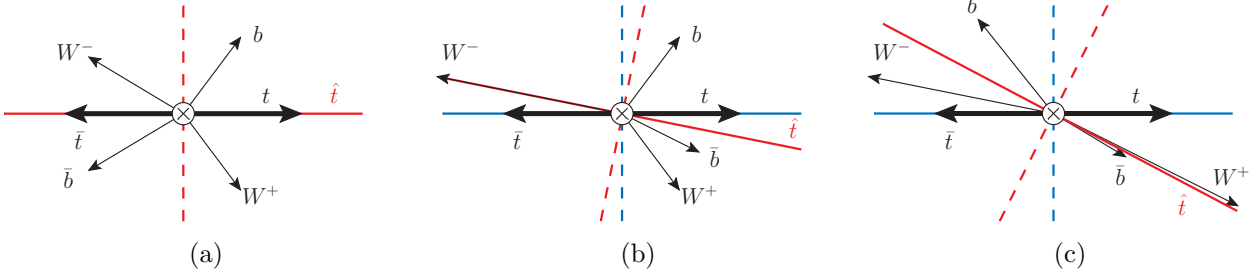

(a) (b) (c)

Figure 4.3: Illustration of $e^+e^- \to t\bar{t} \to W^+b\,W^-\bar{b}$ with fully aligned (a), misaligned $\bar{t}$ and aligned t (b) and fully misaligned (c) decays. The fact that misaligned decays change the event-shape values of the event can be seen by comparing the thrust axis (solid) and hemisphere division (dashed) of the final state (red) and an event where a stable on-shell top-antitop pair (blue) is produced.

To make this notation more precise, the difference of aligned and misaligned decays is shown schematically in Fig. 4.3 for the example of $t\bar{t}$ production which then subsequently decay into two particles each (e.g. $t \to W^+b$). In the exemplary case of thrust the original heavy quark pair momentum axis will align with the final state thrust axis if all decay products end up in the correct hemisphere (defined by the heavy quark pair momentum axis) which will correspond to an aligned decay. If this is not the case the final state thrust axis will not align with the thrust axis of the event which would only contain the initially produced heavy quarks as stable particles, hence the thrust value would change and we would speak of a misaligned decay.

For event shapes which do not have the clustering property, as an example let us look at C-parameter, the effect of the decay, as shown for example in Fig. 4.2, can be understood quite intuitively. When the massive on-shell top quark decays into lighter particles which also must be on-shell an angle between the trajectories of the decay products will be introduced. Even with fully aligned decays the P-scheme C-parameter measurement which is given in Eq. (3.5) would be nonzero while the corresponding event with a stable top-antitop pair would give zero. This shows that for *non-clustering event shapes* (i.e. event shapes without clustering property) even for aligned decays we have to expect changes with respect to the stable case beyond the convolution with a BW.

In the following we will explore this heavy quark decay kinematics dependence of different differential event shape distributions in more detail and explore how aligned and misaligned decays contribute. For this we again look at a study with simulated data (PYTHIA 8.219) at $e^+e^- \to t\bar{t} \to W^+b\,W^-\bar{b}$ with a center of mass energy of $Q = 700$ GeV and $\Gamma_t = 0$ GeV at hard process level (parton shower and hadronization turned off), which is just a numerical version of doing the leading order calculation.

In Fig. 4.4 we show the results for M-scheme thrust and C-parameter with different cuts applied. For that purpose we also define so-called *collinear decay* events which are characterized by the fact that all of the decay products are collinear with respect to the SCET power counting. This is realized by checking explicitly that all decay products are harder than soft particles, i.e. $|\vec{p}|/Q > m_t^2/Q^2 \sim \lambda^2$. For comparison the distributions for the full unstable situation (blue), only fully aligned events (or-
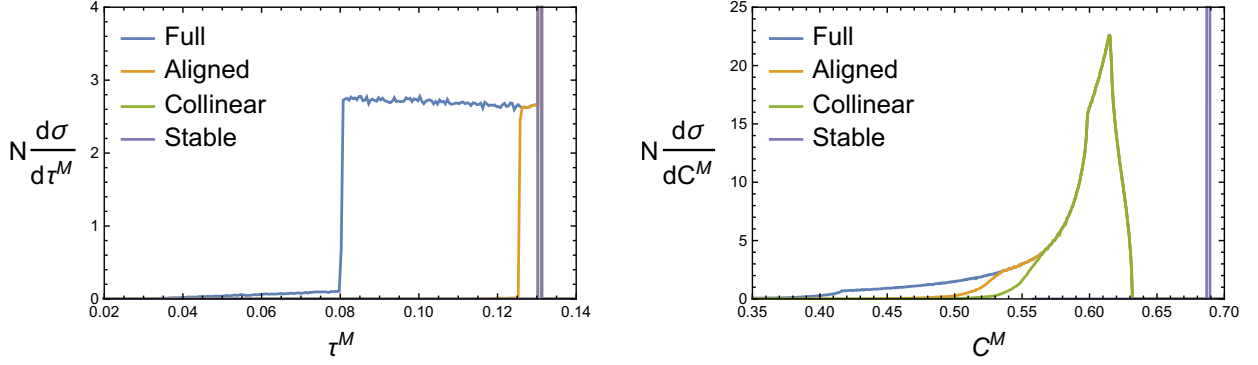
Figure 4.4: Differential $e^+e^- \to t\bar{t} \to W^+bW^-\bar{b}$ cross section from PYTHIA for M-scheme thrust (normalized to $[0, 0.5]$) and C-parameter (normalized to $[0.35, 0.80]$) for all decays (blue), only aligned decays (orange), only collinear decays (green) and for comparison events with a stable $t\bar{t}$ final state. For the thrust case collinear and stable results are on top of each other.

ange), only collinear decay events (green) and the stable $t\bar{t}$ final state (purple) are shown.

Looking first at the full M-scheme thrust distribution we find all the situations discussed so far. Most of the events involve collinear decays[1] (for this situation $\sim 86.2\%$ of the events) which are represented by a delta function at the stable threshold position. Additionally there are a few aligned but not collinear decay events ($\sim 1.4\%$) for which the angle of the decay products is so large that although they are aligned the thrust axis still gets modified and we find a deviation from the stable threshold position. On top of that there are misaligned events ($\sim 12.4\%$) left of the peak giving rise to most of what we called "decay-shoulder" before. Taking a closer look at the M-scheme C-parameter distribution shows a shift and distortion to a much broader distribution. Apart from that we see a similar behavior where the central part of the peak is made up by collinear decay events, aligned decays include a slightly larger set of events and the rest of the events are given by misaligned decays which do only contribute farther away from the peak.

In this section we studied how different prototypical decay kinematics enter the fully unstable distribution of boosted top quark pair production and found the following: (1) The so-called collinear decay events contribute most of the peak of the distribution. (2) There are a few aligned but not collinear decay events which contribute close to the peak. (3) The remaining events come from the power suppressed situation of misaligned decay events which only contribute to the tail of the distribution.

4.2 Fixed Order Calculation for $t\bar{t}$ Production and Decay

In the last section the qualitative behavior of event shapes for boosted unstable top quark pair production was studied. It turns out that for event shapes with the clustering property, as expected, the usual approach of convolution of the stable distribution with a Breit-Wigner function works very well. For non-clustering event shapes (i.e. event shapes without clustering property) this treatment is not sufficient. The aim of the remainder of this chapter is to improve this situation by creating a setup which also allows us to carry out a quantitative analysis for non-clustering event shapes.

As a starting point let us again consider the situation of top quark pair production in e^+e^--annihilation which then subsequently decay (via intermediate W-bosons) into b-quarks and leptons, neutrinos or

---

[1]Note that all collinear decay events are also fully aligned.

light quarks, i.e. $e^+e^- \to t\bar{t} \to bW^+\bar{b}W^- \to Y_i$ with the four possible final states Y_i given by

$$Y_1 = bl^+\nu_l\,\bar{b}l'^-\bar{\nu}_{l'} \;, \qquad\qquad\qquad Y_2 = bl^+\nu_l\,\bar{b}q''\bar{q}''' \;, \tag{4.5}$$

$$Y_3 = b\bar{q}q'\,\bar{b}l^-\bar{\nu}_l \;, \qquad\qquad\qquad Y_4 = b\bar{q}q'\,\bar{b}q''\bar{q}''' \;, \tag{4.6}$$

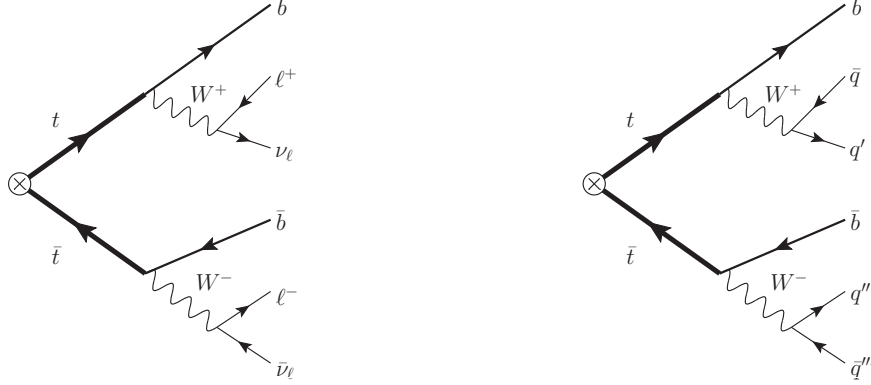As a representative example Y_1 and Y_4 are also shown in Fig. 4.5.

Figure 4.5: Feynman diagram for $t\bar{t}$ production with the subsequent decay into the Y_1 and Y_4 final state which consists of b-quarks, leptons and the corresponding neutrinos as well as light quarks.

It is easy to show (for more details see among others [70]) that for $e^+e^- \to \gamma^*, Z^0 \to Q\bar{Q} \to X$ the fixed order cross section can be factorized into a so called leptonic and hadronic[2] tensor which factorize initial and final state physics at leading order in the electroweak interaction. The total cross section is then given by

$$\sigma = \sum_X \int d\Pi_X (2\pi)^d \delta^{(d)}(q - P_X) \sum_{i=v,a} L^i_{\mu\nu} H_i^{\mu\nu} \;, \tag{4.7}$$

where q is the total (initial state) momentum which in the c.o.m. frame is given by $\hat{q} = (\hat{q}^0, \hat{\vec{q}}) = (Q, 0)$ involving the c.o.m. energy Q. The hadronic tensor involves the vector and axial-vector $Q\bar{Q}$ current $\mathcal{J}^\mu_{\mathrm{QCD},i}$ given in Eq. (3.48) and reads (with an implicit trace over spin, polarization and color indices)

$$H_i^{\mu\nu} = \langle 0| \mathcal{J}_i^{\mu\dagger}(0) |X\rangle \langle X| \mathcal{J}_i^\nu(0) |0\rangle \;. \tag{4.8}$$

The leptonic tensor for unpolarized e^+e^- annihilation is given by

$$L^v_{\mu\nu} = \tilde{\mu}^{4\varepsilon}\left(\frac{1-\varepsilon}{3-2\varepsilon}\right)\frac{8\pi^2\alpha^2}{Q^4}\left(\frac{q_\mu q_\nu}{Q^2} - g_{\mu\nu}\right)$$
$$\times \left[Q_e^2 Q_f^2 + \frac{v_f^2(v_e^2+a_e^2)}{\left(1-(m_Z/Q)^2\right)^2 + \left(\Gamma_Z/m_Z\right)^2} + \frac{2\,Q_e\,Q_f\,v_e\,v_f\left(1-(m_Z/Q)^2\right)}{\left(1-(m_Z/Q)^2\right)^2 + \left(\Gamma_Z/m_Z\right)^2}\right], \tag{4.9}$$

$$L^a_{\mu\nu} = \tilde{\mu}^{4\varepsilon}\left(\frac{1-\varepsilon}{3-2\varepsilon}\right)\frac{8\pi^2\alpha^2}{Q^4}\left(\frac{q_\mu q_\nu}{Q^2} - g_{\mu\nu}\right)\left[\frac{a_f^2(v_e^2+a_e^2)}{\left(1-(m_Z/Q)^2\right)^2 + \left(\Gamma_Z/m_Z\right)^2}\right], \tag{4.10}$$

with $\tilde{\mu} = (\frac{\mu^2 e^{\gamma_E}}{4\pi})^\varepsilon$ and the electromagnetic coupling constant α. Furthermore the v and a factors from the coupling of the fermion f to the Z-boson are given by

$$v_f = \frac{T^f_{3,L} - 2Q_f\sin^2\theta_w}{\sin 2\theta_w} \;, \qquad\qquad a_f = -\frac{T^f_{3,L}}{\sin 2\theta_w} \;, \tag{4.11}$$

---

[2]This naming convention should be taken with a grain of salt. In this case the final state can also include leptons from the W-boson decay.

where $T_{3,L}^f$ stands for the weak isospin, Q_f denotes the electric charge of the fermion f and θ_w is the weak mixing angle which is also called *Weinberg angle*.

4.2.1 Six Particle Phase Space

Before looking at the hadronic tensor let us first investigate the phase space which is opened up by the six particle final state of interest, e.g. $Y_1 = bl^+\nu_l\,\bar{b}l^-\bar{\nu}_l$ (for our purposes using $d = 4$ is sufficient):

$$\int \mathrm{d}\Pi_{Y_1}(2\pi)^4\delta^{(4)}(q - P_Y) = \int \prod_{i=1}^{6} \frac{\mathrm{d}^3\vec{p}_i}{(2\pi)^3 2p_i^0}(2\pi)^4\delta^{(4)}\left(q - \sum_{i=1}^{6} p_i\right), \tag{4.12}$$

where the index i refers to the particles in the same order as the final state particle list given above the equation (referring to the final state particles in Fig. 4.5 from top to bottom), all momenta are considered outgoing and where q again refers to the total momentum. By introducing the W^+, W^- momentum r_1, r_2, the t, $\bar{t}$ momentum q_1, q_2:

$$r_1 = p_2 + p_3, \qquad\qquad q_1 = r_1 + p_1 = p_1 + p_2 + p_3, \tag{4.13}$$
$$r_2 = p_5 + p_6, \qquad\qquad q_2 = r_2 + p_4 = p_4 + p_5 + p_6, \tag{4.14}$$

as well as the invariant mass of the intermediate particles $s_i = q_i^2$ and $t_i = r_i^2$ for $i = 1, 2$ it is possible to write the following identity for the t quark kinematics:

$$\mathbb{1} = \int \frac{\mathrm{d}s_1}{2\pi} \int \frac{\mathrm{d}^4 q_1}{(2\pi)^4} (2\pi)\delta(s_1 - q_1^2)\,\theta(q_1^0)\,(2\pi)^4\delta^{(4)}(q_1 - p_1 - r_1)$$
$$= \int \frac{\mathrm{d}s_1}{2\pi} \frac{\mathrm{d}^3\vec{q}_1}{(2\pi)^3 2q_1^0}(2\pi)^4\delta^{(4)}(q_1 - p_1 - r_1) \qquad \text{with} \qquad q_1^0 = \sqrt{s_1 + \vec{q}_1^2}\,, \tag{4.15}$$

and analogously for the cases of $\bar{t}$, W^+ and W^-. Next let us boost to the W^+ rest frame and look at the W^+ decay kinematics for massless decay products[3]:

$$\int \frac{\mathrm{d}^3\hat{\vec{p}}_2}{(2\pi)^3 2p_2^0} \frac{\mathrm{d}^3\hat{\vec{p}}_3}{(2\pi)^3 2p_3^0} (2\pi)^4\delta(\sqrt{t_1} - p_2^0 - p_3^0)\delta(\hat{\vec{p}}_2 + \hat{\vec{p}}_3)$$
$$= \int \frac{\mathrm{d}(\cos\hat{\theta})}{2} \frac{\mathrm{d}\hat{\varphi}}{2\pi} \frac{\mathrm{d}(|\hat{\vec{p}}_2|^2)|\hat{\vec{p}}_2|}{8\pi} \frac{\delta\left(\sqrt{t_1} - \sqrt{m_1^2 + |\hat{\vec{p}}_2|^2} - \sqrt{m_2^2 + |\hat{\vec{p}}_2|^2}\right)}{\sqrt{m_1^2 + |\hat{\vec{p}}_2|^2}\sqrt{m_2^2 + |\hat{\vec{p}}_2|^2}} \tag{4.16}$$
$$= \frac{1}{8\pi}\left[1 - \frac{2(m_2^2 + m_3^2)}{t_1} + \frac{(m_2^2 - m_3^2)^2}{t_1^2}\right]^{\frac{1}{2}} \int \frac{\mathrm{d}(\cos\hat{\theta})}{2} \frac{\mathrm{d}\hat{\varphi}}{2\pi} = \frac{1}{8\pi} \frac{\lambda^{\frac{1}{2}}(t_1, m_2^2, m_3^2)}{t_1} \int \frac{\mathrm{d}(\cos\hat{\theta})}{2} \frac{\mathrm{d}\hat{\varphi}}{2\pi}\,,$$

where we used on-shell conditions for all final state particles, introduced some polar angle $\hat{\varphi}$ and azimuthal angle $\hat{\theta}$ defined w.r.t. the W^+ rest frame and also used the usual notation for the Källén function $\lambda(t_1, m_2^2, m_3^2) = t_1^2 - 2t_1(m_2^2 + m_3^2) + (m_2^2 - m_3^2)^2$. Using the same strategy for the W^- and subsequently for the (anti-)top quark decay products we can write the six particle phase space from Eq. (4.12) as

$$\int \mathrm{d}\Pi_6 = \int \frac{\mathrm{d}s_1}{2\pi} \frac{\mathrm{d}s_2}{2\pi} \int \frac{\mathrm{d}^3\vec{q}_1}{(2\pi)^3 q_1^0} \frac{\mathrm{d}^3\vec{q}_2}{(2\pi)^3 q_2^0}(2\pi)^4\delta^{(4)}(P - q_1 - q_2)$$
$$\int \frac{\mathrm{d}t_1}{2\pi} \frac{\lambda^{\frac{1}{2}}(s_1, t_1, m_1^2)}{8\pi\, s_1} \frac{\mathrm{d}(\cos\hat{\theta}_{q_1})}{2} \frac{\mathrm{d}\hat{\varphi}_{q_1}}{2\pi} \int \frac{\lambda^{\frac{1}{2}}(t_1, m_2^2, m_3^2)}{8\pi\, t_1} \frac{\mathrm{d}(\cos\hat{\theta}_{r_1})}{2} \frac{\mathrm{d}\hat{\varphi}_{r_1}}{2\pi} \tag{4.17}$$
$$\int \frac{\mathrm{d}t_2}{2\pi} \frac{\lambda^{\frac{1}{2}}(s_2, t_2, m_4^2)}{8\pi\, s_2} \frac{\mathrm{d}(\cos\hat{\theta}_{q_2})}{2} \frac{\mathrm{d}\hat{\varphi}_{q_2}}{2\pi} \int \frac{\lambda^{\frac{1}{2}}(t_2, m_5^2, m_6^2)}{8\pi\, t_2} \frac{\mathrm{d}(\cos\hat{\theta}_{r_2})}{2} \frac{\mathrm{d}\hat{\varphi}_{r_2}}{2\pi}\,,$$

---

[3]Note that particle momenta p defined in the c.o.m. frame, will be denoted as $\hat{p}$ in the rest frame of their parent particle.

where $\hat{\theta}_{q_1}$ now refers to the azimuthal angle defined w.r.t. the rest frame of the top quark where $q_1 = (\sqrt{s_1}, \vec{0})$ is valid (analogously for the other angles).

4.2.2 Matrix Elements

After discussing the phase space let us now focus on the calculation of the hadronic tensor for the final states Y_j, which is given by (with $i = v, a$)

$$H_i^{\mu\nu} = \sum_{j=1}^{4} \sum_{\substack{\text{spins} \\ \text{pol,color}}} \mathcal{M}_{i,j}^{\mu} \big(\mathcal{M}_{i,j}^{\nu}\big)^{\dagger} \qquad \text{with} \qquad \mathcal{M}_{i,j}^{\mu} = \langle Y_j | \, \mathcal{J}_i^{\mu}(0) \, |0\rangle \; . \tag{4.18}$$

Using the chiral projector $P_L = \frac{1-\gamma_5}{2}$ we can write down an expression for the involved amplitude which reads (using $\Gamma_v^{\mu} = \gamma^{\mu}$ and $\Gamma_a^{\mu} = \gamma^{\mu}\gamma_5$)

$$\mathcal{M}_{i,j}^{\mu} = \left[\overline{u}(p_1, s_1)\left\{\frac{g}{i\sqrt{2}}\gamma_\alpha P_L V_{tb}\right\} \frac{i(\slashed{q}_1 + m_t)}{q_1^2 - m_t^2 + i\,m_t\Gamma_t} \Gamma_i^{\mu} \frac{i(-\slashed{q}_2 + m_t)}{q_2^2 - m_t^2 + i\,m_t\Gamma_t}\left\{\frac{g}{i\sqrt{2}}\gamma_\beta P_L V_{tb}\right\} v(p_4, s_4)\right]$$
$$\times \frac{-i\big(g^{\alpha\delta} - (r_1^\alpha r_1^\delta/m_W^2)\big)}{r_1^2 - m_W^2 + i\,m_W\Gamma_W} \left[\overline{u}(p_3, s_3)\left\{\frac{g}{i\sqrt{2}}\gamma_\delta P_L(V_{ff'})\right\} v(p_2, s_2)\right] \tag{4.19}$$
$$\times \frac{-i\big(g^{\beta\rho} - (r_2^\beta r_2^\rho/m_W^2)\big)}{r_2^2 - m_W^2 + im_W\,\Gamma_W} \left[\overline{u}(p_5, s_5)\left\{\frac{g}{i\sqrt{2}}\gamma_\rho P_L(V_{f''f'''})\right\} v(p_6, s_6)\right] \; ,$$

with the weak coupling strength g related to Fermi's constant G_F by $g^2 = 8m_W^2 G_F/\sqrt{2}$, the intermediate particle momenta q_i for the tops and r_i for the W bosons and where unitary gauge (usually Feynman gauge is used in this work) is employed for the W boson propagators to avoid diagrams involving goldstone bosons. Furthermore the appropriate factors of $V_{ff'}$ need to be included if the W boson decays hadronically. It is important to note that when discussing the top quark and its mass treating the final state lepton and the corresponding neutrino to be massless[4] is sufficient and also that due to the conservation of the massless (axial) vector current, i.e. $r_1^\mu\big[\overline{u}(p_3)\gamma_\mu(\gamma_5)v(p_2)\big] = 0$, the second part of the $W^\pm$ propagator does not contribute to the final amplitude. The spin sum of the squard matrix element is then given by

$$\sum_{\text{spins}} \mathcal{M}_i^{\mu}(\mathcal{M}_i^{\nu})^{\dagger} = \left(\frac{2\pi\alpha}{\sin^2\theta_w}\right)^4 \frac{|V_{tb}|^2}{\big[(q_1^2 - m_t^2)^2 + m_t^2\Gamma_t^2\big]} \frac{|V_{tb}|^2}{\big[(q_2^2 - m_t^2)^2 + m_t^2\Gamma_t^2\big]}$$
$$\times \text{Tr}\Big[(\slashed{p}_1 + m_1)\gamma_\alpha P_L(\slashed{q}_1 + m_t)\Gamma_i^{\mu}(-\slashed{q}_2 + m_t)\gamma_\beta P_L(\slashed{p}_4 - m_4)\gamma_\delta P_L(-\slashed{q}_2 + m_t)\Gamma_i^{\nu}(\slashed{q}_1 + m_t)\gamma_\sigma P_L\Big]$$
$$\times \frac{1}{2}\text{Tr}\Big[\slashed{p}_5\gamma^\beta\slashed{p}_6\gamma^\delta\Big] \frac{(|V_{ff'}|^2)}{\big[(r_1^2 - m_W^2)^2 + m_W^2\Gamma_W^2\big]} \frac{1}{2}\text{Tr}\Big[\slashed{p}_2\gamma^\alpha\slashed{p}_3\gamma^\sigma\Big] \frac{(|V_{f''f'''}|^2)}{\big[(r_2^2 - m_W^2)^2 + m_W^2\Gamma_W^2\big]} \; . \tag{4.20}$$

In the next step we proceed along the lines of the narrow width approximation (see [108] for a review) and assume that the top quarks and W's are very close to on-shell (off-shellness $\sim m\Gamma$). For the top quark one can then write[5] $\slashed{q}_1 + m_t = \sum_a u(q_1, a)\overline{u}(q_1, a)\big[1 + \mathcal{O}(\Gamma_t/m_t)\big]$ and analogously for the $W^\pm$

---

[4]This also means that the flavor mixing which would be implemented via PMNS matrix elements in the $W^\pm$ coupling to the lepton/neutrino is omitted. For the corresponding hadronic decays also the light quarks are considered to be massless.

[5]Parametrically the NWA introduces corrections of order Γ/m [109].

one can write $-g^{\mu\nu} + \frac{r_1^\mu r_2^\nu}{M_W^2} = \sum_\sigma (\varepsilon^\mu(r_1,\sigma))^* \varepsilon^\nu(r_1,\sigma)\left[1+\mathcal{O}(\Gamma_W/m_W)\right]$, which allows us to rewrite the expression from Eq. (4.20) as

$$
\sum_{\text{spins}} \mathcal{M}_i^\mu (\mathcal{M}_i^\nu)^\dagger = \left[1 + \mathcal{O}\left(\frac{\Gamma_t}{m_t}, \frac{\Gamma_W}{m_W}\right)\right] \left\{ \frac{1}{\Gamma_t^2\, \Gamma_W^2}\, f_{\text{BW}}(q_1^2, m_t, \Gamma_T)\, f_{\text{BW}}(q_2^2, m_t, \Gamma_T) \right.
$$

$$
\times \sum_{\substack{a_1,a_2,a_3,a_4 \\ b_1,b_2,b_3,b_4}} \left[\overline{u}(q_1,a_1)\Gamma_i^\mu v(q_2,a_2)\overline{v}(q_2,a_3)\Gamma_i^\nu u(q_1,a_4)\right]|V_{tb}|^2\,|V_{tb}|^2\left(|V_{ff'}|^2\right)\left(|V_{f''f'''}|^2\right) \qquad (4.21)
$$

$$
\times \left(\frac{2\pi^2\alpha}{\sin^2\theta_w\, m_t}\right)\left[\overline{u}(q_1,a_4)\gamma_\sigma P_L(\slashed{p}_1 + m_1)\gamma_\alpha P_L u(q_1,a_1)\right](\varepsilon^\alpha(r_1,b_1))^*\varepsilon^\sigma(r_1,b_4)
$$

$$
\times \left(\frac{2\pi^2\alpha}{\sin^2\theta_w\, m_t}\right)\left[\overline{v}(q_2,a_2)\gamma_\beta P_L(\slashed{p}_4 + m_4)\gamma_\delta P_L v(q_2,a_3)\right](\varepsilon^\beta(r_2,b_2))^*\varepsilon^\delta(r_2,b_3)
$$

$$
\times \left(\frac{\pi^2\alpha}{\sin^2\theta_w\, m_W}\right)\text{Tr}\left[\slashed{p}_2\gamma_{\alpha_2}\slashed{p}_3\gamma_{\sigma_2}\right](\varepsilon^{\sigma_2}(r_1,b_4))^*\varepsilon^{\alpha_2}(r_1,b_1)\, f_{\text{BW}}(r_1^2, m_W, \Gamma_W)
$$

$$
\left. \times \left(\frac{\pi^2\alpha}{\sin^2\theta_w\, m_W}\right)\text{Tr}\left[\slashed{p}_5\gamma_{\beta_2}\slashed{p}_6\gamma_{\delta_2}\right](\varepsilon^{\delta_2}(r_2,b_3))^*\varepsilon^{\beta_2}(r_2,b_2)\, f_{\text{BW}}(r_2^2, m_W, \Gamma_W) \right\},
$$

with the well known Breit-Wigner distribution f_{BW} given by

$$
f_{\text{BW}}(s,m,\Gamma) = \frac{m\Gamma}{\pi\left[\left(s - m^2\right)^2 + m^2\Gamma^2\right]}\,. \qquad (4.22)
$$

For the subsequent simplifications the usual strategy which is frequently used in the context of the NWA is to average over intermediate spins and polarizations[6]. For the here occuring example of a spin-$\frac{1}{2}$ particle and a massive gauge boson with momentum p this schematically looks like [108]

$$
\sum_a \left|\mathcal{M}_1\, u(p,a)\,\overline{u}(p,a)\,\mathcal{M}_2\right|^2 = \frac{1}{2}\sum_{a_1,a_2}\left|\mathcal{M}_1 u(p,a_1)\right|^2 \left|\overline{u}(p,a_2)\mathcal{M}_2\right|^2, \qquad (4.23)
$$

$$
\sum_a \left|\mathcal{M}_1^\mu\, \varepsilon_\mu^*(p,a)\varepsilon_\nu(p,a)\,\mathcal{M}_2^\nu\right|^2 = \frac{1}{3}\sum_{a_1,a_2}\left|\mathcal{M}_1^\mu\, \varepsilon_\mu^*(p,a_1)\right|^2 \left|\varepsilon_\nu(p,a_2)\,\mathcal{M}_2^\nu\right|^2. \qquad (4.24)
$$

4.2.3 Result

In the next step we put the results from Eqs. (4.17) and (4.21) together with Eq. (4.7) and factorize the cross section using the discussed trick from the NWA as given in Eqs. (4.23) and (4.24). This leaves us with:

$$
\sigma_{e^+e^- \to t\bar{t} \to Y_j} = \left\{ \int \mathrm{d}s_1 \mathrm{d}t_1\, f_{\text{BW}}(s_1, m_t, \Gamma_t)\frac{\sqrt{s_1}\,\Gamma_{t\to Wb}(s_1,t_1,m_b^2)}{m_t\,\Gamma_t}\, f_{\text{BW}}(t_1, m_W, \Gamma_W)\frac{\sqrt{t_1}\,\Gamma_{W\to Y_j}(t_1)}{m_W\,\Gamma_W} \right.
$$

$$
\times \int \mathrm{d}s_2\, \mathrm{d}t_2\, f_{\text{BW}}(s_2, m_t, \Gamma_t)\frac{\sqrt{s_2}\,\Gamma_{t\to Wb}(s_2,t_2,m_b^2)}{m_t\,\Gamma_t}\, f_{\text{BW}}(t_2, m_W, \Gamma_W)\frac{\sqrt{t_2}\,\Gamma_{W\to Y_j}(t_2)}{m_W\,\Gamma_W}
$$

$$
\times \int \frac{\mathrm{d}(\cos\hat{\theta}_{q_1})}{2}\frac{\mathrm{d}\hat{\varphi}_{q_1}}{2\pi} \int \frac{\mathrm{d}(\cos\hat{\theta}_{r_1})}{2}\frac{\mathrm{d}\hat{\varphi}_{r_1}}{2\pi} \int \frac{\mathrm{d}(\cos\hat{\theta}_{q_2})}{2}\frac{\mathrm{d}\hat{\varphi}_{q_2}}{2\pi} \int \frac{\mathrm{d}(\cos\hat{\theta}_{r_2})}{2}\frac{\mathrm{d}\hat{\varphi}_{r_2}}{2\pi} \qquad (4.25)
$$

$$
\left. \times\, \sigma_{e^+e^- \to t\bar{t}}(s_1, s_2) \right\} \left[1 + \mathcal{O}\left(\frac{\Gamma_t}{m_t}, \frac{\Gamma_W}{m_W}\right)\right],
$$

---

[6]This approximation works well because event shapes are usually not sensitive to spins and polarizations of final state particles.

where we defined the partial widths as

$$\Gamma_{t \to Wb}(s_1, t_1, m_b^2) = \frac{\alpha \, |V_{tb}|^2}{16 \sin^2 \theta_w} \frac{\lambda^{\frac{1}{2}}(s_1, t_1, m_b^2)}{s_1^{3/2} \, t_1} \left[(s_1 - m_b^2)^2 + (s_1 + m_b^2) \, t_1 - 2 \, t_1^2 \right] , \tag{4.26}$$

$$\Gamma_{W \to \text{lep}}(t_1) = \frac{\alpha \sqrt{t_1}}{12 \sin^2 \theta_w} , \qquad\qquad \Gamma_{W \to qq'}(t_1) = \frac{\alpha |V_{qq'}|^2 \sqrt{t_1}}{12 \sin^2 \theta_w} , \tag{4.27}$$

which reduce to the known expressions for the tree level widths of the top quark $\Gamma_{t \to Wb}^0$ and W boson $\Gamma_{W \to Y_j}^0$ (see for example [110] and [111], respectively) in the corresponding channels if all the particles are on-shell, i.e. $s_{1/2} = m_t^2$ and $t_{1/2} = m_W^2$. Moreover we introduced the tree level $e^+ e^- \to t\bar{t}$ cross section given by

$$\sigma_{e^+ e^- \to t\bar{t}} = \int \mathrm{d}\Pi_2(\vec{q}_1, \vec{q}_2, s_1, s_2) S_0(\vec{q}_1, \vec{q}_2, s_1, s_2) \tag{4.28}$$

$$= \int \frac{\mathrm{d}^3 \vec{q}_1}{(2\pi)^3 \, 2q_1^0} \frac{\mathrm{d}^3 \vec{q}_2}{(2\pi)^3 \, 2q_2^0} L^i_{\mu\nu} \, \mathrm{Tr}\left[(\slashed{q}_1 + \sqrt{s_1}) \, \Gamma_i^\mu \, (\slashed{q}_2 - \sqrt{s_2}) \, \Gamma_i^\nu \right] ,$$

with $q_i^0 = \sqrt{s_i + \vec{q}_i^{\,2}}$ and the leptonic tensor $L^i_{\mu\nu}$ given in Eqs. (4.9) and (4.10).

To simplify the expression given in Eq. (4.25) further one can take the final step of the NWA for the W-bosons (i.e. consider $\Gamma_W \to 0$) which reduces the Breit-Wigner function in the following way:

$$f_{\mathrm{BW}}(s, m, \Gamma) \quad \overset{\Gamma \to 0}{\longrightarrow} \quad \delta(s - m^2) . \tag{4.29}$$

Also making the usual assumption that the dependence of the factor involving the partial width on the invariant mass of the top quarks $s_{1/2}$ is negligible for an off-shellness of order $s_{1/2} - m_t^2 \sim m_t \Gamma_t$ is sensible in this context and reduces the complexity of the final expression further. This reduces the factor to the tree level top quark branching fraction for the $t \to Wb$ channel which is essentially 1:

$$\frac{\sqrt{s_1} \, \Gamma_{t \to Wb}(s_1, t_1, m_b^2)}{m_t \, \Gamma_t} \sim B(t \to Wb) = \frac{\Gamma_{t \to Wb}^0}{\Gamma_t} \sim 1 . \tag{4.30}$$

Since we are interested in differential cross sections, in the last step a measurement delta function for the event shape e (giving the event shape value e_Y for the final state Y) is introduced. The differential cross section for $e^+ e^- \to t\bar{t} \to X$ (summing over all possible final states) with the described simplifications is then given by

$$\frac{\mathrm{d}\sigma_{e^+ e^- \to Y}}{\mathrm{d}e} = \int \mathrm{d}s_1 \, f_{BW}(s_1, m_t, \Gamma_t) \int \mathrm{d}s_2 \, f_{BW}(s_2, m_t, \Gamma_t)$$

$$\times \int \frac{\mathrm{d}(\cos \hat{\theta}_{q_1})}{2} \frac{\mathrm{d}\hat{\varphi}_{q_1}}{2\pi} \int \frac{\mathrm{d}(\cos \hat{\theta}_{r_1})}{2} \frac{\mathrm{d}\hat{\varphi}_{r_1}}{2\pi} \int \frac{\mathrm{d}(\cos \hat{\theta}_{q_2})}{2} \frac{\mathrm{d}\hat{\varphi}_{q_2}}{2\pi} \int \frac{\mathrm{d}(\cos \hat{\theta}_{r_2})}{2} \frac{\mathrm{d}\hat{\varphi}_{r_2}}{2\pi} \tag{4.31}$$

$$\times \int \mathrm{d}\Pi_2(\vec{q}_1, \vec{q}_2, s_1, s_2) S_0(\vec{q}_1, \vec{q}_2, s_1, s_2) \, \delta\Big(e - e_Y\big(\vec{q}_1, \vec{q}_2, s_1, s_2, \{\hat{\theta}_i, \hat{\varphi}_i\}\big)\Big) \Bigg\} \left[1 + \mathcal{O}\left(\frac{\Gamma_t}{m_t}\right) \right] ,$$

where we used that the sum over all partial widths for the W boson gives the total W width.

4.3 Measurement Factorization for Unstable Heavy Quarks in the Dijet Limit

In this section we want to follow Sec. 3.4.1 while considering the heavy quark to be unstable and decaying into two or three final state decay products. In particular we want to answer how the measurement outcome is changing when compared to the stable case discussed before.

As we have seen in Sec. 4.1.2 the M-scheme C-parameter is a strongly decay sensitive observable and also has non-trivial factorization properties which makes it an illustrative event shape to discuss in this context. First, let us consider that in the dijet limit particles can be either soft or collinear, hence one can write

$$C^M = \sum_{\substack{a\in\{s,n,\bar{n}\} \\ b\in\{s,n,\bar{n}\}}} C_{ab}^M = \frac{3}{2\,Q^2} \sum_{\substack{a\in\{s,n,\bar{n}\} \\ b\in\{s,n,\bar{n}\}}} \sum_{\substack{i\in a \\ j\in b}} \frac{1}{p_i^0 p_j^0} \left[(p_i \cdot p_j)(2p_i^0 p_j^0 - p_i \cdot p_j) + \delta_{ab}\delta_{ij} m^4 \right].$$ (4.32)

The qualitative analysis of Sec. 4.1.3 shows that the events which give the biggest contribution to the peak region of the event shape distribution are so-called collinear decay events where all decay products of a collinear particle are again collinear. When considering the SCET power counting for this situation it can be quickly realized that the unstable event shape measurement, in analogy to what is shown in Sec. 3.4.1, will reduce to the stable situation. This happens because, at leading power, the measurement is linear in the particle momenta of collinear particles and therefore does not take note of a decay in any of the collinear sectors.

For the peak region of the cross section bHQET is usually more relevant. Since this region is the most mass sensitive it is also the most interesting one in this context. Again we employ the prescription of not expanding contributions which contain purely kinematical information about the initially produced heavy quark (and its decay) in $\frac{m^2}{Q^2}$ but keeping those to all orders and at the same time consider the dynamical terms, which are related to ultracollinear gluon radiation, at leading power. Using this one can see major changes for the unstable case with respect to the stable case. To illustrate what happens, let us start by considering a simplified scenario and then progress in generality to the case of arbitrary decays.

4.3.1 Four Massless Particles in the Final State

One very simple final state is the one where the (anti-)top quark decays into two massless particles, i.e. $t \to 1+2\,(\bar{t} \to 3+4), m_i = 0$. For this case the decay products momenta will be pairwise back to back in the (anti-)top quark rest frame and thereby only depend on the decay axis $\vec{n}(\vec{n}')$ defined in the same frame of reference with $\vec{n}^2 = (\vec{n}^\perp)^2 = 1$. With the residual momentum $\hat{k}_i = (\hat{k}_i^+, \hat{k}_i^-, \hat{\vec{k}}_i^\perp) \sim \Delta(1,1,1)$ (also defined in the heavy quark rest frame), which originates from recoil against ultracollinear gluon radiation, the momenta for the top quark decay products in the center-of-mass frame then read

$$p_{1/2} = \frac{m}{2} v_{1/2} + k_{1/2}$$

$$= \frac{Q}{2}\left(\frac{1}{2}\left(1 - \sqrt{1 - 4\frac{m^2}{Q^2}}\right)(1 \pm n_3 \frac{m}{Q}), \frac{1}{2}\left(1 + \sqrt{1 - 4\frac{m^2}{Q^2}}\right)(1 \mp n_3 \frac{m}{Q}), \pm n_1 \frac{m}{Q}, \pm n_2 \frac{m}{Q} \right)$$

$$+ Q\left(\frac{m\hat{k}_{1/2}^+}{Q^2}, \frac{\hat{k}_{1/2}^-}{m} - \frac{m\hat{k}_{1/2}^-}{Q^2}, \frac{\hat{\vec{k}}_{1/2}^\perp}{Q} \right) + \mathcal{O}\left(\frac{m^3\Delta}{Q^4}\right),$$ (4.33)

where the anti-top quark decay products momenta are given in a completely analogous way.

Simple Case: $\hat{\theta}_{q_1} = \hat{\theta}_{q_2} = \pi/2$ (alternatively $n_3 = n_3' = 0$)

First let us consider a decay configuration which is characteristic for collinear decay events. This is realized for a situation where the azimuthal decay angle for the decay products of the (anti-)top quark is $\pi/2$ in the respective (anti-)top quark rest frame and where the (anti-)top moves along the

z-direction. This configuration makes sure that in case a large enough boost is considered, all decay products end up to be in the same hemisphere as defined by the initially produced heavy quark and also that the event will be a collinear decay event (none of the decay products has soft momentum which would be $|\vec{p}|/Q \lesssim m_t^2/Q^2 \sim \lambda^2$).

For this case we can now calculate the different parts contributing to Eq. (4.32). It is easy to see that the part which involves soft particles is given by the expressions from the SCET case (see for example Ref. [70]) and therefore the only change will occur in the purely ultracollinear contributions. For example the C_{nn} contribution for the stable case is given by

$$C_{nn}^{\text{stable}} = C_{nn}^{tt} + 2\,C_{nn}^{tg} + C_{nn}^{gg} \,, \tag{4.34}$$

where the fact that the C-parameter is a sum of contributions which consider a pair of particles is used, hence C_{nn}^{tt} is the contribution which originates from considering only the n-ultracollinear top quark, C_{nn}^{tg} are the contributions which arise from considering the top quark with the n-ultracollinear gluons and C_{nn}^{gg} are then contributions where only n-ultracollinear gluons are involved. Using the same notation the C_{nn} contribution for the unstable case can then be divided into

$$C_{nn}^{\text{unstable}} = \left(C_{nn}^{11} + 2\,C_{nn}^{12} + C_{nn}^{22} \right) + 2 \left(C_{nn}^{1g} + C_{nn}^{2g} \right) + C_{nn}^{gg} \,. \tag{4.35}$$

The strategy to determine these contributions is then the same as in the stable case (see Sec. 3.4.1 and use Eq. (4.33)) which results in the following expressions for the different parts of C_{nn} (up to $\mathcal{O}(m^3\Delta/Q^4)$ corrections):

$$C_{nn}^{11} = \frac{3}{2} \left(\frac{m\hat{k}_1^-}{Q^2} + \frac{m\hat{k}_1^+}{Q^2} - 2\,\frac{m(\vec{n}\cdot\hat{\vec{k}}_1^\perp)}{Q} \right) , \qquad C_{nn}^{22} = \frac{3}{2} \left(\frac{m\hat{k}_2^-}{Q^2} + \frac{m\hat{k}_2^+}{Q^2} + 2\,\frac{m(\vec{n}\cdot\hat{\vec{k}}_2^\perp)}{Q} \right) ,$$

$$2\,C_{nn}^{12} = \frac{3}{2} \left(2\,\frac{m^2}{Q^2} - 8\,\frac{m^4}{Q^4} + \frac{m\hat{k}_1^-}{Q^2} + \frac{m\hat{k}_1^+}{Q^2} + \frac{m\hat{k}_2^-}{Q^2} + \frac{m\hat{k}_2^+}{Q^2} + 2\,\frac{m(\vec{n}\cdot\hat{\vec{k}}_1^\perp)}{Q} - 2\,\frac{m(\vec{n}\cdot\hat{\vec{k}}_2^\perp)}{Q} \right) ,$$

$$2\,C_{nn}^{1g} = \frac{3}{2} \sum_{i\in x_n} \left(\frac{m\hat{k}_i^+}{Q^2} + \frac{m\hat{k}_i^-}{Q^2} - 2\,\frac{m(\vec{n}\cdot\hat{\vec{k}}_i^\perp)}{Q} \right) , \quad 2\,C_{nn}^{2g} = \frac{3}{2} \sum_{i\in x_n} \left(\frac{m\hat{k}_i^+}{Q^2} + \frac{m\hat{k}_i^-}{Q^2} + 2\,\frac{m(\vec{n}\cdot\hat{\vec{k}}_i^\perp)}{Q} \right) ,$$

$$C_{nn}^{gg} = 0 \,, \tag{4.36}$$

where x_n is now the set of n-ultracollinear gluons. Using the analogous result from the stable situation (just the nn-contribution to the threshold) which is given by

$$C_{nn}^{\text{stable}} = 3\,\frac{m^2}{Q^2} \left(1 - \frac{m^2}{Q^2} \right) , \tag{4.37}$$

the nn-contribution to the M-scheme C-parameter for the unstable situation is given by

$$C_{nn}^{\text{unstable}} = 3 \left(\frac{m^2}{Q^2} - 4\,\frac{m^4}{Q^4} + \sum_{i\in n} \frac{m(\hat{k}_i^+ + \hat{k}_i^-)}{Q^2} \right) + \mathcal{O}(m^3\Delta/Q^4)$$

$$= C_{nn}^{\text{stable}} - 9\,\frac{m^4}{Q^4} + \mathcal{O}(m^3\Delta/Q^4) \,. \tag{4.38}$$

The analogous calculation for $C_{\bar{n}\bar{n}}^{\text{unstable}}$ and $C_{n\bar{n}}^{\text{unstable}}$ gives

$$C_{\bar{n}\bar{n}}^{\text{unstable}} = C_{nn}^{\text{stable}} - 9\,\frac{m^4}{Q^4} + \mathcal{O}(m^3\Delta/Q^4) \,, \tag{4.39}$$

$$2\,C_{n\bar{n}}^{\text{unstable}} = 2\,C_{nn}^{\text{stable}} - 18\,\frac{m^4}{Q^4} + \mathcal{O}(m^3\Delta/Q^4) \,. \tag{4.40}$$

All other C_{ab}^{unstable} contributions coincide with the stable results. For this very simple case the M-scheme C-parameter measurement in the dijet limit and with bHQET power counting is therefore given by the stable measurement plus an additional mass dependent shift. The stable measurement is given by (up to $\mathcal{O}(m^3\Delta/Q^4)$ corrections)

$$C^{M,\text{stable}} = 12\,\frac{m^2}{Q^2}\left(1-\frac{m^2}{Q^2}\right) + \frac{m}{Q}\sum_{i\in n}\frac{k_i^+}{Q} + \frac{m}{Q}\sum_{i\in\overline{n}}\frac{k_i^-}{Q} + \sum_{i\in s}\frac{k_i^+k_i^-}{k_i^+ + k_i^-} \,, \tag{4.41}$$

and the final result for the unstable M-scheme C parameter measurement with this simple decay configuration reads

$$C_{(4),\text{ml},\pi/2}^{M,\text{unstable}} = C^{M,\text{stable}} - 36\,\frac{m^4}{Q^4} + \mathcal{O}(m^3\Delta/Q^4) \,. \tag{4.42}$$

where the subscripts indicate the decay configuration of four massless particles with a specified decay angle of $\pi/2$ in the (anti-)top quark rest frame. One thing which immediately stands out is the fact that the involved shift is parametrically of order m^4/Q^4 which in the literature was omitted so far (also see Sec. 3.3). Furthermore it turns out (see Sec. 5.2) that considering this configuration which is prototypical for collinear decay events gives a good parametrization of the M-scheme C-parameter peak position $C^{M,\text{peak}}$ when considering the contribution where no radiation is present ("norad", unstable tree level configuration) which is given by

$$C_{\text{peak}}^{M} \equiv C_{(4),\text{ml},\pi/2}^{M,\text{norad}} = 12\,\frac{m^2}{Q^2}\left(1-4\,\frac{m^2}{Q^2}\right) \,. \tag{4.43}$$

More Realistic Case: $\hat{\theta}_{q_1}, \hat{\theta}_{q_2} \in [0,\pi]$ **(alternatively $n_3, n_3' \in [0,1]$)**

To cover the more realistic case of the top quark decaying into massless particles but with an arbitrary decay axis it is sensible to automatize the presented calculation[7] to some extent using computer algebra programs (in this case Mathematica [112]). Also in this case the collinear contributions involving gluons do not receive any correction when compared to the stable case. It turns out that the remaining ultracollinear contributions C_{cc}^{unstable} (c for collinear, i.e. either n or $\overline{n}$) are closely related to the contributions from the situation of an unstable heavy quark where no radiation is present C_{cc}^{norad} (unstable tree level configuration which means that the residual momentum is zero $\hat{k}_i = 0$ for $i \in \{1,2,3,4\}$).

Following the same procedure as before the different contributions to C_{cc}^{unstable} are then given by (again up to $\mathcal{O}(m^3\Delta/Q^4)$ corrections)

$$C_{nn}^{tt} - C_{nn}^{tt,\text{norad}} = 3\,\frac{m}{Q}\left(\frac{k_1^- + k_1^+ + k_2^- + k_2^-}{Q}\right) \,, \tag{4.44}$$

$$C_{\overline{nn}}^{\overline{tt}} - C_{\overline{nn}}^{\overline{tt},\text{norad}} = 3\,\frac{m}{Q}\left(\frac{k_3^- + k_3^+ + k_4^- + k_4^-}{Q}\right) \,, \tag{4.45}$$

$$2\,C_{n\overline{n}}^{t\overline{t}} - 2\,C_{n\overline{n}}^{t\overline{t},\text{norad}} = 3\,\frac{m}{Q}\sum_{i=1}^{4}\left(\frac{k_i^- + k_i^+}{Q}\right) \,. \tag{4.46}$$

Finally putting all expressions which contribute to Eq. (4.32) together, it is straightforward to arrive at the final expression for the unstable M-scheme C parameter measurement which is valid

---

[7]This was done by implementing the momenta as given before and expanding the expressions of interest for small $y = \frac{m^2}{Q^2}$ and $z = \frac{\Delta}{Q}$ separately. Then terms with arbitrary high orders only in y were kept while terms suppressed w.r.t. terms which scale like $\sqrt{y}\,z$ are omitted.

for four massless particles in the final state and arbitrary decay angles. Using the result for the stable measurement result $C^{M,\text{stable}}$ which is given in Eq. (4.41) and the stable threshold position $C^M_{\text{min}} = 12\frac{m^2}{Q^2}\left(1 - \frac{m^2}{Q^2}\right)$ the obtained result can be written as follows:

$$C^{M,\text{unstable}}_{(4),\text{ml}} = (C^{M,\text{stable}} - C^M_{\text{min}}) + C^{M,\text{norad}}_{(4),\text{ml}} + \mathcal{O}(m^3\Delta/Q^4) \,. \tag{4.47}$$

Here the subscripts again indicate that the final state consists of four massless particles. Comparing this result to Eq. (4.42) we find a very similar situation: The unstable measurement result is given by the full result for the stable situation (including ultracollinear radiation) shifted to zero plus the unstable tree level contribution (no radiation "norad") which parametrizes the full decay kinematics.

4.3.2 Six (Massive) Particles in the Final State

Finally let us cover the case of the previously discussed six particle final states Y_j. To investigate what happens we setup a decay chain with $t \to W^+b \to ff'b$ where we keep the W and b invariant mass nonzero. Using the same notation as for Eq. (4.35) the contributions to C^{unstable}_{cc} can then be written as follows:

$$C^{tt}_{nn} = C^{ff}_{nn} + C^{f'f'}_{nn} + C^{bb}_{nn} + 2\,C^{ff'}_{nn} + 2\,C^{fb}_{nn} + 2\,C^{f'b}_{nn} \,, \tag{4.48}$$

$$C^{t\bar{t}}_{n\bar{n}} = C^{f\bar{f}}_{n\bar{n}} + C^{f'\bar{f}'}_{n\bar{n}} + C^{b\bar{b}}_{n\bar{n}} + C^{f\bar{f}'}_{n\bar{n}} + C^{f'\bar{f}}_{n\bar{n}} + C^{f\bar{b}}_{n\bar{n}} + C^{b\bar{f}}_{n\bar{n}} + C^{f'\bar{b}}_{n\bar{n}} + C^{b'\bar{f}}_{n\bar{n}} \,, \tag{4.49}$$

and analogous for all others. Implementing the procedure which was used in the case of four massless final state particles can now be generalized to other event shapes like M-scheme thrust, C-parameter, Heavy Jet Mass and P-scheme angularities and a final state consisting of six (possibly) massive particles. Using the same automatized setup, the outcome, which holds for all the investigated cases, is consistent with what we found in Eq. (4.47) and is given by

$$e^{\text{unstable}}_{(6)} = \left(e^{\text{stable}} - e_{\text{min}}\right) + e^{\text{norad}}_{(6)} + \mathcal{O}(m^3\Delta/Q^4) \,, \tag{4.50}$$

where e^{stable} is the result for the measurement of the stable situation, e_{min} is the corresponding stable threshold (explicit expressions can be found in Tab. 3.1) and $e^{\text{norad}}_{(6)}$ is the measurement for the unstable tree level configuration. In conclusion the general situation confirms what we found for the simpler cases before: The full unstable event shape measurement is given by the measurement for the stable situation shifted to zero plus the contribution from the unstable tree level (no radiation "norad") measurement which parametrizes the full decay kinematics.

4.4 Cross Section Calculation with Unstable Heavy Quarks

Leading Order Cross Section

Using the results from Sec. 4.2 and Sec. 4.3 we can now write down a formula for the $e^+e^- \to t\bar{t} \to W^+bW^-\bar{b} \to b\bar{f}f'\bar{b}f''\bar{f}'''$ cross section at leading order which should be valid in the peak region where the top quarks are produced close to resonance and also where the collinear-soft power counting used in the previous chapter is applicable. For this formula we use the fact that the leading mass dependence of the stable cross section is contained in the on-shell threshold position e_{min}, hence in the NWA the stable cross section is independent of s_1 and s_2. Putting everything together we then arrive at

$$\frac{d\sigma}{de} = \left[1 + \mathcal{O}\left(\frac{\Gamma_t}{m_t}\right)\right] \int d\bar{e} \, \frac{d\sigma^{\text{stable}}}{de}(e - \bar{e}) \, F^{\text{decay}}(\bar{e}) \,, \tag{4.51}$$

with the stable cross section given by (shifted to a threshold of 0 if q_1 and q_2 are on-shell)

$$\frac{\mathrm{d}\sigma^{\text{stable}}}{\mathrm{d}e}(e) = \int \mathrm{d}\Pi_2(\vec{q}_1, \vec{q}_2) S_0(\vec{q}_1, \vec{q}_2)\, \delta\left(e - e^{\text{stable}}(\vec{q}_1, \vec{q}_2) + e_{\min}\right), \tag{4.52}$$

and the so called *decay function* defined as

$$
\begin{aligned}
F_{\text{decay}}(e) = {}& \int \mathrm{d}s_1\, f_{BW}(s_1, m_t, \Gamma_t) \int \mathrm{d}s_2\, f_{BW}(s_2, m_t, \Gamma_t) \\
& \times \int \frac{\mathrm{d}(\cos\hat{\theta}_{q_1})}{2} \frac{\mathrm{d}\hat{\varphi}_{q_1}}{2\pi} \int \frac{\mathrm{d}(\cos\hat{\theta}_{r_1})}{2} \frac{\mathrm{d}\hat{\varphi}_{r_1}}{2\pi} \int \frac{\mathrm{d}(\cos\hat{\theta}_{q_2})}{2} \frac{\mathrm{d}\hat{\varphi}_{q_2}}{2\pi} \\
& \times \int \frac{\mathrm{d}(\cos\hat{\theta}_{r_2})}{2} \frac{\mathrm{d}\hat{\varphi}_{r_2}}{2\pi}\, \delta\left(e - e^{\text{norad}}\left(s_1, s_2, \{\hat{\theta}_i, \hat{\varphi}_i\}\right)\right).
\end{aligned}
\tag{4.53}
$$

This result shows that for the peak region and within the uncertainties introduced by the assumptions made in the derivation, the cross section can be expressed as a convolution of the stable cross section and what we called decay function which parametrizes the decay kinematics and which was already briefly discussed in Ref. [55]. The decay function as defined in Eq. (4.53) can easily be extracted from a very basic MC integration program or any of the available multi-purpose numerical FO codes (also based on a MC integration). Details on the extraction of the decay function are given in Sec. 5.2.

Adding Radiation

Next we want to consider higher order QCD corrections. It is clear that with the same simplifications as used before one can keep the factorization of top pair production and decay shown in Eq. (4.51) intact. In the discussed partial narrow width approximation initially an off-shell $\bar{t}t$ quark pair is produced which radiates until both particles are on-shell which ends the production stage. During the subsequent decay stage the (anti-)top quark decays into a W-boson and a b-quark while additional radiation can come both from the top or bottom quark. The interpretation of this would then be a very long lived top quark which radiates and long after that, the decay happens where the decay products and additional radiation is produced.

For the radiation associated with the top pair production cross section one can again use effective field theory methods to resum large logarithms as for the usual stable case. The decay function as it is defined in Eq. (4.53) would then need to be generalized to higher orders which should be straightforward following the presented recipe.

Chapter 5

Numerical Investigations

5.1   Comparing Thrust: M-Scheme vs. P/E-Scheme

One area of application for high precision event shape calculations are α_s-fits using data from e^+e^- annihilation experiments. One such analysis is discussed in Ref. [100] where P-scheme thrust data with $Q \geq 35$ GeV from the TASSO, AMY, JADE, SLC, L3, DELPHI, OPAL and ALEPH experiments[1] was used to extract a highly precise value for $\alpha_s(m_Z)$.

To estimate mass effects of bottom quarks which become more important at low energies the calculation for M-scheme thrust from Ref. [7,8] was used. This is done because the initially produced (close to) on-shell heavy quarks hadronize and subsequently the heavy hadrons decay into light hadrons which are measured in the detector. It is easy to check that for the situation of massless final state particles which originate from an intermediate heavy particle the P-scheme thrust distribution gets a non-zero threshold location which is exactly situated at the M-scheme thrust threshold. When a heavy on-shell particle decays into massless particles the angle between the trajectories of the decay products will be non-zero, which gives rise to the mentioned shift of the threshold position in comparison with the stable case. To account for this effect, which can also be seen experimentally in flavor tagged analyses [113–115], the approximate treatment of using M-scheme thrust with the massless hadronization function is used.

Another approach which is cleaner in terms of factorization between partonic and non-perturbative contributions would be to calculate the partonic cross section using the jet function for P-scheme thrust from Sec. 3.5.4 and include effects from the heavy hadron decay in the non-perturbative shape function, which would now induce the shift as well as potentially other decay related non-perturbative effects. This would of course mean that the shape function which includes the effects from the decay of the B-hadrons would need to be fitted to data from tagged analyses which is beyond the scope of this work.

Nevertheless it is interesting to compare the predictions for the singular partonic M- and P-scheme thrust cross section for $e^+e^- \to b\bar{b}$. As discussed, the shift of the P-scheme cross section to the M-scheme threshold is part of the corresponding hadronization function but to improve the comparability we shift the P-scheme cross section to the same threshold. Using the massive M-scheme thrust profiles, discussed in Sec. 3.8, for both cross section calculations (for P-scheme for the shifted case) the obtained result for this comparison is shown in Fig. 5.1. Furthermore also the massless singular thrust distribution with massless profiles shifted to the M-scheme threshold is shown for comparison.

Analyzing the shown plots one can see that for most of the event shape range the two schemes lead

---
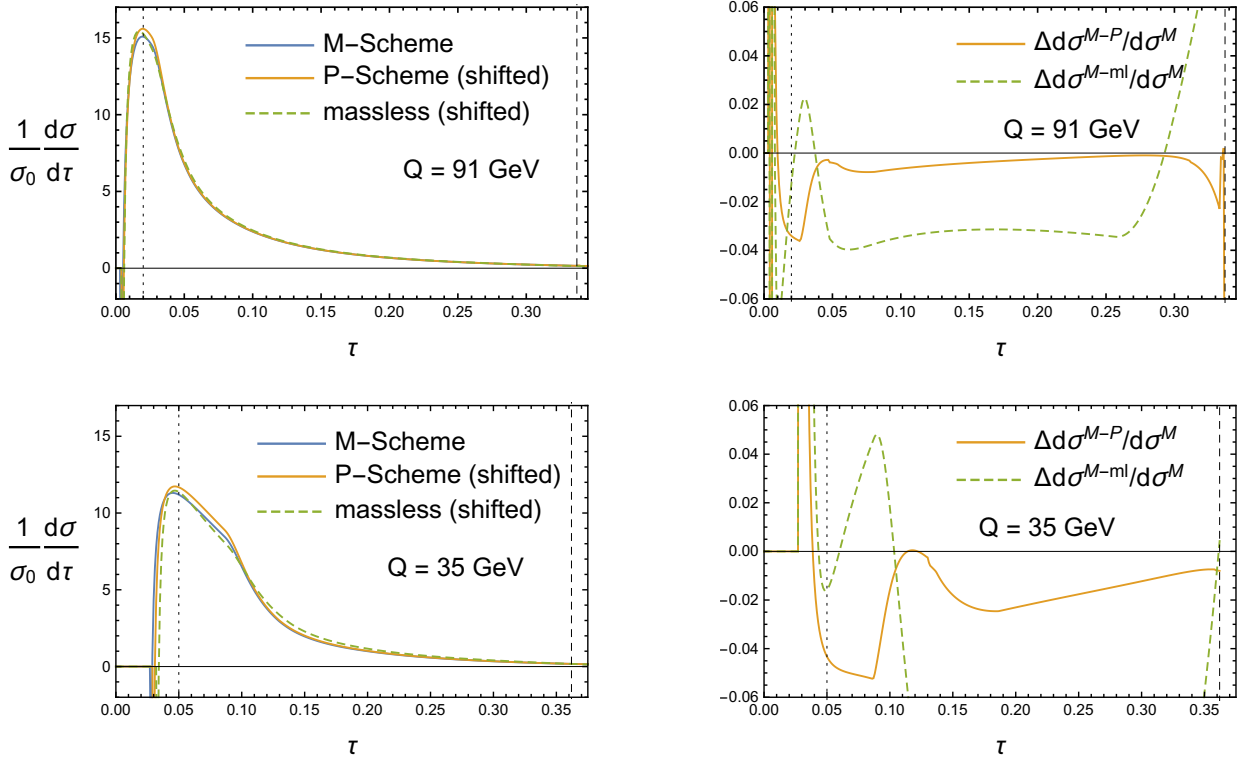
[1]References can be found in [100].

Figure 5.1: Comparison plots (left) for the M- and shifted P-scheme singular thrust cross section with $\overline{m}_b(\overline{m}_b) = 4.2$ GeV as well as the shifted massless singular thrust distribution at a center of mass energy of $Q = 91.187$ GeV (upper) and 35 GeV (lower). Furthermore the relative difference (right) with respect to the M-scheme cross section is shown for both energies. Also the approximate peak position (black dotted) and the $\mathcal{O}(\alpha_s)$ partonic end point for M-sheme thrust $\tau_{\max}^M = \left(5 - 4\sqrt{1 - 3m^2/Q^2}\right)/3$ (black dashed) are plotted.

to very similar results. Ignoring the region of small cross section values left of the peak, the biggest difference can be seen close to the peak position which still does not exceed 5% relative difference (with respect to the M-scheme thrust).

Using the assumption that the non-singular cross-section is small in the region where the singular cross section is sizable (this is true for the massless case - see Fig. 7 in Ref. [100]) and that hadronization differences are small with the exception of the discussed threshold shift, we can conclude that indeed using the M-scheme thrust distribution to approximate the P-scheme cross section is justified and that the additional uncertainty is of order five percent.

5.2 Decay Functions

In Chap. 4 event shape distributions for boosted unstable top quark pair production were discussed. It turns out that so-called non-clustering event shapes are sensitive to the decay of the top quark beyond what is captured by including width effects via the convolution with a Breit-Wigner function. After this qualitative observation the decay function framework was developed in which the unstable cross section is given by a convolution of the stable cross section and a so-called decay function which parametrizes the exact decay configuration. The aim of this section is to develop the notion of the decay function further and to extract the exact form from numerical fixed-order calculations.

5.2.1 Theoretical Discussion

As we have seen in Sec. 4.1.2 the peak position of the event shape distribution $e_{\text{peak}}(y \equiv m^2/Q^2)$ for non-clustering event shapes does not necessarily coincides with the tree level threshold position e_{min}. Using the assumption that the leading heavy quark mass dependence of the unstable tree level measurement (no radiation "norad") in the peak region is contained in the peak position e_{peak} it is possible to further factorize the decay function as follows:

$$
\begin{aligned}
F_{\text{decay}}(e) = \int \frac{\mathrm{d}(\cos \hat{\theta}_{q_1})}{2} \frac{\mathrm{d}\hat{\varphi}_{q_1}}{2\pi} \int \frac{\mathrm{d}(\cos \hat{\theta}_{r_1})}{2} \frac{\mathrm{d}\hat{\varphi}_{r_1}}{2\pi} \int \frac{\mathrm{d}(\cos \hat{\theta}_{q_2})}{2} \frac{\mathrm{d}\hat{\varphi}_{q_2}}{2\pi} \\
\times \int \frac{\mathrm{d}(\cos \hat{\theta}_{r_2})}{2} \frac{\mathrm{d}\hat{\varphi}_{r_2}}{2\pi} \int \mathrm{d}\hat{e}\, \delta\Big(e - e^{\text{norad}}\big(m_t^2, m_t^2, \{\hat{\theta}_i, \hat{\varphi}_i\}\big) + e_{\text{peak}}(\tfrac{m_t}{Q^2}) - \hat{e}\Big) \\
\times \int \mathrm{d}s_1\, \mathrm{d}s_2\, f_{BW}(s_1, m_t, \Gamma_t)\, f_{BW}(s_2, m_t, \Gamma_t)\, \delta\big(\hat{e} - e_{\text{peak}}(\tfrac{s_1}{Q^2})/2 - e_{\text{peak}}(\tfrac{s_2}{Q^2})/2\big)\,,
\end{aligned}
\tag{5.1}
$$

where we used that the top and anti-top both contribute half of the peak position. At this point it is easy to see that there is no real dependence on e_{peak}. Choosing the appropriate expression which captures the leading mass dependence of the distribution will optimize how well the above factorization works.

In a next step we exploit the fact that in the peak region $\big(s_{1/2} - m_t^2\big)/Q^2 \equiv a_{1/2}$ will be small and therefore we can write

$$
\hat{e} - e_{\text{peak}}(\tfrac{s_1}{Q^2})/2 - e_{\text{peak}}(\tfrac{s_2}{Q^2})/2 = \hat{e} - e_{\text{peak}}(\tfrac{m_t^2}{Q^2}) - e'_{\text{peak}}(\tfrac{m_t^2}{Q^2})\,(a_1 + a_2)/2 + \mathcal{O}\big(a_1 a_2, a_1^2, a_2^2\big)
\tag{5.2}
$$

which by using the substitutions $a = a_1 + a_2$ and $\tilde{e} = \hat{e} - e_{\text{peak}}(m_t^2/Q^2)$ gives a single Breit-Wigner with width $2\Gamma_t$ convoluted with $\delta\big(\tilde{e} - e'_{\text{peak}}(m_t^2/Q^2)\, a/2\big) = 2\,\delta\big(a - 2\tilde{e}/e'_{\text{peak}}(m_t^2/Q^2)\big)/e'_{\text{peak}}(m_t^2/Q^2)$.

Using this, the decay function factorizes further and can be written in the following way:

$$
\begin{aligned}
\hat{F}_{\text{decay}}(e) = \int \frac{\mathrm{d}(\cos \hat{\theta}_{q_1})}{2} \frac{\mathrm{d}\hat{\varphi}_{q_1}}{2\pi} \int \frac{\mathrm{d}(\cos \hat{\theta}_{r_1})}{2} \frac{\mathrm{d}\hat{\varphi}_{r_1}}{2\pi} \int \frac{\mathrm{d}(\cos \hat{\theta}_{q_2})}{2} \frac{\mathrm{d}\hat{\varphi}_{q_2}}{2\pi} \int \frac{\mathrm{d}(\cos \hat{\theta}_{r_2})}{2} \frac{\mathrm{d}\hat{\varphi}_{r_2}}{2\pi} \\
\times \int \mathrm{d}\tilde{e}\, \delta\Big(e - e^{\text{norad}}\big(m_t^2, m_t^2, \{\hat{\theta}_i, \hat{\varphi}_i\}\big) - \tilde{e}\Big)\, f_{BW}\Big(Q^2\, \tilde{e}, m_t, \Gamma_t\, e'_{\text{peak}}(\tfrac{m_t^2}{Q^2})\Big) \\
= \int \mathrm{d}\tilde{e}\, F_{\text{decay}}^{\text{NWA}}(e - \tilde{e})\, f_{BW}\Big(Q^2\, \tilde{e}, m_t, \Gamma_t\, e'_{\text{peak}}(\tfrac{m_t^2}{Q^2})\Big)\,.
\end{aligned}
\tag{5.3}
$$

where $F_{\text{decay}}^{\text{NWA}}$ denotes the original decay function in the narrow width approximation (NWA).

In comparison with Eq. (4.4) we find that even for event shapes with the clustering property Eq. (5.3) captures subleading Breit-Wigner effects not present in Eq. (4.4). For the originally discussed case of jet masses the two coincide. As a representative example let us consider top quark pair production with $m_t = 173$ GeV and $Q = 700$ GeV for the case of M-scheme thrust and C-parameter where we choose

$$
\tau_{\text{peak}}^M = 1 - \sqrt{1 - 4\frac{m^2}{Q^2}}\,, \qquad\qquad C_{\text{peak}}^M = 12\,\frac{m^2}{Q^2}\left(1 - 4\frac{m^2}{Q^2}\right).
\tag{5.4}
$$

For thrust e_{peak} is simply set to the stable threshold position due to the realized clustering property and for C-parameter we take the result from Eq. (4.43) which is related to the prototypical collinear decay configuration studied in Sec. 4.3.1. Using this we find a correction to the width due to the subleading Breit-Wigner effects of 15% for thrust and -12% for C-parameter.
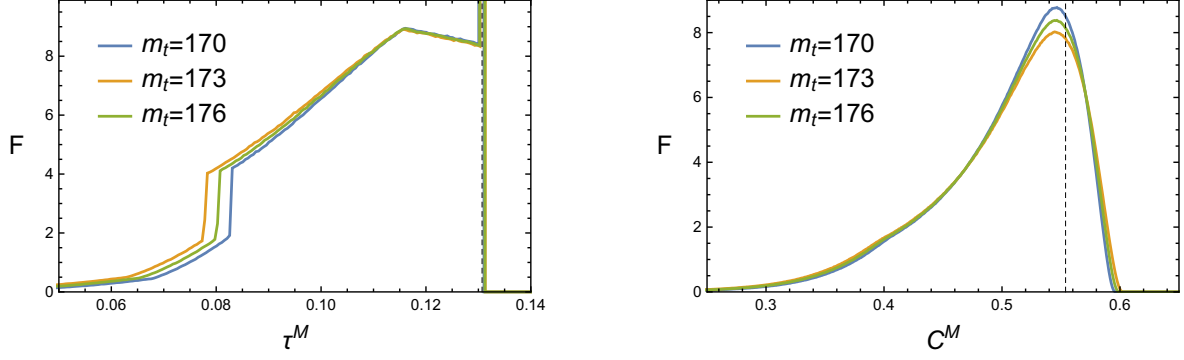
Figure 5.2: Comparison plots for the NWA decay function shiftet by $e_{\text{peak}}(\frac{m^2}{Q^2})$ (dashed black for $m_t = 173$ GeV) for M-scheme thrust and C-parameter for a center of mass energy $Q = 700$ GeV. The normalization factor N is chosen in such a way so that the decay function is normalized.

5.2.2 Extracting the Decay Function from Simulation

Leading Order

The decay function is given in Eq. (4.53) which involves the collinear measurement of the tree level process including heavy quark decay denoted by e^{norad} (alternatively no-radiation measurement) which in general depends on the (anti-)top invariant mass $s_1(s_2)$. Such a function can easily be extracted from a MC simulation[2], e.g. PYTHIA 8.2, where the parton shower and hadronization is turned off. Using data from a high-statistics run with 10^7 events at a center of mass energy $Q = 700$ GeV and with different top quark mass one can straightforwardly extract the decay functions of interest. As an example the full decay function for M-scheme thrust and C-parameter are shown in Fig. 5.3.

Following the discussion from the previous subsection it is interesting to check how well the additional factorization of Eq. (5.3) works. For that a precise extraction of the Decay function in the NWA is needed. The result for M-scheme thrust and C-parameter which is shifted by the appropriate e_{peak} (again we use the choice of Eq. (5.4)) for a c.o.m. energy $Q = 700$ GeV and a top quark mass of $m_t = \{170, 173, 176\}$ GeV is shown in Fig. 5.2.

One thing which immediately becomes clear when looking at Fig. 5.2 is that close to the peak position for thrust indeed the dependence on the exact mass value seems to be quite small (when shifted correctly). For C-parameter the central mass value still has some effect on the width of the distribution but it is much smaller than the effect of the shift and it is clear that the choice for C_{peak}^M works very well.

Next let us consider the example of the full decay function for $m_t = 170$ GeV and $\Gamma_t = 1.4$ GeV at a c.o.m. energy $Q = 700$ GeV and compare it with the $m_t = 170$ GeV NWA decay function convoluted with the Breit-Wigner with modified width of $\Gamma = \Gamma_t\, e'_{peak}(\frac{m_t^2}{Q^2})$ (according to Eq. (5.3)). The result of this comparison for M-scheme thrust and C-parameter is shown in Fig. 5.3 which shows that the decay function factorization of Eq. (5.3) works very well for both investigated event shapes.

As we have seen in Fig. 5.2 the dependence on the exact mass value beyond shifting the distribution to the appropriate value of e_{peak} is quite small. It is now interesting to check if it is possible to

---

[2]Caveat: Due to the setup of the decay chain, in some MC generators e.g. PYTHIA, spin correlations are not fully considered. Investigations carried out with WHIZARD show no noticable differences for the observables presented here. Nevertheless for the case of light jet mass (LJM) the differences were severe which is why in general one should consider this when looking at new observables.
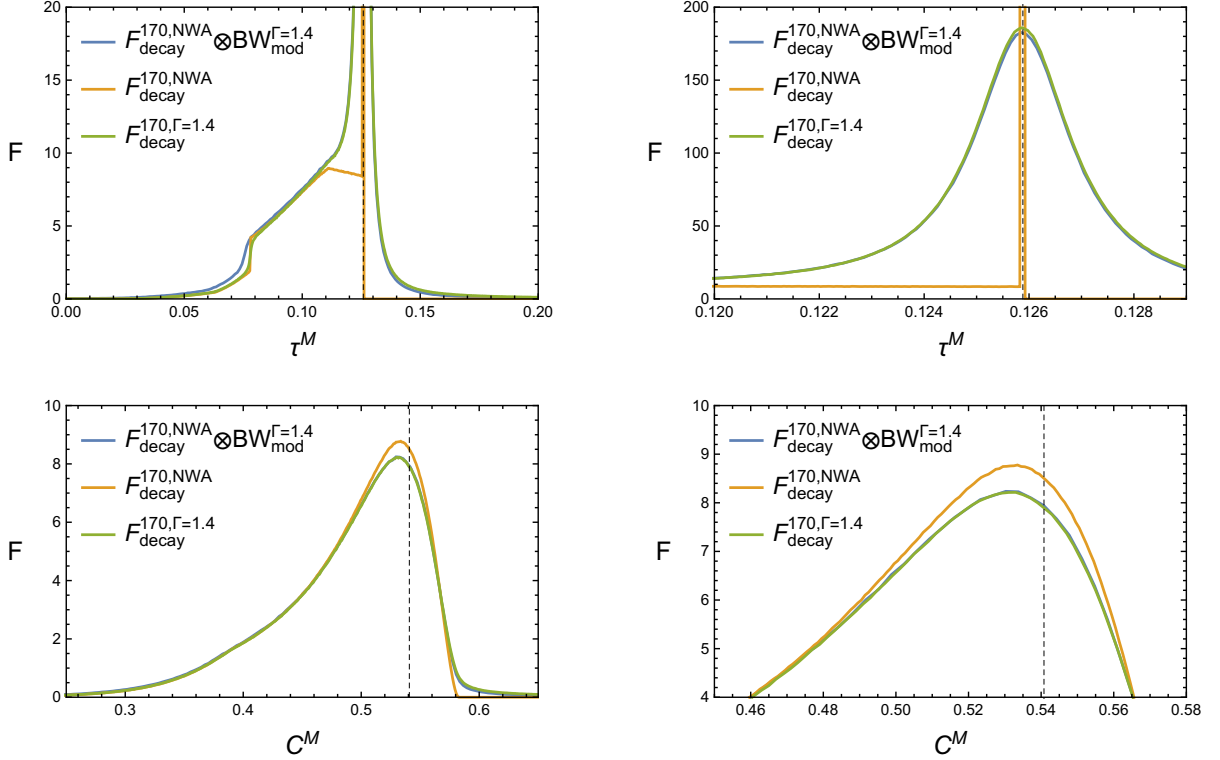
Figure 5.3: Comparison plot for M-scheme thrust (upper row) and C-parameter (lower row) with $m_t = 170$ GeV and c.o.m. energy $Q = 700$ GeV plotted as an overview (left) and just for the peak region (right) including $e_{\text{peak}}(\frac{m^2}{Q^2})$ (dashed black for $m_t = 170$ GeV). The plots contain the full decay function (green), the NWA decay function (orange) and the convolution of the same NWA decay function with the modified width Breit-Wigner with $\Gamma = \Gamma_t\, e'_{peak}(\frac{m_t^2}{Q^2})$ (blue). The normalization factor N is chosen in such a way so that the whole distribution is normalized.

use a NWA decay function for a generic mass (here we take $m_t = 173$ GeV) which is shifted to the appropriate e_{peak} as a replacement for the NWA decay functions for other mass values. In order to investigate this we again compare the full decay function for $m_t = 170$ GeV and $\Gamma_t = 1.4$ GeV at a c.o.m. energy $Q = 700$ GeV with the shifted $m_t = 173$ GeV NWA decay function convoluted with the Breit-Wigner with modified width. The result is then shown in Fig. (5.4) and we find that the use of a generic mass NWA decay function works very well for thrust. In the case of C-parameter the mass dependence of the NWA decay function width which was seen in Fig. 5.2 is also visible for this case but overall we find that this still leads to a good approximation.

Overall we conclude that the additional decay function factorization of Eq. (5.3) works very well for both investigated event shapes. Moreover, we find that for thrust any correctly shifted NWA decay function is suitable. For the case of C-parameter using the correct NWA decay function seems to be the better choice.

Higher Order

To achieve a full next-to-leading order cross section calculation in principle also a NLO decay function is needed in addition to the NLO stable event shape distribution. In principle this can be extracted from any multi-purpose fixed order Monte Carlo generator which fully implements the factorization between production and and decay and describes the decay at NLO-QCD. On the decay side the
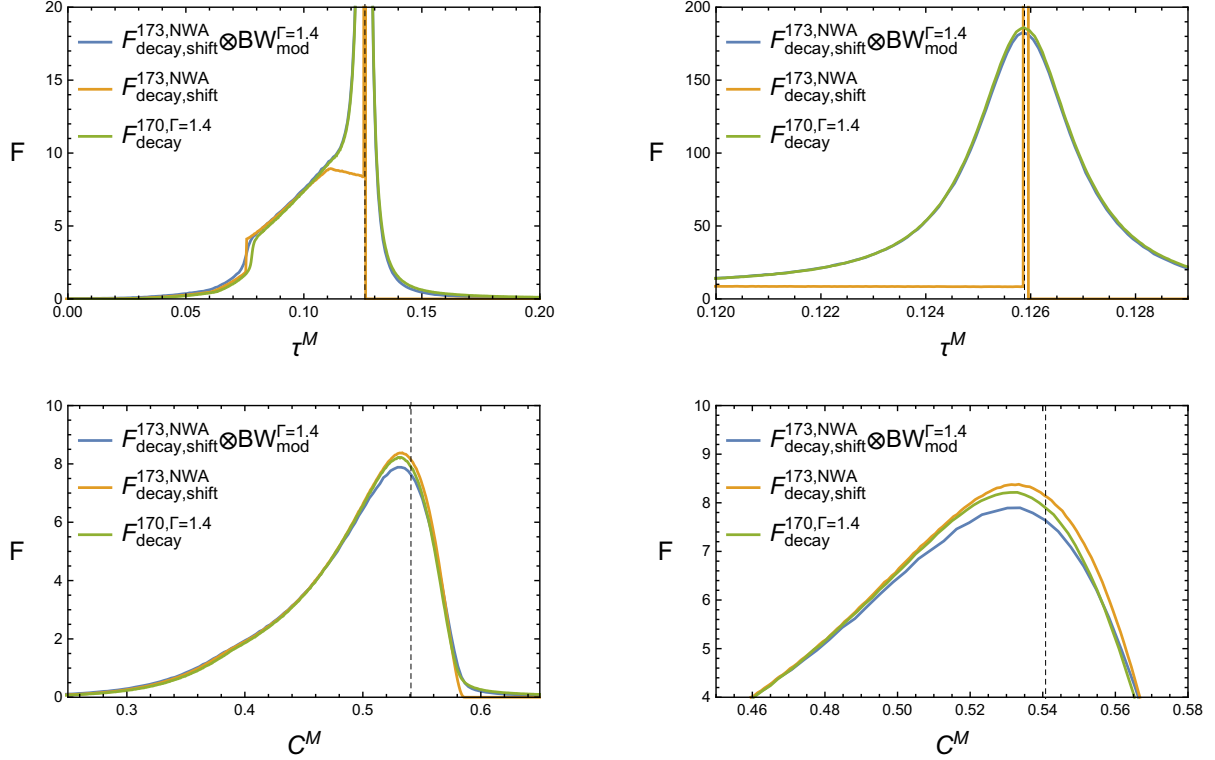
Figure 5.4: Comparison plot for M-scheme C-parameter with $m_t = 170$ GeV and c.o.m. energy $Q = 700$ GeV plotted as an overview (left) and just for the peak region (right) including $e_{\text{peak}}(\frac{m_t^2}{Q^2})$ (dashed black for $m_t = 170$ GeV). The plots contain the full decay function (green), the shifted NWA decay function (orange) and the convolution of the same shifted NWA decay function with modified width Breit-Wigner with $\Gamma = \Gamma_t\, e'_{peak}(\frac{m_t^2}{Q^2})$ (blue). As the input mass for the shifted NWA decay function $m_t = 173$ GeV is used. The normalization factor N is chosen in such a way so that the whole distribution is normalized.

additional gluon can be radiated off the final state $(\bar{b})b$ quark or originate from the "initial" state on-shell top which also involves non-trivial IR cancellations between the final and initial state radiation. This is discussed in more detail in Ref. [116] and should be correctly treated in the "SM_threshold" mode of WHIZARD (only for the case of $e^+e^- \to t\bar{t} \to W^+b\,W^-\bar{b}$ - with a form factor of 1). Unfortunately extracting the decay function at NLO was not yet successful and with the used version of WHIZARD (2.5.0) does lead to numerical inconsistencies. This issue was pointed out to the authors of the software and will hopefully be resolved in the future which will then allow to extract a full NLO decay function.

It is nevertheless interesting to investigate the difference compared to the LO result of the previous section when running PYTHIA with parton shower turned on (still without hadronization) and implementing a veto on events where radiation off the top and anti-top quark happens. We note that, vetoing events with (anti-)top radiation is not gauge invariant and in principle also vetoes radiation off the top which normally would contribute to the top quark decay at NLO. Analyzing this for the appropriate event shape should nevertheless give a partial higher order decay function. For this we generate data with $m_t = 173$ GeV, a c.o.m. energy of $Q = 700$ GeV and 2×10^7 events and apply the appropriate veto. The result and comparison to the LO decay function for M-scheme thrust and C-parameter can be seen in Fig. 5.5.

It can clearly be seen that adding radiation off the $(\bar{b})b$ quark which is produced in the parton shower step of the MC event generator does only slightly modify the extracted NWA decay function. For
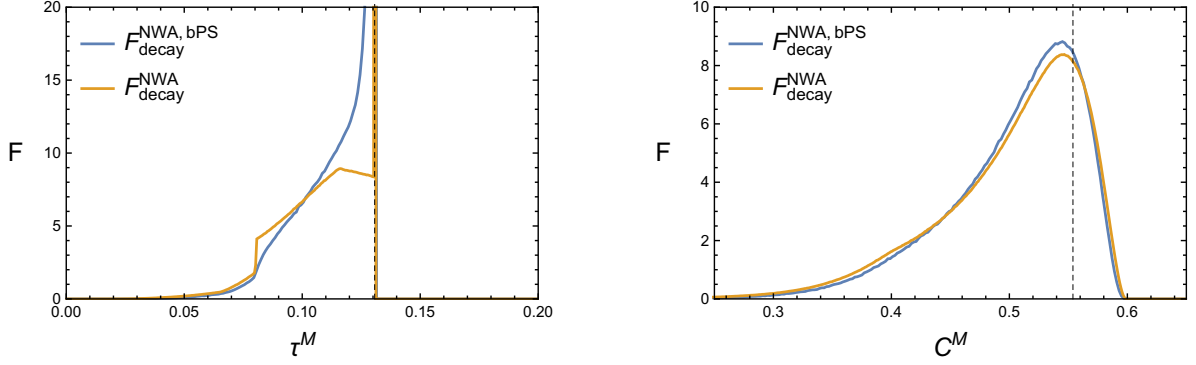
Figure 5.5: Comparison plots for the NWA decay function with $m_t = 173$ GeV and a center of mass energy $Q = 700$ GeV for M-scheme thrust and C-parameter. The plots show the NWA decay function at leading order (orange) and with additional parton shower radiation off the $(\bar{b})b$ quark (blue) and for comparison $e_{\text{peak}}(\frac{m^2}{Q^2})$ (dashed black for $m_t = 173$ GeV). The normalization factor N is chosen in such a way so that the decay function is normalized.

thrust less events are part of the delta function peak and the structure left of the peak gets smeared out. For C-parameter a small shift of the peak position to the left and a slightly smaller overall width is visible.

5.2.3 Testing Decay Factorization for PYTHIA at Parton Level

In this subsection the aim is to check how the derived factorization of the cross section into stable cross section, decay function and Breit Wigner function with modified width works at parton shower level. Using the same setup as before but now with parton shower turned on gives the result for M-scheme thrust and C-parameter which can be seen in Fig. 5.6.

From the shown plots it is quite clear that the discussed factorization also works well at parton shower level. One can observe that for the case of thrust the decay function which includes the radiation off the $(\bar{b})b$ quark works significantly better in describing the peak position and width. For the C-parameter one can conclude that adding radiation off the top decay products has less influence on the already much wider peak.

The fact that including radiation off the bottom quarks leads to a much better description for thrust could hint to either of the following possibilities: (1) The radiation off the top quark which is part of the top decay at NLO does not contribute much to the overall distribution. The decay function with radiation off the bottom then leads to an improved overall result when compared with the LO decay function. (2) For some technical reason all gluons which in the event record are labeled as coming from the top quark (events which include any such gluon are vetoed) are in fact only the ones which are part of the production step of the event. Gluons which originate from the top but belong to the decay stage are marked as "coming from the b" in the event record and are therefore correctly included in the extracted higher order decay function which then leads to an improved overall result when compared with the LO decay function.

5.3 Unstable M-scheme C-parameter and PYTHIA Comparison

In this subsection we want to present a first qualitative comparison of M-scheme C-parameter (here just C-parameter) in the peak region between the resummed full unstable singular cross section
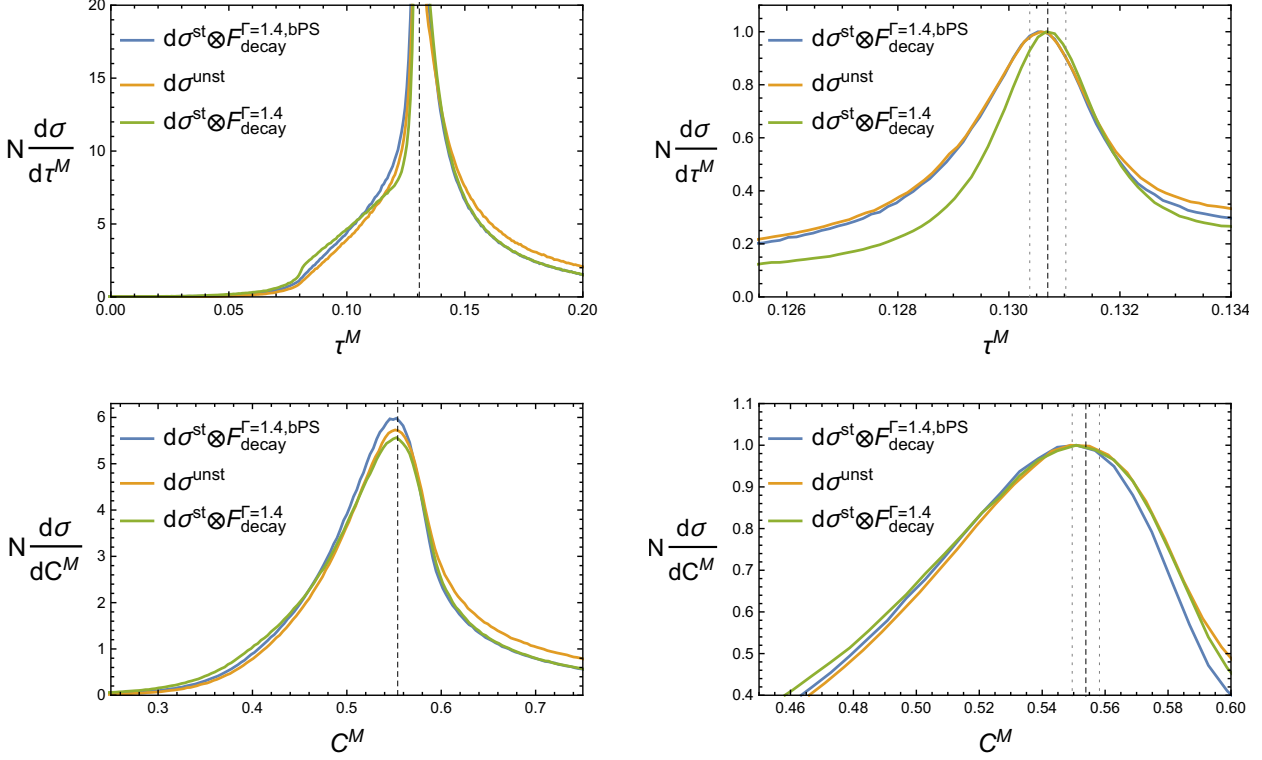
Figure 5.6: Comparison plot for the PYTHIA 8 parton level cross section with $m_t = 173$ GeV, $\Gamma_t = 1.4$ GeV and a c.o.m. energy $Q = 700$ GeV for M-scheme thrust and C-parameter. The plots show the full unstable cross section result (orange), the stable cross section convoluted with the LO decay function (green) and the same stable cross section convoluted both with the NWA decay function including radiation off the $(\bar{b})b$ quark and with the Breit-Wigner function with modified width $\Gamma = \Gamma_t\, e'_{peak}(\frac{m_t^2}{Q^2})$ (blue). For comparison $e_{\text{peak}}(\frac{m^2}{Q^2})$ is plotted for $m_t = 173$ GeV (dashed black) as well as for $m_t = 173.0 \pm 0.2$ GeV for thrust and $m_t = 173 \pm 1$ GeV for C-parameter (gray dotted). The normalization factor N for the overview plot (left) is chosen in such a way so that the distribution is normalized and for the peak region plot (right) so that the maximum of the distribution equals 1.

(NNLL+NLO) and PYTHIA 8.2 at hadron level. The aim of this comparison is to study how well the discussed description works when compared to the case of 2-jettiness (M-scheme thrust - here just thrust) which was extensively studied in the context of Ref. [6,9]. Furthermore we want to get a first qualitative impression on the general suitability and expected precision for using the full unstable C-parameter for Monte Carlo top quark mass calibrations as explained in Sec. 2.4.

In the following we will show plots involving uncertainty bands representing perturbative uncertainties. These bands are obtained by choosing 100 random sets of profile function parameters (flat random distribution in the specified range) and the band then shows the envelope of all of these cross section predictions.

5.3.1 Profile Functions and Convergence

To get meaningful predictions for the resummed singular C-parameter cross section in the peak region the profile functions need to be checked and optimized first. In Sec. 3.8 a general discussion concerning the profile functions and their generalization to the massive and stable case was presented. The default profile function parameters for the unstable case of thrust were optimized in Ref. [9] and the final parameter choices are given in Tab. 3.4. Comparing the convergence of the resummed result for the
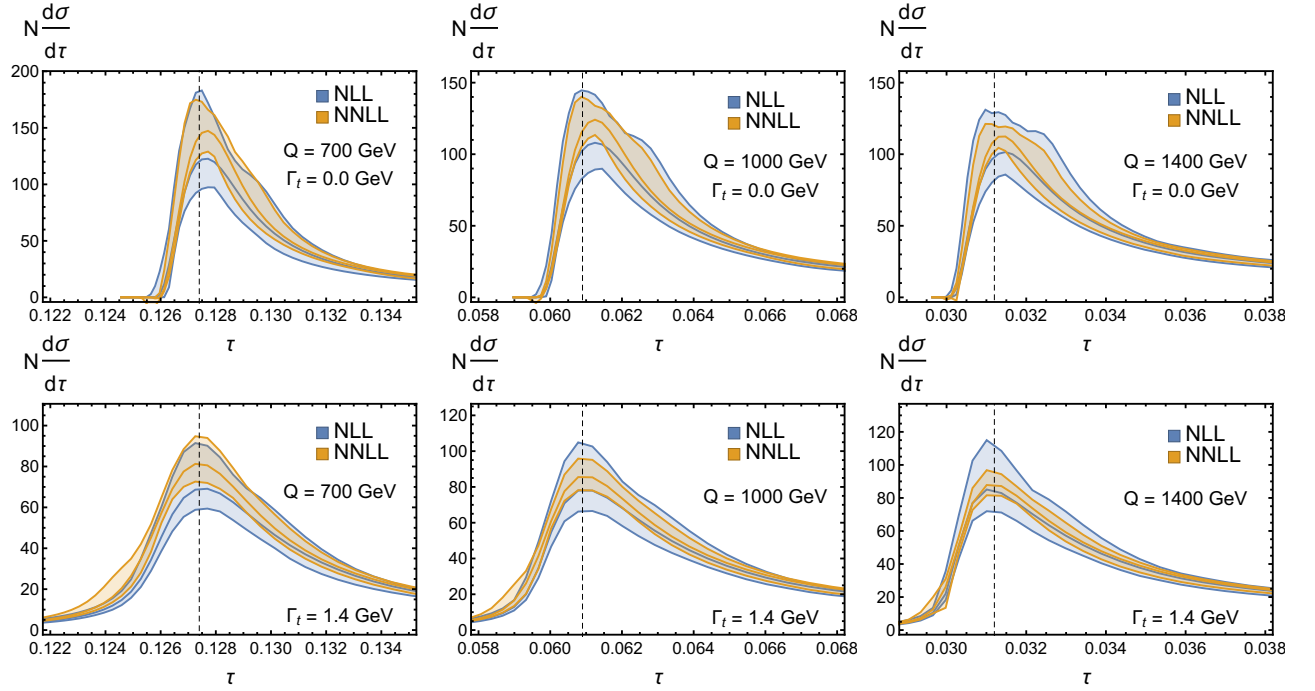
Figure 5.7: Convergence plots for M-scheme thrust with $\overline{m}_t(\overline{m}_t) = 160$ GeV (converted to the MSR mass scheme which is used for the calculation), $\alpha_s(m_Z) = 0.118$ and different c.o.m. energies Q for the stable (upper row) and the unstable (lower row) case with $\Gamma_t = 1.4$ GeV. Furthermore the approximate stable peak position (black dashed) is plotted for comparison between the two rows. The normalization factor N is chosen in such a way so that the distribution is normalized. For additional profile function information see Sec. 3.8.

| e | τ | C | |
	default	default	optimized
μ_0	3.00	3.00	1.7
R_0	2.25	2.25	1.275
abs	0	1	1

Table 5.1: Subset of default profile function parameter choices for the unstable case of M-scheme thrust and C-parameter. Note that these parameters have no variation. For C-parameter the optimized choice leads to an improvement in peak position stability with respect to the default choice which is inspired by the thrust case. For a complete list of the other default profile function parameters and their variation see Tab. 3.4
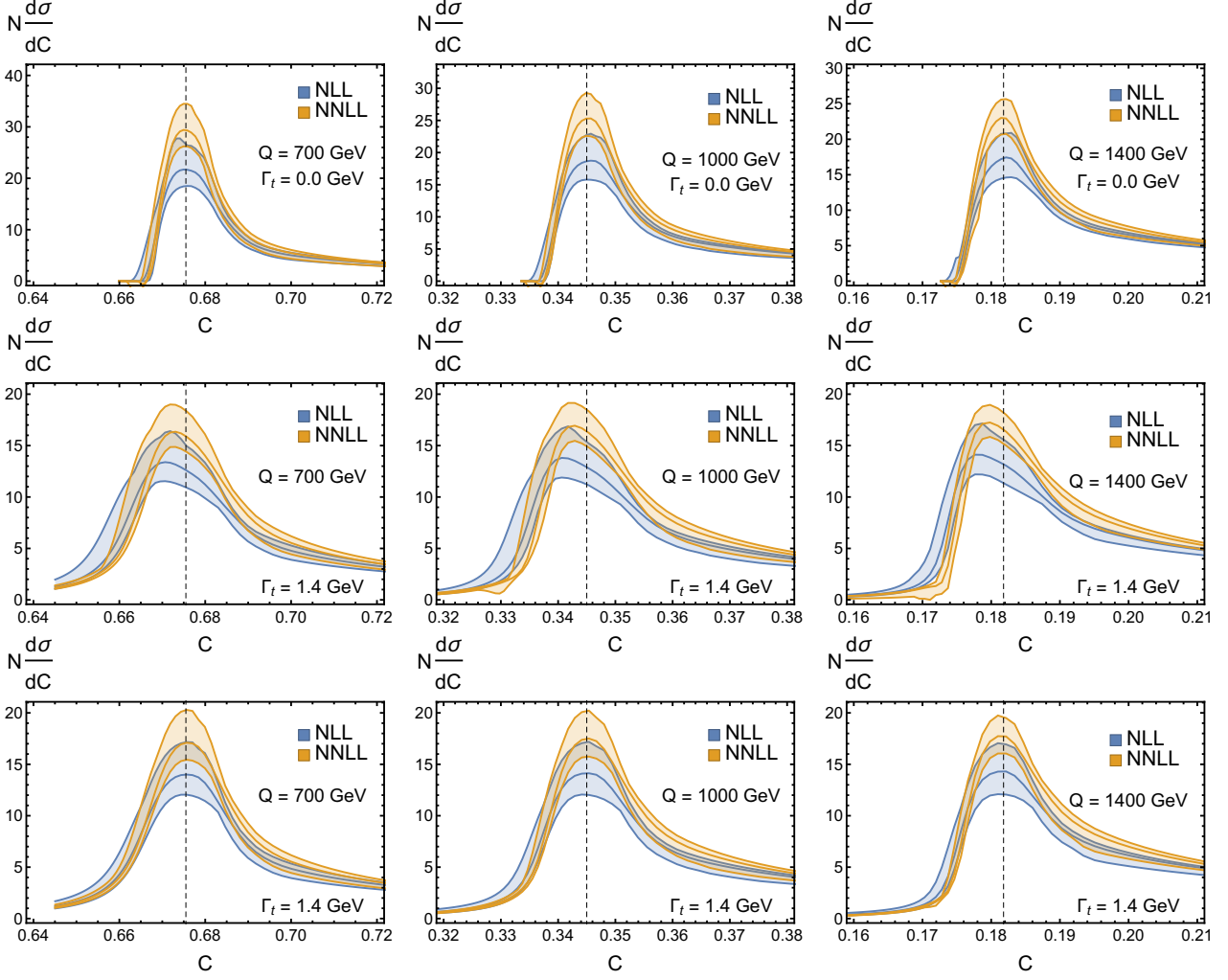
Figure 5.8: Convergence plots for M-scheme C-parameter with $\overline{m}_t(\overline{m}_t) = 160$ GeV, $\alpha_s(m_Z) = 0.118$ and different c.o.m. energies Q for the stable (upper row) and the unstable case with default profiles (middle row) and the unstable case with optimized profiles (lower row), both with $\Gamma_t = 1.4$ GeV. Furthermore the approximate stable peak position (black dashed) is plotted for comparison between the rows. The normalization factor N is chosen in such a way so that the full distribution is normalized. For additional profile function information see Sec. 3.8.

stable and unstable without decay function case at next-to-leading (NLL) vs. next-to-next-to-leading order (NNLL) for the case of thrust is shown in Fig. 5.7 for different c.o.m. energies. The default profile function parameters which are different with respect to the stable case are summarized in Tab. 5.1.

From the shown plots a good convergence of the thrust cross section predictions can be seen when going from NLL to NNLL. It is clearly visible that the width of the uncertainty band decreases, the peak position is stable and also the peak width shows nice stability at all the center of mass energies which were investigated.

In case of the unstable top C-parameter we start with the generalization of the massless profile functions for the massive stable case (discussed in Sec. 3.8). Next we setup the unstable C-parameter profiles in analogy to the case of thrust. The result of this first try with the default parameter choice summarized in Tab. 5.1, is shown in Fig. 5.8. While generating those plots, it turns out that for the unstable case of C-parameter it is necessary to keep the absorption of nonsingular distributions into the singular cross section turned on, which will therefore be used as the default.

From the shown plots for the default profile function parameter choices (top two rows) we see the following: For the stable case one finds reasonably good convergence in the peak region. The width of the band decreases while the peak position shows nice stability. The peak width is not as stable as in the case of thrust but the changes are small and consistent for the investigated energies. On the other hand the unstable case without decay function and with default profile parameter choice is problematic. Although the width of the band still decreases, the peak position becomes unstable and also a shift of the position with respect to the stable case is visible which is not present for the thrust case.

To improve this situation we next take an optimized set of profile function parameters, also see Tab. 5.1. The results for this choice is also shown in Fig. 5.8 (lower row) where a significant improvement with respect to the default case is visible. In this case the width of the uncertainty band decreases and also the peak positions show good stability. The width of the peak behaves consistently with the stable case and more importantly there is no shift in the peak position with respect to the stable case. Overall we find a qualitatively similar result as for the case of thrust when using the optimized profile parameters for C-parameter.

5.3.2 Comparison with PYTHIA

In this subsection we now take the singular unstable hadron level prediction at NNLL for the peak region of thrust and C-parameter and compare it with pseudo data obtained from PYTHIA 8.2. The numerical value for the top quark mass and the first shape function moment which leads to the best fitting prediction (in a wide range of c.o.m. energies) for the thrust peak region was determined in the MC top quark mass calibration of Ref. [6]. Using the gap input value of $\overline{\Delta}(R = 2\,\text{GeV}, \mu = 2\,\text{GeV}) = 0.1$ GeV and the top quark mass parameter input for the simulation of $m_t^{\text{MC}} = 173$ GeV the following results were obtained for the mass and first moment of the shape function:

$$m_t^{\text{MSR}}(R = 1\,\text{GeV}) = (172.82 \pm 0.22)\ \text{GeV}\ , \tag{5.5}$$
$$\Omega_1^{\tau,\text{PYTHIA}} = (0.84 \pm 0.16)\ \text{GeV}\ . \tag{5.6}$$

This corresponds to a $\overline{\text{MS}}$ mass of $\overline{m}_t(\overline{m}_t) = 162.95$ GeV and for the most simple shape function i.e. $\{c_0 = 1, c_{i \neq 0} = 0\}$ the only free model parameter is given by $\xi = 0.74$ GeV.

Next we generate theory predictions for the unstable thrust cross section (no decay function, just Breit-Wigner, as in Ref. [6]) with a c.o.m. energy of $Q = 700$ GeV and $Q = 1000$ GeV, the above input parameters, a top width of $\Gamma_t = 1.4$ GeV and a ± 1 GeV variation for the top mass. These predictions are then compared to PYTHIA pseudo data. The obtained result is then shown in Fig. 5.9. From this plot one can see that regarding the peak position and within the perturbative uncertainties the input parameters indeed lead to a good fit with the PYTHIA pseudo data. Furthermore for thrust a change of ± 1 GeV in the input mass leads to very different peak positions (in particular for $Q = 700$ GeV) which made it possible to carry out a MC top quark mass calibration with a calibration uncertainty of 220 MeV [6].

After this check for thrust one can take the next step and look at the analogous plots for C-parameter which is shown in Fig. 5.10. Due to the lower expected mass sensitivity for the full unstable C-parameter we take a ± 3 GeV variation for the input value of the top quark mass. Comparing the unstable result without decay function (dashed) with the pseudo data obtained from PYTHIA it becomes clear that the discussed convolution with the decay function (see Sec. 4.4) is needed.

To achieve that, we follow Eqs. (4.51) and (5.3) and convolute each of the 100 inclusive unstable cross section predictions (which make up the perturbative uncertainty band and which already contain the convolution with the Breit-Wigner function) with the respective NWA decay function (with $m_t = \{170, 173, 176\}$ GeV respectively).
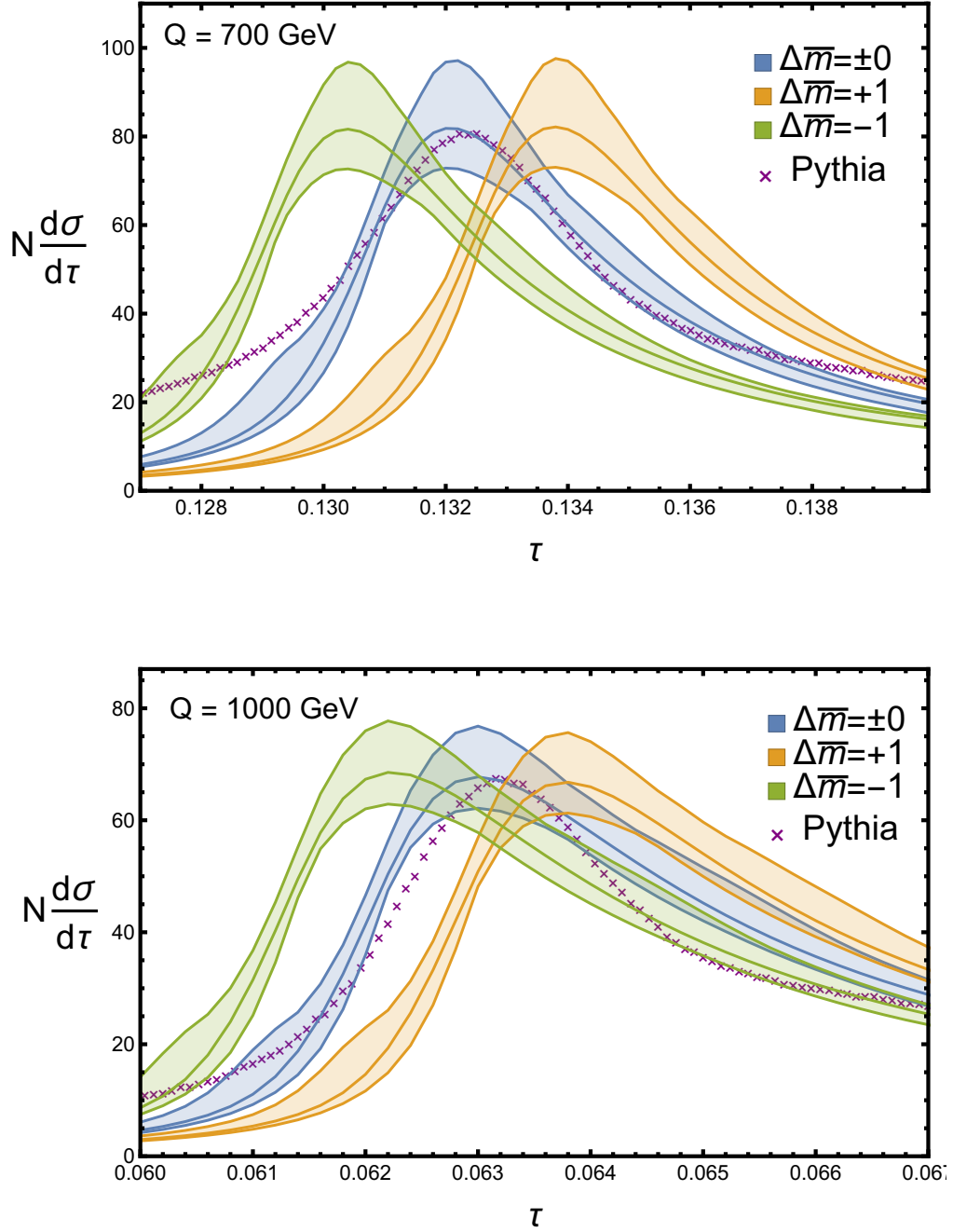
Figure 5.9: Comparison for M-scheme thrust between PYTHIA data (purple crosses) with $m_t^{\text{MC}} = 173$ GeV and unstable theory output without decay function (solid) with different mass values $\overline{m}_t(\overline{m}_t) = (162.95 + \Delta\overline{m})$ GeV at NNLL. Furthermore a c.o.m. energy of $Q = 700$ GeV and $Q = 1000$ GeV as well as a top width of $\Gamma_t = 1.4$ GeV was used. The normalization factor N for the theory curves is chosen in such a way so that the full cross section is normalized. The PYTHIA cross section was rescaled so that the maximum has the same height as the maximum of the theory curve with intermediate mass value.
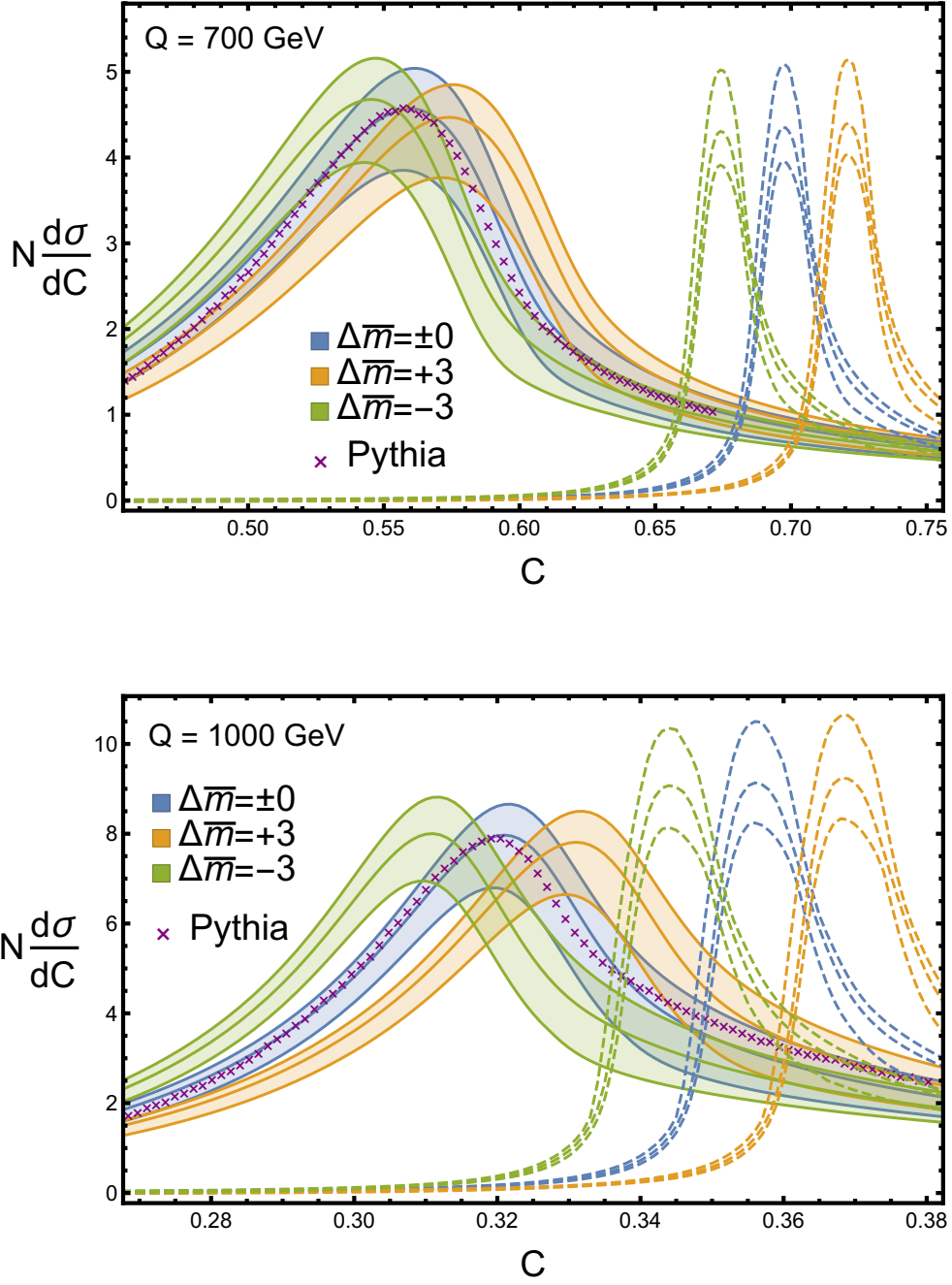
Figure 5.10: Comparison for M-scheme C-parameter between PYTHIA data (purple crosses) with $m_t^{\mathrm{MC}} = 173$ GeV and unstable theory output (solid) with different mass values $\overline{m}_t(\overline{m}_t) = (162.95 + \Delta\overline{m})$ GeV at NNLL. Furthermore a c.o.m. energy of $Q = 700$ GeV and $Q = 1000$ GeV as well as a top width of $\Gamma_t = 1.4$ GeV was used. The normalization factor N for the theory curves is chosen in such a way so that the full cross section is normalized. For the unstable cross section without decay function (dashed) the analogous normalization is $1/4$ and $1/2$ for $Q = 700$ GeV and $Q = 1000$ GeV, respectively, to fit the plot range. The PYTHIA cross section was rescaled so that the maximum has the same height as the maximum of the theory curve with intermediate mass value.

Carrying out the described procedure it is possible to include the previously neglected but important decay effects into our theoretical cross section predictions and obtain an uncertainty band for the full unstable case of C-parameter which is also shown in Fig. 5.10 (solid). Comparing this with the `PYTHIA` pseudo data one can see a significant improvement with respect to the unstable case without decay function where the central mass value leads to a good agreement for the peak position and also the shape of the peak.

Analyzing the shown plots we find that the convolution with the decay function will decrease the mass sensitivity with respect to the stable case because it causes the peak to get much wider. Moreover, a very interesting effect is visible when comparing the two different energies of $Q = 700$ GeV and $Q = 1000$ GeV. We note that at higher energies the effect of reduced mass sensitivity due to the decay function convolution is suppressed and also that this suppression is stronger than the reduction of mass sensitivity in the stable distribution due to the higher center-of-mass energy. Overall this effectively causes the mass sensitivity to be higher for this special case of an intermediately high energy of $Q = 1000$ GeV. At even higher values for Q we anticipate that the decreased mass sensitivity of the stable distribution will eventually fully compensate this effect leading to an overall reduced mass sensitivity with respect to lower energies, as in the case of thrust.

In conclusion we expect that with the discussed theory setup it is possible to use the M-scheme C-parameter to carry out a sensible MC top quark mass calibration similar to the one in Ref. [6]. From the presented "proof of concept" no inconsistencies were visible and a compatible calibration seems feasible. Based on the shown plots the associated calibration uncertainty is expected to be larger than for thrust and we estimate it to be around $1 - 2$ GeV (compared to 200 MeV for 2-jettiness/thrust).

Appendix A

Evolution

A.1 General

The Beta function [117, 118] is given by the following:

$$\mu \frac{\mathrm{d}\alpha_s}{\mathrm{d}\mu}(\mu) = \beta[\alpha_s(\mu)] = -\frac{\alpha_s^2(\mu)}{2\pi} \sum_{i=0} \beta_i \left(\frac{\alpha_s}{4\pi} \right)^i , \tag{A.1}$$

$$\beta_0 = \frac{11}{3} C_A - \frac{4}{3} T_R \, n_f , \tag{A.2}$$

$$\beta_1 = \frac{34}{3} C_A^2 - 4 C_F \, T_R \, n_f - \frac{20}{3} C_A \, T_R \, n_f , \tag{A.3}$$

$$\beta_2 = \frac{2857}{54} C_A^3 + T_R \, n_f \left(2 C_F^2 - \frac{205}{9} C_F \, C_A - \frac{1415}{27} C_A^2 \right) + T_R^2 \, n_f^2 \left(\frac{44}{9} C_F + \frac{158}{27} C_A \right) . \tag{A.4}$$

Furthermore the 4- and 5-loop coefficient β_3 [119, 120] and β_4 [21] are also known but omitted here to save space.

The QCD cusp anomalous dimension [121–124] is given by:

$$\Gamma^{\mathrm{cusp}}[\alpha_s] = \sum_{i=0} \Gamma_i \left(\frac{\alpha_s}{4\pi} \right) , \tag{A.5}$$

$$\Gamma_0 = 4 , \tag{A.6}$$

$$\Gamma_1 = 4 \, C_A \left(\frac{67}{9} - \frac{\pi^2}{3} \right) , \tag{A.7}$$

$$\Gamma_2 = 4 \, C_A^2 \left(\frac{245}{6} - \frac{134\pi^2}{27} + \frac{11\pi^4}{45} + \frac{22}{3} \zeta_3 \right) + 32 \, C_A \, T_R \, n_f \left(-\frac{209}{108} + \frac{5\pi^2}{27} - \frac{7}{3} \zeta_3 \right)$$
$$+ 4 \, C_F \, T_R \, n_f \left(16 \zeta_3 - \frac{55}{3} \right) - \frac{64}{27} T_R^2 \, n_f^2 \tag{A.8}$$

A.2 Cross Section Factors

A.2.1 Evolution Kernels

$$\omega^{\mathrm{N^3LL}}(\mu, \mu_0, \Gamma, j) = \frac{2}{j} \int_{\alpha_s(\mu_0)}^{\alpha_s(\mu)} d\alpha \, \frac{\Gamma[\alpha]}{\beta[\alpha]}$$

$$= \frac{\Gamma_0}{\beta_0 \, j} \left[-\ln(r) + \frac{\alpha_s(\mu_0)}{4\pi} \left(\frac{\beta_1}{\beta_0} - \frac{\Gamma_1}{\Gamma_0} \right)(r-1) + \frac{1}{2} \left(\frac{\alpha_s(\mu_0)}{4\pi} \right)^2 \left(\frac{\beta_2}{\beta_0} + \frac{\beta_1 \Gamma_1}{\beta_0 \Gamma_0} - \frac{\beta_1^2}{\beta_0^2} - \frac{\Gamma_2}{\Gamma_0} \right)(r^2-1) \right.$$

$$\left. + \frac{1}{3} \left(\frac{\alpha_s(\mu_0)}{4\pi} \right)^3 \left(\frac{\beta_1^3}{\beta_0^3} - \frac{2\beta_1 \beta_2}{\beta_0^2} + \frac{\beta_3}{\beta_0} - \frac{\beta_1^2 \Gamma_1}{\beta_0^2 \Gamma_0} + \frac{\beta_2 \Gamma_1}{\beta_0 \Gamma_0} + \frac{\beta_1 \Gamma_2}{\beta_0 \Gamma_0} - \frac{\Gamma_3}{\Gamma_0} \right)(r^3-1) \right] , \tag{A.9}$$

$$K^{\mathrm{N^2LL}}(\mu, \mu_0, \Gamma, \gamma) - \omega^{\mathrm{N^2LL}}(\mu, \mu_0, \gamma, 2) = 2 \int_{\alpha_s(\mu_0)}^{\alpha_s(\mu)} d\alpha \, \frac{\Gamma[\alpha]}{\beta[\alpha]} \int_{\alpha_s(\mu_0)}^{\alpha} \frac{d\alpha'}{\beta[\alpha']}$$

$$= \frac{\Gamma_0}{2\beta_0^2} \left[\frac{4\pi}{\alpha_s(\mu_0)} \left(\frac{1}{r} + \ln(r) - 1 \right) + \left(\frac{\Gamma_1}{\Gamma_0} - \frac{\beta_1}{\beta_0} \right) \left[r - 1 - \ln(r) \right] - \frac{\beta_1}{2\beta_0} \ln^2(r) \right.$$

$$+ \frac{\alpha_s(\mu_0)}{4\pi} \left[\left(\frac{\Gamma_1 \beta_1}{\Gamma_0 \beta_0} - \frac{\beta_1^2}{\beta_0^2} \right) \left[r - 1 - r \ln(r) \right] - B_2 \ln(r) + \left(\frac{\Gamma_2}{\Gamma_0} - \frac{\Gamma_1 \beta_1}{\Gamma_0 \beta_0} + B_2 \right) \frac{(r^2-1)}{2} \right.$$

$$\left. \left. + \left(\frac{\Gamma_2}{\Gamma_0} - \frac{\Gamma_1 \beta_1}{\Gamma_0 \beta_0} \right)(1-r) \right] . \tag{A.10}$$

where the $B_2 = \beta_1^2/\beta_0^2 - \beta_2/\beta_0$ and $r = \alpha_s(\mu)/\alpha_s(\mu_0)$ which depends on the 4-loop running coupling.

A.2.2 Anomalous Dimensions

For the $(n_\ell + 1)$ active flavor cross section factors the cusp anomalous dimension is given by

$$\Gamma_H[\alpha_s] = -\Gamma_J[\alpha_s] = \Gamma_S[\alpha_s] = -2 \, \Gamma^{\mathrm{cusp}}[\alpha_s] . \tag{A.11}$$

and the non-cusp anomalous dimensions up to 2-loop read [97, 125]

$$\gamma_{H,0} = -12 \, C_F \tag{A.12}$$

$$\gamma_{J,0} = 6 \, C_F \tag{A.13}$$

$$\gamma_{S,0} = 0 \tag{A.14}$$

$$\gamma_{H,1} = -\frac{7976}{27} - \frac{136}{9}\pi^2 + \frac{736}{3}\zeta_3 + \left(\frac{1040}{81} + \frac{16}{9}\pi^2 \right) n_f , \tag{A.15}$$

$$\gamma_{J,1} = \frac{7220}{27} + \frac{8}{3}\pi^2 - \frac{704}{3}\zeta_3 - \left(\frac{968}{81} + \frac{16}{27}\pi^2 \right) n_f , \tag{A.16}$$

$$\gamma_{S,1} = -\gamma_{H,1} - 2\gamma_{J,1} . \tag{A.17}$$

Appendix B

Bubble Chain Insertions and Renormalons

The contribution from a massless fermion bubble inserted into the gluon propagator is given by

$$
\Pi_{AB}^{0,\mu\nu}(p,\mu) = -i\delta_{AB}(p^2 g^{\mu\nu} - p^\mu p^\nu)\frac{\alpha_s T_F n_f}{\pi}\left[2\Big(\frac{\mu^2 \mathrm{e}^{\gamma_E}}{-p^2 - i0}\Big)^\varepsilon \frac{\Gamma(\varepsilon)\Gamma(2-\varepsilon)^2}{\Gamma(4-2\varepsilon)} - \frac{1}{3\varepsilon}\right]
$$

$$
= -i\delta_{AB}(p^2 g^{\mu\nu} - p^\mu p^\nu)\frac{\alpha_s T_F n_f}{3\pi}\ln\frac{\mu^2 \mathrm{e}^{\frac{5}{3}}}{-p^2 - i0} + \mathcal{O}(\varepsilon)\ . \tag{B.1}
$$

In the next step we look at n insertions of such renormalized massless fermion bubbles into the gluon propagator which gives us the n'th *bubble chain gluon propagator*. This modified propagator is given by

$$
P_{AB}^{\mu\nu,n}(p,\mu) = \frac{-i\delta_{AB}\Big(p^2 g^{\mu\nu} - p^\mu p^\nu\Big)}{\big(p^2 + i0\big)^2}\left[\frac{\alpha_s(-\frac{4}{3}T_F n_f)}{4\pi}\right]^n \ln^n\Big(\frac{\mu^2 \mathrm{e}^{\frac{5}{3}}}{-p^2 - i0}\Big) + \mathcal{O}(\varepsilon)\ . \tag{B.2}
$$

For Renormalon calculations the Borel transform of the sum of diagrams with insertions of all orders of bubble chain gluon propagators is important. After naive nonabelianization i.e. $\frac{4}{3}T_F n_f \to -\beta_0$ and by using the modified Borel variable $u = \frac{t\beta_0}{4\pi}$ the relevant expression therefore reads

$$
B\left[P_{AB}^{\mu\nu}(p,\mu)\right](u) = \sum_{n=0}^{\infty}\frac{P_{AB}^{\mu\nu,n}(p,\mu)}{n!}\Big(\frac{4\pi}{\alpha_s\beta_0}\Big)^{n+1} = \frac{-i\delta_{AB}\Big(p^2 g^{\mu\nu} - p^\mu p^\nu\Big)}{(p^2 + i0)^2}\Big(\frac{\mathrm{e}^{\frac{5}{3}}\mu^2}{-p^2 - i0}\Big)^u\Big(\frac{4\pi}{\alpha_s\beta_0}\Big)\ . \tag{B.3}
$$

In the above expression the last factor enters due to the fact that the propagator will be part of some diagram which induces one additional α_s. Since only the Borel transform of the full object is of interest this additional power of α_s is included into the Borel transform already at this point.

Appendix C

Integrals for the P-scheme Angularities Jet Function

C.1   SCET Single Quark Contribution

When calculating the single heavy quark final state contribution in Sec. 3.5.1 we encountered the following integral which comes from virtual radiative corrections:

$$
\mathcal{I}_{\text{virt}}(p, m) = \tilde{\mu}^{4-d} \int \frac{\mathrm{d}^d q}{(2\pi)^d} \frac{p^- - q^-}{[(p-q)^2 - m^2 + i0][q^- + i0][q^2 + i0]} \ . \tag{C.1}
$$

In the next step we use that the quark is on-shell, hence $p^\mu = (p^+, p^-, \vec{p}^\perp) = (m^2/Q, Q, 0)$, the fact that $\mathrm{d}^d q = \frac{1}{4} \mathrm{d}\Omega_{\text{tot}}^{d-2} \mathrm{d}q^- \, \mathrm{d}q^+ \, \mathrm{d}(q_\perp^2)(q_\perp^2)^{-\varepsilon}\theta(q_\perp^2)$ and also the substitution $x = q^-/Q$, $y = q^+/Q$, $z = q_\perp^2/Q^2$ with $q_\perp = |\vec{q}^\perp|$. Since nothing depends on angles between particle momenta it is easy to carry out the solid angle integral which gives $\Omega_{\text{tot}}^{d-2} = (2\pi^{\frac{d-2}{2}})/\Gamma(\frac{d-2}{2}) = 2\pi^{1-\varepsilon}/\Gamma(1-\varepsilon)$. With this we arrive at the following expression:

$$
\mathcal{I}_{\text{virt}}(p, m) = \frac{(\mu^2/Q^2 \mathrm{e}^{\gamma_E})^\varepsilon}{32\pi^3 \, \Gamma(1-\varepsilon)} \int \frac{\mathrm{d}x \, \mathrm{d}y \, \mathrm{d}z \, \theta(z) \, z^{-\varepsilon} \, (1-x)}{[x+i0][x\,y - z + i0] \left[\left(\frac{m^2}{Q^2} - y \right)(1-x) - z - \frac{m^2}{Q^2} + i0 \right]} \ . \tag{C.2}
$$

To solve this we carry out the y integration as a contour integral which also imposes $0 \leq x \leq 1$. The z and x integration is then straightforward which leaves us with the final result:

$$
\mathcal{I}_{\text{virt}}(p, m) = -i \, \frac{(\mu^2/m^2 \, \mathrm{e}^{\gamma_E})^\varepsilon}{16\pi^2} \, \frac{\Gamma(\varepsilon)}{2\,\varepsilon\,(1-2\,\varepsilon)} \ . \tag{C.3}
$$

C.2   SCET Real Radiation Contribution

First Real Radiation Integral

In the real radiation contribution we need to look into two integrals which we encountered in Sec. 3.5.1. The first one which was given in Eq. (3.112) reads:

$$
J_{n,\tau_a}^c = \frac{\alpha_s C_F}{\pi} \int \mathrm{d}t \, \frac{8\pi \, \tilde{\mu}^{4-d}}{t - m^2} \int \frac{\mathrm{d}^d q}{(2\pi)^d} \, (2\pi)^2 \theta(p^0 - q^0)\theta(q^0)\delta((p-q)^2 - m^2)\delta(q^2) \, \frac{Q - q^-}{q^-}
$$

$$
\times \delta\left\{ Q(Q - q^-)^{a-1} \left[(Q - q^-)(\frac{t}{Q} - q^+) - m^2 \right]^{\frac{2-a}{2}} + Q(q^-)^{a-1} \left[q^+ q^- \right]^{\frac{2-a}{2}} - s \right\} \ . \tag{C.4}
$$

As in the case of the single quark contribution we use the convenient substitution $x = q^-/Q$, $y = q^+/Q$, $z = q_\perp^2/Q^2$ with $q_\perp = |\vec{q}^{\perp}|$ and carry out the solid angle integral. Using collinear power counting for the real momenta we are left with the following expression:

$$
J_{n,\tau_a}^c = \frac{\alpha_s C_F}{\pi} \frac{((\mu/Q)^2 e^{\gamma_E})^\varepsilon}{Q^2 \, \Gamma(1-\varepsilon)} \int \mathrm{d}t \, \frac{1}{t-m^2} \int \mathrm{d}x \, \mathrm{d}y \, \mathrm{d}z \, \frac{1-x}{x} \, z^{-\varepsilon}
$$
$$
\times \, \theta(z) \, \theta(1-x) \, \theta(x) \, \delta\left[(1-x)(\frac{t}{Q^2} - y) - z - \frac{m^2}{Q^2}\right] \delta(xy - z) \tag{C.5}
$$
$$
\times \, \delta\left\{(1-x)^{a-1}\left[(1-x)(\frac{t}{Q^2} - y) - \frac{m^2}{Q^2}\right]^{\frac{2-a}{2}} + x^{a-1} [xy]^{\frac{2-a}{2}} - \frac{s}{Q^2}\right\}.
$$

Now we use the gluon on-shell delta functions to carry out the y integration and in the next step make use of the quark on-shell delta function for the t integration. For that we need:

$$
\delta\left\{(1-x)\left(\frac{t}{Q^2} - \frac{z}{x}\right) - z - \frac{m^2}{Q^2}\right\} = \frac{1}{1-x}\delta\left\{\frac{t}{Q^2} - \frac{z + \frac{m^2}{Q^2}x}{x(1-x)}\right\}. \tag{C.6}
$$

After the t integration we manipulate the remaining delta function as follows:

$$
\delta\left\{z^{\frac{2-a}{2}}\left[(1-x)^{a-1} + x^{a-1}\right] - \frac{s}{Q^2}\right\} = \frac{2}{2-a}\left(\frac{Q^2}{s}\right)^{\frac{a}{a-2}}\left[(1-x)^{a-1} + x^{a-1}\right]^{\frac{2}{a-2}}
$$
$$
\times \, \delta\left\{z - \left(\frac{s}{Q^2}\left[(1-x)^{a-1} + x^{a-1}\right]^{-1}\right)^{\frac{2}{2-a}}\right\}, \tag{C.7}
$$

which allows us to carry out the z integration and by defining $g(x,a) = \frac{Q^2}{s}\left[(1-x)^{a-1} + x^{a-1}\right]$ we arrive at the final integral (with $\tilde{s} = s/\mu^2$)

$$
\mu^2 J_{n,\tau_a}^c = \frac{\alpha_s C_F}{\pi} \frac{((\mu/Q)^2 e^{\gamma_E})^\varepsilon}{\tilde{s}\,\Gamma(1-\varepsilon)} \frac{2}{2-a} \int_0^1 \mathrm{d}x \, \frac{1-x}{x} \, \frac{g(x,a)^{\frac{2(1-\varepsilon)}{a-2}}}{g(x,a)^{\frac{2}{a-2}} + \frac{m^2}{Q^2}x^2}. \tag{C.8}
$$

As it turns out a direct integration is not feasible which is why we use the well known trick of subtracting and adding the divergent structure leaving us with a simpler integral to solve $J_{n,\tau_a}^{c,\mathrm{div}}$ and a finite numerical integral $J_{n,\tau_a}^{c,\mathrm{ndiv}} = J_{n,\tau_a}^c - J_{n,\tau_a}^{c,\mathrm{div}}$. For $0 \le a \le 1$ the integral is divergent for $x \to 0$ where the singular part is given by

$$
\mu^2 J_{n,\tau_a}^{c,\mathrm{div}} = \frac{\alpha_s C_F}{\pi} \frac{((\mu/Q)^2 e^{\gamma_E})^\varepsilon}{\tilde{s}\,\Gamma(1-\varepsilon)} \frac{2}{2-a} \int_0^1 \mathrm{d}x \, \frac{\left(\frac{Q^2}{s}x^{a-1}\right)^{\frac{2-2\varepsilon}{a-2}}}{\left(\frac{Q^2}{s}x^{a-1}\right)^{\frac{2}{a-2}} + \frac{m^2}{Q^2}x^2} \frac{1-x}{x}
$$
$$
= -\frac{\alpha_s C_F}{\pi} \frac{((\mu/Q)^2 e^{\gamma_E})^\varepsilon}{\tilde{s}\,\Gamma(1-\varepsilon)} \left(\frac{Q^2}{s}\right)^{\frac{2\varepsilon}{2-a}}
$$
$$
\times \left\{ \frac{{}_2F_1\left(1, 1-\varepsilon + a\left(\varepsilon - \frac{1}{2}\right); 2-\varepsilon + a\left(\varepsilon + \frac{1}{2}\right); -\frac{m^2}{Q^2}\left(\frac{Q^2}{s}\right)^{\frac{2}{2-a}}\right)}{1 - \varepsilon + a\left(\varepsilon - \frac{1}{2}\right)} \right. \tag{C.9}
$$
$$
\left. + \frac{{}_2F_1\left(1, \varepsilon(a-1); 1 + \varepsilon(a-1); -\frac{m^2}{Q^2}\left(\frac{Q^2}{s}\right)^{\frac{2}{2-a}}\right)}{\varepsilon(1-a)} \right\}.
$$

Next we carry out the small ε expansion for $J_{n,\tau_a}^{c,\mathrm{div}}$. The first term in the curly brackets of Eq. (C.9) becomes 0 for $s \to 0$ at order ε^0 and order ε^1 which is why we can expand the prefactor and the first term in the curly brackets separately and multiply them together afterwards. This leaves us with a non-distributional expression for the first contribution to $J_{n,\tau_a}^{c,\mathrm{div}}$:

$$\mu^2 J_{n,\tau_a}^{c,\mathrm{div},1} = \frac{\alpha_s C_F}{\pi} \frac{2}{a-2} \frac{\theta(\tilde{s})}{\tilde{s}} \,_2F_1\left(1, 1 - \frac{a}{2}; 2 - \frac{a}{2}; -\frac{m^2}{Q^2}\left(\frac{\mu^2}{Q^2}\tilde{s}\right)^{\frac{2}{a-2}}\right) . \tag{C.10}$$

The second term in Eq. (C.9) is not well behaved in the same limit which is why we look into the cumulative distribution of this term denoted by $\mathcal{J}_{n,\tau}^{c,\mathrm{div},2}(\Delta) = \int_0^\Delta \mathrm{d}s\, J_{n,\tau}^{c,\mathrm{div},2}$. From this it is straightforward to identify distributional and non-distributional terms and we get the following expression for the second contribution to $J_{n,\tau_a}^{c,\mathrm{div}}$:

$$\mu^2 J_{n,\tau_a}^{c,\mathrm{div},2} = \frac{\alpha_s C_F}{\pi}\left\{\delta(\tilde{s})\left[\frac{1}{2(1-a)\varepsilon^2} + \frac{1}{2(1-a)\varepsilon}\left((1-a)\ln\frac{m^2}{Q^2} + a\ln\frac{Q^2}{\mu^2}\right)\right.\right.$$
$$\left. + \frac{1-4a+2a^2}{24(1-a)}\pi^2 + \frac{1}{4(1-a)}\left((1-a)\ln\frac{m^2}{\mu^2} + a\ln\frac{Q^2}{\mu^2}\right)^2\right] + \frac{2}{(1-a)}\left[\frac{\theta(\tilde{s})\ln\tilde{s}}{\tilde{s}}\right]_+$$
$$\left. - \frac{1}{(1-a)}\left[\frac{\theta(\tilde{s})}{\tilde{s}}\right]_+\left[\frac{1}{\varepsilon} + (1-a)\ln\frac{m^2}{\mu^2} + a\ln\frac{Q^2}{\mu^2}\right] - \frac{\theta(\tilde{s})}{\tilde{s}}\ln\left(1 + \frac{(\tilde{s}\mu^2/Q^2)^{\frac{2}{2-a}}}{m^2/Q^2}\right)\right\} . \tag{C.11}$$

The remaining part is then given by the numerical integral involving the mentioned subtraction:

$$\mu^2 J_{n,\tau_a}^{c,\mathrm{ndiv}} = -\frac{\alpha_s C_F}{\pi} \frac{2}{2-a} \frac{\theta(\tilde{s})}{\tilde{s}} \mathcal{I}_1(s;a) , \tag{C.12}$$

where $\mathcal{I}_1(s;a)$ was already defined in Eq. (3.116). The full expression for J_{n,τ_a}^c is finally obtained by putting all contributions together:

$$J_{n,\tau_a}^c = J_{n,\tau_a}^{c,\mathrm{div},1} + J_{n,\tau_a}^{c,\mathrm{div},2} + J_{n,\tau_a}^{c,\mathrm{ndiv}} . \tag{C.13}$$

which leads to the result already given in Eq. (3.114).

Second Real Radiation Integral

The second integral one encounters in the real radiation contribution is given in Eq. (3.113) and reads:

$$J_{n,\tau_a}^d = -\frac{\alpha_s C_F}{\pi}\int \mathrm{d}t \frac{2\pi Q^2 \tilde{\mu}^{4-d}}{(t-m^2)^2}\int\frac{\mathrm{d}^d q}{(2\pi)^d}(2\pi)^2\theta(p^0 - q^0)\theta(q^0)\delta((p-q)^2 - m^2)\delta(q^2)$$
$$\times (d-2)\left[\frac{m^2}{Q^2}\left(\frac{2d}{d-2} - \frac{Q-q^-}{Q} - \frac{Q}{Q-q^-}\right) - \frac{Q}{Q-q^-}\frac{q_\perp^2}{Q^2}\right] \tag{C.14}$$
$$\times \delta\left\{Q(Q-q^-)^{a-1}\left[(Q-q^-)(\frac{t}{Q} - q^+) - m^2\right]^{\frac{2-a}{2}} + Q(q^-)^{a-1}\left[q^+q^-\right]^{\frac{2-a}{2}} - s\right\} .$$

Using the same substitutions, the fact that again we have no dependence on angles between different particles, collinear power counting for the real momenta and simplifying the involved expressions we arrive at the following integral:

$$J_{n,\tau_a}^d = -\frac{\alpha_s C_F}{\pi}\frac{((\mu/Q)^2 \mathrm{e}^{\gamma_E})^\varepsilon}{4\,\Gamma(1-\varepsilon)}\int \mathrm{d}t \frac{1}{(t-m^2)^2}\int \mathrm{d}x\,\mathrm{d}y\,\mathrm{d}z\, z^{-\varepsilon}\left[4\frac{m^2}{Q^2} - (2-2\varepsilon)\frac{z + \frac{m^2}{Q^2}x^2}{1-x}\right]$$
$$\times \theta(z)\,\theta(1-x)\,\theta(x)\,\delta\left[(1-x)(\frac{t}{Q^2} - y) - z - \frac{m^2}{Q^2}\right]\delta(xy - z) \tag{C.15}$$
$$\times \delta\left\{(1-x)^{a-1}\left[(1-x)(\frac{t}{Q^2} - y) - \frac{m^2}{Q^2}\right]^{\frac{2-a}{2}} + x^{a-1}[xy]^{\frac{2-a}{2}} - \frac{s}{Q^2}\right\} .$$

Following along the lines of the first integral the y integration is carried out first by using the gluon on-shell delta function. In the next step we employ Eq. (C.6) and (C.7) to do the t and z integral. In analogy to Eq. (C.8) this leaves us with an integral expression which splits into two main contributions, again involves $g(x,a) = \frac{Q^2}{s}\left[(1-x)^{a-1} + x^{a-1}\right]$ and reads (with $\tilde{s} = s/\mu^2$):

$$\mu^2 J_{n,\tau_a}^d = \mu^2(J_{n,\tau_a}^{d,1} + J_{n,\tau_a}^{d,2}) \,, \tag{C.16}$$

$$\mu^2 J_{n,\tau_a}^{d,1} = \frac{\alpha_s C_F}{\pi} \frac{((\mu/Q)^2 e^{\gamma_E})^\varepsilon}{\tilde{s}\,\Gamma(1-\varepsilon)} \frac{1-\varepsilon}{2-a} \int_0^1 dx \, \frac{x\,g(x,a)^{\frac{2(1-\varepsilon)}{a-2}}}{g(x,a)^{\frac{2}{a-2}} + \frac{m^2}{Q^2}x^2} \,, \tag{C.17}$$

$$\mu^2 J_{n,\tau_a}^{d,2} = -\frac{\alpha_s C_F}{\pi} \frac{((\mu/Q)^2 e^{\gamma_E})^\varepsilon}{\tilde{s}\,\Gamma(1-\varepsilon)} \frac{2}{2-a} \frac{m^2}{Q^2} \int_0^1 dx \, \frac{x\,(1-x)\,g(x,a)^{\frac{2(1-\varepsilon)}{a-2}}}{\left[g(x,a)^{\frac{2}{a-2}} + \frac{m^2}{Q^2}x^2\right]^2} \,. \tag{C.18}$$

It turns out that the expression in Eq. (C.17) is finite for $\tilde{s} \geq 0$ and $0 \leq a \leq 1$ and can be expressed as a numerical integral involving the expression already given in Eq. (3.117). The result then reads

$$\mu^2 J_{n,\tau_a}^{d,1} = \frac{\alpha_s C_F}{\pi} \frac{1}{2-a} \frac{\theta(\tilde{s})}{\tilde{s}} \, \mathcal{I}_2(s;a) \,. \tag{C.19}$$

For the second part which is given in Eq. (C.18) we again have to use subtractions. The divergent part of this integral is then given by

$$\mu^2 J_{n,\tau_a}^{d,2,\text{div}} = -\frac{\alpha_s C_F}{\pi} \frac{((\mu/Q)^2 e^{\gamma_E})^\varepsilon}{\tilde{s}\,\Gamma(1-\varepsilon)} \frac{2}{2-a} \frac{m^2}{Q^2} \int_0^1 dx \, \frac{x\,(1-x)\,\left(\frac{Q^2}{s}x^{a-1}\right)^{\frac{2(1-\varepsilon)}{a-2}}}{\left[\left(\frac{Q^2}{s}x^{a-1}\right)^{\frac{2}{a-2}} + \frac{m^2}{Q^2}x^2\right]^2} \,. \tag{C.20}$$

As it turns out this expression is not well behaved in the limit $s \to 0$ when looking at small ε and furthermore it seems not feasible to do the x integral right away. It is still possible to solve this integral by looking at the cumulative distribution $\mathcal{J}_{n,\tau}^{d,2,\text{div}}(\Delta) = \int_0^\Delta ds \, J_{n,\tau}^{d,2,\text{div}}$ and afterwards carrying out the x integral with the convenient substitution $\tilde{x} = x^{\frac{2}{2-a}}$. Next we expand the obtained result for small ε, subsequently it is straightforward to extract distributional and non-distributional contributions as follows:

$$\mu^2 J_{n,\tau_a}^{d,2,\text{div}} = \frac{\alpha_s C_F}{\pi} \left\{ \delta(\tilde{s})\left[\frac{1}{2\varepsilon} + \frac{1}{2}\left((1-a)\ln\frac{m^2}{\mu^2} + a\ln\frac{Q^2}{\mu^2}\right)\right] - \left[\frac{\theta(\tilde{s})}{\tilde{s}}\right]_+ \right.$$

$$+ \theta(\tilde{s})\left[\frac{2-a}{2}\frac{\mu^2}{m^2}\left(\frac{m^2}{Q^2}\right)^{\frac{a}{2}}\Gamma\left(1-\frac{a}{2}\right)\Gamma\left(\frac{a}{2}\right)\right.$$

$$\left.\left. - \frac{2-a}{a}\frac{\mu^2}{m^2}\left(\frac{Q^2}{\mu^2}\right)^{\frac{-a}{2-a}}\tilde{s}^{\frac{a}{2-a}}\,{}_2F_1\left(1,\frac{a}{2};\frac{2+a}{2}; -\frac{\mu^2}{m^2}\left(\frac{Q^2}{\mu^2}\right)^{\frac{-a}{a-2}}\tilde{s}^{\frac{2}{2-a}}\right)\right]\right\} \,. \tag{C.21}$$

The remaining part is then given by the numerical integral involving the appropriate subtraction. For $m \neq 0$ it reads

$$\mu^2 J_{n,\tau_a}^{d,2,\text{ndiv}} = -\frac{\alpha_s C_F}{\pi} \frac{2}{2-a} \frac{\theta(\tilde{s})}{\tilde{s}} \left[\mathcal{I}_1(s;a) - \mathcal{I}_3(s;a)\right] \,, \tag{C.22}$$

where $\mathcal{I}_1(s;a)$ and $\mathcal{I}_3(s;a)$ was defined in Eq. (3.116) and (3.118) respectively. The full expression for J_{n,τ_a}^d is then obtained by putting all the contributions together:

$$J_{n,\tau_a}^d = J_{n,\tau_a}^{d,1} + J_{n,\tau_a}^{d,2,\text{div}} + J_{n,\tau_a}^{d,2,\text{ndiv}} \,, \tag{C.23}$$

which leads to the result already given in Eq. (3.115).

C.3 SCET Massless Limit

Since the single quark contribution to the massless jet function is trivial we start right away with the real radiation part. To find the massless analog to J^c_{n,τ_a} we have to consider the subtraction used in Eq. (C.9) in the massless limit. For this we then find

$$
\begin{aligned}
\mu^2 J^{c,\text{div}}_{n,\tau_a,\text{ml}} &= \frac{\alpha_s C_F}{\pi} \frac{((\mu/Q)^2 e^{\gamma_E})^\varepsilon}{\Gamma(1-\varepsilon)} \frac{2}{2-a} \left(\frac{Q^2}{\mu^2}\right)^{\frac{2\varepsilon}{2-a}} \frac{1}{\tilde{s}^{1+\frac{2\varepsilon}{2-a}}} \int_0^1 \mathrm{d}x\, x^{\frac{-2\varepsilon(1-a)}{2-a}} \frac{1-x}{x} \\
&= \frac{\alpha_s C_F}{\pi} \Bigg\{ \delta(\tilde{s})\bigg[\frac{(1-a/2)}{(1-a)\varepsilon^2} + \frac{1}{\varepsilon} - \frac{a/2}{(1-a)\varepsilon} \ln\left(\frac{Q^2}{\mu^2}\right) + \frac{(1-a)}{(1-a/2)} - \frac{\pi^2}{24}\frac{(2-a)}{(1-a)} \\
&\qquad + \frac{a^2}{8(1-a/2)(1-a)} \ln^2\left(\frac{Q^2}{\mu^2}\right) + \frac{a}{(2-a)} \ln\left(\frac{Q^2}{\mu^2}\right) \bigg] \\
&\quad - \left[\frac{\theta(\tilde{s})}{\tilde{s}}\right]_+ \left[\frac{1}{(1-a)\varepsilon} + \frac{a}{2(1-a/2)(1-a)} \ln\left(\frac{Q^2}{\mu^2}\right) + \frac{2}{2-a} \right] \\
&\quad + \frac{2}{(1-a)(2-a)} \left[\frac{\theta(\tilde{s})\ln\tilde{s}}{\tilde{s}}\right]_+ \Bigg\},
\end{aligned}
\tag{C.24}
$$

with $\tilde{s} = s/\mu^2$. For the corresponding integral containing the subtraction we get

$$
\mu^2 J^{c,\text{ndiv}}_{n,\tau_a,\text{ml}} = -\frac{\alpha_s C_F}{\pi} \frac{2}{2-a} \delta(\tilde{s}) \Bigg\{ (1-a)\left(-1 + \frac{\pi^2}{6}\right) + \int_0^1 \mathrm{d}x\, \frac{1-x}{x} \ln\left(x^{1-a} + (1-x)^{1-a}\right) \Bigg\}.
\tag{C.25}
$$

In the case of the second real radiation contribution it is clear that the contribution corresponding to $J^{d,2}_{n,\tau_a}$ does not exist in the massless limit. For $J^{d,1}_{n,\tau_a}$ in the massless limit we again do not need to employ subtractions and find

$$
\begin{aligned}
\mu^2 J^{d,1}_{n,\tau_a,\text{ml}} &= \frac{\alpha_s C_F}{\pi} \frac{((\mu/Q)^2 e^{\gamma_E})^\varepsilon}{\Gamma(1-\varepsilon)} \frac{1-\varepsilon}{2-a} \left(\frac{Q^2}{\mu^2}\right)^{\frac{2\varepsilon}{2-a}} \frac{1}{\tilde{s}^{1+\frac{2\varepsilon}{2-a}}} \int_0^1 \mathrm{d}x\, x \left(\frac{x^{1-a}+(1-x)^{1-a}}{x^{1-a}(1-x)^{1-a}}\right)^{\frac{2\varepsilon}{2-a}} \\
&= \frac{\alpha_s C_F}{\pi} \Bigg\{ \delta(\tilde{s})\bigg[-\frac{1}{4\varepsilon} - \frac{2-3a}{4(2-a)} - \frac{a}{4(2-a)} \ln\left(\frac{Q^2}{\mu^2}\right) \bigg] + \left[\frac{\theta(\tilde{s})}{\tilde{s}}\right]_+ \frac{1}{2(2-a)} \\
&\quad - \delta(\tilde{s}) \frac{1}{2-a} \int_0^1 \mathrm{d}x\, x \ln\left(x^{1-a}+(1-x)^{1-a}\right) \Bigg\}.
\end{aligned}
\tag{C.26}
$$

By putting everything together:

$$
J^c_{n,\tau_a,\text{ml}} = J^{c,\text{div}}_{n,\tau_a,\text{ml}} + J^{c,\text{ndiv}}_{n,\tau_a,\text{ml}},
\tag{C.27}
$$

$$
J^d_{n,\tau_a,\text{ml}} = J^{d,1}_{n,\tau_a,\text{ml}},
\tag{C.28}
$$

we arrive at the final result which was given in Eq. (3.148).

C.4 bHQET Real Radiation Contribution

First Real Radiation Integral

In analogy to the SCET case we encountered two integrals in the real radiation contribution (see Sec. 3.5.2). The first one from Eq. (3.126) is given by

$$
J^c_{B,n,\tau_a} = \frac{\alpha_s C_F}{\pi} \int dt \, \frac{8\pi \tilde{\mu}^{2\varepsilon}}{t} \int \frac{d^d q}{(2\pi)^d}
$$

$$
\times (2\pi)^2 \theta(p^0 - q^0)\theta(q^0)\delta((p-q)^2 - m^2)\delta(q^2) \frac{mv^-}{\bar{n} \cdot q} \delta\left\{ s - Q^2 \tau^P_{a,n} \right\}. \tag{C.29}
$$

Using the same substitutions as in App. C.2, the fact that again we have no dependence on angles between different particles, bHQET power counting for the real momenta and simplifying the involved expressions we arrive at the following integral:

$$
J^c_{B,n,\tau_a} = \frac{\alpha_s C_F}{\pi} \frac{mv^-}{Q} \frac{((\mu/Q)^2 \exp^{\gamma_E})^\varepsilon}{\Gamma(1-\varepsilon)} \int \frac{d\tilde{t}}{\tilde{t}} \int dx \, dy \, dz \, \frac{z^{-\varepsilon}}{x} \theta(z) \, \theta(x+y) \, \delta(xy - z) \tag{C.30}
$$

$$
\times \delta\left[\tilde{t} - \left(\frac{mv^+}{Q} x + \frac{mv^-}{Q} y \right) \right] \delta\left\{ s - Q^2 \left(\frac{mv^-}{Q} \right)^{a-1} \left[\tilde{t} - \left(\frac{mv^+}{Q} x + \frac{mv^-}{Q} y \right) \right]^{\frac{2-a}{2}} - Q^2 x^{\frac{a}{2}} y^{\frac{2-a}{2}} \right\},
$$

with $\tilde{t} = t/Q^2$. After the trivial y and $\tilde{t}$ integration we use the measurement delta function for the z integration by rewriting it in the following way:

$$
\delta\left(s - Q^2 x^{a-1} z^{\frac{2-a}{2}} \right) = \frac{2}{2-a} \frac{1}{Q^2} \left(\frac{s}{Q^2} \right)^{\frac{a}{2-a}} x^{\frac{2(1-a)}{2-a}} \delta\left(z - \left(\frac{s}{Q^2} \right)^{\frac{2}{2-a}} x^{\frac{2(1-a)}{2-a}} \right). \tag{C.31}
$$

After carrying out the z integration we now look into the cumulative distribution denoted by $\mathcal{J}^c_{B,n,\tau}(\Delta) = \int_0^\Delta ds \, J^c_{B,n,\tau}$. It is now possible to carry out the x integration by using the convenient substitution of $\tilde{x} = x^{\frac{2}{2-a}}$ and identify the distributional structure of J^c_{B,n,τ_a}. The final result is then given by

$$
\mu^2 J^c_{B,n,\tau_a} = \frac{\alpha_s C_F}{\pi} \left\{ \delta(\tilde{s}) \left[\frac{1}{2(1-a)\varepsilon^2} + \frac{1}{2(1-a)\varepsilon} \left((1-a)L_m + aL_Q \right) \right. \right.
$$

$$
+ \frac{1 - 4a + 2a^2}{24(1-a)} \pi^2 + \frac{1}{4(1-a)} \left((1-a)L_m + aL_Q \right)^2 \right] \tag{C.32}
$$

$$
\left. - \frac{1}{1-a} \left[\frac{\theta(\tilde{s})}{\tilde{s} \, for} \right]_+ \left[\frac{1}{\varepsilon} + \left((1-a)L_m + aL_Q \right) \right] + \frac{2}{1-a} \left[\frac{\theta(\tilde{s}) \ln \tilde{s}}{\tilde{s}} \right]_+ \right\},
$$

with $\tilde{s} = \frac{s}{\mu^2}$, $L_m = \ln \frac{Q^2}{\mu^2} \frac{v^+}{v^-}$ and $L_Q = \ln \frac{Q^2}{\mu^2}$.

Second Real Radiation Integral

The second real radiation integral was given in Eq. (3.126) and reads

$$
J^d_{B,n,\tau_a} = -\frac{\alpha_s C_F}{\pi} m^2 \int dt \, \frac{8\pi \tilde{\mu}^{2\varepsilon}}{t^2} \int \frac{d^d q}{(2\pi)^d} (2\pi)^2 \theta(p^0 - q^0)\theta(q^0)\delta((p-q)^2 - m^2)\delta(q^2) \delta\left\{ s - Q^2 \tau^P_{a,n} \right\}. \tag{C.33}
$$

Following the same steps as for the first real radiation integral we first get:

$$
J^d_{B,n,\tau_a} = -\frac{\alpha_s C_F}{\pi} \frac{m^2}{Q^2} \frac{((\mu/Q)^2 \exp^{\gamma_E})^\varepsilon}{\Gamma(1-\varepsilon)} \int \frac{d\tilde{t}}{\tilde{t}^2} \int dx \, dy \, dz \, z^{-\varepsilon} \, \theta(z) \, \theta(x+y) \, \delta(xy - z) \tag{C.34}
$$

$$
\times \delta\left[\tilde{t} - \left(\frac{mv^+}{Q} x + \frac{mv^-}{Q} y \right) \right] \delta\left\{ s - Q^2 \left(\frac{mv^-}{Q} \right)^{a-1} \left[\tilde{t} - \left(\frac{mv^+}{Q} x + \frac{mv^-}{Q} y \right) \right]^{\frac{2-a}{2}} - Q^2 x^{\frac{a}{2}} y^{\frac{2-a}{2}} \right\},
$$

with $\tilde{t} = t/Q^2$. Still following the strategy of the previous integral we carry out $\tilde{t}$, y and z integration and while looking into the cumulative distribution carry out the remaining x integration. This allows us to identify the distributional structure which is given by

$$\mu^2 J^d_{B,n,\tau_a} = \mathcal{C} \, \frac{\alpha_s C_F}{\pi} \left\{ \delta(\tilde{s}) \left[\frac{1}{2\varepsilon} + \frac{1}{2} \Big((1-a) L_m + a L_Q \Big) \right] - \left[\frac{\theta(\tilde{s})}{\tilde{s}} \right]_+ \right\},$$

with $\tilde{s} = \frac{s}{\mu^2}$, $L_m = \ln \frac{Q^2}{\mu^2} \frac{v^+}{v^-}$ and $L_Q = \ln \frac{Q^2}{\mu^2}$. Furthermore the global constant $\mathcal{C}$ is given by:

$$\mathcal{C} = \frac{m^2}{Q^2} \frac{v^+}{v^-} \left(\frac{mv^+}{Q} \right)^{-2} = \frac{1}{1 + \mathcal{O}(\frac{m^2}{Q^2})} \, . \tag{C.35}$$

Considering the used power counting, we keep the leading dynamical terms scaling like $s/Q^2 \sim m\Delta/Q^2$ and neglect suppressed terms which are scaling like $m^3\Delta/Q^4$. In the case when $\mathcal{C}$ is multiplied with a $\delta(\tilde{s})$ or $[\theta(\tilde{s})/\tilde{s}]_+$ the used power counting effectively gives $\mathcal{C} = 1$ at leading power.

Appendix D

Soft-Drop Groomed Jet Mass and the Soft Renormalon

In recent years so called jet grooming techniques became increasingly popular. These tools can be used to remove soft radiation appearing in experimentally measured jets at hadron colliders which does not directly originate from the hard interaction of interest. Origins of such soft radiation contamining the jet is for example the underlying event or pile-up. One of the more recent grooming techniques which turns out to be theoretically quite fruitful is the so called *soft-drop* grooming [126, 127].

Soft-drop grooming depends on two parameters i.e. z_{cut} and β and is defined by the following procedure: (0) The particles of the jet are identified with some type of jet clustering algorithm. (1) The jet is reclustered using the so called Cambridge/Aachen algorithm [128, 129], i.e. sequentially the two particles which are the least separated in terms of angle are combined until all particles are clustered together, the resulting momentum is the jet momentum. (2) Next one goes step-by-step through the branching history (momentum of the two branches given by p_i and p_j) and checks the so called soft-drop criterion. For e^+e^- this criterion reads

$$\frac{\min(p_i^0, p_j^0)}{p_i^0 + p_j^0} \equiv z > z_{\text{cut}} \left(\sqrt{2} \, \frac{\sin(\theta_{ij}/2)}{\sin(R/2)} \right)^\beta , \tag{D.1}$$

with θ_{ij} being the angle between the two branches and R being the total jet radius. If this requirement is not fulfilled the softer of the two branches is removed from the jet and one continues with the harder one of the two branches. (3) This procedure continues through the branching history until the above criterion is met. At this point soft-drop stops and the sum of the two remaining branches gives the soft-drop groomed jet momentum.

For jets with radius $R \sim 1$ it was shown in Ref. [101] that it is possible to write down a factorization theorem for observables like soft-drop groomed jet mass. For the situation where the produced jet is far away from the beam axis the factorization theorem takes the following very simple form:

$$\frac{\mathrm{d}\sigma}{\mathrm{d}\rho_{\text{SD}}} = N \times \int \mathrm{d}s \, J_n(s, \mu) \, S_C(E_J \, \rho_{\text{SD}} - s/E_J, \mu) , \tag{D.2}$$

with the soft drop groomed jet mass $\rho_{\text{SD}} = \sum_{i \in \text{SD-jet}} p_i^+ / E_j$ and the total ungroomed jet energy E_J. Furthermore N denotes a normalization factor, $J_n(s, \mu)$ is the massless hemisphere jet function discussed also in Sec. 3.5.5 and $S_C(\ell, \mu)$ is the so called collinear-soft function.

The perturbative part of this collinear-soft function is defined as

$$S_{C,\text{pert},\rho_{\text{SD}}}(\ell, \mu) = \frac{1}{N_c} \langle 0| \left(W_n Y_n^\dagger \right)(0) \delta \left[\ell - (1 - \hat{\Theta}_{\text{SD}}) \, E_J \, \hat{\rho}_J \right] \left(Y_n W_n^\dagger \right)(0) |0\rangle , \tag{D.3}$$

with the W_n and Y_n Wilson lines being the same as in the jet and soft function respectively but which now depend on collinear-soft fields [101]. Furthermore the above expression depends on the jet mass measurement acting like $\hat{\rho}_J |X\rangle = \rho_J(X) |X\rangle$ and the soft-drop groomer $\hat{\Theta}_{\mathrm{SD}}$ which gives 1 for final state configurations where (parts of) the radiation are groomed by soft-drop.

For the singular case of e^+e^- annihiliation (i.e. small ρ_J) and $R \sim 1$ the soft-drop criterion of Eq. D.1 reduces to $z > z_{\mathrm{cut}}\theta^\beta$ which for only a single radiated gluon and SCET power counting (which is applicable for the singular situation) reduces to:

$$p^- > (2E_J)\, 2^\beta z_{\mathrm{cut}} \left(\frac{p^+}{p^-}\right)^{\frac{\beta}{2}}. \tag{D.4}$$

In order to calculate the leading soft renormalon which is contained in the collinear soft function we proceed as in Sec. 3.7.1 as well as App. E of Ref. [101] (particularly up to Eq. E.3). Following the calculation of the Borel-transformed soft function with gluon bubble chain propagator insertion, which was shown in Eqs. (3.170) to (3.173), and applying the power counting for collinear-soft momenta it is straightforward to arrive at the following expression:

$$B\big[\mu\, S^{(1)}_{C,\mathrm{pert},\rho_{\mathrm{SD}}}(\ell,\mu)\big](u) = \frac{4C_F}{\beta_0} \frac{(\mathrm{e}^{\gamma_E})^\varepsilon\, \mathrm{e}^{\frac{5u}{3}}}{\Gamma(1+u)\,\Gamma(1-\varepsilon-u)} \tag{D.5}$$
$$\times \int \mathrm{d}\tilde{k}^+\, \mathrm{d}\tilde{k}^-\, \theta(\tilde{k}^-)\, \theta(\tilde{k}^+\tilde{k}^-)\, \theta\Big[\tilde{k}^- - \big(\tfrac{2E_J}{\mu}\big) 2^\beta z_{\mathrm{cut}} \big(\tfrac{\tilde{k}^+}{\tilde{k}^-}\big)^{\frac{\beta}{2}}\Big] \Big\{\delta(\ell-\tilde{k}^+) - \delta(\ell)\Big\} \big(\tilde{k}^+\tilde{k}^-\big)^{-1-\varepsilon-u},$$

To make the calculation a bit simpler we next look at the Fourier transform of the collinear-soft function with bubble chain insertions (including tree level) $\tilde{S}_{C,\mathrm{pert},\rho_{\mathrm{SD}}}(y,\mu)$ and subsequently take the Borel transform of the leading term of $\ln\tilde{S}_{C,\mathrm{pert},\rho_{\mathrm{SD}}}(y,\mu)$ which gives

$$B\big[\ln\tilde{S}_{C,\mathrm{pert},\rho_{\mathrm{SD}}}(y,\mu)\big](u) = \frac{4C_F}{\beta_0} \frac{(\mathrm{e}^{\gamma_E})^\varepsilon\, \mathrm{e}^{\frac{5u}{3}}}{\Gamma(1+u)\,\Gamma(1-\varepsilon-u)} \tag{D.6}$$
$$\times \int_0^\infty \mathrm{d}\tilde{k}^+ \int_{x_-}^\infty \mathrm{d}\tilde{k}^- \Big\{\mathrm{e}^{-iy\mu\tilde{k}^+} - 1\Big\} \big(\tilde{k}^+\tilde{k}^-\big)^{-1-\varepsilon-u},$$

where $x_- = \big(\big(\tfrac{2E_J}{\mu}\big) 2^\beta z_{\mathrm{cut}}\big)^{\frac{2}{2+\beta}} (\tilde{k}^+)^{\frac{\beta}{2+\beta}}$. Evaluating the remaining integrals gives

$$B\big[\ln\tilde{S}_{C,\mathrm{pert},\rho_{\mathrm{SD}}}(y,\mu)\big](u) = \tag{D.7}$$

$$\frac{4C_F}{\beta_0} \frac{(\mathrm{e}^{\gamma_E})^\varepsilon\, \mathrm{e}^{\frac{5u}{3}}}{\Gamma(1+u)\,\Gamma(1-\varepsilon-u)} \frac{\big(2^{1+\beta}\frac{E_J}{\mu} z_{\mathrm{cut}}\big)^{\frac{-2(\varepsilon+u)}{2+\beta}}\, \Gamma\big(-\frac{2(1+\beta)(\varepsilon+u)}{2+\beta}\big)}{\varepsilon+u} \big(iy\mu\big)^{\frac{2(1+\beta)(\varepsilon+u)}{2+\beta}}.$$

For this expression one recovers the result from Ref. [101] at one loop by using $u=0$, the appropriate change of variables and the $\frac{\alpha_s\beta_0}{4\pi}$ prefactor, which is then given by

$$\tilde{S}_{C,\mathrm{pert},\rho_{\mathrm{SD}}}(y,\mu) = 1 + \frac{\alpha_s C_F}{\pi} \frac{\Gamma\big(-\frac{2\varepsilon(1+\beta)}{2+\beta}\big)}{\varepsilon\,\Gamma(1-\varepsilon)} \mathrm{e}^{-\frac{\gamma_E\varepsilon\beta}{2+\beta}} \big(i\mu\tilde{y}\big)^{\frac{2\varepsilon(1+\beta)}{2+\beta}} \tag{D.8}$$

$$= 1 + \frac{\alpha_s C_F}{2\pi}\bigg\{ -\frac{2+\beta}{(1+\beta)\,\varepsilon^2} - \frac{2+\beta}{(1+\beta)\,\varepsilon} \ln\big(\tilde{y}^{2\frac{1+\beta}{2+\beta}}\big) - \frac{2+\beta}{2(1+\beta)} \ln\big(\tilde{y}^{2\frac{1+\beta}{2+\beta}}\big)$$

$$- \frac{2+\beta}{2(1+\beta)} \ln^2\big(\tilde{y}^{2\frac{1+\beta}{2+\beta}}\big) - \pi^2 \frac{\beta(4+3\beta)}{12(1+\beta)(2+\beta)} \bigg\} + \mathcal{O}(\alpha_s^2), \tag{D.9}$$

with $\tilde{y} = y\, \mathrm{e}^{\gamma_E} (\mu/E_J)^{\frac{1}{1+\beta}} / \big(2 z_{\mathrm{cut}}^{\frac{1}{1+\beta}}\big)$.

Now it is straightforward to investigate the renormalon structure. For that we look at Eq. D.7 for the case of $\varepsilon = 0$ and $u \neq 0$ which gives

$$B\big[\ln \tilde{S}_{C,\text{pert},\rho_{\text{SD}}}(y,\mu)\big](u) = \frac{4C_F}{\beta_0} \frac{\mathrm{e}^{\frac{5u}{3}}}{\Gamma(1+u)\,\Gamma(1-u)} \frac{\big(2^{1+\beta}\frac{E_J}{\mu}z_{\text{cut}}\big)^{\frac{-2u}{2+\beta}}\Gamma\big(-\frac{2(1+\beta)u}{2+\beta}\big)}{u}\,(iy\mu)^{\frac{2(1+\beta)u}{2+\beta}}\,.$$

(D.10)

The leading IR renormalon pole (positive and closest to $u = 0$) of the above function clearly is situated at $u = \frac{2+\beta}{2(1+\beta)}$. This value depends on how aggressive the grooming is and therefore lies between $u = \frac{1}{2}$ for no grooming or $\beta \to \infty$ and $u = 1$ for the groomer being an energy cut for $\beta = 0$. Up to now only observables with IR renormalon poles at $u = \frac{2n+1}{2}$ with $n \in \mathbb{N}_0$ were studied and the fact that in the case of soft-drop groomed jet mass the leading renormalon pole position can be changed to a real number which lies in the interval $\{\frac{1}{2}, 1\}$ is a novelty. Expanding around this leading renormalon pole gives

$$B\big[\ln \tilde{S}_{C,\text{pert},\rho_{\text{SD}}}(y,\mu)\big](u)\Big|_{u=\frac{2+\beta}{2(1+\beta)}} = \frac{4C_F}{\beta_0} \frac{\mathrm{e}^{\frac{5(2+\beta)}{6(1+\beta)}}}{\Gamma\big(\frac{\beta}{2(1+\beta)}\big)\Gamma\big(\frac{4+3\beta}{2(1+\beta)}\big)} \frac{\big(z_{\text{cut}}\frac{E_J}{\mu}\big)^{\frac{-1}{1+\beta}}}{2\big(u-\frac{2+\beta}{2(1+\beta)}\big)}\,(iy\mu)$$
$$+\, \mathcal{O}\Big(\big(u-\tfrac{2+\beta}{2(1+\beta)}\big)^0\Big)\,.$$

(D.11)

As discussed in Sec. 3.7.1 this leading renormalon also corresponds to a $\delta'(\tilde{\ell})$ distribution and can therefore be absorbed into the gap parameter of the soft model function by an appropriate subtraction. It is furthermore interesting to note that by increasing the strength of the grooming to a large β value the overall normalization of the pole decreases until it becomes 0 for $\beta \to \infty$, hence vanishes for the renormalon pole position of $u = 1$. Furthermore for this limit all higher renormalon poles in Eq. (D.10) vanish as well. In conclusion this just confirms that soft-drop grooming removes parts of the nonperturbative soft radiation which causes the pathological renormalon behavior. The amount of radiation removed is connected to the strength of the grooming and the limit of implementing an energy cutoff (for $\beta \to 0$) then removes all radiation softer than $E_J z_{\text{cut}}$ and all connected renormalon divergences.

Bibliography

[1] **CDF** Collaboration, F. Abe *et al.*, "Observation of top quark production in $\bar{p}p$ collisions," *Phys. Rev. Lett.* **74** (1995) 2626–2631, `arXiv:hep-ex/9503002 [hep-ex]`.

[2] **D0** Collaboration, S. Abachi *et al.*, "Observation of the top quark," *Phys. Rev. Lett.* **74** (1995) 2632–2637, `arXiv:hep-ex/9503003 [hep-ex]`.

[3] **CDF, D0** Collaboration, T. E. W. Group, "Combination of CDF and D0 results on the mass of the top quark using up to 9.7 fb^{-1} at the Tevatron," `arXiv:1407.2682 [hep-ex]`.

[4] **CMS** Collaboration, V. Khachatryan *et al.*, "Measurement of the top quark mass using proton-proton data at $\sqrt{(s)} = 7$ and 8 TeV," *Phys. Rev.* **D93** no. 7, (2016) 072004, `arXiv:1509.04044 [hep-ex]`.

[5] **ATLAS** Collaboration, M. Aaboud *et al.*, "Measurement of the top quark mass in the $t\bar{t} \rightarrow$ dilepton channel from $\sqrt{s} = 8$ TeV ATLAS data," *Phys. Lett.* **B761** (2016) 350–371, `arXiv:1606.02179 [hep-ex]`.

[6] M. Butenschoen, B. Dehnadi, A. H. Hoang, V. Mateu, M. Preisser, and I. W. Stewart, "Top Quark Mass Calibration for Monte Carlo Event Generators," *Phys. Rev. Lett.* **117** no. 23, (2016) 232001, `arXiv:1608.01318 [hep-ph]`.

[7] S. Fleming, A. H. Hoang, S. Mantry, and I. W. Stewart, "Jets from massive unstable particles: Top-mass determination," *Phys.Rev.* **D77** (2008) 074010, `arXiv:hep-ph/0703207 [hep-ph]`.

[8] S. Fleming, A. H. Hoang, S. Mantry, and I. W. Stewart, "Top Jets in the Peak Region: Factorization Analysis with NLL Resummation," *Phys.Rev.* **D77** (2008) 114003, `arXiv:0711.2079 [hep-ph]`.

[9] B. Dehnadi, "Heavy quark mass determinations with sum rules and jets," 2016. Doctoral Thesis, `http://othes.univie.ac.at/42936/`.

[10] A. V. Manohar and M. B. Wise, "Heavy quark physics," *Camb. Monogr. Part. Phys. Nucl. Phys. Cosmol.* **10** (2000) 1–191.

[11] M. Neubert, "Heavy quark symmetry," *Phys. Rept.* **245** (1994) 259–396, `arXiv:hep-ph/9306320 [hep-ph]`.

[12] C. W. Bauer, S. Fleming, and M. E. Luke, "Summing Sudakov logarithms in B —¿ X(s gamma) in effective field theory," *Phys. Rev.* **D63** (2000) 014006, `arXiv:hep-ph/0005275 [hep-ph]`.

[13] C. W. Bauer, S. Fleming, D. Pirjol, and I. W. Stewart, "An Effective field theory for collinear and soft gluons: Heavy to light decays," *Phys. Rev.* **D63** (2001) 114020, `arXiv:hep-ph/0011336 [hep-ph]`.

[14] C. W. Bauer, D. Pirjol, and I. W. Stewart, "Soft collinear factorization in effective field theory," *Phys. Rev.* **D65** (2002) 054022, `arXiv:hep-ph/0109045 [hep-ph]`.

[15] C. W. Bauer and I. W. Stewart, "Invariant operators in collinear effective theory," *Phys. Lett.* **B516** (2001) 134–142, `arXiv:hep-ph/0107001 [hep-ph]`.

[16] A. H. Hoang, S. Mantry, A. Pathak, and I. W. Stewart, "Extracting a Short Distance Top Mass with Light Grooming," `arXiv:1708.02586 [hep-ph]`.

[17] A. H. Hoang, A. Jain, C. Lepenik, V. Mateu, M. Preisser, I. Scimemi, and I. W. Stewart, "The MSR Mass and the $\mathcal{O}(\Lambda_{\mathrm{QCD}})$ Renormalon Sum Rule," `arXiv:1704.01580 [hep-ph]`.

[18] A. H. Hoang, C. Lepenik, and M. Preisser, "On the Light Massive Flavor Dependence of the Top Quark Mass," *PoS* **RADCOR2017** (2018) 051, `arXiv:1802.04334 [hep-ph]`.

[19] P. Marquard, A. V. Smirnov, V. A. Smirnov, M. Steinhauser, and D. Wellmann, "$\overline{\mathrm{MS}}$-on-shell quark mass relation up to four loops in QCD and a general SU(N) gauge group," *Phys. Rev.* **D94** no. 7, (2016) 074025, `arXiv:1606.06754 [hep-ph]`.

[20] A. H. Hoang, C. Lepenik, and M. Preisser, "On the Light Massive Flavor Dependence of the Large Order Asymptotic Behavior and the Ambiguity of the Pole Mass," *JHEP* **09** (2017) 099, `arXiv:1706.08526 [hep-ph]`.

[21] P. A. Baikov, K. G. Chetyrkin, and J. H. Kühn, "Five-Loop Running of the QCD coupling constant," *Phys. Rev. Lett.* **118** no. 8, (2017) 082002, `arXiv:1606.08659 [hep-ph]`.

[22] B. A. Kniehl, A. V. Kotikov, A. I. Onishchenko, and O. L. Veretin, "Strong-coupling constant with flavor thresholds at five loops in the anti-MS scheme," *Phys. Rev. Lett.* **97** (2006) 042001, `arXiv:hep-ph/0607202 [hep-ph]`.

[23] R. Tarrach, "The Pole Mass in Perturbative QCD," *Nucl. Phys.* **B183** (1981) 384–396.

[24] N. Gray, D. J. Broadhurst, W. Grafe, and K. Schilcher, "Three Loop Relation of Quark $\overline{\mathrm{MS}}$ and Pole Masses," *Z. Phys.* **C48** (1990) 673–680.

[25] K. G. Chetyrkin and M. Steinhauser, "Short distance mass of a heavy quark at order α_s^3," *Phys. Rev. Lett.* **83** (1999) 4001–4004, `arXiv:hep-ph/9907509 [hep-ph]`.

[26] K. G. Chetyrkin and M. Steinhauser, "The Relation between the $\overline{\mathrm{MS}}$ and the on-shell quark mass at order α_s^3," *Nucl. Phys.* **B573** (2000) 617–651, `arXiv:hep-ph/9911434 [hep-ph]`.

[27] K. Melnikov and T. v. Ritbergen, "The Three loop relation between the $\overline{\mathrm{MS}}$ and the pole quark masses," *Phys. Lett.* **B482** (2000) 99–108, `arXiv:hep-ph/9912391 [hep-ph]`.

[28] P. Marquard, L. Mihaila, J. H. Piclum, and M. Steinhauser, "Relation between the pole and the minimally subtracted mass in dimensional regularization and dimensional reduction to three-loop order," *Nucl. Phys.* **B773** (2007) 1–18, `arXiv:hep-ph/0702185 [hep-ph]`.

[29] P. Marquard, A. V. Smirnov, V. A. Smirnov, and M. Steinhauser, "Quark Mass Relations to Four-Loop Order in Perturbative QCD," *Phys. Rev. Lett.* **114** no. 14, (2015) 142002, `arXiv:1502.01030 [hep-ph]`.

[30] A. S. Kronfeld, "The Perturbative pole mass in QCD," *Phys. Rev.* **D58** (1998) 051501, `arXiv:hep-ph/9805215 [hep-ph]`.

[31] M. Beneke, "Renormalons," *Phys. Rept.* **317** (1999) 1–142, `arXiv:hep-ph/9807443 [hep-ph]`.

[32] M. Beneke and V. M. Braun, "Naive nonAbelianization and resummation of fermion bubble chains," *Phys. Lett.* **B348** (1995) 513–520, `arXiv:hep-ph/9411229 [hep-ph]`.

[33] M. Beneke and V. M. Braun, "Heavy quark effective theory beyond perturbation theory: Renormalons, the pole mass and the residual mass term," *Nucl. Phys.* **B426** (1994) 301–343, `arXiv:hep-ph/9402364 [hep-ph]`.

[34] M. Beneke, P. Marquard, P. Nason, and M. Steinhauser, "On the ultimate uncertainty of the top quark pole mass," *Phys. Lett.* **B775** (2017) 63–70, `arXiv:1605.03609 [hep-ph]`.

[35] M. Beneke, "More on ambiguities in the pole mass," *Phys. Lett.* **B344** (1995) 341–347, `arXiv:hep-ph/9408380 [hep-ph]`.

[36] A. Czarnecki, K. Melnikov, and N. Uraltsev, "NonAbelian dipole radiation and the heavy quark expansion," *Phys. Rev. Lett.* **80** (1998) 3189–3192, `arXiv:hep-ph/9708372 [hep-ph]`.

[37] M. Beneke, "A Quark mass definition adequate for threshold problems," *Phys. Lett.* **B434** (1998) 115–125, `arXiv:hep-ph/9804241 [hep-ph]`.

[38] A. H. Hoang, Z. Ligeti, and A. V. Manohar, "B decay and the Upsilon mass," *Phys. Rev. Lett.* **82** (1999) 277–280, `arXiv:hep-ph/9809423 [hep-ph]`.

[39] A. H. Hoang, Z. Ligeti, and A. V. Manohar, "B decays in the upsilon expansion," *Phys. Rev.* **D59** (1999) 074017, `arXiv:hep-ph/9811239 [hep-ph]`.

[40] A. H. Hoang, "1S and MS-bar bottom quark masses from Upsilon sum rules," *Phys. Rev.* **D61** (2000) 034005, `arXiv:hep-ph/9905550 [hep-ph]`.

[41] A. Pineda, "Determination of the bottom quark mass from the Upsilon(1S) system," *JHEP* **06** (2001) 022, `arXiv:hep-ph/0105008 [hep-ph]`.

[42] A. Jain, I. Scimemi, and I. W. Stewart, "Two-loop Jet-Function and Jet-Mass for Top Quarks," *Phys. Rev.* **D77** (2008) 094008, `arXiv:0801.0743 [hep-ph]`.

[43] A. H. Hoang, A. Jain, I. Scimemi, and I. W. Stewart, "Infrared Renormalization Group Flow for Heavy Quark Masses," *Phys. Rev. Lett.* **101** (2008) 151602, `arXiv:0803.4214 [hep-ph]`.

[44] A. H. Hoang, A. Jain, I. Scimemi, and I. W. Stewart, "R-evolution: Improving perturbative QCD," *Phys. Rev.* **D82** (2010) 011501, `arXiv:0908.3189 [hep-ph]`.

[45] A. Buckley *et al.*, "General-purpose event generators for LHC physics," *Phys. Rept.* **504** (2011) 145–233, `arXiv:1101.2599 [hep-ph]`.

[46] T. Ježo, J. M. Lindert, P. Nason, C. Oleari, and S. Pozzorini, "An NLO+PS generator for $t\bar{t}$ and Wt production and decay including non-resonant and interference effects," *Eur. Phys. J.* **C76** no. 12, (2016) 691, `arXiv:1607.04538 [hep-ph]`.

[47] A. Juste, S. Mantry, A. Mitov, A. Penin, P. Skands, E. Varnes, M. Vos, and S. Wimpenny, "Determination of the top quark mass circa 2013: methods, subtleties, perspectives," *Eur. Phys. J.* **C74** (2014) 3119, `arXiv:1310.0799 [hep-ph]`.

[48] **ATLAS, CDF, CMS, D0** Collaboration, , "First combination of Tevatron and LHC measurements of the top-quark mass," `arXiv:1403.4427 [hep-ex]`.

[49] S. Mrenna and P. Skands, "Automated Parton-Shower Variations in Pythia 8," *Phys. Rev.* **D94** no. 7, (2016) 074005, `arXiv:1605.08352 [hep-ph]`.

[50] J. Bellm, S. Plätzer, P. Richardson, A. Siódmok, and S. Webster, "Reweighting Parton Showers," *Phys. Rev.* **D94** no. 3, (2016) 034028, `arXiv:1605.08256 [hep-ph]`.

[51] A. H. Hoang and I. W. Stewart, "Top Mass Measurements from Jets and the Tevatron Top-Quark Mass," *Nucl. Phys. Proc. Suppl.* **185** (2008) 220–226, `arXiv:0808.0222 [hep-ph]`.

[52] A. Andreassen and M. D. Schwartz, "Reducing the Top Quark Mass Uncertainty with Jet Grooming," *JHEP* **10** (2017) 151, `arXiv:1705.07135 [hep-ph]`.

[53] A. H. Hoang, S. Plätzer, and D. Samitz, "On the Cutoff Dependence of the Quark Mass Parameter in Angular Ordered Parton Showers," `arXiv:1807.06617 [hep-ph]`.

[54] T. Sjöstrand, S. Ask, J. R. Christiansen, R. Corke, N. Desai, P. Ilten, S. Mrenna, S. Prestel, C. O. Rasmussen, and P. Z. Skands, "An Introduction to PYTHIA 8.2," *Comput. Phys. Commun.* **191** (2015) 159–177, `arXiv:1410.3012 [hep-ph]`.

[55] B. Dehnadi, A. H. Hoang, V. Mateu, M. Preisser, and I. W. Stewart, "Monte Carlo Top Quark Mass Calibration," *PoS* **RADCOR2017** (2018) 062, `arXiv:1803.02321 [hep-ph]`.

[56] M. Dasgupta and G. P. Salam, "Event shapes in e^+e^- annihilation and deep inelastic scattering," *J.Phys.* **G30** (2004) R143, `arXiv:hep-ph/0312283 [hep-ph]`.

[57] S. Kluth, "Tests of Quantum Chromo Dynamics at e^+e^- Colliders," *Rept.Prog.Phys.* **69** (2006) 1771–1846, `arXiv:hep-ex/0603011 [hep-ex]`.

[58] A. Banfi, G. P. Salam, and G. Zanderighi, "Resummed event shapes at hadron - hadron colliders," *JHEP* **08** (2004) 062, `arXiv:hep-ph/0407287 [hep-ph]`.

[59] A. Banfi, G. P. Salam, and G. Zanderighi, "Phenomenology of event shapes at hadron colliders," *JHEP* **06** (2010) 038, `arXiv:1001.4082 [hep-ph]`.

[60] E. Farhi, "A QCD Test for Jets," *Phys. Rev. Lett.* **39** (1977) 1587–1588.

[61] S. Brandt, C. Peyrou, R. Sosnowski, and A. Wroblewski, "The Principal axis of jets. An Attempt to analyze high-energy collisions as two-body processes," *Phys. Lett.* **12** (1964) 57–61.

[62] R. K. Ellis, D. Ross, and A. Terrano, "The Perturbative Calculation of Jet Structure in e^+e^- Annihilation," *Nucl.Phys.* **B178** (1981) 421.

[63] L. Clavelli, "Jet Invariant Mass in Quantum Chromodynamics," *Phys. Lett.* **85B** (1979) 111–114.

[64] T. Chandramohan and L. Clavelli, "Consequences of Second Order QCD for Jet Structure in e^+e^- Annihilation," *Nucl. Phys.* **B184** (1981) 365–380.

[65] L. Clavelli and D. Wyler, "Kinematical Bounds on Jet Variables and the Heavy Jet Mass Distribution," *Phys. Lett.* **103B** (1981) 383–387.

[66] C. F. Berger, T. Kucs, and G. F. Sterman, "Interjet energy flow / event shape correlations," *Int. J. Mod. Phys.* **A18** (2003) 4159–4168, `arXiv:hep-ph/0212343 [hep-ph]`.

[67] C. F. Berger, T. Kucs, and G. F. Sterman, "Event shape / energy flow correlations," *Phys. Rev.* **D68** (2003) 014012, `arXiv:hep-ph/0303051 [hep-ph]`.

[68] G. Parisi, "Super Inclusive Cross-Sections," *Phys.Lett.* **B74** (1978) 65.

[69] J. F. Donoghue, F. Low, and S.-Y. Pi, "Tensor Analysis of Hadronic Jets in Quantum Chromodynamics," *Phys.Rev.* **D20** (1979) 2759.

[70] M. Preißer, "C-Parameter with Massive Quarks," 2014. Master's Thesis, http://othes.univie.ac.at/34188/.

[71] S. Catani, G. Turnock, and B. R. Webber, "Jet broadening measures in e^+e^- annihilation," *Phys. Lett.* **B295** (1992) 269–276.

[72] G. Salam and D. Wicke, "Hadron masses and power corrections to event shapes," *JHEP* **0105** (2001) 061, arXiv:hep-ph/0102343 [hep-ph].

[73] V. Mateu, I. W. Stewart, and J. Thaler, "Power Corrections to Event Shapes with Mass-Dependent Operators," *Phys.Rev.* **D87** no. 1, (2013) 014025, arXiv:1209.3781 [hep-ph].

[74] I. W. Stewart, F. J. Tackmann, and W. J. Waalewijn, "N-Jettiness: An Inclusive Event Shape to Veto Jets," *Phys. Rev. Lett.* **105** (2010) 092002, arXiv:1004.2489 [hep-ph].

[75] E. Gardi and L. Magnea, "The C parameter distribution in e^+e^- annihilation," *JHEP* **0308** (2003) 030, arXiv:hep-ph/0306094 [hep-ph].

[76] T. Becher, G. Bell, and M. Neubert, "Factorization and Resummation for Jet Broadening," *Phys. Lett.* **B704** (2011) 276–283, arXiv:1104.4108 [hep-ph].

[77] T. Becher and G. Bell, "NNLL Resummation for Jet Broadening," *JHEP* **11** (2012) 126, arXiv:1210.0580 [hep-ph].

[78] S. Catani, L. Trentadue, G. Turnock, and B. R. Webber, "Resummation of large logarithms in e+ e- event shape distributions," *Nucl. Phys.* **B407** (1993) 3–42.

[79] L. G. Almeida, S. D. Ellis, C. Lee, G. Sterman, I. Sung, and J. R. Walsh, "Comparing and counting logs in direct and effective methods of QCD resummation," *JHEP* **04** (2014) 174, arXiv:1401.4460 [hep-ph].

[80] H. Contopanagos, E. Laenen, and G. F. Sterman, "Sudakov factorization and resummation," *Nucl. Phys.* **B484** (1997) 303–330, arXiv:hep-ph/9604313 [hep-ph].

[81] C. W. Bauer, S. P. Fleming, C. Lee, and G. F. Sterman, "Factorization of e+e- Event Shape Distributions with Hadronic Final States in Soft Collinear Effective Theory," *Phys.Rev.* **D78** (2008) 034027, arXiv:0801.4569 [hep-ph].

[82] A. V. Manohar, "Effective field theories," *Lect. Notes Phys.* **479** (1997) 311–362, arXiv:hep-ph/9606222 [hep-ph].

[83] T. Becher, A. Broggio, and A. Ferroglia, "Introduction to Soft-Collinear Effective Theory," *Lect. Notes Phys.* **896** (2015) pp.1–206, arXiv:1410.1892 [hep-ph].

[84] P. Pietrulewicz, "Variable flavor scheme for final state jets," 2014. Doctoral Thesis, http://othes.univie.ac.at/34439/.

[85] A. K. Leibovich, Z. Ligeti, and M. B. Wise, "Comment on quark masses in SCET," *Phys. Lett.* **B564** (2003) 231–234, arXiv:hep-ph/0303099 [hep-ph].

[86] A. H. Hoang, D. W. Kolodrubetz, V. Mateu, and I. W. Stewart, "C-parameter distribution at N³LL' including power corrections," *Phys. Rev.* **D91** no. 9, (2015) 094017, arXiv:1411.6633 [hep-ph].

[87] S. Gritschacher, A. H. Hoang, I. Jemos, and P. Pietrulewicz, "Secondary Heavy Quark Production in Jets through Mass Modes," *Phys. Rev.* **D88** (2013) 034021, arXiv:1302.4743 [hep-ph].

[88] P. Pietrulewicz, S. Gritschacher, A. H. Hoang, I. Jemos, and V. Mateu, "Variable Flavor Number Scheme for Final State Jets in Thrust," *Phys. Rev.* **D90** no. 11, (2014) 114001, `arXiv:1405.4860 [hep-ph]`.

[89] P. Pietrulewicz, D. Samitz, A. Spiering, and F. J. Tackmann, "Factorization and Resummation for Massive Quark Effects in Exclusive Drell-Yan," *JHEP* **08** (2017) 114, `arXiv:1703.09702 [hep-ph]`.

[90] C. Lepenik, "Heavy jet mass with massive quarks," 2016. Master's Thesis, `http://othes.univie.ac.at/42441/`.

[91] M. Dasgupta and G. P. Salam, "Resummation of nonglobal QCD observables," *Phys. Lett.* **B512** (2001) 323–330, `arXiv:hep-ph/0104277 [hep-ph]`.

[92] P. A. Baikov, K. G. Chetyrkin, A. V. Smirnov, V. A. Smirnov, and M. Steinhauser, "Quark and gluon form factors to three loops," *Phys. Rev. Lett.* **102** (2009) 212002, `arXiv:0902.3519 [hep-ph]`.

[93] T. Gehrmann, E. W. N. Glover, T. Huber, N. Ikizlerli, and C. Studerus, "The quark and gluon form factors to three loops in QCD through to $\mathcal{O}(\epsilon^2)$," *JHEP* **11** (2010) 102, `arXiv:1010.4478 [hep-ph]`.

[94] M. D. Schwartz, "Resummation and NLO matching of event shapes with effective field theory," *Phys. Rev.* **D77** (2008) 014026, `arXiv:0709.2709 [hep-ph]`.

[95] A. Hornig, C. Lee, and G. Ovanesyan, "Effective Predictions of Event Shapes: Factorized, Resummed, and Gapped Angularity Distributions," *JHEP* **05** (2009) 122, `arXiv:0901.3780 [hep-ph]`.

[96] A. J. Larkoski, D. Neill, and J. Thaler, "Jet Shapes with the Broadening Axis," *JHEP* **04** (2014) 017, `arXiv:1401.2158 [hep-ph]`.

[97] T. Becher and M. Neubert, "Toward a NNLO calculation of the anti-B → X(s) gamma decay rate with a cut on photon energy. II. Two-loop result for the jet function," *Phys. Lett.* **B637** (2006) 251–259, `arXiv:hep-ph/0603140 [hep-ph]`.

[98] H. Boos, T. Feldmann, T. Mannel, and B. D. Pecjak, "Can anti-B → X(c) l anti-nu l help us extract |V(ub)|?," *JHEP* **05** (2006) 056, `arXiv:hep-ph/0512157 [hep-ph]`.

[99] A. H. Hoang, A. Pathak, P. Pietrulewicz, and I. W. Stewart, "Hard Matching for Boosted Tops at Two Loops," *JHEP* **12** (2015) 059, `arXiv:1508.04137 [hep-ph]`.

[100] R. Abbate, M. Fickinger, A. H. Hoang, V. Mateu, and I. W. Stewart, "Thrust at N³LL with Power Corrections and a Precision Global Fit for alphas(mZ)," *Phys. Rev.* **D83** (2011) 074021, `arXiv:1006.3080 [hep-ph]`.

[101] C. Frye, A. J. Larkoski, M. D. Schwartz, and K. Yan, "Factorization for groomed jet substructure beyond the next-to-leading logarithm," *JHEP* **07** (2016) 064, `arXiv:1603.09338 [hep-ph]`.

[102] W. Kilian, T. Ohl, and J. Reuter, "WHIZARD: Simulating Multi-Particle Processes at LHC and ILC," *Eur. Phys. J.* **C71** (2011) 1742, `arXiv:0708.4233 [hep-ph]`.

[103] B. W. Harris and J. F. Owens, "The Two cutoff phase space slicing method," *Phys. Rev.* **D65** (2002) 094032, `arXiv:hep-ph/0102128 [hep-ph]`.

[104] G. P. Korchemsky and S. Tafat, "On power corrections to the event shape distributions in QCD," *JHEP* **10** (2000) 010, `arXiv:hep-ph/0007005 [hep-ph]`.

[105] A. H. Hoang and I. W. Stewart, "Designing gapped soft functions for jet production," *Phys.Lett.* **B660** (2008) 483–493, arXiv:0709.3519 [hep-ph].

[106] C. Lee and G. F. Sterman, "Universality of nonperturbative effects in event shapes," *eConf* **C0601121** (2006) A001, arXiv:hep-ph/0603066 [hep-ph].

[107] Z. Ligeti, I. W. Stewart, and F. J. Tackmann, "Treating the b quark distribution function with reliable uncertainties," *Phys. Rev.* **D78** (2008) 114014, arXiv:0807.1926 [hep-ph].

[108] C. F. Uhlemann and N. Kauer, "Narrow-width approximation accuracy," *Nucl. Phys.* **B814** (2009) 195–211, arXiv:0807.4112 [hep-ph].

[109] D. Berdine, N. Kauer, and D. Rainwater, "Breakdown of the Narrow Width Approximation for New Physics," *Phys. Rev. Lett.* **99** (2007) 111601, arXiv:hep-ph/0703058 [hep-ph].

[110] **Particle Data Group** Collaboration, C. Patrignani *et al.*, "Review of Particle Physics," *Chin. Phys.* **C40** no. 10, (2016) 100001.

[111] J. L. Rosner, M. P. Worah, and T. Takeuchi, "Oblique corrections to the W width," *Phys. Rev.* **D49** (1994) 1363–1369, arXiv:hep-ph/9309307 [hep-ph].

[112] W. R. Inc., "Mathematica, Version 11.3.". Champaign, IL, 2018.

[113] **L3** Collaboration, P. Achard *et al.*, "Studies of hadronic event structure in e^+e^- annihilation from 30-GeV to 209-GeV with the L3 detector," *Phys. Rept.* **399** (2004) 71–174, arXiv:hep-ex/0406049 [hep-ex].

[114] **ALEPH** Collaboration, D. Buskulic *et al.*, "Test of the flavor independence of alpha-s," *Phys. Lett.* **B355** (1995) 381–393.

[115] **OPAL** Collaboration, G. Abbiendi *et al.*, "Test of the flavor independence of alpha(s) using next-to-leading order calculations for heavy quarks," *Eur. Phys. J.* **C11** (1999) 643–659, arXiv:hep-ex/9904013 [hep-ex].

[116] F. Bach, B. C. Nejad, A. Hoang, W. Kilian, J. Reuter, M. Stahlhofen, T. Teubner, and C. Weiss, "Fully-differential Top-Pair Production at a Lepton Collider: From Threshold to Continuum," *JHEP* **03** (2018) 184, arXiv:1712.02220 [hep-ph].

[117] O. V. Tarasov, A. A. Vladimirov, and A. Yu. Zharkov, "The Gell-Mann-Low Function of QCD in the Three Loop Approximation," *Phys. Lett.* **93B** (1980) 429–432.

[118] S. A. Larin and J. A. M. Vermaseren, "The Three loop QCD Beta function and anomalous dimensions," *Phys. Lett.* **B303** (1993) 334–336, arXiv:hep-ph/9302208 [hep-ph].

[119] T. van Ritbergen, J. A. M. Vermaseren, and S. A. Larin, "The Four loop beta function in quantum chromodynamics," *Phys. Lett.* **B400** (1997) 379–384, arXiv:hep-ph/9701390 [hep-ph].

[120] M. Czakon, "The Four-loop QCD beta-function and anomalous dimensions," *Nucl. Phys.* **B710** (2005) 485–498, arXiv:hep-ph/0411261 [hep-ph].

[121] G. P. Korchemsky and A. V. Radyushkin, "Renormalization of the Wilson Loops Beyond the Leading Order," *Nucl. Phys.* **B283** (1987) 342–364.

[122] A. Vogt, "Next-to-next-to-leading logarithmic threshold resummation for deep inelastic scattering and the Drell-Yan process," *Phys. Lett.* **B497** (2001) 228–234, arXiv:hep-ph/0010146 [hep-ph].

[123] C. F. Berger, "Higher orders in A(alpha(s))/[1-x]+ of nonsinglet partonic splitting functions," *Phys. Rev.* **D66** (2002) 116002, `arXiv:hep-ph/0209107 [hep-ph]`.

[124] S. Moch, J. A. M. Vermaseren, and A. Vogt, "Three-loop results for quark and gluon form-factors," *Phys. Lett.* **B625** (2005) 245–252, `arXiv:hep-ph/0508055 [hep-ph]`.

[125] T. Becher, M. Neubert, and B. D. Pecjak, "Factorization and Momentum-Space Resummation in Deep-Inelastic Scattering," *JHEP* **01** (2007) 076, `arXiv:hep-ph/0607228 [hep-ph]`.

[126] M. Dasgupta, A. Fregoso, S. Marzani, and G. P. Salam, "Towards an understanding of jet substructure," *JHEP* **09** (2013) 029, `arXiv:1307.0007 [hep-ph]`.

[127] A. J. Larkoski, S. Marzani, G. Soyez, and J. Thaler, "Soft Drop," *JHEP* **05** (2014) 146, `arXiv:1402.2657 [hep-ph]`.

[128] Y. L. Dokshitzer, G. D. Leder, S. Moretti, and B. R. Webber, "Better jet clustering algorithms," *JHEP* **08** (1997) 001, `arXiv:hep-ph/9707323 [hep-ph]`.

[129] M. Wobisch and T. Wengler, "Hadronization corrections to jet cross-sections in deep inelastic scattering," in *Monte Carlo generators for HERA physics. Proceedings, Workshop, Hamburg, Germany, 1998-1999*, pp. 270–279. 1998. `arXiv:hep-ph/9907280 [hep-ph]`.